ENGINEERING PHOTOSYNTHETIC SYSTEMS FOR BIOREGENERATIVE LIFE SUPPORT

Alexandra Masot Mata

PhD Thesis

May 2007

UAB
Universitat Autònoma
de Barcelona

Universitat Autònoma de Barcelona

Escola Tècnica Superior d'Enginyeria

Departament d'Enginyeria Química

ENGINEERING PHOTOSYNTHETIC SYSTEMS FOR BIOREGENERATIVE LIFE SUPPORT

Alexandra Masot Mata

PhD Thesis

May 2007

Title	Engineering Photosynthetic Systems For Bioregenerative Life Support
Author	Alexandra Masot Mata
Directors	Francesc Gòdia Casablancas Joan Albiol Sala Geoffrey Waters
Financial Support	The author acknowledges 'Centre de Referència en Biotecnologia (CeRBa) de la Generalitat de Catalunya' for the grant FI 0045. This work was supported by the 'Departament d'Educació i Universitats de la Generalitat de Catalunya i del Fons Social Europeu'.

PhD Program in Biotechnology
Departament d'Enginyeria Química
Escola Tècnica Superior d'Enginyeria
Universitat Autònoma de Barcelona

FRANCESC GÒDIA CASABLANCAS, catedràtic del Departament d'Enginyeria Química de la Universitat Autònoma de Barcelona, JOAN ALBIOL SALA, professor agregat del Departament d'Enginyeria Química de la Universitat Autònoma de Barcelona i GEOFFREY WATERS, research associate of CESRF Department of Environmental Biology of University of Guelph (Canada),

CERTIFIQUEM:

Que l'enginyera química ALEXANDRA MASOT MATA ha dut a terme amb la nostra direcció el treball amb el títol "Engineering photosynthetic systems for bioregenerative life support" que es presenta en aquesta memòria i que constitueix la seva Tesi per optar al Grau de Doctora per la Universitat Autònoma de Barcelona.

I perquè se'n prengui coneixement i consti als efectes oportuns, presentem a l'Escola Tècnica Superior d'Enginyeries de la Universitat Autònoma de Barcelona l'esmentada Tesi, signant el present certificat a

Bellaterra, Maig 2007

Dr. Francesc Gòdia Casablancas Dr. Joan Albiol Sala Dr. Geoffrey Waters

A l’Eudald,
als meus pares, Josep i Modesta,
i a l’Òscar.

AGRAÏMENTS/ACKNOWLEDGEMENTS

Reconec que el fet d'escriure els agraïments m'entristeix una mica, perque significa que aquesta etapa de la vida que he dedicat a fer la tesi està arribant a la fi. I tot i que estic molt il·lusionada en començar nous projectes, quan recordo tot el que he viscut durant aquest anys i totes les persones amb les que he fet el camí, no puc evitar que m'envaeixi la melancolia. Bé, no patiu, faré el cor fort, i començaré d'una vegada, que encara us queda molt per llegir ;).

Clarament aquesta tesi no l'hagués realitzat sense la confiança que en Quico va dipositar en mi per desenvolupar aquest projecte. Moltes gràcies per encoratjar-me a seguir sempre endavant i per les teves aportacions al treball, he après molt de tu.

Vull agraïr de forma molt especial l'ajuda d'en Joan, que ha seguit el treball del dia a dia i ha dedicat incomptables hores del seu temps a guiar-me i a discutir junts els resultats. De veritat Joan, moltíssimes gràcies per tot.

I would also want to express my gratitude to my third supervisor, Geoff. I appreciate your valuable contribution to the thesis. During these years, I've not only learned a lot from you, but also I've enjoyed working together. Thanks for the inexhaustible enthusiasm you've shown for my work.

Moltes gràcies Vane per tota la teva inestimable ajuda amb els cultius de *Spirulina* i la teva amistat. També, vull agraïr a tots els altres companys de MELiSSA, per ajudar-me quan ho he necessitat i per les hores compartides durant les reunions de grup.

Thanks a lot Danuta for your work in the plant cultures, you know that part of this thesis belongs to you. I would also like to thank Jen, Dave, Urbee and Youbin for their friendship and hospitality. Definitely, you are my Canadian family.

I és clar, moltes gràcies a tots vosaltres companys, que heu estat al meu costat compartint les penes i alegries típiques de qualsevol investigador jove precari. He disfrutat molt treballant al laboratori, però crec que el que més recordaré són les nostres converses durant cafés, dinars, hores de despatx i sortides de nit.

Per últim, vull agrair al meus amics de Lleida per cuidar-me tant...gràcies nenes! També gràcies a la gent de Cassà, especialment a l'Agustí i la Dolors, per acollir-me com una més de la familia.

Moltíssimes gràcies i un petó ben fort a tots!

Barcelona, 7 de maig del 2007.

SUMMARY

The MELiSSA project (Micro-Ecological Life Support System Alternative) of the European Space Agency (ESA) is an artificial ecosystem conceived as a tool to study and develop technology for a future biological life support system required for long term manned space missions. The fact that the MELiSSA project is formed by several independent organizations of different countries made possible that part of the experimental work of this thesis was carried out in the MELiSSA Pilot Plant (MPP) located at Universitat Autònoma de Barcelona (Spain) and the Controlled Environmental Systems Research Facility (CESRF) located at University of Guelph (Canada).

Based on the principle of an aquatic ecosystem, MELiSSA aims to produce food, fresh water and oxygen from organic wastes (inedible biomass, faeces, urine and CO_2) using the combined activity of several microorganisms and higher plants, which colonize five interconnected compartments. The main contribution of this thesis is in the engineering of the photosynthetic compartments of the MELiSSA loop. These photosynthetic compartments consist of a continuous photobioreactor for the culture of *Arthrospira sp.*, and a number of sealed higher plant chambers. The first *Arthrospira* reactor has been already built and is in operation at the MPP. This work is contributing to an increase in the knowledge on its operation and characterization. While the Higher Plant Chamber (HPC) is still in the construction phase, the work of this thesis focuses on the collection of basic data for the culture of beet and lettuce. These data are then used in the design of the HPC prototype, which will be built and integrated within the MPP. Finally, the work evaluates the impact of the integration of these two compartments in the complete system, using a static mass balance model for assessing the nitrogen, CO_2 and O_2 balances.

Particularly, the work has been structured in the following three main units.

Unit I - *Arthrospira* Compartment (CIVa):

Several continuous cultures have been carried out at different dilution rates and light intensities, planned using a Box-Wilson Central Composite Design, to determine the operational limits and maximum productivity of *Arthrospira* pilot plant photobioreactor. The highest *Arthrospira* productivity attained in the pilot plant photobioreactor is 27 $mg \cdot L^{-1} \cdot h^{-1}$ at a dilution rate of 0.044 h^{-1} and a light intensity of 194 $W \cdot m^{-2}$. Disturbances of normal operating conditions affecting pH, liquid and gas flow rate influence *Arthrospira* growth, but the tested deviations, in all cases, allows the recovery of the initial biomass values after the reestablishment of normal operational conditions along a discontinuous operational period.

Moreover, the effect of ammonium and light intensity on *Arthrospira* production and biomass composition has been studied and it is determined that in order to avoid inhibition of the *Arthrospira* growth, the steady-state ammonium concentration must be lower than 5.6 mM.

Unit II – Higher Plant Compartment (CIVb/HPC):

Three batch cultures and two staggered cultures in sealed environment chambers have been performed to collect baseline data of productivity, tissue composition, nutrient uptake and canopy photosynthesis from beet and lettuce trials. For beet, the mean total plant productivity among batch and staggered cultures is 15.31 g $dw \cdot m^{-2} \cdot d^{-1}$ with a harvest index of 89%. For lettuce, total plant productivity is 13.85 g $dw \cdot m^{-2} \cdot d^{-1}$ and the percentage of edible biomass is 72%. The net CO_2 exchange rate (NCER) technique is a good alternative to classical growth analysis for estimating plant growth and dry weight production inside the chamber without using destructive analyses. In addition to this, the ionic uptake of the nutrient solution has been proven to be a good predictor of total canopy mineral content using the estimated biomass.

Moreover, the photosynthetic study performed at leaf level has contributed to estimates of light energy related parameters for the canopy model. The rectangular hyperbola model (RH) is suitable in defining the leaf photosynthetic response to light at different CO_2 levels and crop ages. No significant differences are detected for the quantum yield (α) and dark respiration rate (R_d) among CO_2 levels, but in contrast, the maximum photosynthetic rate (P_{max}) was found to depend on CO_2 concentration. Moreover, it is observed that that α, P_{max} and R_d values remain constant through crop development. It is also concluded that the RH model coupled with direct estimation of α, P_{max} and R_d from leaf light curve studies is an appropriate first step in the development of an HPC control law for managing gas exchange.

Unit III - Photosynthetic Compartments Integration:

The knowledge gained in the performance of beet and lettuce cultures in sealed environment chambers has been used to design the HPC prototype to be integrated into the MPP. Using plant productivity data obtained in the previous trials, it is concluded that 3 HPC prototypes with 5 m^2 of growing area each, will be constructed to provide 20% of the daily crew diet with beet, lettuce and wheat. The selected configuration is an elongated chamber with a growing area 5 m long and 1 m wide with two air-locks at each end. Such configuration will allow the semi-continuous (staggered) production of plant biomass while ensuring gas environment isolation during sowing and harvest.

Finally, the impact of the integration of the photosynthetic compartments into the MPP has been evaluated using a static mass balance model for assessing the nitrogen, CO_2 and O_2 balances, while determining the conditions under which the closure of the mass balances can be expected.

TABLE OF CONTENTS

RESULTS UNIT III: Photosynthetic Compartments Integration

CONCLUSIONS

REFERENCES

ANNEXES

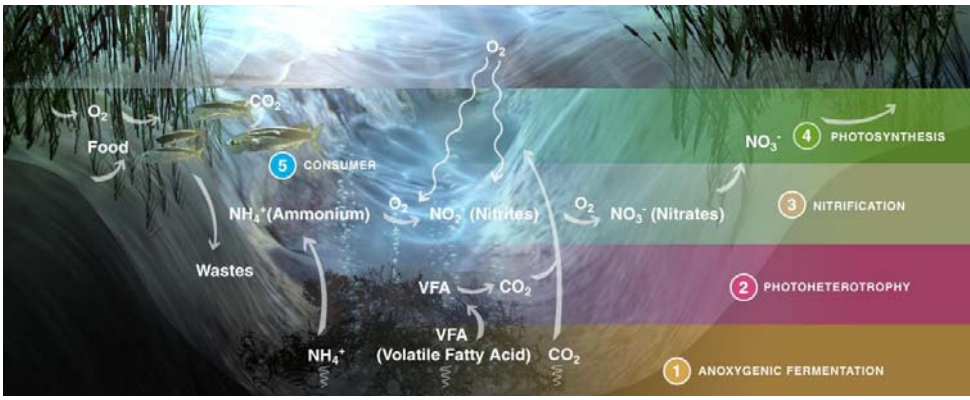

Introduction

Chapter **1**

General Introduction

Chapter **2**

Objectives and outline

Chapter 1

GENERAL INTRODUCTION

1.1 LIFE SUPPORT SYSTEMS

The main objective of life support systems is to maintain life in an environment or situation in which, without external aid, it would not be possible to sustain the vital functions of an exploration mission's crew. The support of life requires supply of food, water and O_2 and removal of generated wastes, faeces, urine and CO_2. In addition to this, the environmental conditions (such as temperature and pressure) must be controlled, so that the system can be habitable (Tamponnet *et al.*, 1994).

The need of life support systems emerged in the start of human presence in extreme environments such as in space. In short manned space missions, all the material required to support life is taken as part of the mission support materials or supplied regularly from Earth. As the duration, distance and crew size of missions increase, so does the shipped mass and volume of food and wastes. This leads to a higher mission cost and mass transportation requirements. Moreover, the choice to rely on periodic re-supply is associated with a high economical cost and risk. Therefore a self-sustainable system able to support life in a hostile environment, such as the Moon or Mars, would overcome serious limitations in the extent of

human space exploration (Mitchell, 1994). Additionally, the technology developed could also be used in some terrestrial environments on Earth, such as at Poles or submarine bases.

Depending on the recycling capacity for wastes, life support systems are classified in several types. In open systems, the material necessary for sustaining life is taken initially or supplied periodically from the original biosphere, while the wastes are stored and returned. Such systems are suitable for short manned space missions near Earth such as the International Space Station (ISS). In the semi-closed or closed systems, there is a higher degree of recycling of wastes, and subsequently, a higher degree of system closure. The type of process used for recycling defines whether the system is physicochemical or biological. Some of the characteristics of both process types are shown in Table 1.1.

Table 1.1 Classification of the semi-closed or closed life support systems based on the type of recycling process used.

PROCESS	CHARACTERISTICS
PHYSICOCHEMICAL	Atmospheric management Wastes management Water management No production of edible material (food) Suitable for long mission in Earth orbits
BIOLOGICAL	Atmospheric management Wastes management Water management Production of edible material (food) Mimic of the terrestrial biosphere Suitable for long term mission on Moon or Mars

The prospect for use of biologically based life support systems rests in the development of a system with a high degree of closure by means of the progressive incorporation of biological subsystems rather than physicochemical ones.

Research and development of bioregenerative life support systems is done by several organizations. Some of the government funded projects include those of the European Space Agency (ESA), the Canadian Space Agency (CSA), the National Aeronautics and Space Administration (NASA) in the USA and the National Space Development Agency (NASDA) in Japan.

The primary activity of ESA and CSA in bioregenerative life support systems is the MELiSSA (Micro-Ecological Life Support System Alternative) project, which is described in detail below.

The NASA activity in Controlled Ecological Life-Support System (CELSS) has been carried out in different research installations. In the Kennedy Space Centre (KSC), a Biomass Production Chamber (BPC) was designed to provide the food, water and atmospheric regeneration needs for one person. The chamber, with a total crop growing area of 20 m^2, is used for several crop tests focused mainly on the effects of high intensity lighting and the effect of CO_2 concentration on crop growth development (Wheeler, 2003). In the Johnson Space Centre, research was performed using a variable plant growth chamber (VPGC) with a growing

area of 11 m^2 (Barta *et al.*, 1996). Currently, the research activity on biomass production involving higher plants and cyanobacteria is focused in the NASA Specialized Center of Research and Training (NSCORT) located at Purdue University (Mitchell, 1994).

In 1973, the Bios-3 experiments conducted as part of the former Soviet space program demonstrated the feasibility of sustaining human life inside a small, essentially closed ecological system with a plant growing area of 63 m^2. Bios-3 was a further step of Bios-1 constructed in 1965, where the atmosphere was regenerated for one human in a sealed 12 m^3 chamber connected through air ducts with an 18 L algal culture of *Chlorella vulgaris* (Salisbury *et al.*, 1997).

One of the private projects for the development of life support systems was Biosphere 2, which is a sealed air conditioned greenhouse occupying 1.2 hectares in Arizona (USA). The first mission involved the closure of Biosphere 2 with eight crew members for 2 years (1991-1993). The objectives, results and main conclusions of the first experimental closure and the subsequent engineering improvements of the facility are reported by several authors (Allen and Nelson, 1999; Marino *et al.*, 1999; Silverston *et al.*, 1999, 2003; Allen *et al.* 2003). However, the experiments were heavily criticized by the space community.

Another life support system project is the Japanese Closed Ecology Experiment Facility (CEEF) based on the connection of a several modules colonized by plants and animals (Kibe *et al.*, 1997). This project is currently testing the closure of two humans using physicochemical waste recycling.

1.2 MELiSSA PROJECT

The MELiSSA project was started at ESA in 1989. The MELiSSA project, coordinated by ESA, is formed by several independent organizations of different countries: EPAS (Nazareth, Belgium), SCK-CEN and VITO (Mol, Belgium), Universiteit Gent (Gent, Belgium), SHERPHA Engineering (Nanterre, France), Université Blaise Pascal (Clermont-Ferrand, France), Universitat Autònoma de Barcelona (UAB) (Bellaterra, Spain) and University of Guelph (UoG) (Guelph, Canada). The project is co-funded by ESA, the MELiSSA partners, and the authorities of Belgium (SSTC), Spain (Generalitat de Catalunya, CDTI and PNE) and Canada (OCE and CSA). The organization of the MELiSSA project is based in five different phases related to basic research and development, preliminary flight experiments, ground and space demonstration, technology transfer and education and communication (Lasseur *et al.*, 2005).

1.2.1 MELiSSA CONCEPT

MELiSSA is an artificial ecosystem conceived as a tool for the study and development of technology for a future biological life support system required for long term manned space missions (Mergeay *et al.*, 1988). Based on the principle of an aquatic ecosystem (Figure 1.1), MELiSSA aims to produce food, fresh water and oxygen from organic wastes (inedible biomass, faeces, urea and CO_2) using the combined activity several microorganisms and higher plants.

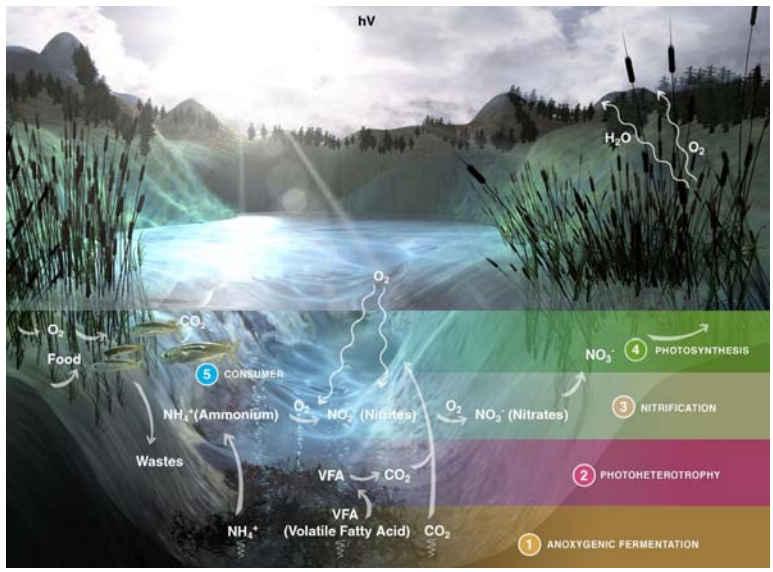

Figure 1.1 Lake ecosystem used to illustrate the concept of MELiSSA and its compartments.

In order to simplify the behaviour of such an artificial ecosystem and to allow a deterministic engineering approach, MELiSSA was structured in five interconnected compartments colonized respectively by thermophilic anoxygenic bacteria (CI), photoheterotrophic bacteria (CII), nitrifying bacteria (CIII), photoautotrophic bacteria (CIVa), higher plants (CIVb or HPC) and the crew (CV), as schematically shown in Figure 1.2. Each compartment has its own function that contributes to achieve the complete recycling of the wastes, while regenerating air, water and food required by the crew. When possible, the various compartments defined in the MELiSSA loop are operated in axenic conditions, using pure cultures of microorganisms.

The thermophilic anaerobic bacteria of the first compartment (CI) are responsible for the degradation of the organic wastes, such as the inedible parts of the plants and the crew wastes (faeces and urine). The compartment converts these wastes into CO_2, volatile fatty acids and ammonium. However, since the fibrous compounds of the plant material have low degradation efficiency in CI, the incorporation of a fungal sub-compartment or even a physical treatment for further degradation is currently under consideration. The liquid outlet mixture resulting from the anaerobic degradation (CI) is fed into the second compartment (CII), where the anaerobic photoheterotrophic bacteria transform the fatty acids into *Rhodospirillum rubrum* biomass. Ammonium present in the output of CII is converted by the nitrifying bacteria (CIII) to nitrate, which is the main nitrogen source for the following compartment (CIV). This compartment is divided into a photoautotrophic cyanobacteria compartment (CIVa) colonized by *Artrosphira sp.* and a Higher Plant Compartment (CIVb or HPC). Both photosynthetic compartments are responsible of removal of CO_2, regeneration of O_2, recovery of water, and production of edible biomass for the crew.

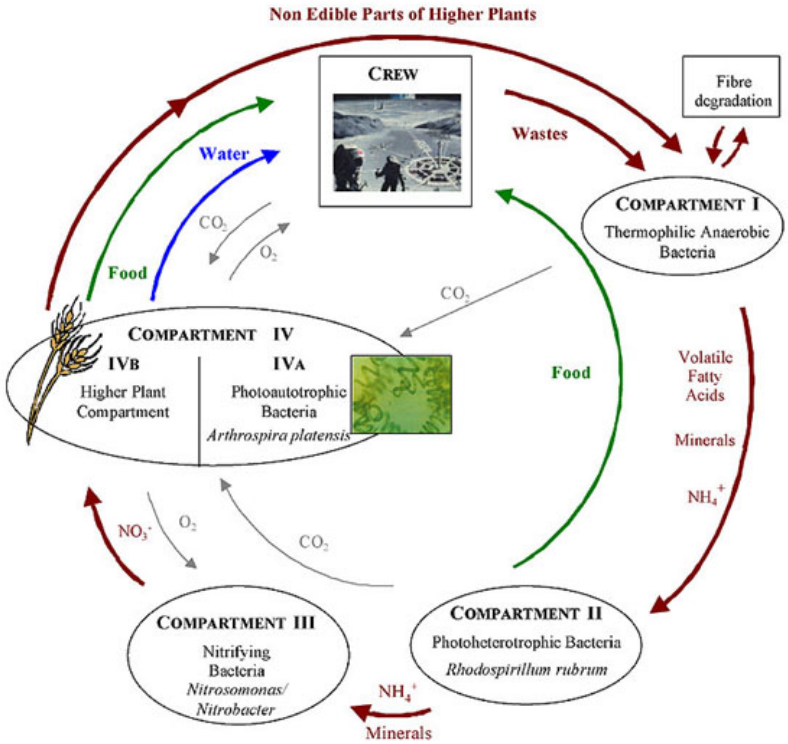

Figure 1.2 Compartmentalized structure of the MELiSSA loop concept.

1.2.2 MELiSSA COMPARTMENTS

1.2.2.1 CI: FERMENTATIVE, ANAEROBIC AND THERMOPHILIC COMPARTMENT

The liquid and solid wastes generated by the crew, mainly biomass not used for human consumption and inedible parts of plants, are degraded biologically in CI (breaking polymers such as cellulose and hemicellulose). In order to minimize the consumption of oxygen, the degradation is anaerobic.

The classical anaerobic degradation approach encompasses four main phases:

- Hydrolysis: The hydrolytic-fermentative bacteria hydrolyze macromolecular compounds into water soluble polymers.
- Acidogenesis: The polymers produced in the previous step are further fermented along with the production of fermentation products such as volatile fatty acids, alcohols, lactic acid, ammonia, H_2, CO_2 and minerals.
- Acetogenesis: The acetogenic bacteria carry out the degradation of volatile fatty acids and the alcohols into acetic acid, CO_2 and H_2.
- Methanogenesis: The acetoclastic and hydrogenotrophic methanogenic bacteria convert the former products into methane.

Unlike the conventional anaerobic systems, where methane production is enhanced, in the MELiSSA loop methane is not a valuable product since can not be further used in the following steps. Thus, in order to avoid the methane production and the presence of contaminants, the bioreactor is operated at a slightly acidic pH (6.5) under thermophilic conditions (50ºC) and with an ammonium concentration inside the reactor around 80 $mg \cdot L^{-1}$. In those conditions the main products generated in CI would be volatile fatty acids (VFA), CO_2 and ammonium.

The strains initially selected for colonizing CI (*Clostridium thermocellum*, *Clostridium thermosaccharolyticum* and *Coprothermobacter proteolyticus*) were not capable of degrading in an efficient way complex substrates such as faeces. Thus, they were substituted by an inoculum cultivated using natural selection of strains present in faecal material (Lasseur and Paillé, 2001). Both species degraded efficiently some of the substrates present in faeces such as proteins (65%), but still presented low degradation efficiency of fiber material. Nowadays, the possibility to include another compartment colonized by fibrobacter to enhance fiber degradation of CI is under study (Lasseur and Viera da Silva, 2005).

1.2.2.2 CII: PHOTOAUTO/HETEROTROPHIC COMPARTMENT

The aim of CII is to metabolize the compounds generated in the anaerobic degradation of CI, mainly volatile fatty acids (VFA), alcohols, CO_2, ammonium, amino acids and H_2, as shown in Table 1.2.

Table 1.2 Possible compounds of the effluent to the photoheterotrophic compartment. (Albiol, 1994).

Carbon sources	Acetic, Propionic, Butyric, Isobutyric, Valeric, Isovaleric, Caproic, Isocaproic, Lactic, Ethanol and CO_2
Nitrogen sources	Ammonium, Urea, Uric acid, Amino acids and amines
Others	H_2, Mineral nutrient and Vitamins

In order to convert such product into biomass under anaerobic conditions, two different phototrophic bacteria were selected. One of the species, *Rhodospirillum rubrum*, degrades the organic carbon source and the other, *Rhodobacter capsulata*, consumes H_2 and CO_2. Both species can grow in photoheterotrophic conditions using several compounds as a carbon source (lactic, acetic, butyric and ethanol) and as a nitrogen source (ammonium, urea, betaine and glutamate). In a photoautotrophic culture carried out with both strains, *Rhodobacter capsulata* showed a higher growth rate in the absence of organic compounds in the culture media (Albiol, 1994).

However, the presence of organic compounds inhibits the autotrophic growth, for this reason, it was decided to split CII into two different subsystems: the photoheterotrophic subcompartment, where the VFAs are used as a carbon and electron sources and the photoautotrophic subcompartment, where the H_2 electrons are used for the assimilation of CO_2 gas (Figure 1.3).

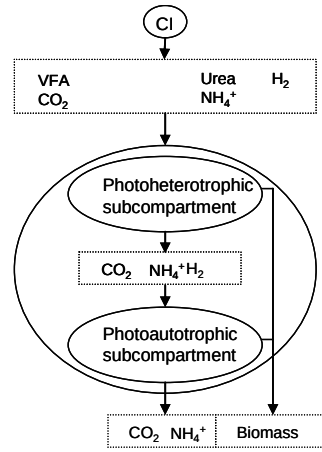

Figure 1.3 Schematic of CII subcompartments (Albiol, 1994).

Although, the former phototrophic bacteria are able to degrade sulphide, the extracellular accumulation of elemental sulphur (Hansen *et al.*, 1972; Kompatseva, 1981) requires the action of other phototrophic anoxygenic bacteria (*Thiocapsa roseopersicina*) which are able to reduce sulphidric acid to sulfate.

Phototrophic bacteria are considered as a source of Single Cell Protein (SCP) due to their high composition and quality. Particularly for *R. rubrum* biomass, the addition of freeze-dried preparation of *R. rubrum* to the food of experimental animals considerably reduces the blood cholesterol level of these animals (Emeis and Lasseur, 2006). Thus, biomass produced in CII can be included in the crew diet.

1.2.2.3 CIII: NITRIFYING COMPARTMENT

This compartment is devoted to the degradation of ammonium, present in the effluent from CII, into nitrate, which is used subsequently in the photosynthetic compartments (CIVa and CIVb). Although ammonium can also be used in the photosynthetic compartments as a nitrogen source, it is necessary to convert ammonium to nitrate, since ammonium is toxic to most cyanobacteria and plants at relatively low concentrations.

The oxidation of ammonium to nitrate is performed in two consecutive stages:

- Ammonium to nitrite oxidation (*Nitrosomonas europaea*):

$$NH_4^+ + 1.5\ O_2 \longrightarrow NO_2^- + 2\ H^+ + H_2O$$

- Nitrite to nitrate oxidation (*Nitrobacter winogradskyi*):

$$NO_2^- + 0.5\ O_2 \longrightarrow NO_3^-$$

Due to the low efficiency in energy use (20%), the ammonium consumption is high and the growth rate of both bacteria is low (Hunik *et al.,* 1994; Hanaki *et al.*, 1990).This slow growth rate together with a long lay phase and the non edibility of biomass, led to the selection of an immobilized system for the culture of this bacteria.

1.2.2.4 CIVa: PHOTOAUTOTROPHIC COMPARTMENT

The objective of this compartment is to produce edible biomass using as carbon source the CO_2 produced mainly by the crew and other compartments, and as nitrogen source the nitrates present in the CIII effluent.

The photoautotrophic microorganism should have high photosynthetic efficiency, low duplication time, high nutritional value, high digestibility, low contamination risk and non toxic effect. The cyanobacteria selected, *Arthrospira sp*., not only have the aforementioned characteristics, but is also of high nutritional quality. The quality and quantity of its protein, measured as utilizable protein, ranges between 30 and 42% of its dry weight which is similar to the protein values found in lactic products and meat (36%) and higher than that in vegetables (<24%). Moreover, due to the high content of vitamins A, B_{12} and Fe in *Arthrospira* biomass, only 4.3 g, 1.8 g and 12 $g \cdot d^{-1}$ de *Arthrospira* is required to satisfy the recommended daily human requirements of these compounds respectively. In addition to this, its content in essential amino acids, minerals and other vitamins contributes to *Arthrospira*'s nutritional value (Jassby, 1988).

1.2.2.5 CIVb: HIGHER PLANT COMPARTMENT (HPC)

The incorporation of a higher plant compartment inside the MELiSSA loop allows to produce a more rich and healthy diet for the crew. Its main function is similar to the one developed by the *Arthrospira* compartment (CIVa): atmospheric regeneration, water purification and the production of edible biomass to be used as food in the crew compartment.

Due to the fact that the work developed in this thesis is focused on the photoautotrophic compartments colonized by the cyanobacteria *Arthrospira* (CIVa) and higher plants (CIVb), their more extensive description is included later in this chapter.

1.2.2.6 CV: CREW COMPARTMENT

The main objective of the MELiSSA loop is to support life of the crew compartment. The other compartments have been conceived to achieve, under interconnected operation (i) the degradation of the crew's wastes (faeces, urine, CO_2 and minerals), (ii) the regeneration of O_2, (iii) and the production of food.

Initially during the first interconnection of the loop, animals will mimic the crew compartment consuming oxygen and producing CO_2, though their faeces will not be introduced into the MELiSSA loop. Instead, human faeces and urine will be collected and introduced into the first compartment. The crew compartment is still under preliminary development phase and the animals are still to be defined more specifically.

1.2.3 MELiSSA PILOT PLANT (MPP)

Over the last 15 years, the development of MELiSSA technologies has followed a progressive approach of integration and validation.

Each compartment is studied, designed and demonstrated at laboratory scale before being scaled-up for subsequent integration into the MELiSSA Pilot Plant (MPP). The facility, presently located at UAB, serves as a test bed to study the robustness and stability of the continuous operation of the MELiSSA loop (Gòdia *et al.*, 2002, 2004).

The research performed in the MPP has been focused up to the present on the development of compartments II, III and IVa. Some of the topics studied of each compartment comprise cell growth, gas-liquid mass transfer characterization, light distribution inside the photosynthetic cell cultures, compartment scale-up, development of control systems and interconnection of the MELiSSA loop at bench scale.

A brief description of the bioreactor configuration for each compartment present in the MPP is included below:

- Compartment II: Several photobioreactors are being used for bench scale testing of *R.rubrum* culture, including a 2.5 L mechanically stirred and a 7 L air-lift photobioreactors. The scale-up of CII has been recently performed and currently the pilot scale photobioreactor is under construction, with a total volume of 50 L (Cabello, 2007).
- Compartment III: The nitrifying compartment is a packed-bed reactor with immobilized cells of *Nitrosomonas* and *Nitrobacter*. Biostyr® is the polystyrene support in the form of 4 mm diameter beads used for immobilization of the cells by adhesion. The bench reactors are 600 mL total volume fixed bed columns and the pilot nitrifying compartment is a fixed bed of 8 dm^3 total volume (Pérez, 2001). Ammonium and nitrate in-line analyzers were incorporated for the monitoring of the nitrogen concentration in the liquid flows (Montràs, 2003).
- Compartment IVa: As for CII, several photobioreactors are being used for bench scale testing of *Arthrospira* culture, including mechanically stirred photobioreactors with volumes ranging from 1 L to 3 L and air-lift photobioreactor with culture volumes between 3 L and 7 L. The pilot scale bioreactor of this compartment is a 77 L external loop airlift photobioreactor.

1.3 THE PHOTOSYNTHETIC COMPARTMENTS OF MELiSSA

1.3.1 THE ROLE OF ALGAE AND HIGHER PLANTS IN BIOREGENERATIVE LIFE SUPPORT SYSTEMS

The use of microalgae and higher plants for life support systems was considered as early as 1950s. Algae were considered for biological life support because of their high photosynthetic efficiency, its low volume requirements to growth and its ability to regenerate atmosphere via the photosynthetic process, where CO_2 is consumed, while O_2 is evolved.

In addition to this, algal biomass (*Chlorella, Scenedesmus*) presented high nutritional qualities to be used as food, though its high nucleic acid content limited the percentage to be consumed humans. Hence, higher plants were incorporated to satisfy human nutritional needs more completely. Moreover, the incorporation of higher plants allowed for the regeneration of fresh water through the transpiration process and provided a more psychologically friendly environment for the crew.

Recently, Lehto *et al.* (2006) reviewed the growth requirements of microalgae and higher plants in life support systems, with particular attention to their suitability for use in harsh Martian conditions.

1.3.2 BIOREGENERATIVE PLANT FUNCTION: THE PHOTOSYNTHESIS

Photosynthetic organisms, such as cyanobacteria and higher plants capture light energy and form adenosine triphosphate (ATP) and nicotinamide adenine dinucleotide phosphate (reduced form, NADPH), which they use as energy sources to make organic compounds from CO_2 and H_2O; while simultaneously evolving O_2 into the atmosphere.

The photosynthetic process carried out by cyanobacteria and plants is remarkably similar, only differing in some details. This section aims to summarize some of the basic aspects of photosynthesis for both cyanobacteria and plants (Lehninger *et al*., 2004).

The balanced overall chemical reaction for photosynthesis can be described as a redox reaction in which water donates electrons for the reduction of CO_2 to carbohydrates (CH_2O):

$$CO_2 + H_2O \xrightarrow{\text{light}} O_2 + (CH_2O)$$

Photosynthesis in plants includes two processes, as depicted schematically in Figure 1.4:

- Light-dependent reactions: In these reactions, which take place only when plants are illuminated, photosynthetic pigments absorb light energy and convert it as NADPH and ATP, while O_2 from water is evolved. In photosynthetic eukaryotic cells, light reaction and ATP synthesis are carried out by the photosynthetic pigments and the enzyme complexes embedded in the thylakoid membranes of the chloroplasts.

- Carbon-assimilation reactions: In these reactions, the NADPH and ATP generated in the light-dependent reactions are used to reduce CO_2 to form carbohydrates and other organic compounds. In photosynthetic eukaryotic cells, these reactions takes places in the stroma of the chloroplasts, which is the aqueous phase enclosed by the inner membrane. Although sometimes are called dark reactions, they can occur in light or darkness.

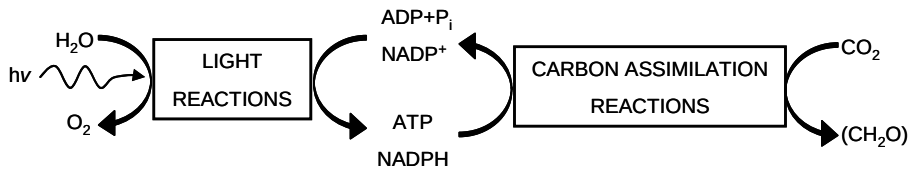

Figure 1.4 Photosynthetic reactions. The ATP and NADPH generated in the light reactions, using the light as energy source, are used for reducing the CO_2 in the carbon assimilation reactions to carbohydrates. (Figure adapted from Lehninger *et al*., 2004).

- **Light-dependent reactions**

In plants, the most important light-absorbing pigments in the thylakoid membranes are the chlorophylls, while in cyanobacteria phycobilins are employed. Phycobilins pigments are bound to specific proteins, forming phycobiliproteins, which can be classified in phycocyanin (PC), allophycocyanin (AP) and phycoerythrin (PE). Phycobiliproteins are associated in phycobilisomes, which are the main light harvesting structure of cyanobacteria.

The thylakoid membranes of chloroplasts have two photosystems, each with its distinct and complementary functions and its own type of photochemical reaction center and set of antenna molecules:

- Photosystem II (PSII): The excitation of its reaction center P680 passes electrons through the cytochrome b_6f complex with associated movement of protons across the thylakoid membrane. This photosystem contain similar amounts of chlorophylls *a* and *b*.
- Photosystem I (PSI): The excitation of its reaction center P700 drives electrons to the Fe-S protein ferredoxin, then to $NADP^+$, producing NADPH. PSI has higher amounts of chlorophyll *a* than chlorophyll *b*.

The combined activity of both photosystems allows to achieve the light-driven movement of electrons from H_2O to $NADP^+$. A schematic of the electron flow between PSII and PSI in the light reaction is depicted in Figure 1.5.

Each photosystem requires one photon, which is used to raise the energy of electrons, obtained from water, to the energy level required to reduce $NADP^+$ to NADPH. Then, the excited electrons flow down through the carrier chains. In order to replace the electrons that flows from PSII through PSI to $NADP^+$, cyanobacteria and plants oxidize H_2O, producing O_2. The proton gradient generated during the split reaction of water and the electron transfer through the cytochrome b_6f complex allows for the formation of ATP.

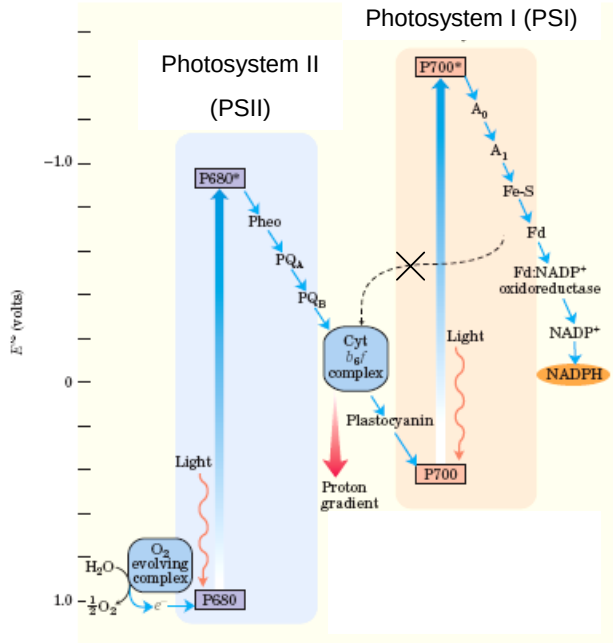

Figure 1.5 Schematic of light reactions of non cyclic photosynthesis (also known as Z scheme), which represents electron transfer from H_2O to $NADP^+$ achieved with the combined activity of photosystems I and II. The standard reduction potential of each electron is show in the vertical axis depicted in the left side of figure (Lehninger *et al*., 2004).

The overall equation of the electron flow from H_2O to $NADP^+$ is:

$$2\ H_2O + 2\ NADP^+ + 8\ photons \longrightarrow O_2 + 2\ NADPH + 2\ H^+$$

In order to form a molecule of O_2 four electrons are required from two H_2O to two $NADP^+$. Moreover, eight photons must be absorbed, since for every two absorbed photons (one by each photosystem), one electron is transferred.

- **Carbon-assimilation reactions**

As mentioned above, the ATP and NADPH generated light-dependent reactions of photosynthesis are used as energy and reducing power by the plants and photosynthetic microorganisms to synthesize carbohydrates from CO_2 and water.

Higher plants and other photoautotrophic organisms can use CO_2 as the sole carbon source required for the synthesis of cell organic components such as proteins, lipids or cellulose. The CO_2 assimilation is the process where CO_2 is converted to reduced organic compounds.

CO_2 is assimilated via the Calvin cycle, which is a cyclic pathway with its key intermediates being constantly regenerated, as depicted in Figure 1.6.

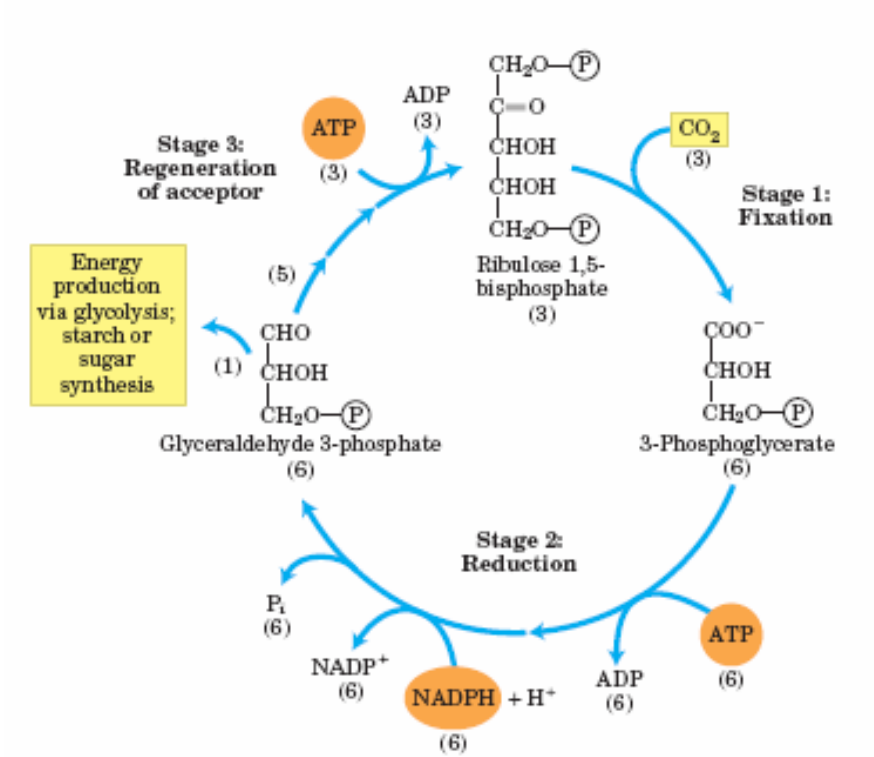

Figure 1.6 Schematic of the Calvin cycle, which represents the photosynthetic carbon reduction cycle. The CO_2 assimilation in photosynthetic organisms has 3 main stages (fixation, reduction and regeneration of acceptor). Number in parentheses represents the number of carbon atoms entering and leaving the cycle and of the three key intermediates (Lehninger *et al*., 2004).

The assimilation of CO_2 has three main stages:

- Assimilation of CO_2 into biomolecules. Condensation of CO_2 with ribulose 1,5-bisphosphate to form two molecules of 3-phosphoglycerate, which is the precursor of more complex biomolecules. Overall, the fixation of 3 molecules of CO_2 (3C) on 3 molecules of ribulose 1,5-bisphosphate (15C) form 6 molecules of glyceraldehydes 3-phosphate (18 C).

- Reduction of 3-phosphoglycerate to triose phosphate. These 6 molecules of 3-phosphoglycerate are reduced to 6 molecules of glyceraldehyde 3-phosphate (which is in equilibrium with dihydroxyacetone phosphate), using 6 ATP (in the synthesis of 1,3-bisphosphoglycerate) and 6 NADPH (in the reduction of 1,3-bisphosphoglycerate to glyceraldehyde 3-phosphate).

- Regeneration of 3 molecules of ribulose 1,5-bisphosphate (15 carbons), the carbon acceptor molecule, using 5 of the 6 molecules of triose phosphate (15 carbons). Triose phosphate is used to form several compounds such as hexoses, sucrose or starch.

Photorespiration

Photosynthetic cells with both photosystems PSI and PSII evolve oxygen and consume CO_2 during the light reactions, so the net gaseous change during photosynthesis is described as:

$$CO_2 + H_2O \longrightarrow O_2 + (CH_2O)$$

However, in the dark, plants also carry out mitochondrial respiration, the oxidation of substrates to CO_2 and the conversion of O_2 to H_2O. In addition to this, there is a side reaction of photosynthesis, called the photorespiration, where light drives the consumption of O_2 and the production of CO_2 due to the lack of specificity of the enzyme ribulose 1,5-bisphosphate carboxylase/oxygenase (Rubisco).

Rubisco is not specific for CO_2 as a substrate and can also catalyzes the condensation of O_2 with ribulose 1,5-bisphosphate to form 3-phosphoglycerate and 2-phosphoglycolate, a metabolically useless product. In this case, carbon is not fixed and in order to recover the carbons from 2-phosphoglycolate significant amounts of cellular energy is consumed and some previously fixed CO_2 is released, which appears to be a net loss to the cell.

Some plants have evolved a mechanism to decrease the photorespiration rates, using a temporary fixation of CO_2 into a four carbon compound. Such plants are referred to as C_4 plants and usually grow at high light intensity and high temperatures, such as in the tropics.

Plants using the carbon-assimilation method described above, in which the first step is reaction of CO_2 with ribulose 1,5-bisphosphate to form 3-phosphoglycerate, are known as C_3 plants.

1.4 CIVa: *ARTHROSPIRA* COMPARTMENT

Spirulina is the common name used for the filamentous cyanobacteria *Arthrospira sp.* of the *Oscillatoriales* order. This oxygenic photosynthetic prokaryote is characterized by the arrangement of the multicellular cylindrical trichomes in an open left-hand helix along the entire length (Vonshak, 1997), which can derive to abnormal morphologies such as irregularly curved and even linear shape under unsuitable culture conditions (Ciferri and Tiboni, 1985; Wang and Zhao, 2005). The cell dimension, length of the filaments and degree of coiling vary between the species and also within the species depending on the environmental growth conditions.

Unlike other cyanobacteria, *Arthrospira* cells cannot fix atmospheric nitrogen (N_2) because they lack of heterocysts. *Arthrospira* can adjust their buoyancy with special gas vesicles in order to receive optimal light incidence for photosynthesis. Moreover, they can excrete extracellular polysaccharides to form floating aggregates, a fact that facilitates their harvest in natural lakes and outdoor cultures.

The cell wall is composed of four thin layers, mainly formed of mucopolymers and polysaccharides without cellulose. The absence of cellulose cell walls involves that no chemical or physical processing steps are required for human consumption, since humans lack the cellulose enzyme and could not digest cellulose components.

Thylakoids present in the cytoplasm are the membrane structures where the photosynthetic pigments, (chlorophyll and phycobilisomes) for the light dependent reactions of photosynthesis, are embedded. Phycobilisomes are light-harvesting supramolecular aggregates, which collect light energy in a region of the visible spectrum where chlorophyll has low absorbance (Siegelman and Kycia, 1982). Around 80–85% of the phycobilisomes are composed of brilliantly colored polypeptides named phycobiliproteins, which are the major photosynthetic accessory pigments in cyanobacteria. According to their structure, phycobiliproteins can be classified in phycocyanin (PC), allophycocyanin (APC) and phycoerythrin (PE), which are the major phycobiliproteins found in *Arthrospira* (Siegelman and Kycia, 1982, Patel *et al.*, 2005).

Historically, *Arthrospira* has been consumed by humans for years (Cifferri, 1983). Since ancient times, the Aztecs living near Lake Texcoco in Mexico (Farrar, 1966) and people near Lake Chad in Africa (Dangeard, 1940) harvested *Arthrospira* from the lakes to use as food after drying (Abdulqader *et al.*, 2000). *Arthrospira* grows naturally in these lakes due to an optimal pH and a high content of carbonate (Vonshak, 1997; Belay *et al.*, 1993). In fact, *Arthrospira* is considered an extremophilic cyanobacterium since it can grow at highly levels of carbonates and bicarbonates and alkaline pH, which minimizes the contamination risk during its culture (Walach *et al.*, 1987).

1.4.1 METABOLIC NETWORK

Recently a metabolic network was built up from literature data for describing biomass synthesis, exopolysaccharides production and energy aspects of *Arthrospira* (Cogne *et al.*, 2003).

In this work, a simplified overview of the major metabolic routes of *Arthrospira* grown under photoautotrophic conditions was carried out. The major reactions considered for metabolic flux estimations included:

- The carbon uptake. The bicarbonate ion is the primary carbon source for *Arthrospira* and enters the cell by active transport. The intracellular bicarbonate is first incorporated into the Calvin cycle via Rubisco after being dehydrated and then is distributed for the synthesis of the macromolecular elements (proteins, carbohydrates, lipids and nucleic acids).
- The central metabolic pathways:
    - The Emben-Meyerhof-Parnas pathway.

- The tricarboxylic acid (TCA) cycle, this is not operating as a cycle, but rather as two branches yielding succinate and α-ketoglutarate.
- The oxidative and non oxidative branches of pentose phosphate (PP) pathway.
- The Calvin cycle for the CO_2 fixation which is closely related to the PP pathway.

- The anaplerotic reactions of phosphoenolpyruvate carboxylase to maintain the operability of TCA pathway and of malate.
- The energy metabolism reactions, based on the photosynthetic process that takes place in the thylakoids membranes, where the photosynthetic pigments are located.
- The anabolism network reactions.
- The synthesis of biomass macromolecules (protein, carbohydrates, lipids, RNA and DNA) biomass and exopolysaccharides.

1.4.2 BIOCHEMICAL COMPOSITION AND BENEFICIAL PROPERTIES

Nowadays, *Arthrospira* is one of the most utilized microalgae in the health food market due to its highly valuable nutritional and medicinal properties (Belay *et al.*, 1993). Hence, increasing attention is being given to *Arthrospira* properties and to its biochemical composition under different culture conditions. This section includes a bibliographic review of such studies, including not only the content of each macromolecular compound, but also some their valuable nutritional properties and the effects of some growth conditions on their content.

- **Protein**

Arthrospira is characterized by its uncommonly high protein content ranging from 60 to 70% of the biomass (Ciferri and Tiboni, 1985), which is higher than the averaged values of many food products, such as meat, fish, soy, evaporated milk, peanuts, eggs or grains. Several authors confirmed such high values of protein levels in *Arthrospira* biomass (Becker and Venkataraman, 1984; Vonshak, 1997; Cornet *et al.*, 1998; Morist *et al.*, 2001; Pelizer *et al.*, 2003; Babadzhanov *et al.*, 2004), though others reported lower values comprised between 30% and 50% (Cañizares-Villanueva *et al.*, 1995; Marty, 1997; Vernerey, 2000), which usually are obtained under non optimal growth conditions, such as limitation in light, nitrogen or carbon source.

The nutritional value of proteins is determined by its amino acid profile and particularly by the content of essential amino acids. *Arthrospira* protein contains all essential amino acids (Babadzhanov *et al.*, 2004) and its amino acid content is in agreement with the one recommended by Food Agriculture Organization (FAO) and World Health Organization (WHO), except for lysine and sulphur-containing amino acids such as methionine and cystine, which are present in lower levels (Becker and Venkataraman, 1984; Ciferri and Tiboni, 1985). A list of the amino acid profile of *Arthrospira* can be found in bibliographic studies under several conditions (Becker and Venkataraman ,1984; Ahlgren *et al.* 1992; Cañizares-Villanueva *et al.*, 1995; Morist

et al., 2001; Babadzhanov *et al.*, 2004). The most important in relative abundance is aspartic acid (Asp), glutamic acid (Glu), arginine (Arg), alanine (Ala), leucine (Leu) and valine (Val) (Morist *et al.*, 2001).

Besides the amino acid profile, the nutritional quality of *Arthrospira* protein can be determined using other parameters such Protein Efficiency Ratio (PER), which is based on the weight increase of the tested individual divided by the intake of the protein food, and the Net Protein Utilization (NPU), which is the proportion (0-100%) of dietary nitrogen retained by the body for protein synthesis. *Arthrospira* PER values range between 0.6 and 2.6 (Becker and Venkataraman, 1984; Anupama and Ravindra, 2000) and NPU levels are between 43-63% (Bourges *et al*., 1971).

Regarding the influence of culture conditions on protein content, several authors reported that at higher light intensities protein content decreases (Tadros *et al.*, 1993; Tomaselli *et al.*, 1997; Vernerey, 2000; Olguín *et al.*, 2001). Moreover, the protein levels found in biomass grown using ammonium as a nitrogen source instead of nitrate were lower (Olguín *et al.*, 2001).

- **Carbohydrates**

Carbohydrates represent between 5-16% of *Arthrospira* biomass (Becker and Venkataraman, 1984; Ciferri and Tiboni, 1985; Marty, 1997; Vonshak, 1997; Cornet *et al.*, 1998; Morist *et al.*, 2001; Pelizer *et al.*, 2003). Glucose, rhamnose, mannose, xylose and galactose are the principal *Arthrospira* sugars and glycogen is its carbon reserve (Shekharam *et al.*, 1987). Olguín *et al.* (2001) found that nitrogen deficiency stimulated the synthesis of carbohydrates.

- **Lipids**

Arthrospira contains between 4-14% lipids (Ciferri and Tiboni, 1985; Vonshak, 1997, Cornet, *et al.* 1998), of which more than 75% correspond to fatty acids (FA) (Babadzhanov *et al.*, 2004). The total fatty acids can be further classified into saturated (SFA), monounsaturated (MUFA) and polyunsaturated (PUFA).

The predominant fatty acid found in *Arthrospira* are palmitic acid (C16:0), γ-linoleic acid (C18:3) (GLA), linoleic acid (C18:2), oleic acid (C18:1), palmitoleic acid (C16:1) (Oliveira *et al.,* 1999; Morist *et al.,* 2001; Babadzhanov *et al.,* 2004; Mühling *et al.,* 2005b).

The high content of GLA, an essential FA representing between 7 and 30% of total FA (Oliveira *et al.*, 1999; Morist *et al.,* 2001; Olguín *et al.*, 2001), is of great value since it has been found to have therapeutic effects on humans such as the reduction of serum triglycerides and low density lipoproteins levels and the stimulation of the immune system (Ciferri and Tiboni, 1985; Ahlgren *et al.*, 1992; Mühling *et al.*, 2005b). Moreover, the higher the PUFA content, the higher the nutritional value of foods. Usually the PUFA/SFA ratio found in *Arthrospira* is higher than the recommended ratio for the human diet.

Composition of FA can vary considerably between *Arthrospira* grown in different environments (Piorreck 1984). In fact, *Arthrospira* fatty acid composition can be found under different culture conditions in bibliography (Ahlgren *et al.*, 1992; Cañizares-Villanueva, *et al.*, 1995; Morist *et al.,* 2001; Xue *et al.*, 2002; Babadzhanov *et al.*, 2004; Maslova *et al.*, 2004; Palmegiano *et al.*, 2005). Particularly, Mühling *et al.* (2005b) studied the variation in fatty acid profile composition of *Arthrospira* strains.

- **Nucleic acids**

The nucleic acid content in *Arthrospira* is reported to be between 4% and 6%, distributed into 78% RNA and 22% DNA (Becker and Venkataraman, 1984; Ciferri and Tiboni, 1985; Vonshak, 1997).

It is noteworthy to mention that the nucleic content of single cell protein (SCP) is a major limiting factor of *Arthrospira* to be used as human food. The intake of a nucleic acids leads to the production of uric acid, which accumulate in the body due to a lack of the uricase enzyme in humans. Human consumption of higher than 2 g nucleic acids equivalent per day may lead to kidney stone formation and gout, so SCP consumption should be reduced to acceptable limits. The safety evaluation of SCP products for human and animal food has been extensively discussed, sometimes involving the use of specific methods to reduce its nucleic content (Anupama and Ravindra, 2000).

- **Pigments**

As mentioned above, the light-harvesting pigments of *Arthrospira* include chlorophyll *a* (Chl *a*) and phycobiliproteins, which can be classified into phycoerythrins (PE), phycocyanin (PC) and allophycocyanin (APC) (Siegelman and Kycia, 1982).

Chlorophyll contents in *Arthrospira* are found around 1% (Vonshak, 1997; Danesi *et al*., 2004; Rangel-Yagui *et al*., 2004; Bhattacharya and Shivaprakash, 2005). Hence, Arthrospira is an attractive alternative source of chlorophyll, which is used as a natural colour in food, cosmetic, and pharmaceutical products (Ciferri and Tiboni, 1985; Pulz and Gross, 2004).

Phycocyanin is the major component of phycobiliproteins. Although most of the PC levels reported in literature ranged from 7 to 17% (Pervushkin *et al.*, 2001; Bhattacharya and Shivaprakash, 2005; Patel *et al.*, 2005), Morist *et al.* (2001) obtained lower content of PC (0.4-4%). PC has been identified as the component mainly responsible for the antioxidant activity of *Arthrospira* (Estrada *et al.*, 2001). Thus, PC is not only used for food and cosmetic applications, but also as potential therapeutic agent due to its antioxidant, anti-inflammatory, immunomodulating, and hepatoprotective properties (Pervushkin *et al.*, 2001).

The content of the other two major phycobiliproteins is lower than PC, being around 3.8% for APC and between 0.4-1.2% for PE (Patel *et al.*, 2005; Bhattacharya and Shivaprakash, 2005).

Because of the valuable applications of pigments, several authors studied the effects of culture conditions, such as light intensity or nitrogen source, on pigment content in order to optimize their production (Rangel-Yagui *et al.*, 2004; Carvalho *et al.*, 2004). Specifically, under nitrogen source limitation, pigment content decreases, showing a yellowish colour instead of the deep green blue characteristic of *Arthrospira* (Carvalho *et al.*, 2004). In fact, Miller *et al.* (2002) reported that such nitrogen chlorosis is due to the rapid loss of light-harvesting phycobiliproteins by phycobilisome degradation and repression of phycobiliprotein synthesis at the transcriptional level. Besides, *Arthrospira* regulates its pigmentation in response to light intensity, leading to a decrease in chlorophyll levels under increased irradiances (Tomaselli *et al.*, 1997; Danesi *et al.*, 2004).

- **Vitamins**

Arthrospira contains a high percentage of vitamins, especially of provitamin A (as β-carotene) and B_{12}. The *Arthrospira* vitamin profile also contains vitamin B_1 (Thiamin), B_2 (Riboflavin), B_3 (Niacin), B5 (Phantothenic acid), B_6 (Pyridoxine), B_7 (Biotin), B_9 (Folic acid), E (Tocopherol and Tocotrienol) and K (Naphthoquinone) (Ciferri and Tiboni, 1985; Belay *et al.*, 1993; Annapurna *et al.*, 1991; Vonshak, 1997).

1.4.3 *ARTHROSPIRA* CULTURE

1.4.3.1 *ARTHROSPIRA* GROWTH CONDITIONS

Several factors can influence the growth and composition of Arthrospira, such as carbon source, pH, temperature, nitrogen source and light intensity (Vonshak et al., 1982). The following section aims to review the main characteristics and optimal values of these culture conditions for *Arthrospira* growth.

- **Carbon source**

Traditionally, *Arthrospira* has been considered as a photoautotrophic cyanobacterium, since its primary carbon source is the inorganic carbon present as CO_2 in the atmosphere or as carbonate or bicarbonate ions in the culture media. In this case, carbon is photosynthetically fixed by Rubisco, as in the metabolism of the C_3 higher plants, entering into the incomplete cyanobacterial tricarboxylic acid cycle, as explained in section 1.3.2.

Although most of the photoautotrophic cultures of *Arthrospira* are performed using carbon source mixtures of bicarbonate/carbonate, the photosynthetic and carbon utilization efficiencies has also been determined using carbon dioxide as sole carbon source (Binaghi *et al.*, 2003). Gordillo *et al.* (1998) studied the effects of CO_2 enrichment (1%) on biomass yield, cell composition and photosynthesis in batch cultures of *Arthrospira* under both nitrogen sufficiency and limitation. Under N sufficiency, increased CO_2 levels did not cause any change in maximum growth rate while it decreased maximum biomass yield. In such conditions, its protein and

chlorophyll content decreased and the synthesis of carbohydrates was stimulated, hence no effect on C:N atomic ratio was detected.

Recently, the ability of *Arthrospira* strains to grow using organic sources such as acetate, glucose and fructose has been demonstrated, though none grew with fructose or sucrose (Mühling *et al.*, 2005a; Chen *et al.*, 2006). However, heterotrophic growth is not suitable for the production of valuable photosynthetic *Arthrospira* pigments such as PC and APC (Chen and Zhang, 1997). Therefore, the mixotrophic growth of *Arthrospira*, which combines both (i) the autotrophic photosynthesis, mainly influenced by light intensity, and (ii) heterotrophic assimilation of organic compounds, affected by the availability of organic carbon, has been also studied (Marquez *et al.*, 1993; Chen *et al.*, 2006).

This culture strategy is currently an interesting alternative to conventional photoautotrophic mass culture systems for production of high value chemicals (Zhang *et al.*, 1999; Vonshak *et al.*, 2000), since some studies demonstrated the improvement in yield and composition of *Arthrospira* (Marquez *et al.*, 1995; Chen and Zhang, 1997; Chojnacka and Noworyta, 2004; Cerón *et al.*, 2005).

- **Nitrogen source**

Arthrospira is able to assimilate several nitrogen sources such as nitrate, ammonium, urea and some aminoacids (glutamine and adenine) as numerous studies prove (Azov and Goldman, 1982; Ciferri, 1983; Richmond, 1986; Boussiba and Gibson, 1991; Becker, 1994; Liotenberg *et al.*, 1996; Filali *et al.*, 1997; Stanca and Popovici, 1996; Miller *et al.*, 2002; Costa *et al.*, 2004; Carvalho *et al.*, 2004; Danesi *et al.*, 2004; Rangel-Yagui *et al.*, 2004; Soletto *et al.*, 2005; Converti *et al.*, 2006).

Nitrate is the nitrogen form used in the conventional culture media described for *Arthrospira* (Zarrouk, 1966; Paoletti *et al.*, 1975; Schlösser, 1982). Currently, the use of ammonium and urea in *Arthrospira* cultures has been studied not only because their cheaper cost would decrease production costs, but also to evaluate the possibility of using *Arthrospira* cultures as an alternative for nitrogen removal in wastewater treatment (Lodi *et al.* 2003; Sassano *et al.* 2004; Carvalho *et al.*, 2004; Converti *et al.*, 2006).

Nonetheless, a main limitation of using urea and ammonium as nitrogen sources is that their inhibitory and toxic concentrations thresholds values for *Arthrospira* growth, which are between 1.7 mM and 10 mM (Abeliovich and Azov, 1976; Belkin and Boussiba, 1991; Converti *et al.*, 2006), are much lower than inhibitory nitrate concentrations (around 1.2 M) (Ciferri, 1983). Therefore, nitrate is considered the most suitable nitrogen source for *Arthrospira* growth.

In addition, when several nitrogen sources are supplied, *Arthrospira* consumes first the ammonium, since the associated energetic cost for its assimilation is lower (Boussiba and Gibson, 1991; Guerrero and Lara, 1987; Converti *et al.*, 2006).

Muro-Pastor and Florencio (2003) in a review of the ammonium assimilation in cyanobacteria reported than ammonium enters into the cell, either by diffusion of its gaseous form ammonia (NH_3) or by the action of specific permeases, and is directly incorporated into the GS-GOGAT pathway (GS:glutamine synthetase; GOGAT:glutamate synthase) (Figure 1.7). However, the assimilation of the other nitrogen forms (nitrate, urea and amino acids) requires first their reduction to ammonium, which implies an energy expense for the cell compared with the directly assimilation of the ammonium. Particularly, nitrate is sequentially reduced to nitrite by nitrate reductase (NiR) and later to ammonium by nitrite reductase (NaR), urea is metabolized by urease enzymes and amino acids usually require specific transport systems and further metabolization to produce ammonium (Flores *et al.*, 1994; Herrero *et al.*, 2001).

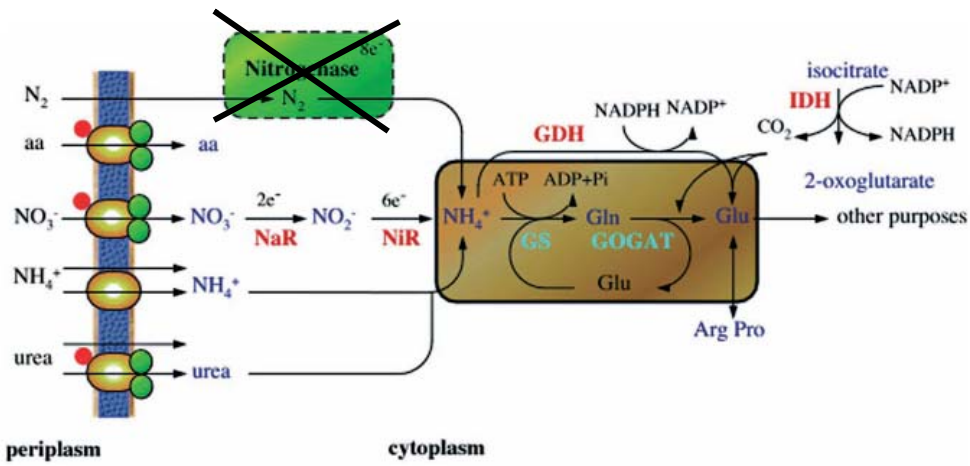

Figure 1.7 Nitrogen metabolism pathways in cyanobacteria. *Arthrospira* has the present nitrogen metabolism except for the assimilation of N_2, since *Arthrospira* cannot uptake atmospheric nitrogen A continuous line encloses the GS-GOGAT cycle. NaR: nitrate reductase; NiR: nitrite reductase; GS: glutamine synthetase; GOGAT: glutamate synthase; IDH: isocitrate dehydrogenase; GDH: glutamate dehydrogenase; aa: amino acids; e^-: electrons (adapted from Muro-Pastor and Florencio ,2003).

Regarding the influence of nitrogen source on biomass composition, one of the main effects is the decrease of protein and chlorophyll content under nitrogen limitation (Piorreck *et al.*, 1984; Gordillo *et al.*, 1998; Rangel-Yagui *et al.* 2004).

- **pH**

Arthrospira growth in high alkaline environments, with pH values ranging from 8.3 to 11 and an optimal value around pH 9.6.

In outdoor cultures, the high pH required for *Arthrospira* growth is an advantage since it increase the gradient of CO_2 from the atmosphere, which represents an increase in the available carbon source, and prevent the contamination from other species (Richmond and Grobbelaar, 1986).

- **Temperature**

The optimal growth temperature for *Arthrospira* culture is between 35ºC and 37ºC (Vonshak and Richmond, 1988), although the minimum and the maximum temperature for its growth are 18ºC and 40ºC.

Oliveira *et al.* (1999) studied the effects of temperature on *Arthrospira* composition and observed that an increase of temperature caused a marked decrease in protein content, while carbohydrate synthesis was stimulated.

- **Light intensity**

In the photoautotrophic growth of *Arthrospira*, light availability is the main factor influencing the photosynthetic rate, the biomass productivity and composition when no other factors such as carbon or nitrogen source are limiting. Hence, several authors studied the effect of different illumination levels on *Arthrospira* growth (Kebede, 1996; Hirata *et al.*, 1998; Masojidek *et al.*, 2003; Rangel-Yagui *et al.*, 2004).

As in most of the photosynthetic organisms, the following regions can be identified in the *Arthrospira* growth curve at increasing irradiances:

- Light limited region: At low light intensities, irradiance limit growth rate. In this region an increase in light intensity produces a linearly increase in photosynthesis.
- Saturated region: At increased irradiances, growth rate become independent of light, (Molina *et al.*, 1996; Hirata *et al.*, 1997; Chojnacka and Noworyta, 2004; Andrade and Costa, 2007).
- Photoinhibited region: At higher light intensities than the ones corresponding to saturation of the photosynthetic rate, the cell growth is inhibited. Under photoinhibited conditions, the growth rate decrease and cell look chlorotic with filaments forming clusters (Kebede 1996, Hirata *et al.*, 1997; Chojnacka and Noworyta, 2004). This phenomenon can be also observed at light intensities below the saturation of the photosynthetic rate in cultivations under stress conditions (Samuelson *et al.*, 1985).
- Photoxidation region: In this region the cell inhibition due to the high light intensities produces severe cell damage and, in extreme cases, cell death (Jensen and Knutsen, 1993; Vonshak *et al.*, 1994).

One of the major concerns in photosynthetic cultures is to determine the averaged irradiance received per cell. At a constant radiation level, the averaged irradiance level depends on the biomass concentration in the culture, and on the cell position within the culture system. Cells nearer the light surface receive higher irradiance while at the same time shading cells located further from the light source. Hence, several authors devoted efforts to modelling the light distribution within the culture of *Arthrospira* for different photobioreactors geometries and at different levels of complexity (Cornet, 1992a, b, 1998; Molina *et al.*, 1996; Hirata *et al.*, 1997; Molina *et al.* 1999; Masojidek *et al.*, 2003; Chojnacka and Noworyta, 2004).

Regarding the effect of light intensity on biomass composition, under poor illumination conditions, biomass increases its chlorophyll and phycobiliprotein content in order to optimize light capture (Tomaselli *et al.*, 1997; Vernerey, 2000; Rangel-Yagui *et al.*, 2004). Similarly, protein content was lower at high irradiances (Olguín *et al.*, 2001). During a shift in light intensity from low to high levels, carbohydrate biosynthesis increased (Tomaselli *et al.*, 1997; Olguín *et al.*, 2001). Moreover, Olguín *et al.* (2001) reported that a higher light intensity produced a lower total lipid concentration.

1.4.3.2 *ARTHROSPIRA* PRODUCTION AND CULTURE SYSTEMS

The commercial production of *Arthrospira* is carried out almost exclusively in outdoor open systems. The operating factories located worldwide (Japan, USA, Taiwan, Israel, Thailand) have an overall yearly production rate of 2000-3000 tones of *Arthrospira* (Anupama and Ravindra, 2000). Recently, Jiménez *et al.* (2003) reported the viability of the industrial production of *Arthrospira* in Southern Spain and Shimamatsu (2004) described the mass culture of *Arthrospira*, deriving information from two commercial facilities: Siam Algae Company (Thailand) and Earthrise Farms (USA). Such a worldwide production is used by the food industry for producing a variety of health products such as powder, tablets, capsules, or for extracting bioactive ingredients such as phycocyanin. Moreover, in order to enhance the nutritive value of some foods, algal biomass is added to some common products such as breads, biscuits, pasta, yogurt, tea or beer (Shizhong *et al.*, 2004). In addition to the food market, *Arthrospira* is currently being used in other industries such as the cosmetic, pharmaceutical and environmental (Pulz and Gross, 2004).

An alternative to the open *Arthrospira* ponds are the closed photobioreactors, which in most of the cases are used for research purposes. Some of the advantages of the closed systems are that: (i) the environmental conditions, such as temperature, light, carbon and nitrogen source, can be controlled and set to optimal levels; (ii) contamination can be completely prevented (iii); light availability can be increased using different photobioreactors configurations and (iv) higher cell densities can be attained (Vonshak, 1997; Converti *et al.*, 2006). Different configurations of photobioreactors, which usually can be identified as flat or tubular, are used for *Arthrospira* culture (Torzillo *et al.*; 1986; Watanabe and Hall, 1996; Molina *et al.*, 1999; Vernerey, 2001;Travieso *et al.*, 2001; Sanchez-Mirón *et al.*, 2002; Converti *et al.*, 2006).

1.5 CIVb: HIGHER PLANT COMPARTMENT (HPC)

1.5.1 PLANT CULTURAL REQUIREMENTS FOR LIFE SUPPORT

In the field frame of life support systems, where the external environmental conditions are expected to be extreme, plants are grown in closed environments (also known as plant chambers) that allow the control of the atmospheric conditions while supplying all the requirements for proper crop development.

This section briefly reviews some of the basic plant culture requirements such as light, carbon dioxide, temperature, humidity, air circulation and mineral nutrients.

- **Light**

Radiation is the sole source of energy for plant growth and development, hence light intensity is considered to be one of the most important environmental factors for growing plants in closed environments.

Light spectrum

Photosynthetically active radiation (PAR) is a term used to describe radiation in wavelengths of the electromagnetic light spectrum useful for photosynthesis of plants. Generally, PAR is accepted to be between 380 and 780 nm and most of the photosynthetic reactions are controlled by wavelengths either in the blue region (400 to 500 nm) or in the red region (600 to 700nm) (Langhans *et al.*, 1997). The photosynthetic photon flux (PPF) corresponds to the number of photons emitted inside the PAR region and is usually expressed as $\mu mols \cdot m^{-2} \cdot s^{-1}$. The conversion factor between the light flux emitted by a lamp and the PPF received by the plant depends on the spectrum of emission and therefore type of light source.

Photoperiod

Plants present a photomorphogenic response to photoperiod, which is the relative length of alterning periods of light and darkness. According to their sensitivity to photoperiod, plants can be identified either as short-day (when the crop is intolerant or show injury to very long photoperiods, such as potatoes), neutral-day and long-day (when the crop is able to grow under continuous light, such as wheat). Thus, the sensitivity to photoperiod would limit the cultivation of several crops inside the same growth chamber (Wheeler, 2001).

- **CO_2 concentration**

One of the limiting factors in photosynthesis in plants grown in field is the low atmospheric CO_2 concentration of 350 $\mu L\ CO_2 \cdot L^{-1}$ Air (350 ppm). Bearing in mind that a higher CO_2 concentration would enhance CO_2 diffusion, the photosynthetic rate can be increased under higher CO_2 concentration. In fact, several studies carried out in plant closed chambers have demonstrated that CO_2 concentrations up to 1200 ppm increase plant yield, though the effects of higher concentrations are not still clear (Wheeler, 2001).

- **Temperature**

Optimal temperature for plant cultures ranges between 15 and 28 ºC. When temperature falls out of this optimal range, plant growth rate is diminishes due to a decrease in the enzymatic rate of biochemical reactions.

In plant cultures inside closed environmental chambers, night temperature is usually set at lower levels in order to slow down the respiration rate and to decrease the carbon losses (Ambrosio *et al.*, 2006).

- **Humidity**

Atmospheric humidity should be maintained between 60 or 80%. Below these levels, plants can decrease their growth rate because of water stress. High humidity levels can condensate water on leaf, especially during cold night temperatures, thereby decreasing transpiration efficiency and increasing the risk for pathogen infection such as powdery mildew.

- **Air circulation**

Air circulation is required inside the plant chamber to supply CO_2 to the crop, to maintain temperature gradient and to remove heat generated by the lamps. Barta *et al.* (1996) recommended an air velocity between 0.1 and 1 $m \cdot s^{-1}$ as an optimal range.

- **Nutrients**

Mineral nutrients have specific and essential functions in plant metabolism. When all the essential nutrients and energy are supplied, plants can synthesize all the compounds they need for their growth and development. Usually, essential nutrients are classified as macronutrients or micronutrients according to their relative requirements (Marschner, 1995). Another classification according to the nutrients' biochemical role and physiological function identifies four main groups:

- Nutrients that form the organic compounds of plants (N, S).
- Nutrients that are important in energy storage or structural integrity (P, B, Si).
- Nutrients that remain in ionic form and are required by the activity of many enzymes (K, Na, Mg, Ca, Mn, Cl).
- Nutrients that are involved in electron transfers (Fe, Cu, Zn, Mo, Ni).

This classification scheme does not consider hydrogen, carbon and oxygen as mineral elements, because they are obtained from water or carbon dioxide (Taiz and Zeiger, 1998). Although over the years, different nutrient solutions have been used to sustain rapid plant growth, currently the modified Hoagland solution (Hoagland and Arnon, 1950) is the most widely used, since it contains all the essential mineral elements at the highest possible levels without producing toxicity effects or salinity stress.

1.5.2 CROP SELECTION FOR AN OPTIMIZED MENU WITHIN MELiSSA APPROACH

Initially, the selection of the crops to be included in the HPC of the MELiSSA loop was carried out taking into account some of the basic criteria recommended for plant selection in life support systems. Lane *et al.* (1999) identified the following as the most critical ones:

- Nutritional value: Any candidate crop for life support system must have a high nutritional value, particularly with regard to protein, lipid and carbohydrate content. Vitamin and mineral content would be also considered, though to a less extent since they can be added as a dietary supplement. The rich fatty acid profile should provide dietary diversity.
- Plant yield: Because space habitats must make efficient use of area and volume restrictions, crops with higher productivity rates and species with short stature (dwarf cultivars) are often rated favorably.
- Harvest index: A crop with a high harvest index (ratio of edible to total biomass) increases not only the edible production for human consumption, but also reduces the amount of inedible material to be degraded as waste material.
- Processing requirements: A crop with low processing requirements after harvest is advantageous, since the support equipment, energy and crew time is reduced leading to a more efficient and economical life support system.
- Palatability and dietary acceptability: Flavourful and familiar crops could have a positive psychological effect on the crew.

Previous authors have defined an optimized menu for crew using a linear programming routine that assumed a high degree of food closure. Particularly, the menu selected the lowest cost diet from a number of surveyed foods considering the crew's nutritional requirements, food acceptability and variety (Olabi *et al.*, 1999). The menu was designed for 6 crew members under the assumption of 10-day staggered planting. The optimized menu required 66.7 kg of dry edible crop biomass to feed a six member crew for a 10 day menu cycle. Plant biomass was supplied from a total of 27 crops (broccoli, beet, bean, cauliflower, carrot, cucumber, 15 different herbs, kale, lettuce, onion, green onion, peppers, peanut, potato, rice, sweet potato, swiss chard, soybean, spinach, tomato, wheat, alfalfa, cabbage, chili peppers, mushrooms, snow peas and squash) (Waters *et al.*, 2002).

Although such a large number of crops will ultimately provide dietary diversity for the crew compartment, three species were selected in order to develop HPC within the MPP, as a first step to demonstrate the viability of the MELiSSA concept. The selected species - wheat (*Triticum aestivum* L.), lettuce (*Lactuca sativa* L. cv. Grand Rapids) and beet (*Beta vulgari*s cv. Detroit Medium Red) - are representatives of plants with a predominant nutritional value in seeds, leaves and hypocotyls respectively.

The nutritional composition of the selected crops may be affected by the optimized environmental conditions of the closed plant chambers for life support systems. Plants grown in the field often are exposed to stresses that can limit plant growth and that can consequently affect tissue composition. Typical plant stresses, such as fluctuations in temperature, humidity, water or nutrient availability, are eliminated in plant growth chambers, since they operate near or at optimal plant growth conditions. Therefore, a difference in nutrient composition between crops grown in field and in environmentally controlled plants chambers is expected.

This section aims to review tissue composition data for each of the selected crops (beet, lettuce and wheat) grown in closed environments, when available, in order to provide more reliable data for estimating the nutritional quality of the diet designed for the crew.

The elemental and macromolecular composition of plant tissues is usually expressed as content per unit dry weight (% dw) of one plant part. Depending on the mineral nutrient, crop and age, the most suitable part to be analyzed for representing the mineral status of the plant differs. Thus, the elemental (Na, K, P, Mg, Ca, Cl, N and C) and macromolecular (protein, fat, ash, carbohydrates, fiber, energy or caloric content and moisture) composition has been reviewed per plant part.

1.5.3 BEET

- **Elemental Composition**

The composition of red beet (*Beta vulgaris*) in terms of Na, K, P, Mg, Ca, N and C content is presented below. Data are grouped separately for roots (Table 1.3) hypocotyl and leaves (Table 1.4). Culture conditions, under which these data were obtained, have been included when available; unfortunately in some cases growth conditions weren't specified in detail within the literature source.

Table 1.3 Beet Roots Elemental and Mineral Composition. Acronyms for cultivars correspond to: Zwaanpoly (Z), Kawemegapoly (K), Top (T), Desprez poly (D), Nejma (N).
(1) Culture conditions: sunlight, 12/12 h day/night photoperiod, 15 ºC and 350 ppm CO_2. Nitrogen content of the roots was 0.04%.

Growth Conditions	Irrigation solution	[NaCl]	Cultivar	Crop Age	Beet Roots			Reference
					Na	K	Cl	
		mM		d	%	%	%	
soil+ NK fertilizer	Rain water	-	-	150	0.04	0.84	-	Mahn *et al.* 2002 (1)
Sand + NPK fertilizer	½ strength Hoagland	0	Z	60	0.2	2.1	2	Ghoulam *et al.* 2002
			K		0.3	2.9	3	
			T		0.3	2.7	2	
			D		0.2	2.9	2	
			N		0.4	2.9	2	
		50	Z	60	0.9	2.1	4	
			K		0.9	2.3	4	
			T		0.8	2.3	4.5	
			D		1	2.5	5	
			N		0.8	2.1	5	
		100	Z	60	1.2	2.3	7	
			K		1	1.9	7	
			T		1.6	2.4	6	
			D		2.3	3.4	9.5	
			N		1.1	2.1	6	
		200	Z	60	1.6	2	7	
			K		1.6	1.8	7	
			T		2	1.9	11	
			D		2.2	2.7	10	
			N		2.2	2.7	9	

Table 1.4 Beet hypocotyl and leaves elemental and mineral composition. Acronyms for cultivars correspond to: Zwaanpoly (Z), Kawemegapoly (K), Top (T), Desprez poly (D), Nejma (N).

(1) Culture conditions: sunlight, 12/12 h day/night photoperiod, 15 ºC, 350 ppm CO_2, plant density of $4 \cdot 10^5$ - $12 \cdot 10^5$ plants·ha^{-1} under different K and N application (0-160 kg K·ha^{-1} and 120-240 kg N·ha^{-1}).

(2) Other mineral content is also available: P 0.32%, Mg 0.19%, Ca 0.13% Zn 0.03%, Mn 0.003%, Fe 0.01%; Cu 0.001%.

Growth Conditions	Irrigation solution	[NaCl] mM	Cultivar	Crop Age (d)	Beet Leaves Elemental Compo (%).					Reference
					Na	K	Cl	NO_3^-	N	
Hypocotyl										
Soil + NK fertilizer	Rain water	-	-	150	0.07	0.93	-	-	0.07	Mahn *et al.* 2002 (1)
Soil	-	-	-	-	0.63	2.62	-	-	-	USDA 2005 (2)
Leaves										
Soil + NK fertilizer	Rain water	-	-	150	0.18	1.34	-	0.03	0.16	Mahn *et al.* 2002 (1)
				150	0.08	0.97	-	0.05	0.10	
Sand + NPK fertilizer	½ strength Hoagland	0	Z	60	0.8	4.5	5.5	4.2	-	Ghoulam *et al.* 2002
			K		1	5.5	6	4.5	-	
			T		0.8	4.7	6	2.2	-	
			D		0.8	5	6	3.6	-	
			N		1	5.2	5	2.4	-	
		50	Z	60	2.6	4	8	4.5	-	
			K		2.7	3.8	8	4.8	-	
			T		2.7	3.3	8.5	2.9	-	
			D		2.9	4.5	9	4.1	-	
			N		3	4.1	8.5	4.9	-	
		100	Z	60	2.7	2.8	13	3.4	-	
			K		3	3.7	14	4.7	-	
			T		3	3	10	3.7	-	
			D		3	3.1	8	2.4	-	
			N		3.1	4	10	5	-	
		200	Z	60	3.3	3.1	14	5	-	
			K		4.2	4.1	16	5.1	-	
			T		3.5	2.8	12	4.3	-	
			D		4	3.7	12	3.1	-	
			N		4.1	3.8	14	2.6	-	

The effect of salinity on mineral composition in plants of 5 varieties of beet has been investigated by Ghoulam *et al.* (2002). They concluded that high NaCl concentrations caused a decrease in K content, but Na and Cl contents were highly increased in the leaves. Subbabarao *et al.* (2001) already mentioned the enormous capability by red beet to take up Na^+ and utilize it in non-specific functions instead of K^+. Nearly 95% of the K in red-beet can be replaced by Na, with Na levels reaching close to 2000 μmol·g^{-1} dw (Subbarao *et al.*, 1999).

In addition to this, the effect of salt concentration on NO_3^- content was not significant. Under salt stress, the tested varieties accumulated more inorganic ions in the leaves than in the roots (Ghoulam *et al.*, 2002). Therefore, salinity stress plays an important role in mineral composition of beets.

Comparing mineral content between morphological parts, a non uniform distribution of elements within beet is detected. Data reported by Mahn *et al.* (2002) show a considerable increase of K, Na and N content from the root to the upper stem. In contrast to this, nitrate content does not change markedly. Accordingly, Ghoulam *et al.* (2002) report that beets without salinity stress have a higher K, Na and Cl content in leaves than in roots.

- **Macromolecular Composition**

The nutrient composition of foods found in USDA nutrient database (2005) includes extensive and detailed information about mineral and proximate content in plants. The macromolecular composition of red beet as percentage of biomass dry weight provided by USDA is: 12.96% protein, 1.37% fat, 8.7% ash and 76.97% carbohydrates (calculated by difference). The total dietary fiber content is 22.54 %dw and the caloric content is of 3.5 $kcal \cdot g^{-1}$.

Moreover, its profile of fatty acids, vitamins and amino acids is shown in Table 1.5. Unfortunately, no macromolecular composition of red beets grown in controlled environmental plant chambers was found in literature.

Table 1.5 Beet lipid, vitamin and amino acid composition (USDA, 2005)

Lipids	Units	Value per 100 g dw
Fatty acids, total saturated	g	0.22
16:00	g	0.21
18:00	g	0.01
Fatty acids, total monounsaturated	g	0.27
18:1 undifferentiated	g	0.27
Fatty acids, total polyunsaturated	g	0.49
18:2 undifferentiated	g	0.45
18:3 undifferentiated	g	0.04
Phytosterols	mg	0.20
Vitamins		
Vitamin C, total ascorbic acid	mg	3.95E-02
Thiamin	mg	2.50E-04
Riboflavin	mg	3.22E-04
Niacin	mg	2.69E-03
Pantothenic acid	mg	1.25E-03
Vitamin B_6	mg	5.39E-04
Folate, total	mcg	8.78E-04
Vitamin A, IU	IU	2.66E-04
Vitamin E (alpha-tocopherol)	mg	3.22E-04
Vitamin K (phylloquinone)	mcg	1.61E-06

Amino Acids	Value (% dw)
Tryptophan	0.15
Threonine	0.38
Isoleucine	0.39
Leucine	0.55
Lysine	0.47
Methionine	0.14
Cystine	0.15
Phenylalanine	0.37
Tyrosine	0.31
Valine	0.45
Arginine	0.34
Histidine	0.17
Alanine	0.48
Aspartic acid	0.93
Glutamic acid	3.45
Glycine	0.25
Proline	0.34
Serine	0.48

1.5.4 LETTUCE

- **Elemental Composition**

The elemental composition (Na, K, P, Mg, Ca, N, C, Mo, Zn, B, Mn, Fe, Cu) of lettuce leaves is shown in Table 1.6. The K, P, Mg and Ca content of lettuce leaves grown using the hydroponic nutrient film technique (NFT) were increased compared to the field and were decreased for Zn, B, Mn, Fe and Cu (McKeehen, 1994). Analyzing the effect of CO_2, the composition of K, P, Mg, Ca and N has lower values at the highest CO_2 level (10000 ppm). Therefore, CO_2 level is a factor to be considered as an environmental condition influencing elemental condition.

A study of Na, K, and Ca composition of lettuce under salinity stress was carried out by Bie *et al.* (2004). The study reports that increasing salinity levels, values of leaf area, dry weight, photosynthetic rate and stomatal conductance diminished. Moreover, using Na_2SO_4, the content of K and Ca decreased, whereas Na content increased (Table 1.7). In comparison to this, under $NaHCO_3$ stress the K content decreased and Na content increased. They mentioned that the rapid uptake of Na and the decrease in K content, leading to a decrease in K/Na ratio, would have influenced the K/Na selectivity in the root system and disrupted the regular osmotic adjustment resulting in osmotic stress (Bie *et al.*, 2004).

Table 1.7 Lettuce Elemental and Mineral Composition under salt stress (Bie *et al.*, 2004). Culture conditions: butterhead cultivars ('P' Sumitomo Chemistry, and 'L-2', Mikado Seed) grown using the hydroponic technique of deep water culture under PPF of 1150 μmol $\cdot m^{-2} \cdot s^{-1}$. Crop age at harvest is 39 days for sulphates cultures and 34 days for carbonates cultures.

Na_2SO_4	Culti.	Photosynthetic rate	Mineral Composition		
			Na	K	Ca
mM		μmol $CO_2 \cdot m^{-2} \cdot s^{-1}$	%	%	%
Leaves					
0	P	8.6	0.2	14.9	1.1
	L-2	9.3	0.3	13.8	0.9
20	P	8.5	1.4	11.5	0. 6
	L-2	8.8	2.7	10.7	0. 6
40	P	8.4	2.2	9.0	0.4
	L-2	8.4	3.3	9.4	0.4
60	P	7.7	2.8	8.3	0.4
	L-2	7.9	4.1	8.3	0.4
Roots					
0	P	8.6	0.3	11.8	0.9
	L-2	9.3	0.3	11.0	0.7
20	P	8.5	2.5	10. 7	0.4
	L-2	8.8	1.3	9.7	0.5
40	P	8.4	3.5	9.2	0.4
	L-2	8.4	2.1	8.4	0.4
60	P	7.7	3.9	8.5	0.4
	L-2	7.9	2.7	7.8	0.4

$NaHCO_3$	Culti.	Mineral Composition		
		Na	K	Ca
mM		%	%	%
Leaves				
0	P	0.3	16.4	1.0
	L-2	0.2	15.9	1.2
2.5	P	0.5	14.7	1.0
	L-2	0.5	15.9	1.0
5	P	0.9	14.9	1.0
	L-2	0.8	14.4	1.0
7.5	P	1. 1	14.9	1.0
	L-2	1.0	13.4	0.9
Roots				
0	P	0.2	12.1	1.3
	L-2	0.2	11.5	1.0
2.5	P	0.4	12.0	1.9
	L-2	0.4	11.0	1.8
5	P	0.5	12.9	1.1
	L-2	0.5	11.5	1.1
7.5	P	0.6	11.5	1.4
	L-2	0.7	11.0	1.2

Table 1.6 Lettuce Elemental and Mineral Composition.
(1) Culture conditions: Field Purdue University, sunlight, 12/12 h day/night photoperiod.
(2) Data obtained by R. M. Wheeler in BPC at KSC. Culture conditions: daylight and fluorescent lamps providing a PPF of 325 μmol ·m^{-2}·s^{-1}, 18/4 h day/night photoperiod, 23 ºC, relative humidity 65%, using a modified 1/2 Hoagland nutrient solution.

Growth Conditions	Cultivar	CO_2 levels	Crop Age	Lettuce Leaves Elemenal Composition												Reference
				Na	K	P	Mg	Ca	N	Mo	Zn	B	Mn	Fe	Cu	
		ppm	d	%	%	%	%	%	%	%	%	%	%	%	%	
Field	-	350	-	0.57	3.94	0.59	0.26	0.73	-	-	4.0E-03	-	1.0E-02	2.0E-02	1.0E-03	USDA,2005
Field	-	350	-	0.045	1.31	0.12	-	0.34	-	-	-	-	-	6.9E-03	-	Watt and Merril, 1975
Soil+NPK	Waldmann G.	-	51	0.01	3.12	0.31	0.18	0.63	3.088	-	5.0E-03	2.0E-03	2.0E-02	1.4E-01	1.3E-03	McKeehen,1994(1)
NFT	Waldmann's Green	400	25	0	8.27	0.68	0.23	0.72	4.72	1.0E-04	3.2E-03	1.4E-03	1.3E-02	6.4E-03	4.0E-04	McKeehen,1994 (2)
		1000		0	8.21	0.62	0.20	0.63	4.464	1.0E-04	2.4E-03	1.5E-03	6.1E-03	5.2E-03	4.0E-04	
		5000		0	8.48	0.63	0.22	0.70	4.768	1.0E-04	2.7E-03	1.5E-03	9.3E-03	5.3E-03	4.0E-04	
		10000		0	7.02	0.54	0.22	0.67	4.144	1.0E-04	2.0E-03	1.6E-03	3.9E-03	5.5E-03	3.0E-04	

Table 1.8 Lettuce Proximate Composition
(1) Culture conditions: Field Purdue University, sunlight, 12/12 h day/night photoperiod.
(2) Data obtained by R.M. Wheeler in BPC located at KSC. Culture conditions: daylight and fluorescent lamps providing a PPF of 325 μmol ·m^{-2}·s^{-1}, 18/4 h day/night photoperiod, 23 ºC, relative humidity 65%, using a modified 1/2 Hoagland nutrient solution.
(3) Culture conditions: MH and HPS Lamps providing a PPF between 280-336 μmol ·m^{-2}·s^{-1}, 16/8 h day/night photoperiod, 23 ºC, relative humidity 75%, density 19.2 plant·m^{-2}, using a modified 1/2 Hoagland nutrient solution, biomass between 5.8-7.7 g dw·$plant^{-1}$ and edible yield between 5.4 and 7.1 g dw·m^{-2}·d^{-1}. Energy calculated by assigning 4 kcal·g^{-1} carbohydrates, 4 kcal·g^{-1} protein and 9 kcal·g^{-1} fat.

Growth Condition	Cultivar	CO_2 levels	Crop Age	Lettuce Leaves Macromolecular Composition				Fiber	Energy	Reference
				Protein	Fat	Ash	CH			
		ppm	d	%	%	%	%	%	cal·g^{-1}	
Field	-	350	-	27.59	3.04	12.58	56.59	26.37	3043	USDA,2005
Field	-	350	-	21.7	5	15	58.3	-	-	Watt and Merril, 1975
Soil+NPK	Waldmann G.	-	51	17.7	4.2	15.6	62.5	-	3905	McKeehen,1994 (1)
NFT	Waldmann's Green	400	25	24	3.6	18.4	54	-	3798	McKeehen, 1994 (2)
		1000		21.8	3.2	16.9	58.1	-	3690	
		5000		22	3.5	17.6	56.9	-	3698	
		10000		19.7	2.6	15.3	62.4	-	3711	
NFT	Waldmann's Green	1000	28	24.6	8.2	22.4	33.6	11.1	3070	Wheeler, 1996 (3)
				30.2	4.1	22	32.7	11.1	2880	
				27.2	4.5	21.8	37	9.4	2970	
				27.8	1.6	21.1	39.8	9.7	2850	

- **Macromolecular Composition**

The macromolecular composition (protein, fat, ash, carbohydrate) and fiber and energy content of lettuce leaves under different culture conditions is presented in Table 1.8.

The protein and ash levels found in lettuce tissue grown in hydroponics cultures are higher than the ones found in field conditions, probably due to an increased uptake of some nutrients such as K and N (Wheeler *et al.*, 1996b).

In a similar way, Davis *et al.* (1988) reported an increase in leaf protein content (27-36%) under controlled environments compared to the field caused by all N nutrition treatments applied. Moreover an increase in nitrogen leads to a better yield per unit area, but also an increase in non-protein N, such as nitrate (Aldrich, 1980). Nevertheless, carbohydrates content of lettuce grown in hydroponics are lower than in the field.

McKeehen (1994) proposed to use CO_2 atmospheric concentration as an interesting strategy to control nitrate accumulation in tissue, since in his study under a CO_2 enriched atmosphere, lettuce presented not only a lower protein and fat content, but also a decrease in the nitrate accumulation.

In Table 1.9 lipid, vitamin and amino acid composition of lettuce is shown.

Table 1.9 Lettuce lipid, vitamin and amino acid composition (USDA, 2005).

Lipids	Units	Value per 100 g dw
Fatty acids, total saturated	g	0.406
16:00	g	0.365
18:00	g	0.041
Fatty acids, total monounsaturated	g	0.122
16:1 undifferentiated	g	0.041
18:1 undifferentiated	g	0.101
Fatty acids, total polyunsaturated	g	1.663
18:2 undifferentiated	g	0.487
18:3 undifferentiated	g	1.176
Phytosterols	mg	0.771
Vitamins		
Vitamin C, total ascorbic acid	mg	3.65E-01
Thiamin	mg	1.42E-03
Riboflavin	mg	1.62E-03
Niacin	mg	7.61E-03
Pantothenic acid	mg	2.72E-03
Vitamin B-6	mg	1.83E-03
Folate, total	mcg	7.71E-04
Vitamin A, IU	IU	1.50E-01
Vitamin A, RAE	mcg	7.51E-03
Vitamin E (alpha-tocopherol)	mg	5.88E-03
Tocopherol, gamma	mg	7.51E-03
Tocopherol, delta	mg	2.03E-04
Vitamin K (phylloquinone)	mcg	3.52E-03

Amino Acids	Value (% dw)
Tryptophan	0.18
Threonine	1.20
Isoleucine	1.70
Leucine	1.60
Lysine	1.70
Methionine	0.32
Cystine	0.32
Phenylalanine	1.12
Tyrosine	0.65
Valine	1.42
Arginine	1.44
Histidine	0.45
Alanine	1.14
Aspartic acid	2.88
Glutamic acid	3.69
Glycine	1.16
Proline	0.97
Serine	0.79

1.5.5 WHEAT

Wheat growth rate increases in direct proportion to increase in photosynthetic photon flux (Salisbury *et al.,* 1987). Wheat yields were increased a 25% by elevating CO_2 from 350 to 700 ppm (Bugbee and Salisbury, 1989).

Smart *et al.* (1998) examined the hypothesis that elevated CO_2 concentrations would increase nitrate absorption. The cultivar "Veery-10" were grown hydroponically using NFT, with HPS lamps providing 1000 $\mu mol \cdot m^{-2} \cdot s^{-1}$, under a photoperiod of 18/6 day/night and with a high plant density (1780 $plants \cdot m^{-2}$) under two levels of CO_2 (360 and 1000 ppm) and two different nitrate concentration in the nutrient solution (100 and 1000 $mmol \cdot m^{-3}$). The productivities obtained were higher when nitrate and/or CO_2 had elevated values, ranging 43 g $dw \cdot m^{-2} \cdot d^{-1}$ for grain and 6-8 g $dw \cdot m^{-2} \cdot d^{-1}$ for roots. Evapotranspiration rates were 4.82 L $H_2O \cdot m^{-2} \cdot d^{-1}$ at 360 ppm CO_2 and 3.26 at 1000 ppm CO_2. They concluded that under high CO_2 levels (1000 ppm), wheat presents higher nitrate consumption, but most of this increase did not lead to higher nitrogen content in plant tissue.

André *et al.* (1989) performed a wheat culture in controlled environment chambers under high CO_2 concentration (800 ppm) with and irradiance of 800 $\mu mol \cdot m^{-2} \cdot s^{-1}$, photoperiod of 14/10 and plant density of 80 $plants \cdot m^{-2}$. The evapotranspiration was found to decrease 20% under high CO_2 values, from 6 to 4.62 L $H_2O \cdot m^{-2} \cdot d^{-1}$. Nutrient uptake was slightly higher at elevated CO_2 levels, with the following averages (expressed in $mmol \cdot m^{-2} d^{-1}$): 60 NO_3^- , 6 NH_4^+ and 12 K^+.

- **Elemental Composition**

Mineral composition reported in Table 1.10 include Na, K, P, Mg, Ca, N, Mo, Zn, B, Mn, Fe, and Cu content for each wheat part (grain, chaff, straw and roots).

McKeehen (1994) concluded that grain Zn and Fe content were decreased in controlled environments compared to the field, whereas other elements in the grain maintained similar values. In addition to this, the controlled environment straw had higher contents of K, P, Ca and Cu compared to field straw.

Table 1.10 Wheat mineral composition

(1) Data obtained by B. Bugbee in the field at Utah State University. Culture conditions: Sunlight, 12/12 h day/night photoperiod

(2) Data obtained by B. Bugbee in Growth Chamber located at Utah State University. Culture conditions: HPS lamps providing a PPF of 1200 μmol $\cdot m^{-2} \cdot s^{-1}$, 24 h photoperiod, 23 ºC, relative humidity 70%, using a modified 1/2 Hoagland nutrient solution with Deep Root Zone (DRZ) technique.

(3) Data obtained by R.M. Wheeler in BPC located at KSC. Culture conditions: HPS lamps providing a PPF of 750 μmol $\cdot m^{-2} \cdot s^{-1}$, 20/4 h day/night photoperiod, temperature 24-20/16 ºC day/night, relative humidity 75%, using a modified 1/2 Hoagland solution for the nutrient film technique (NFT) culture.

Growth Conditions	Cultivar	$[CO_2]$ ppm	Age (d)	Mineral Composition (%)												Reference
				Na	K	P	Mg	Ca	N	Mo	Zn	B	Mn	Fe	Cu	
Grain																
Soil	-	350	-	0.01	1.00	0.95	0.27	0.04	-	-	0.01	-	0.01	0.01	0.001	USDA, 2005
Soil	-	350	-	3.4E-03	0.42	0.42	-	0.05	-	-	-	-	-	3.8E-03	-	Watt and Merril, 1975
Soil	Yecora Rojo	350	105	1.9E-03	0.43	0.35	0.13	0.06	3.71	0	5.0E-03	0	3.4E-03	3.7E-03	5.0E-04	McKeehen,1994 (1)
	Veery-10			1.9E-03	0.49	0.42	0.15	0.06	3.66	1.0E-04	7.7E-03	0	4.2E-03	6.6E-03	6.0E-04	
DRZ	Yecora Rojo	1000	64	0	0.44	0.40	0.14	0.08	4.13	0	3.0E-03	0	3.8E-03	1.8E-03	8.0E-04	McKeehen,1994 (2)
	Veery-10			0	0.59	0.43	0.13	0.05	3.10	0	3.0E-03	0	3.1E-03	1.5E-03	6.0E-04	
NFT	Yecora Rojo	1200	85	0	0.55	0.48	0.19	0.04	3.57	0	2.5E-03	0	4.0E-03	2.6E-03	5.0E-04	McKeehen,1994 (3)
Chaff																
Soil	Yecora Rojo	350	105	2.0E-04	0.16	0.03	0.03	0.09	1.42	0	5.0E-04	0	7.0E-04	7.9E-03	2.0E-04	McKeehen,1994 (1)
	Veery-10			6.3E-03	0.73	0.22	0.17	0.40	2.03	1.0E-04	3.9E-03	2.0E-04	4.3E-03	4.1E-02	1.1E-03	
DRZ	Yecora Rojo	1000	64	8.6E-03	1.27	0.32	0.12	0.25	1.94	1.0E-04	1.0E-03	3.1E-03	3.6E-03	5.3E-03	6.0E-04	McKeehen,1994 (2)
	Veery-10			8.9E-03	2.31	0.21	0.08	0.32	1.76	0	1.6E-03	2.9E-03	2.8E-03	4.9E-03	5.0E-04	
NFT	Yecora Rojo	1200	85	2.4E-03	1.93	0.43	0.34	0.32	2.11	0	1.3E-03	5.8E-03	1.0E-02	1.1E-02	5.0E-04	McKeehen,1994 (3)
Straw																
Soil	Yecora Rojo	350	105	1.2E-02	2.73	0.07	0.09	0.31	0.88	0	2.1E-03	0	1.7E-03	2.0E-02	4.0E-04	McKeehen,1994 (1)
	Veery-10			8.31	2.11	0.11	0.11	0.37	1.39	1.0E-04	2.4E-03	0	2.2E-03	1.8E-02	4.0E-04	
DRZ	Yecora Rojo	1000	64	9.9E-03	4.52	0.18	0.10	0.53	2.30	3.0E-04	1.4E-03	2.3E-03	1.8E-03	1.0E-02	8.0E-04	McKeehen,1994 (2)
	Veery-10			1.3E-02	4.59	0.16	0.19	0.80	2.34	4.0E-04	2.6E-03	3.5E-03	2.8E-03	9.3E-03	8.0E-04	
NFT	Yecora Rojo	1200	85	9.9E-03	6.69	0.35	0.31	0.52	3.73	0	8.0E-04	9.3E-03	5.8E-03	1.6E-02	5.0E-04	McKeehen,1994 (3)
Roots																
NFT	Yecora Rojo	1200	85	1.2E-02	4.56	0.24	0.12	0.18	5.33	0	1.5E-03	4.8E-03	3.5E-03	8.4E-02	5.6E-03	McKeehen,1994 (3)

- **Macromolecular Composition**

Proximate composition for each wheat part is presented in the following tables. Table 1.11 shows protein, fat, ash, carbohydrate, fiber and energy content for wheat grown in field and in controlled environments.

Table 1.11 Wheat macromolecular Composition. Acronym for cultivars (Culti.) are: Yecora Rojo (YR) and Veery-10 (V-10).

(1) Data obtained by B. Bugbee in the field at Utah State University. Culture conditions: Sunlight, 12/12 h day/night photoperiod

(2) Data obtained by B. Bugbee in Growth Chamber located at Utah State University. Culture conditions: HPS lamps providing a PPF of 1200 $\mu mol \cdot m^{-2} \cdot s^{-1}$, 24 h photoperiod, 23 ºC, relative humidity 70%, using a modified 1/2 Hoagland nutrient solution with Deep Root Zone (DRZ) technique.

(3) Data obtained by R.M. Wheeler in BPC located at KSC. Culture conditions: HPS lamps providing a PPF of 750 $\mu mol \cdot m^{-2} \cdot s^{-1}$, 20/4 h day/night photoperiod, 24-20/16 ºC day/night, relative humidity 75%, using a modified 1/2 Hoagland solution with nutrient film technique (NFT).

(4) Culture conditions: MH and HPS lamps providing a PPF between 280-336 $\mu mol \cdot m^{-2} \cdot s^{-1}$, 16/8 h day/night photoperiod, 23 ºC, relative humidity 75%, plant density 19.2 plant/m^2, using a modified 1/2 Hoagland nutrient solution, biomass between 5.8-7.7 g dw·$plant^{-1}$ and edible yield between 5.4-7.1 g dw·$m^{-2} \cdot d^{-1}$). Energy calculated by assigning 4 kcal·g^{-1} carbohydrates (CH), 4 kcal·g^{-1} protein and 9 kcal·g^{-1} fat.

Growth Conditions	Culti.	$[CO_2]$ (ppm)	Age (d)	Macromolecular composition (%)				Fiber (%)	Energy cal·g^{-1}	Reference
				Protein	Fat	Ash	CH			
Grain										
Soil	-	350	-	26.0	10.9	4.7	58.3	14.8	4005	USDA, 2005
Soil	-	350	-	16.3	2.3	1.9	79.5	-	-	Watt and Merril, 1975
Soil	YR	350	105	16.7	1.5	1.9	79.9	-	4173	McKeehen,1994 (1)
	V-10			18.6	1.4	2.1	77.9	-	4172	
DRZ	YR	1000	64	18.9	1.8	1.9	77.4	-	4122	McKeehen,1994 (2)
	V-10			16.5	2.3	2.1	79.1	-	4053	
NFT	YR	1200	85	18.9	1.4	2.3	77.3	-	4105	McKeehen,1994 (3)
NFT	YR	1000	77	18.4	3.2	2	73.3	2.5	3980	Wheeler,1996b (4)
			86	20.9	3.1	2.1	71.6	3.2	3940	
			85	20.1	3.3	1.9	72.3	2.8	3950	
			85	17	2.9	2	75.7	2.4	4050	
Chaff										
Soil	YR	350	105	5.2	1.1	13.9	79.8	-	-	McKeehen,1994 (1)
	V-10			6.5	1.9	10.7	80.9	-	-	
DRZ	YR	1000	64	5.4	0.7	4	89.9	-	-	McKeehen,1994 (2)
	V-10			6.4	0.8	5.6	87.2	-	-	
NFT	YR	1200	85	8	1.1	6	84.9	-	-	McKeehen,1994 (3)
Straw										
Soil	YR	350	105	3.4	1	11	84.6	-	-	McKeehen,1994 (1)
	V-10			4.3	1.3	9.6	84.9	-	-	
DRZ	YR	1000	64	4.5	1	10.7	83.9	-	-	McKeehen,1994 (2)
	V-10			4.8	1.4	11.6	82.2	-	-	
NFT	YR	1200	85	5.6	1.7	16.1	76.6	-	-	McKeehen,1994 (3)
Roots										
NFT	YR	1200	85	14.9	0.4	10.9	73.8	-	-	McKeehen,1994 (3)

Proximate composition of wheat changes at different morphological parts. Protein and fat content in grain is higher than in the other parts, whereas chaff and straw are richer in ashes, carbohydrates and fibers. Protein composition in grain usually present higher values than the range of 11.18% mentioned in Hoff *et al.* (1982) and Gauer *et al.* (1992).

Fat composition is about 0.4 - 1.8 % in Yecora Rojo cultivar and 0.6 – 2.3 % in Veery-10 variety for all plants parts.

Table 1.12 shows amino acid composition in wheat grain is listed under different growing conditions.

Table 1.12 Wheat amino acid composition. Acronym for cultivars (Culti.) are: Yecora Rojo (YR) and Veery-10 (V-10).

(1) Data obtained by B. Bugbee in the field at Utah State University. Culture conditions: Sunlight, 12/12 h day/night photoperiod

(2) Data obtained by B. Bugbee in Growth Chamber located at Utah State University. Culture conditions: HPS lamps providing a PPF of 1200 µmol $\cdot m^{-2} \cdot s^{-1}$, 24 h photoperiod, 23 ºC, relative humidity 70%, using a modified 1/2 Hoagland nutrient solution with DRZ technique.

(3) Data obtained by R.M. Wheeler in BPC located at KSC. Culture conditions: HPS lamps providing a PPF of 750 µmol $\cdot m^{-2} \cdot s^{-1}$, 20/4 h day/night photoperiod, 24-20/16 ºC day/night, relative humidity 75%, using a modified 1/2 Hoagland solution with NFT.

Reference		USDA, 2005	McKeehen, 1994 (1)		McKeehen, 1994 (2)		McKeehen, 1994 (3)	Sosulski, 1990
Growth conditions		Soil	Soil		DRZ		NFT	Soil
CO_2 levels (ppm)		350	350		1000		1200	-
Crop Age (d)		-	105		64		85	-
Cultivar		-	YR	V-10	YR	V-10	YR	-
Amino Acid (%)	Tryptophan	0.36	0.191	0.192	0.179	0.162	0.175	0.102
	Lysine	1.65	0.474	0.492	0.466	0.413	0.473	0.361
	Histidine	0.72	0.462	0.457	0.441	0.349	0.454	0.301
	Arginine	2.1	0.883	0.905	0.847	0.719	0.878	0.484
	Aspartic Acid	2.33	0.936	0.967	0.899	0.815	0.851	0.649
	Threonine	1.09	0.513	0.542	0.504	0.439	0.5	0.367
	Serine	1.24	0.855	0.917	0.893	0.734	0.853	0.605
	Glutamic Acid	4.49	5.848	6.121	6.444	4.858	5.974	3.68
	Cysteine	0.52	0.433	0.439	0.424	0.392	0.42	0.315
	Glycine	1.6	0.764	0.81	0.801	0.67	0.788	0.511
	Alanine	1.66	0.775	0.753	0.724	0.632	0.718	0.468
	Valine	1.35	0.798	0.835	0.79	0.67	0.778	0.54
	Methionine	0.51	0.298	0.285	0.295	0.237	0.286	0.177
	Isoleucine	0.95	0.66	0.707	0.683	0.542	0.652	0.553
	Leucine	1.77	1.258	1.345	1.288	1.05	1.271	0.864
	Tyrosine	0.79	0.564	0.67	0.615	0.537	0.646	0.44
	Phenylalanine	1.04	0.906	0.951	1.008	0.708	0.949	0.607

The amino acid composition presents similar values for all the different cultures. Hoff *et al.* (1982) suggest that a complementation with proteins with higher levels of lysine and tryptophan is recommended, since wheat is deficient in them.

Finally, lipid and vitamin composition is included in Table 1.13.

Table 1.13 Wheat lipid and vitamin composition (USDA, 2005)

Lipids	Value (% dw)
Fatty acids, total saturated	1.87
14:00:	0.01
16:00:	1.79
18:00:	0.06
Fatty acids, total monounsaturated	1.54
16:1 undifferentiated	0.04
18:1 undifferentiated	1.50
Fatty acids, total polyunsaturated	6.76
18:2 undifferentiated	5.95
18:3 undifferentiated	0.81

Vitamins	Units	Value per 100 g dw
Thiamin	mg	2.1E-03
Riboflavin	mg	5.6E-04
Niacin	mg	7.7E-03
Pantothenic acid	mg	2.5E-03
Vitamin B-6	mg	1.5E-03
Folate, total	mcg	3.2E-04
Folate, food	mcg	3.2E-04

1.6 MOTIVATION OF THE WORK

One of the next steps of the MELiSSA project is to integrate all the compartments in the MPP at UAB to demonstrate the feasibility of the terrestrial loop closure. In order to achieve this goal, each compartment is developed and characterized individually before being scaled-up for subsequent integration. Some of the required studies are the collection of standardized empirical data sets allowing for mass balance modelling based on stoichiometry as a deterministic modelling approach. Hence it is important to have empirical data on productivities, biomass compositions, nutrient uptake rates and gas exchange rates of each compartment.

The motivation of this work is to increase and improve the knowledge existing on the photosynthetic compartments of the MELiSSA loop.

Although the photoautotrophic compartment CIVa of the MELiSSA loop has been widely studied for years within the MELiSSA consortium and numerous bibliographic references deal with *Arthrospira sp.* cultures and properties (as reviewed in section 1.4) some basic aspects related to CIVa need to be further studied. This work focuses on two of them. First, the determination of the operational limits, biomass productivity, nitrogen uptake, carbon consumption and oxygen production of the actual photobioreactor for the *Arthrospira* production in the MPP is investigated. Second, the effects of nitrogen source used are also studied. Although the nitrogen source for *Arthrospira* compartment (CIVa) is nitrate present in the outlet from the nitrifying compartment (CIII), a perturbation in CIII, such as a decrease in the oxygen supply, would increase the ammonium concentration in the liquid inlet of the *Arthrospira* compartment. Thus, it is critical to study the effect of ammonium in *Arthrospira sp.* kinetics and

composition since in the literature review it has been seen that high ammonium loading rates could inhibit *Arthrospira* growth, resulting in unstable operational conditions.

This work also aims to contribute to the study of higher plant compartments. After an initial literature review of plant production in closed environments, it was detected that available data was sparse and focused mainly on gas exchange and yield for very specific cultivars and operational conditions. Data on nutrient uptake and composition exist but often not for the specific cultivars and culture conditions of interest to the MPP. Therefore an experimental program needs to be undertaken to collect sufficient baseline data to allow for mass balance and eventually dynamic modelling studies and for the sizing and design of the higher plant compartment (HPC) to be integrated into the MPP.

Chapter 2

OBJECTIVES AND OUTLINE

The aim of this thesis is to further develop and to evaluate the integration of two photosynthetic compartments, one colonized by the microalgae *Arthrospira sp*. (CIVa) and another populated by higher plants (CIVb or HPC), into the MELiSSA bioregenerative life support system. This objective is divided in three main units:

- Unit I - *Arthrospira* Compartment (CIVa):
  - Determine the operational limits and maximum productivity of the *Arthrospira* photobioreactor of the MELiSSA Pilot Plant (MPP) under nominal conditions (Chapter 3).
  - Study the effect of ammonium, light intensity and dilution rate on continuous *Arthrospira* production and biomass composition and determine the threshold values to avoid inhibitory conditions, when using ammonium as nitrogen source (Chapter 4).

- Unit II - Higher Plant Compartment (CIVb or HPC):
  - Obtain baseline data of yield, tissue composition and nutrient uptake from beet and lettuce trials in sealed and environmentally controlled plant chambers (Chapter 5).
  - Compare carbon dynamics between batch and staggered cultures of beet and lettuce (Chapter 6).
  - Estimate the parameters of a full canopy photosynthesis model and evaluate its applicability for prediction of biomass production in HPC (Chapter 6).

- Unit III – Photosynthetic Compartments Integration
  - Design and engineer the HPC compartment and prototype to be integrated in the MPP located at UAB (Chapter 7).
  - Evaluate the impact of the integration of the photosynthetic compartments into the MPP using a static mass balance model for assessing the nitrogen, CO_2 and O_2 balances, while determining the conditions under which mass balances can be expected (Chapter 8).

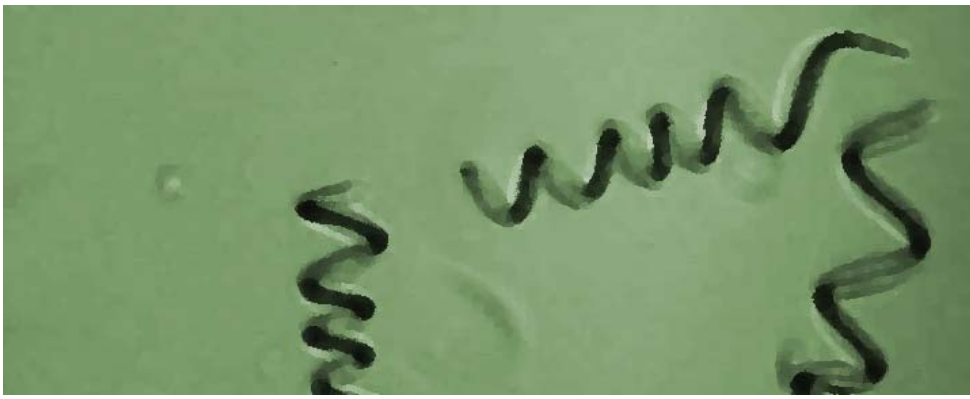

Unit I

Arthrospira Compartment

Chapter **3**

Pilot Plant photobioreactor operational limits

Chapter **4**

Effect of ammonium, light intensity and dilution rate on *Arthrospira* production: Determination of threshold values to avoid inhibitory conditions

3

PILOT PLANT BIOREACTOR OPERATIONAL LIMITS

3.1 INTRODUCTION

The integration of all the MELiSSA compartments is one of the key steps for the terrestrial demonstration of the feasibility of the loop closure, which will take place in the MELiSSA Pilot Plant (MPP) located at Universitat Autònoma de Barcelona (UAB).

As mentioned in the general introduction, the photoautotrophic compartment CIVa of the MELiSSA loop, colonized by *Arthrospira sp*., also know as *Spirulina*, has been widely studied for years within the MELiSSA consortium. Preliminary *Arthrospira* cultures at bench scale contributed to increase available knowledge on *Arthrospira* growth and to develop a biochemical structured model describing it (Cornet *et al.*, 1992a,b, 1998).

For the integration and development scenario defined in the MPP, a new bioreactor with the appropriate size was designed and constructed. Therefore, the scale-up of the photobioreactor for *Arthrospira* culture, carried out at UAB, was a step of key importance for the future integration of the complete loop. Vernerey *et al*. (2001) described in detail the scale-up approach for the *Arthrospira* compartment, the evaluation of the different design constraints and the final design of the pilot scale photobioreactor. In brief, biomass productivity and light

distribution were the main parameters for scaling-up the 7 L photobioreactor with an order of magnitude of 10x its volume. The final geometry of the photobioreactor was selected in order to ensure an optimum light distribution within the culture, using the abovementioned mathematical model, which allows the quantification of the light availability inside the photobioreactor (Cornet *et al.*, 1992a). The designed pilot scale photobioreactor was a 77 L airlift photobioreactor with an external loop and with an illuminated part composed by two polyamide wall cylinders, one acting as a rise and the other as a down-comer.

After the construction of this photobioreactor, its gas-liquid mass transfer and hydrodynamics were analyzed (Vernerey, 2000). The main characteristics of the bioreactor were that, in order to obtain a suitable mixing time without compromising the integrity of the polyamide walls, the range of superficial gas velocities in the riser should be between $[1\text{-}4]\cdot10^{-3}$ $m\cdot s^{-1}$, which corresponds to gas flow rates ranging from 2 to 4 $L\cdot min^{-1}$. Moreover, the values of gas-liquid mass transfer coefficients were found to be in the range of 6.0 - 14.7 h^{-1} for O_2 and of 5.7 - 14.0 h^{-1} for CO_2. Based on the volumetric gas-liquid mass transfer coefficient, it was concluded that CO_2 transfer would not limit the biomass concentration expected at the design phase and that the oxygen produced concomitantly to the biomass generation would be removed from the bioreactor without reaching inhibitory levels.

The next study to be carried out with this bioreactor is to determine the maximum biomass productivity achieved with the pilot plant bioreactor. With this aim, several continuous cultures have been carried out in this work at different dilution rates (D) and light intensities (I) using CO_2 gas as a carbon source.

The specific values of each of the two factors essayed (D and I) were planned using a Box-Wilson Central Composite Design (CCD) in order to estimate effectively the parameters of the Response Surface Model (RSM) used. The RSM methodology was employed to find a relationship between the response variable (biomass concentration and productivity) and the selected factors (D and I) and to determine the operational region in which the responses converge to a local optimum (a more detailed description about the experimental design is provided in the material and methods section).

In addition to this, the elemental and macromolecular composition of *Arthrospira* biomass, harvested at the steady state of each of the continuous cultures, was analyzed. Such data are used to determine whether dilution rate and illumination levels influence the nutritional value of *Arthrospira* biomass.

Finally, the effects of some disturbances of the main culture conditions on the biomass concentration and other key variables were evaluated to define the photobioreactor's operational limits.

3.2 MATERIALS AND METHODS

3.2.1 PILOT PLANT PHOTOBIOREACTOR

The pilot-scale photobioreactor (Bioengineering AG, Wald, CH) used for the *Arthrospira sp*. cultures is a 77-L external-loop airlift bioreactor (Figure 3.1). A detailed description of the scale-up, design, associated instrumentation and physical characterization of this photobioreactor has been already reported (Vernerey, 2000; Vernerey *et al.*, 2001).

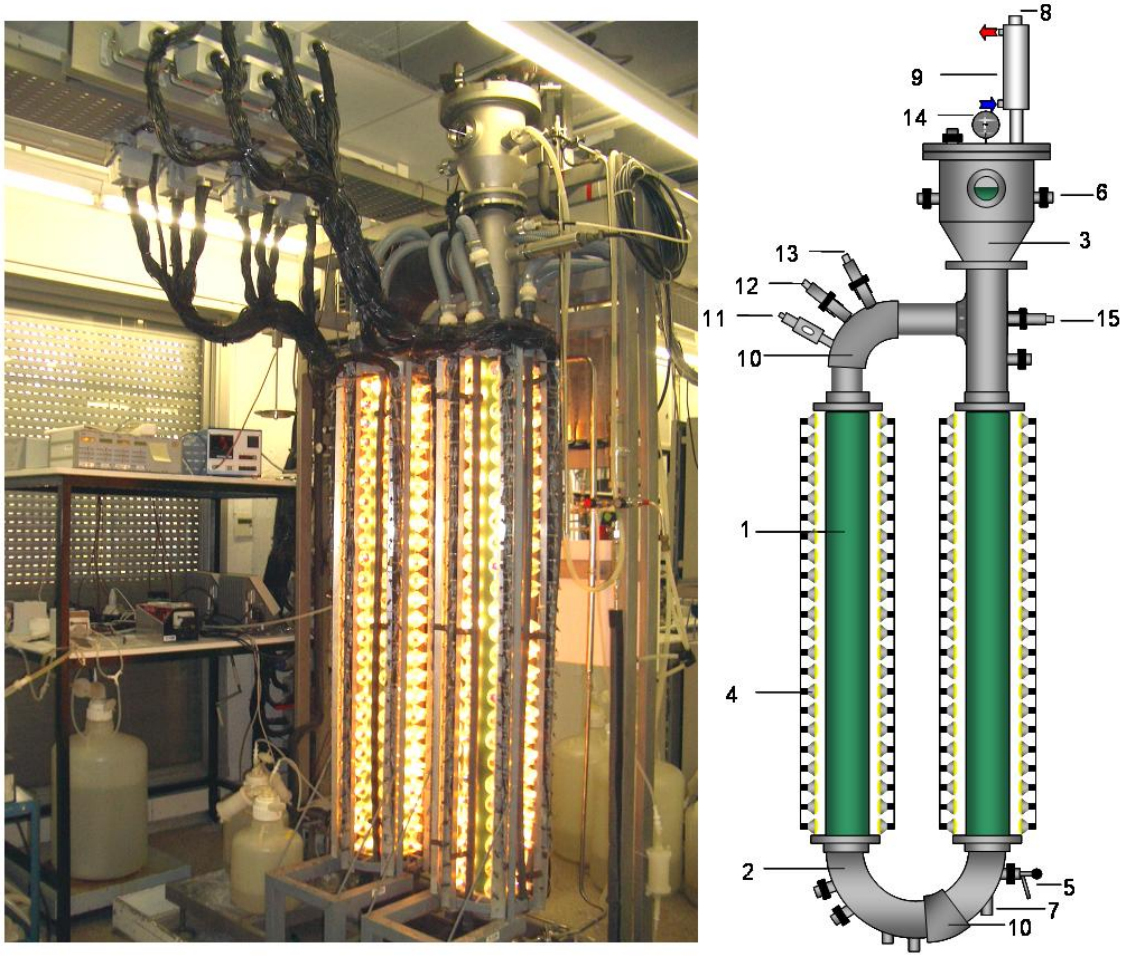

Figure 3.1 Pilot-scale photobioreactor for *Arthrospira sp*. culture. The following parts are indicated in the scheme: (1) transparent cylindrical parts corresponding to the illuminated section -right column: riser; left column: downcomer- (2) stainless steel connection parts (3) gas-liquid separator (4) halogen lamps (5) liquid medium inlet (6) liquid outlet (7) gas inlet (8) gas outlet (9) condenser (10) external cooling jackets (11) pH probe (12) dissolved oxygen sensor (13) temperature probe (14) pressure sensor (15) biomass sensor.

The illuminated part of the bioreactor consists of two cylinders made of polyamide tripan, a transparent plastic foil material, each column with a 15 cm diameter and 1.5 m height. Both cylinders are connected at their lower and upper parts by U-shaped stainless-steel sections with an external jacket for the temperature control, where all the instrumentation is located. The illumination system consists of 350 halogen lamps (Sylvania, 12V, 20W) distributed homogeneously around the plastic cylinders. A voltage regulator allows for different light intensities to the bioreactor.

Liquid media input is done by peristaltic pumps (Reglo-Analoge MS 2/6-160; MS 4/6-100, Ismatec SA, Glattbrugg, CH) from one of the two 50L buffer tanks, through a liquid filter (0.22 µm KVGL04HB3 Millipore, Billerica, MA, USA) to ensure sterility and then to the bottom part of the bioreactor. A U-tube located at the top part of the bioreactor allows the output liquid to flow by gravity, while maintaining a constant culture volume.

The gas circuit is composed by 4 mass flow meter-controllers (Bronkhorst High-Tech BV F202D-FA-44-V, Ruurlo, NL) that measure and regulate both the input CO_2-enriched air, responsible of the culture agitation, and the output gas flow. An IR analyzer for CO_2 coupled to a paramagnetic analyzer for O_2 (Maihak, Multor 610, Hamburg, DE) measures on-line the composition of the gas phase.

Instrumentation associated with the bioreactor allows for the on-line measurement of biomass concentration (Monitek, Düsseldorf, DE), pH, dissolved O_2, temperature and pressure.

3.2.1.1 CONTROL SYSTEM

The control system of the photobioreactor allows for the monitoring and control of the main parameters of the *Arthrospira* cultures. Figure 3.2 shows the control system human interface displays for the culture liquid system (A), gas system (B), pH regulation (C) and temperature control (D). The user can not only define the control mode and change the set point values, but can also follow the on-line measures and the main parameters evolution through time in the graphs automatically plotted.

Biomass concentration is followed on-line with an optical biomass sensor (Monitek, Düsseldorf, DE), which use a factor of 1.6 to convert the optical measure to dry weight units ($g \cdot L^{-1}$).

Liquid input flow rate is maintained at set points by activating one of the two calibrated peristaltic pumps upon the weight of the corresponding buffer tanks. A balance measures the weight of each tank and when the active buffer tank is under a defined volume, the system activates the alternative pump. Then, the empty tank is refilled with liquid medium. If both tanks are under the minimum volume, input and output pumps are stopped.

pH control is done actuating over a base (NaOH) or acid (HCl) feeding pump based on the measurement using a conventional pH probe connected to a pH amplifier (Crison pH Rocon 18, Barcelona, ES).

Gas flow set point is provided by the supervisor system actuating over a set of flow controllers that regulate gas input and output flow rates. When the gas supply is interrupted externally, a gas alarm is activated, the light is decreased to a safety value and the liquid pumps are stopped.

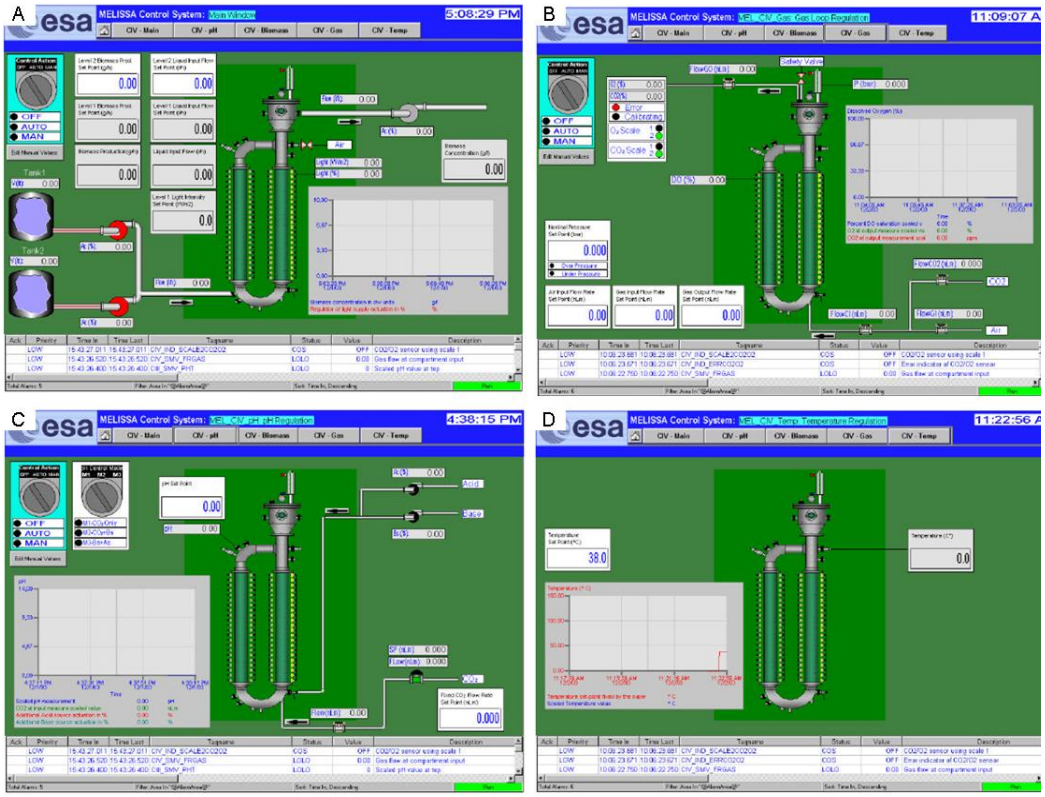

Figure 3.2 Control system regulation displays for the pilot plant photobioreactor CIVa. Some of the parameters shown in the different subsections are (A) buffer tank weights, active pump, input flowrate, light intensity, biomass concentration evolution (B) gas flowrates, CO_2 and O_2 composition evolution and pressure measurement (C) pH evolution and acid/base active pumps (D) temperature value.

Temperature is maintained at 36ºC by the refrigeration system pumping a cooling fluid through the external jacket of the two stainless steel parts of the bioreactor. Besides, a set of perforated tubes located around lamps evacuate hot air outside the laboratory. When the temperature is over a determined value, an alarm is activated, the light is decreased to a safety value and the liquid pumps are stopped.

Control system allows for the data acquisition and storage of the main parameters in a database file (Microsoft Access).

3.2.1.2 PHOTOBIOREACTOR START-UP

The following sequence comprises the main tasks to perform before starting *Arthrospira* cultures in the pilot photobioreactor:

- Bioreactor plastic parts and instrumentation set-up.
- Sterilization of the bioreactor.
- Set-up of the lamps structure.
- Control system and PLC initialization.
- Set-up of the liquid circuit for culture medium entrance and acid/base control.

- Filling the bioreactor with sterilized culture media through a 0.22 μm liquid filter.
- Refrigeration and gas circuit start-up. The cold fluid level inside the cooling system and the gas bottle pressures should be checked first.
- Instrumentation calibration:
  - pH sensor is calibrated using commercial standard solutions at pH 4 and pH 7.
  - O_2 dissolved sensor calibration is done with culture media at 36ºC saturated first with bubbled N_2 (0%) and then with air (100%).
  - Peristaltic pumps for inlet culture media are calibrated based on the decrease in weight of the buffer tanks for a given percentage of the pump controller, during at least 24h for each point. Each peristaltic pump, Reglo-Analoge MS 2/6-160 (2 channels 6 rollers) and MS 4/6-100 (4 channels 6 rollers),are calibrated using two tubes of 2.79 mm ID Ismaprene-PharMed (Ismatec SA, Glattbrugg, CH). The corresponding calibration curves, expressed as pump controller (%) versus liquid flow rate ($L \cdot h^{-1}$) are: $y_{MS2/6-160} = 16.82x+1.40$ ($r^2=0.996$) and $y_{MS4/6-100} = 36.22x+1.54$ ($r^2=0.985$).
  - Gas mass flow meter-controllers (Bronkhorst High-TecH BV F202D-FA-44-V, Ruurlo, NL) were calibrated when installed with 30 $NL \cdot min^{-1}$ air for the air input, total input and output flowmeters and with 5 $NL \cdot min^{-1}$ CO_2 for the CO_2 input flowmeter. Gas flow measures are corrected taking into account the composition of the gas flow measured. The gas used in the calibration and the corresponding factors are chosen as described in the Bronkhorst catalogue 'Mass flow meters and Controllers'.
  - Incident light calibration relates the average light intensity at bioreactor's surface and a percentage of the controller that regulates the voltage supplied to lamps (Vernerey, 2000). The adjusted equation, expressed as light intensity ($W \cdot m^{-2}$) against light controller (%) is: $y=1.83 \cdot 10^{-1} + 7.741 \cdot 10^{-2} x - 2.71 \cdot 10^{-2} x^2 + 2.21 \cdot 10^{-3} x^3 - 2.75 \cdot 10^{-5} x^4 + 1.12 \cdot 10^{-7} x^5$ ($r^2=0.999$ and Standard Error, SE=1.36).
- Photobioreactor inoculation is done using 10% of the working volume.

3.2.2 STRAIN AND CULTURE MEDIUM

The axenic strain used for this study was the cyanobacterium *Arthrospira sp*. (PCC 8005), also known as *Spirulina*, provided by the Pasteur Institute (Paris, FR). The inoculum was grown in Erlenmeyer-flasks containing modified Zarrouk's medium (Zarrouk, 1966) with constant illumination and periodical agitation. The modified Zarrouk medium (Table 3.1) consisting in one macroelement solution and two microelement solutions (A5 and B6) was adjusted to pH 9.5 before its use.

Table 3.1 Culture media composition for *Arthrospira sp*. cultures. (1)-Carbonates are not included during the pilot plant *Arthrospira* continuous cultures.

Compound	$g \cdot L^{-1}$
EDTA-Na·2 H_2O	0.08
NaCl	1
$FeSO_4 \cdot 7\ H_2O$	0.01
(1)Na_2CO_3	4.543
(1)$NaHCO_3$	4.972
$MgSO_4 \cdot 7\ H_2O$	0.20
$CaCl_2$	0.04
K_2SO_4	1
KH_2PO_4	0.5
$NaNO_3$	2.5
Solution	$mL \cdot L^{-1}$
A5	1.00
B6	1.00

A5 Compounds	$g \cdot L^{-1}$
H_3BO_3	2.860
$MnCl_2 \cdot 4\ H_2O$	1.810
$ZnSO_4 \cdot 7\ H_2O$	0.222
$CuSO_4 \cdot 5\ H_2O$	0.079
MoO_3	0.015
B6 Compounds	$g \cdot L^{-1}$
NH_4VO_3	0.023
$KCr(SO_4)_2 \cdot 12\ H_2O$	0.096
$NiSO_4 \cdot 7\ H_2O$	0.048
$(NO_3)_2Co \cdot 6\ H_2O$	0.049
$Na_2WO_4 \cdot 2\ H_2O$	0.018
$Ti(SO_4)_2$ + $TiOSO_4$	0.048

Based on the MELiSSA loop concept, the main carbon source for the *Arthrospira* compartment would be the CO_2 present in the gas loop produced by other compartments such as the crew. In order to better mimic the culture conditions of the future operation of the whole loop, it was decided to supply carbon source via the gas phase instead of the liquid phase. Therefore, for the continuous culture, the carbonates normally used in the media formulation (Na_2CO_3, $NaHCO_3$) were not included and instead the inlet gas flow rate was enriched with CO_2. The quantity of pure CO_2 introduced (0.12 $NL \cdot min^{-1}$) was determined using conservative estimations to ensure that carbon source would not limit *Arthrospira* growth. The total inlet gas flow was set at 2.2 $NL \cdot min^{-1}$ to ensure good mixing in the bioreactor.

3.2.3 EXPERIMENTAL DESIGN

All *Arthrospira* continuous cultures were carried out at the same culture conditions of pH, temperature, culture media and gas flow rates. Particularly, cultures were performed at 36ºC, pH 9.6 and using Zarrouk medium without carbonates as nutrient solution. Total inlet airflow (2.2 $NL \cdot min^{-1}$) enriched with CO_2 (around 5%) provided the agitation of the culture and the supply of the carbon source.

As the aim of this study is to determine the effect of dilution rate and illumination levels on biomass productivity of the photobioreactor, the levels of both parameters used for the several tests were determined using a central composite design. Thus, dilution rate (D) and light intensity (I) were the selected two factors for the experimental design.

Before selecting the experimental design, the experimental domain of both factors has to be defined. With this aim, a review of the *Arthrospira* continuous culture carried out successfully in the MPP, using different type of bioreactors, in previous works, was performed. Table 3.2 shows the summary of this review, including the dilution rate, light intensity and biomass concentration (expressed as dry weight, DW) for each case.

The lower and higher dilution rates are use to define the experimental domain for dilution rate, which ranges from 0.007 h^{-1} to 0.050 h^{-1}. Taking into account that the pilot plant bioreactor has 77 L of culture volume, the experimental domain for the liquid flow rate ranges between 0.54-3.85 $L \cdot h^{-1}$.

Table 3.2 Review of *Arthrospira* biomass concentration achieved during continuous cultures carried out successfully at different dilution rates (D) and illumination levels (I) using different type of bioreactors.

D (h^{-1})	I ($W \cdot m^{-2}$)	DW ($g \cdot L^{-1}$)
A. Bench Bioreactor V=2.5 L- Loop connection tests CII-III-IVa (Creus, 2003)		
0.018	94	2.0
0.017	20	1.25-1.35
0.010	11	0.8
0.020	11	0.5
0.017	20	1.2
0.007	20	2.1
0.012	20	1.2
0.042	94	1.43
B. Bench Bioreactor V=7 L (Vernerey, 2000) p.99-102		
0.025	133	0.91-1.03
0.025	305	1.13-1.18
0.035	133	0.66
0.035	305	0.89-0.92
C. Bench Bioreactor V=7 L Nitrogen limitation tests (Vernerey, 2000) p.123-129		
0.012-0.018	305-50.2	0.41-0.54
0.05	50.2-305	0.25
0.05	50.2	0.50
D. Pilot Plant Bioreactor V=77 L (Vernerey, 2000) p.204-205		
0.026	155	0.60
0.026	223	0.73
0.026	155	0.47
0.026	223	0.46

The number of lamps of the photobioreactor and the voltage supplied to them defines the maximum light intensity that can be provided to the *Arthrospira* culture. Taking this into account, the experimental domain of the light intensity ranges from 10 $W \cdot m^{-2}$ to 225 $W \cdot m^{-2}$.

Once the experimental domain of each variable has been determined, the experimental design that would define the levels at which the several cultures would be carried out has to be chosen. Based on the experimental objective and the number of factors a response surface method was selected. The response surface methodology (RSM) is a mathematical and statistical technique useful for modelling a response of interest influenced by several variables, also called factors. The RSM objective is to determine the region of the factor in which the response variable converges to a local optimum. With this aim, usually a second order polynomial [Eq. 3.1] is employed to find a relationship between the response variable (Y_n) and the independent factors (X_1, X_2). The shape of the response surface can be also used to detect weak points of the process (Montgomery, 1991).

$$Y_n = b_0 + b_1 \cdot X_1 + b_2 \cdot X_2 + b_{11} \cdot X_1^2 + b_{22} \cdot X_2^2 + b_{12} \cdot X_1 \cdot X_2 \quad \text{[Eq. 3.1]}$$

In order to estimate model parameters effectively, proper experimental designs should be used to collect the experimental data. One of the most widely used experimental design for fitting a second-order model is the Box-Wilson Central Composite Design (CCD), which consists of a 2^k factorial (coded as ±1) increased by 2k axial point (± α) and n_c center points (where k is the number of factors or independent variables). These levels correspond to cube points at the corner of a unit cube, which is the product of the interval [-1,1], star points along the axes outside the cube (α) and center point at the origin (0,0) (Figure 3.3).

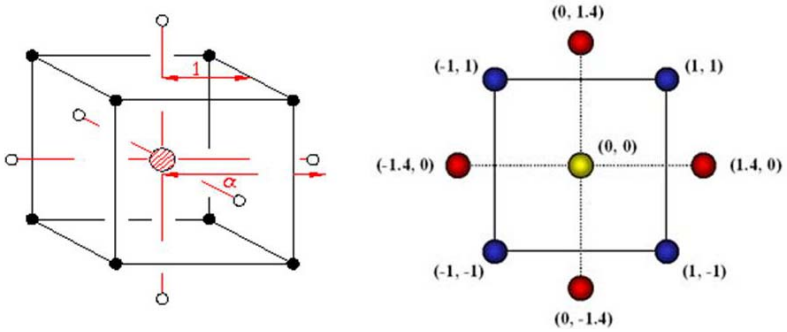

Figure 3.3 Schematic for the Central Composite Design (CCD).

Two important properties in the selection of a response surface design are orthogonality and rotability. Orthogonality is the optimal design property as it minimizes the variance of the regression coefficients, whereas rotability provides equal precision of estimation in all directions.

The CCD can be rotatable choosing the appropriate axial distance value ($\alpha = [2^k]^{1/4}$) and orthogonality selecting the number of center points. In order to ensure the rotability of the present experimental design the α value selected is 1.414 ($\alpha=[2^2]^{1/4} = 1.414$) (Box *et al.*, 1978). The following equation is used for coding the independent variables:

$$X_c = \left[\frac{Xi - cx}{dx}\right] \cdot dc \qquad \text{[Eq. 3.2]}$$

In [Eq. 3.2] Xc is the coded value of the independent variable, which for the selected CCD design ranges from -1.414 to 1.414, Xi is the real value of the independent variable, cx is the real value of the independent variable at the centre point, dx is the distance between the experimental domain selected for the real value of independent variable and dc is the distance between the extremes of the coded experimental domain.

Table 3.3 shows the parameters required for codifying the experimental domain of the independent variables selected, which are dilution rate (D) and illumination level (I).

Table 3.3 Parameters required for codifying the experimental domain of the dilution rate and illumination levels.

Parameter	Light intensity ($W \cdot m^{-2}$)	Dilution rate (h^{-1})
Experimental domain	10-225	0.007-0.05
cx	117.5	0.0285
dx	215	0.043
dc	2.828	2.828

Thus, the coded scaled values of the independent variables are obtained using [Eq. 3.3] and [Eq. 3.4].

$$I_C = \left[\frac{I - 118}{215}\right] \cdot 2.828 \qquad \text{[Eq. 3.3]}$$

$$D_C = \left[\frac{D - 0.029}{0.043}\right] \cdot 2.828 \qquad \text{[Eq. 3.4]}$$

Since the CCD selected as experimental design determines at which coded levels the experiments have to be performed, [Eq. 3.3] and [Eq. 3.4] are used to determine the real values for dilution rate (D) and light intensity (I) that corresponds to their coded values, named respectively as Dc and Ic.

Table 3.4 shows the CCD used with the coded (Dc and Ic) and real values (D and I) for each of the two factors selected.

Table 3.4 Coded levels and real values of the variables used in the factorial and Central Composite Design (CCD) with three replicates on the centre point for the *Arthrospira* continuous cultures. Dc is the codified value for the dilution rate (D) and Ic is the codified value for light intensity (I).

Run	Dc (X1)	Ic (X2)	D (h^{-1})	I ($W \cdot m^{-2}$)
1	-1	-1	0.0133	41
2	1	-1	0.0437	41
3	-1	1	0.0133	194
4	1	1	0.0437	194
5	-1.414	0	0.0070	118
6	1.414	0	0.0500	118
7	0	-1.414	0.0285	10
8	0	1.414	0.0285	225
9	0	0	0.0285	118
10	0	0	0.0285	118
11	0	0	0.0285	118

3.2.4 EXPERIMENTAL PROCEDURE

Data acquired and recorded continuously by the control system were analyzed on a daily basis for verification. Such data contribute not only to follow the evolution of the main culture variables, but also to detect whether any disturbance occurred or to adjust calibration parameters of peristaltic pumps.

Besides the on-line monitoring of the major variables, several off-line analyses were also carried out on a daily basis. The off-line analytical methods include the determination of the pH (micropH 2001, Crison SA, Barcelona, ES), conductivity (microCM2100, Crison SA, Barcelona, ES) and nitrate concentration of the inlet and outlet liquid flow and the measure of the optical density, biomass dry weight and inorganic and organic carbon concentration of the outlet liquid flow. A more detailed description of the sampling and analytical methods is included in the next section.

The occasional formation of foams was detected by direct observation and Sigma Antifoam 289 (A-5551; Sigma-Aldrich, Poole, GB) was added occasionally only when required at the recommended starting concentration for microbiological media (0.005-0.01%). This antifoam is a mixture of both silicone and non-silicone organic compounds.

The culture broth was checked weekly to verify the axenity of *Arthrospira* culture by microscopic examination (Zeiss Axioskop, Carl Zeiss AG, DE).

3.2.5 ANALYTICAL METHODS

3.2.5.1 BIOMASS CONCENTRATION

- **Dry Weight**

Dry weight of *Arthrospira* was obtained filtering 25 mL of culture broth through a 0.47 μm filters (Whatman glass GF/F, Brentford, GB), previously dried and weighted. Then filters with retained biomass were dried until constant weight and cooled to room temperature in a desiccator. Afterwards, filters were weighted again to determine the biomass dry weight by means of the difference between the weight of the filter with retained cells and its weight before filtering the sample. Dry weight value was calculated as the arithmetical average of three determinations for each sample point.

- **Optical Density**

Optical density measured at 750 nm provides a direct measurement of the *Arthrospira* concentration according to the Beer-Lambert law. Neither exopolysaccharides nor cyanobacteria pigments absorb at this wavelength. Thus, these measurements reflect only the absorption of light produced by the presence of the microorganisms, fact that is directly related with biomass concentration. The optical density is measured by a spectrophotometer (Uvikon 941 Plus, Kontron Instruments) and expressed in absorbance units, not concentration ($g \cdot L^{-1}$) and thus not directly comparable to DW or biomass sensor measurement.

3.2.5.2 LIQUID COMPOSITION ANALYSIS

- **Inorganic and Organic Carbon Concentration**

A total organic carbon analyzer OI Analytical 1020A with 1051 vial Autosampler (OI Analytical, TX, USA) was used to measure total carbon (TC), total inorganic carbon (TIC) and total organic carbon (TOC) in liquid samples. The analyzer is based on the complete combustion of carbon compounds to CO_2 in an O_2 rich environment. A Non Dispersive Infra Red (NDIR) sensor detects the resulting CO_2 used for determining TC. For determining TIC, the sample pH is decreased, so carbonate and bicarbonate ions are converted to dissolved CO_2, which is purged from the solution and swept into the NDIR to detect the carbon mass. TOC is determined by subtracting the results of TIC from TC.

The calibration for TC/TIC was done with standard of Na_2CO_3 ranging from 50 to 2000 mg $C \cdot L^{-1}$. The standard solutions were prepared using *Arthrospira* culture media without carbonates (Table 3.1) to minimize the interferences of other compounds. The adjusted equation, expressed as carbon concentration ($mg \cdot L^{-1}$) against area detected by NDIR (counts) was: $y=0.1797+1.182 \cdot 10^{-4}x$ ($r^2=0.999$). In order to verify the correct determination of TOC, several standards solutions of glucose ($C_2H_{12}O_6$), acetic acid ($C_2H_4O_2$) and propionic acid ($C_3H_6O_2$) were analyzed and their TOC content were satisfactorily determined.

The TIC/TOC concentration was determined in triplicate liquid samples, once the biomass had been removed by filtration.

- **Nitrate Concentration**

Nitrate was measured using UV measurement determinations by means of LCK 339 nitrate analysis kits (Dr. Lange Nitrax, analyse range 0.23-13.5 ppm $N\text{-}NO_3^-$). The analysis is based on the reaction of nitrate ions, in presence of sulphuric or phosphoric acid, with 2,6-dimethylphenol forming 4-nitro-2,6-dimethylphenol, which is then quantified measuring the absorption at 370 nm.

For nitrate determination 1 ml of filtered sample, previously diluted to be in the measuring range, was added into the test cuvette. After adding 0.2 ml of LCK 339 solution, the cuvette was mixed vigorously. The absorbance was measured after 15 minutes with the spectrophotometer (Dr. Lange Xion 500, Hach Lange GmbH, Düsseldorf, DE) and the nitrate concentration ($N\text{-}NO_3^-$) was provided directly by the spectrophotometer. Several standard solutions were prepared to verify the correct nitrate determination by Dr. Lange spectrophotometer. The nitrate concentration of the liquid input and output flows was determined in triplicate.

3.2.5.3 BIOMASS ELEMENTAL AND MOLECULAR COMPOSITION

Once a steady state was reached a volume between 3 and 5 L of the culture broth upon biomass concentration, was filtered through a 0.47 μm Whatman filters. The collected cells were washed twice with deionized water and filtered again. The resulting dense biomass solution was first frozen at -80ºC and then lyophilized. The freeze-dried biomass was used for the determination of the elemental and macromolecular composition of *Arthrospira* cells.

All the analysis was determined at least in triplicate and the solutions were prepared with deionized water. Standard calibration plots were prepared for each new sets of sample analysis and have not been included for simplicity. In this way, the influence of slight differences on analytical procedure due to either environmental factors, operator effect, reagent preparation or instrumentation used on molecular content determination are minimized.

- **Elemental Composition**

Elemental analyses were performed by the analytical service of UAB (Servei d'Anàlisi Química, UAB). The determination of C, N, H and S composition is based on sample combustion inside a Sn capsule with O_2 atmosphere in a furnace at 1800ºC.

The procedure is based on the combustion of the organic sample components to the corresponding oxides, obtaining a gas mixture of CO_2, N_2, N_xO_y, H_2O, SO_2 and SO_3. The exothermic reaction, which turns Sn into SnO_2(s), releases heat that increases the capsule temperature until 1800 ºC. SnO_2 and inorganic sample components remain as a solid in the combustion zone. The gases formed and the O_2 excess flow with He as a carrier gas to a reactor with WO_3, which catalyses the transformation of the gas mixture into the unique species for each element, obtaining CO_2, N_2, H_2O, SO_2 and the O_2 and He in excess. This mixture is transported to a reactor at 500 ºC containing CuO, which reacts with the O_2 in excess to give CuO(s). The remaining gases CO_2, N_2, H_2O and SO_2 are carried with He to a gas chromatograph (Porapak column, Waters Associates Inc.) where they are separated and measured using a thermal conductivity detector for determining a signal proportional to the amount of component. The quantification is performed by interpolation in an appropriate calibration plot.

- **Proteins**

Protein content was determined by a modified method of Lowry (Herbert *et al.*, 1971). In the Lowry method, the peptide bonds form a complex with divalent copper ion in the presence of tartrate under alkaline conditions. The subsequent reduction of the added Folin-Ciocalteu phenol reagent, which is essentially a phosphotungstic-phosphomolybdic acid solution, by tyrosine and trypthophan produces a blue coloured complex detectable at 750nm.

For quantifying the protein content, 0.5 mL of 1N NaOH was added to 0.5 mL of cell suspension (0.5 $g \cdot L^{-1}$) and the mixture was kept for 10 min in a boiling water bath. After cooling it in cold water, 0.5 mL of a reagent, which was prepared as 50 mL of 5% Na_2CO_3 and 2 mL of 0.5% $CuSO_4 \cdot 5H_2O$ in 1% sodium potassium tartrate, was added and mixed. After 10 min, 0.5mL of the Folin-Ciocalteu reagent diluted 1:2 (v/v) with water is added and is allowed to stand 30min for full colour development. The standard proteins solutions prepared with bovine serum albumin (0-800 $mg \cdot L^{-1}$) were treated in the same way as biomass samples. Optical densities were read at 750 nm against the reagent blank in a spectrophotometer (Cary 50 Bio, Varian Inc., CA, USA). The standard curve generated with the protein standard solutions was used for obtaining the corresponding amount of protein in the cell samples.

- **Carbohydrates**

Total carbohydrates were analyzed by the phenol method first developed by Dubois *et al*. (1956) as described in Herbert *et al.* (1971). The addition of sulphuric acid produces the hydrolysis of the polysaccharides to monosaccharides by heating. The formed furfural, from pentoses, or hydoxymethyl-furfural, from hexoses, by dehydration and rearrangement of the monosaccharides, reacts with phenol to produce a yellow coloured-compound, which is measured at 488 nm.

The procedure for quantifying carbohydrates involved adding 1 mL of 5% phenol to a 1 mL biomass sample (0.4 $g \cdot L^{-1}$), mixing, adding 5 mL of 96% H_2SO_4 and mixing again completely. After 10 min, tubes were placed in a water bath at 25ºC for 15 min and then the absorbance was read at 488 nm. The same procedure was followed simultaneously for the glucose standard solutions (0-100 $mg \cdot L^{-1}$). The total carbohydrate content was obtained in biomass samples using calibration plots obtained with the standard glucose solutions.

- **Glycogen**

The content of glycogen, a reserve polysaccharide, was determined as described in Smolders *et al.* (1994). The glycogen was hydrolysed adding 5 mL 0.6 M HCl to 10 mg freeze-dried biomass and was placed in a water bath at 100ºC for 1 hour. After cooling and filtering the sample through a 0.22 μm filter, the glucose concentration was quantified directly by a YSI 1700 Select glucose analyzer (Yellow Springs Instruments, OH, USA).

- **Total fatty acids**

Elemental analyses were performed by Servei d'Anàlisi Química (Departament de Química, UAB). The transesterification of fatty acids was done with BF_3 in methanol medium with nonadecanoic acid as internal standard. BF_3 and methanol was added to the sample and the mixture was maintained under reflux for 20 min at 95 ºC. Then, a liquid-liquid extraction with hexane and NaCl saturated water was carried out for 2 min. Afterwards, the mixture was centrifuged and the organic fraction was injected to a gas chromatograph (HP 6890, column HP-23) equipped with a flame ionization detector (FID). The determination and quantification of the fatty acids is done comparing the retention times with an external standard of 37 commercial fatty acids (37 Fame Mix Supelco).

The following fatty acids were determined: palmitic (C16:0), palmitoleic (C16:1(9c)), palmitelaidic (C16:1(9t)), stearic (C18:0), oleic (C18:1(9c)), trans-9-octadecenoic (C18:1(9t)), vaccenic (C18:1(11c)), linoleic (C18:2(9c,12c)) and γ-linoleic (C18:3(6c,9c,12c)).

- **Nucleic acids**

The methods used for the determination of nucleic acids (DNA and RNA) content in biomass are described in Herbert *et al.* (1971). First the removal of acid soluble compounds was done with the addition of 10 mL cold 0.2N $HClO_4$ to 25 mg freeze-dried biomass. After 15 min at 4ºC, the suspension was centrifuged for 5 min. This step was repeated twice. Then, the

lipid extraction was achieved by adding 10 mL chloroform:methanol 2:1 (v/v) and after 5 min, the suspension was centrifuged for 5 min. This step was repeated twice.

For the determination of the DNA content, the obtained pellet is digested with 5 mL $HClO_4$ 0.5 N for 45 min at 70 ºC and then the suspension was centrifuged. The supernatant and the DNA standard solutions prepared with 5 mM NaOH (0-90 $mg \cdot L^{-1}$) were analyzed by the Burton method (1956) as follows. Samples were mixed with 4 mL of the diphenylamine reagent containing acetaldehyde, incubated overnight (16-24h) at 30ºC and their absorbance was read at 600nm. The DNA concentration was obtained with the corresponding calibration plot obtained from the DNA standard solutions.

For the RNA quantification, the pellet was hydrolyzed with 2 mL 0.3 N KOH overnight (18-24 h) at 30ºC and then treated with $HClO_4$, which precipitated DNA and protein. After centrifuging, the RNA supernatant and the RNA standard solution (0-60 $mg \cdot L^{-1}$) were determined by the orcinol method, where 2 mL orcinol is added to the samples and kept for 35 min at 100ºC. The RNA content is determined spectrophotometrically at 665 nm using the corresponding standard calibration plot.

- **Chlorophyll**

Chlorophyll content was quantified according to the method described by Sesták (1971). The extraction of the chlorophyll content was done adding 5 mL of aqueous acetone (80% v/v) to 10 mg of freeze-dried biomass and sonicating for 30 sec. After 2 min, the sample was filtered and the absorbance of the supernatant was measured at 647 and 664 nm.

The chlorophyll content was determined using the following equations defined by Sesták (1971):

$$\text{Chlorophyll } a \text{ (mg L}^{-1}) = 11.78 \cdot A_{664} - 2.29 \cdot A_{647}$$

$$\text{Chlorophyll } b \text{ (mg L}^{-1}) = 20.05 \cdot A_{647} - 4.77 \cdot A_{664}$$

- **Phycobiliproteins**

Phycobiliproteins concentration was estimated following the method reported by Patel *et al.* (2005) based on Bennet and Bogorad (1973). An amount of 10 mg freeze-dried biomass was resuspended in 5 mL of 0.01 M sodium phosphate pH 7 buffer solution. Cell suspensions were first frozen at -20ºC in darkness and after thawing at room temperature, they were sonicated for 4 min and centrifuged at 4ºC for 45 min. The absorbance of the supernatant, where phycobiliproteins were contained, was determined at 562, 615 and 652 nm.

The following equations were used for determining the content of c-phycocyanin (PC), allophycocyanin (APC) and c-phycoerythrin (PE) (Bennet and Bogorad, 1973):

$$PC \text{ (g L}^{-1}) = (A_{615} - 0.474 \cdot A_{652}) / 5.34$$

$$APC \text{ (g L}^{-1}) = (A_{652} - 0.208 \cdot A_{615}) / 5.09$$

$$PE \text{ (g L}^{-1}) = (A_{562} - 2.41 \cdot PC - 0.849 \cdot APC) / 9.62$$

3.3 RESULTS AND DISCUSSION

3.3.1 PILOT PLANT CONTINUOUS CULTURES AT DIFFERENT DILUTION RATES AND LIGHT INTENSITIES

3.3.1.1 BIOMASS PRODUCTION

As mentioned in the materials and methods section, *Arthrospira* concentration is followed on-line with the biomass sensor ([X]sensor) and is also measured off-line on a daily basis by means of the optical density (OD) and the dry weight analysis (DW). Although the steady-state values of biomass concentration and production of each of the continuous cultures performed in the pilot plant photobioreactor are presented later in this section (Table 3.5), for simplicity it is decided to include the biomass evolution only for some of the cultures (Figure 3.4, Figure 3.5, Figure 3.6). Such figures are an example of the typical profiles of biomass concentration obtained for each of the *Arthrospira* cultures performed at different dilution rates (D) and illumination levels (I).

Figure 3.4 shows *Arthrospira* evolution during the continuous culture carried out at a dilution rate of 0.044 $h^{-1}$and and illumination level of 194 $W \cdot m^{-2}$, which corresponds to the culture conditions defined for run 4 with the CCD design (Table 3.4). As can bee seen, biomass concentration present the same trend regardless the technique used for its measurement (value are not the same since OD is measured in absorbance units and DW in $g \cdot L^{-1}$).

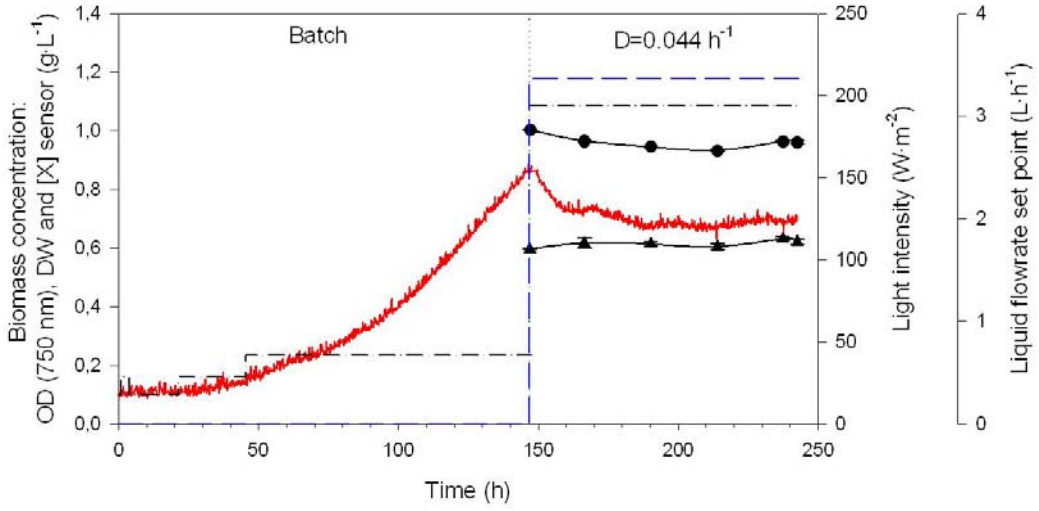

Figure 3.4 Evolution of *Arthrospira* concentration during the batch phase performed at increasing light intensities (dashed-dotted line) from 28 $W \cdot m^{-2}$ to 42 $W \cdot m^{-2}$ until the start-up of the continuous phase, where the illumination level is set at 194 $W \cdot m^{-2}$ and the dilution rate at D=0.044 h^{-1}, which corresponds to a liquid flow rate (dashed line) of 3.4 $L \cdot h^{-1}$. Cell concentration is given based on the measurement of (i) on-line biomass probe ([X]sensor ($g \cdot L^{-1}$), solid line), (ii) off-line dry weight (DW ($g \cdot L^{-1}$), ▲) and (iii) off-line optical density at 750 nm (OD, ●). The corresponding steady-state values of the continuous phase are reported in Table 3.5 (Run 4).

After the inoculation of the photobioreactor, culture is kept in batch mode at low illumination levels (ranging from 28 to 42 $W \cdot m^{-2}$) until biomass levels reached in the bioreactor

are high enough to handle the continuous conditions desired. Thus after 147 hours, illumination is increased to 194W·m^{-2} and liquid flow rate is set at 3.4 L·h^{-1}, which correspond to a dilution rate of 0.044 h^{-1}. At this moment, biomass concentration starts to decrease until a stable value of biomass level is attained and kept for 4 residence times. The corresponding steady-state values of biomass concentration and production of the continuous phase are listed in Table 3.5 (Run 4).

Another example of biomass evolution of this set of continuous cultures is depicted in Figure 3.5. In this case, *Arthrospira* culture is carried out at a fixed dilution rate of 0.028 h^{-1} and at two different illumination levels, 118 and 225 W·m^{-2}.

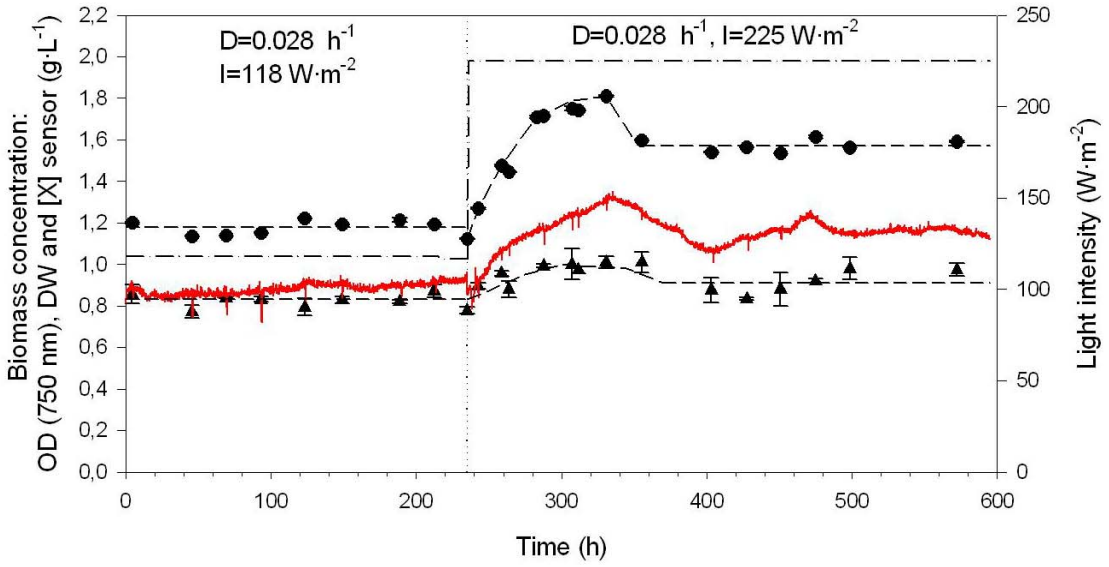

Figure 3.5 Evolution of *Arthrospira* concentration during the continuous cultures carried out at a fixed dilution rate (D) of 0.028 h^{-1} and with changing illumination levels (I, dashed-dotted line) from 118 W·m^{-2} to 225 W·m^{-2}. Cell concentration is given based on the measurement of (i) on-line biomass probe ([X]sensor (g·L^{-1}), solid line), (ii) off-line dry weight (DW (g·L^{-1}), ▲) and (iii) off-line optical density at 750 nm (OD, ●). The steady-state values of the both phases correspond to Run 9 (I=118 W·m^{-2}) and Run 8 (I=225 W·m^{-2}) reported in Table 3.5.

Figure 3.5 starts when the steady-state of the continuous culture at D=0.028 h^{-1} and at 118 W·m^{-2}, which are the conditions determined for run 9 in the CCD design (Table 3.4), is achieved. After 6 residence times under steady-state operation, the illumination levels were increased to 225 W·m^{-2} (run 8, Table 3.4). As can be seen in Figure 3.5, biomass concentration starts to increase until a new steady state is achieved at higher biomass levels than in the previous phase and maintained during 7 residence times. The steady state values of biomass concentration and productivity at both illumination levels are summarized in Table 3.5 (Run 9 and 8).

The last example of a typical biomass profile obtained during this series of experiments is illustrated in Figure 3.6. Particularly, *Arthrospira* concentration is shown for the continuous cultures performed at three different culture conditions, which correspond to the ones defined for runs 1, 3 and 7 (CCD design, Table 3.4).

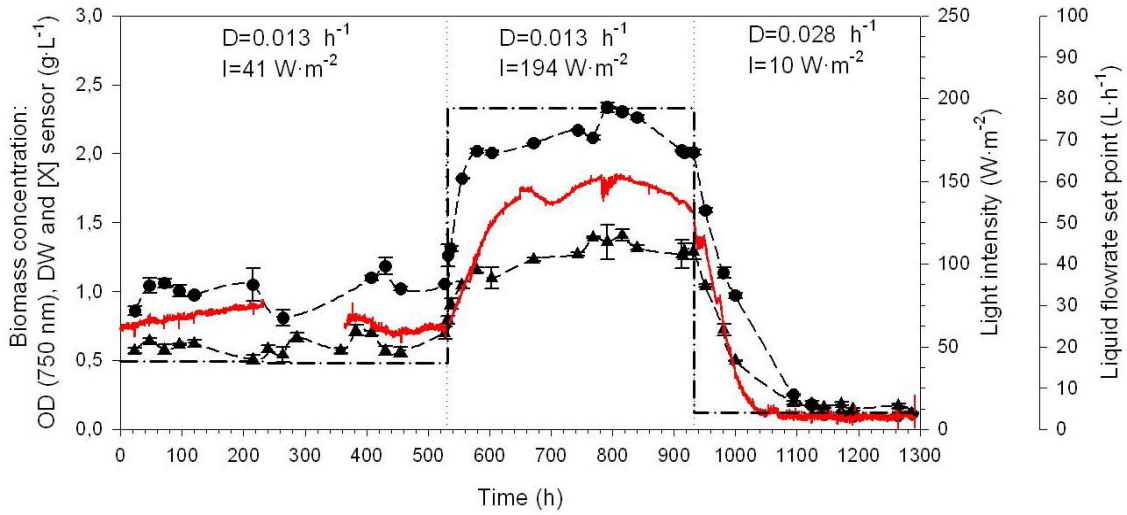

Figure 3.6 Evolution of *Arthrospira* concentration during the continuous cultures carried out at different liquid flow rates (dashed line) and illumination levels (I, dashed-dotted line). Cell concentration is given based on the measurement of (i) on-line biomass probe ([X]sensor ($g \cdot L^{-1}$), solid line), (ii) off-line dry weight (DW ($g \cdot L^{-1}$), ▲) and (iii) off-line optical density at 750 nm (OD, ●). The steady-state values attained at each of the 3 phases are reported in Table 3.5 and correspond to Run 1 (D=0.013 h^{-1}; I=41 $W \cdot m^{-2}$), Run 3 (D=0.013 h^{-1}; I=194 $W \cdot m^{-2}$) and Run 7 (D=0.028 h^{-1}; I=10 $W \cdot m^{-2}$).

Initially, illumination level is fixed at 41 $W \cdot m^{-2}$ and dilution rate at 0.013 h^{-1}, which corresponds to a liquid flow rate of 1 $L \cdot h^{-1}$ (Run 1). After 7 residence times of steady-state operation, illumination was increased to 194 $W \cdot m^{-2}$, while maintaining the same dilution rate (Run 3). At this point, the biomass concentration started to increase indicating that in the previous conditions illumination was the limiting factor. Once the new steady-state values are kept for more than 4 residence times, illumination is decreased to 10 $W \cdot m^{-2}$ and dilution rate is increased to 0.028 h^{-1} (Run 7). Due to the higher liquid flow rates of 2.15 $L \cdot h^{-1}$ and to the lower illumination level, biomass concentration diminished until a stable value is achieved and kept during more than 6 residence times. *Arthrospira* concentration and productivity values attained at each steady state are shown in Table 3.5 (Run 1, 3, and 7). Moreover, the evolution of CO_2 uptake, O_2 production and nitrogen consumption through time corresponding to this tests (Run 1, 3, and 7) are show in Figure 3.9, Figure 3.10 and Figure 3.11, presented in the subsequent sections.

As mentioned, Table 3.5 shows the mean values of such biomass related variables (OD, DW and [X]sensor) at the steady state phase for each of the continuous cultures carried out at different dilution rates (D) and light intensity values (I). In order to determine the steady-state operation of the bioreactor, the linear regression of the biomass concentration along time is calculated. If the p-value associated to the linear regression slope is higher than 0.05, indicates that at an alpha (α) level of 0.05 (95% confidence) the biomass concentration is independent of time. Thus, when time does not influence biomass concentration, it can be considered that the system has finally entered the steady-state phase.

The levels of dilution rates and irradiance were determined using a Central Composite Design where the tree runs in the center point and their corresponding codified values are named as Dc and Ic, respectively. In addition to the CCD runs, four additional tests were repeated at the same conditions of some of the CCD runs (R1, R4, R5 and R6) to verify steady-state values obtained. The biomass productivity values (Px and Px sensor) are obtained multiplying the dilution rate by the biomass composition measured as DW and with the biomass sensor respectively. For repeated runs R1 and R6, biomass sensor measurement is not available because a malfunction of probe transmitter.

Table 3.5 Results of biomass concentration measured for the various steady-states corresponding to CCD analysis, with different dilution rates (D) and illumination intensities (I) (Dc and Ic show the corresponding codified values. In addition to the CCD runs, repeated runs are also provided. Cell concentration is given based on on-line probe measurement, [X]sensor, and direct off-line measurement [X] (equivalent to DW), and similarly for productivity Px and Px sensor.

Test	Dc	Ic	D (h^{-1})	I ($W \cdot m^{-2}$)	OD (750 nm)	DW ($g \cdot L^{-1}$)	[X]sensor ($g \cdot L^{-1}$)	Px ($mg \cdot L^{-1} \cdot h^{-1}$)	Px sensor ($mg \cdot L^{-1} \cdot h^{-1}$)
A. Runs for the experimental Design (CCD, no=3)									
1	-1	-1	0.0133	41	1.0±0.2	0.61±0.06	0.75±0.04	7.8±0.9	11±2
3	-1	1	0.0133	194	2.2±0.1	1.32±0.06	1.73±0.09	16.3±0.8	22±1
4	1	1	0.0437	194	0.95±0.01	0.62±0.01	0.70±0.02	27±1	31±2
5	-1.414	0	0.0070	118	1.56±0.05	1.19±0.04	1.24±0.04	8.6±0.4	9.0±0.3
6	1.414	0	0.0500	118	0.66±0.07	0.44	0.53±0.06	13±9	16±11
7	0	-1.414	0.0285	10	0.14±0.06	0.17±0.03	0.10±0.02	4.3±0.7	2.4±0.4
8	0	1.414	0.0285	225	1.57±0.03	0.91±0.07	1.16±0.05	24±2	31±2
9	0	0	0.0285	118	1.18±0.03	0.83±0.03	0.88±0.03	20.0±0.6	21.7±0.5
10	0	0	0.0285	118	1.12	0.78	0.91±0.02	17.4	19.9
11	0	0	0.0285	118	1.26±0.04	0.92±0.04	0.97±0.04	25±1	27±2
B. Repeated runs of the CCD									
R1	-1	-1	0.0133	41	0.87±0.07	0.49±0.02	-	9±3	-
R4	1	1	0.0437	194	0.59±0.01	0.62±0.05	0.47±0.03	26±2	20±1
R5	-1.414	0	0.0070	118	1.2±0.24	1.0±0.1	1.03±0.21	7.1±0.9	7±2
R6	1.414	0	0.0500	118	0.71±0.04	0.50±0.06	-	21.4±0.2	-

Due to the fact that cell concentrations ($g \cdot L^{-1}$) obtained with the on-line biomass sensor and the off-line DW analyses are in agreement, the reliability of the probe measurement is demonstrated. Moreover, because biomass concentration present the same trend regardless the technique used for its measurement, it was decided to generate the response surface for the *Arthrospira* concentration and productivity adjusting [Eq. 3.5] to the results obtained in the CCD runs and the repeated runs only for DW and Px.

$$Y_n = b_0 + b_1 \cdot D_c + b_2 \cdot I_c + b_{11} \cdot D_c^2 + b_{22} \cdot I_c^2 + b_{12} \cdot D_c \cdot I_c \quad \text{[Eq. 3.5]}$$

In [Eq. 3.5] Yn is the predicted response for the dependent variable (DW, Px), Dc is the codified value for the dilution rate (D, h^{-1}) and Ic is the codified value for the light intensity (I, $W \cdot m^{-2}$).

The surface response for biomass concentration is presented in Figure 3.7 and the corresponding regression coefficients and Analysis of Variance (ANOVA) values are shown in Table 3.6 and Table 3.7 respectively.

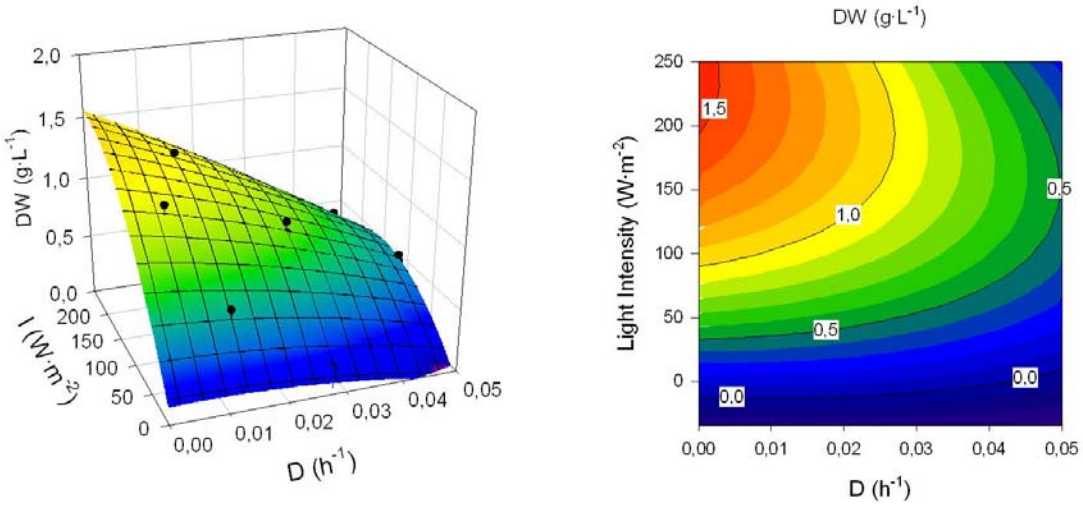

Figure 3.7 Response surface and contour diagrams for the biomass concentration (DW, $g \cdot L^{-1}$) as a function of dilution rate (D, h^{-1}) and light intensity supplied to the bioreactor (I, $W \cdot m^{-2}$).

Table 3.6 Regression coefficient for the biomass DW as a function of coded values for dilution rate (Dc) and light intensity (Ic), with r^2= 0.967 and SE of DW=0.07

Factor	Coefficient	Standard Error	t-value	p-value
b_0	0.84	0.04	20.4	<0.0001
b_1 (Dc)	-0.23	0.02	-10.7	<0.0001
b_2 (Ic)	0.29	0.03	10.3	<0.0001
b_{11} (Dc^2)	-0.02	0.03	-0.9	0.4
b_{22} (Ic^2)	-0.14	0.03	-4.6	0.002
b_{12} (Dc·Ic)	-0.10	0.04	-2.7	0.03

Table 3.7 ANOVA for the biomass DW as a function of dilution rate (Dc) and light intensity (Ic). Acronyms of parameters shown are: degrees of freedom (df), Sum of Squares (SS) and Mean Squares (MS).

	df	SS	MS	F-ratio	p-value
Regression	5	1.21	0.24	47.6	<0.0001
Residual	8	0.04	0.005		
Total	13	1.26	0.097		

A p-value associated to the parameters coefficient estimates higher than 0.05 indicates that the corresponding factor does not contribute to describe the response. Taking this into account, the following model can be used to generate the response surface (Figure 3.7).

$$DW\ (g \cdot L^{-1}) = 0.84 - 0.23 \cdot D_c + 0.29 \cdot I_c - 0.14 \cdot I_c^2 - 0.10 \cdot D_c \cdot I_c \qquad \text{[Eq. 3.6]}$$

Based on the F-test, the model is predictive since its F-ratio is higher than unity, which means that the independent variables contribute to the prediction of the biomass concentration.

Moreover, the regression correlation coefficient (r^2=0.967) is considerably close to unity indicating the equation is a good description of the relation between the independent and the dependent variables.

In order to confirm biomass concentration (DW) estimated with the response surface methodology model [Eq. 3.6], five extra continuous cultures (C1-C5) were done at different dilution rates and illumination levels from the CCD runs. Table 3.8 compares estimated DW values using [Eq. 3.6] with empirical DW obtained in the steady-state phase of the confirmation tests.

Table 3.8 Comparison between empirical DW ($g \cdot L^{-1}$) obtained in the confirmation test C1-C5 carried out at different dilution rates (D) and illumination levels (I) and the estimated DW using the response surface model as described in [Eq. 3.6]. Dc is the codified value for the dilution rate (D) and Ic is the codified value for light intensity (I), calculated as indicated in [Eq. 3.3] and [Eq. 3.4]. Relative error (%) is calculated in respect to the empirical value.

Test	Dc	Ic	D (h^{-1})	I ($W \cdot m^{-2}$)	Estimated DW ($g \cdot L^{-1}$)	Empirical DW ($g \cdot L^{-1}$)	Error (%)
C1	-1	-1.16	0.0133	30	0.43	0.40±0.05	-7.3
C2	-1	0	0.0133	118	1.07	1.13±0.02	5.3
C3	-0.59	-1	0.0195	41	0.49	0.52±0.04	6.4
C4	0	-1	0.0285	41	0.41	0.39±0.02	-5.1
C5	0	-1	0.0285	41	0.41	0.40±0.02	-2.5

The low calculated relative errors ranging from 2-7% (Table 3.8) indicate that the predicted values are in good agreement with experimental *Arthrospira* concentration obtained in the confirmation tests, corroborating the validity of the DW model shown in [Eq. 3.6]. Figure 3.7 illustrates that the highest biomass concentration inside the bioreactor are obtained at the highest light intensity values and at low dilution rates.

The surface response for productivity is shown in Figure 3.8 and the corresponding regression coefficients and ANOVA analysis are summarized in Table 3.9 and Table 3.10 respectively.

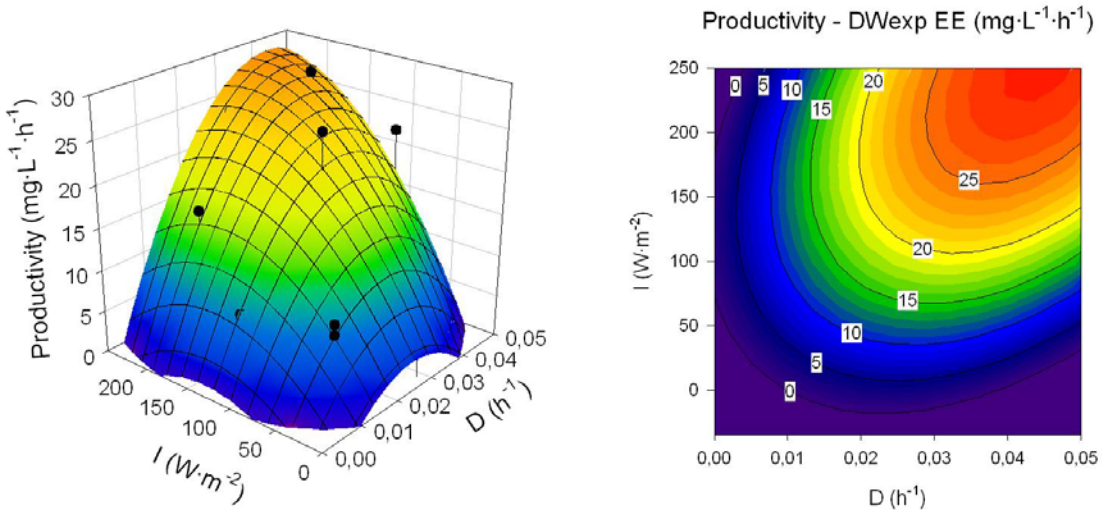

Figure 3.8 Response surface and contour diagrams for the *Arthrospira* productivity (Px, $mg \cdot L^{-1} \cdot h^{-1}$) as a function of dilution rate (D, h^{-1}) and light intensity supplied to the bioreactor (I, $W \cdot m^{-2}$).

Table 3.9 Regression coefficient for the biomass productivity (Px) as a function of dilution rate (Dc) and light intensity (Ic), with r^2= 0.902 and SE of Px=3.16.

Factor	Coefficient	Standard Error	t-value	p-value
b_0	21	1.8	11.4	<0.0001
b_1 (Dc)	2.7	0.9	2.9	0.02
b_2 (Ic)	6.9	1.1	5.9	0.0003
b_{11} (Dc^2)	-4	1.2	-3.4	0.009
b_{22} (Ic^2)	-2.9	1.3	-2.1	0.06
b_{12} (Dc·Ic)	3.2	1.6	1.9	0.09

Table 3.10 ANOVA for the biomass productivity as a function of dilution rate (Dc) and light intensity (Ic). Acronyms of parameters shown are: degrees of freedom (df), Sum of Squares (SS) and Mean Squares (MS).

	df	SS	MS	F-ratio	p-value
Regression	5	738	147	14.8	0.0007
Residual	8	80	10		
Total	13	818	63		

Considering the p-value associated to the parameters coefficient estimates, the model to generate the response surface for the productivity is described by [Eq. 3.7].

$$Px\,(mg{\cdot}L^{-1}{\cdot}h^{-1}) = 21 + 2.7 \cdot D_c + 6.9 \cdot I_c - 4 \cdot D_c^2 \qquad \text{[Eq. 3.7]}$$

Like in the response surface for biomass concentration, the model for productivity can be considered predictive due to the F-ratio value (Table 3.10) and the fairly close regression correlation coefficient value to unity (r^2=0.902). Figure 3.8 shows that the highest productivity value is obtained at the highest irradiance level 250 $W{\cdot}m^2$ and at dilution rates between 0.04-0.05 h^{-1}.

Particularly, as reported in Table 3.5, the maximum empirical productivity of 27 $mg{\cdot}L^{-1}{\cdot}h^{-1}$ is obtained at a dilution rate of 0.044 h^{-1} and at an illumination level of 194 $W{\cdot}m^{-2}$ (Run 4). Such value will be used in the mass balance model developed to evaluate the integration of the photosynthetic compartments within the MPP (Chapter 8).

3.3.1.2 CO_2 UPTAKE

Similarly as done for the biomass production, although steady-state values of carbon dynamics are reported in Table 3.11 for each of the continuous cultures performed at different D and I levels, for simplicity the evolution with time of carbon concentration in liquid and gas flow rates along time is depicted only for some of the tests.

Thus, Figure 3.9 illustrates total carbon (TC) and total organic carbon (TOC) content in the liquid outflow and the CO_2 concentration (%) in inlet and outlet gas flow during the continuous cultures performed at three different culture conditions, which correspond to those defined for runs 1 (D=0.013 h^{-1}, I=41 $W{\cdot}m^{-2}$), 3 (D=0.013 h^{-1}, I=194 $W{\cdot}m^{-2}$) and 7 (D=0.028 h^{-1}, I=10 $W{\cdot}m^{-2}$). The corresponding biomass production of this culture has been previously depicted in Figure 3.6.

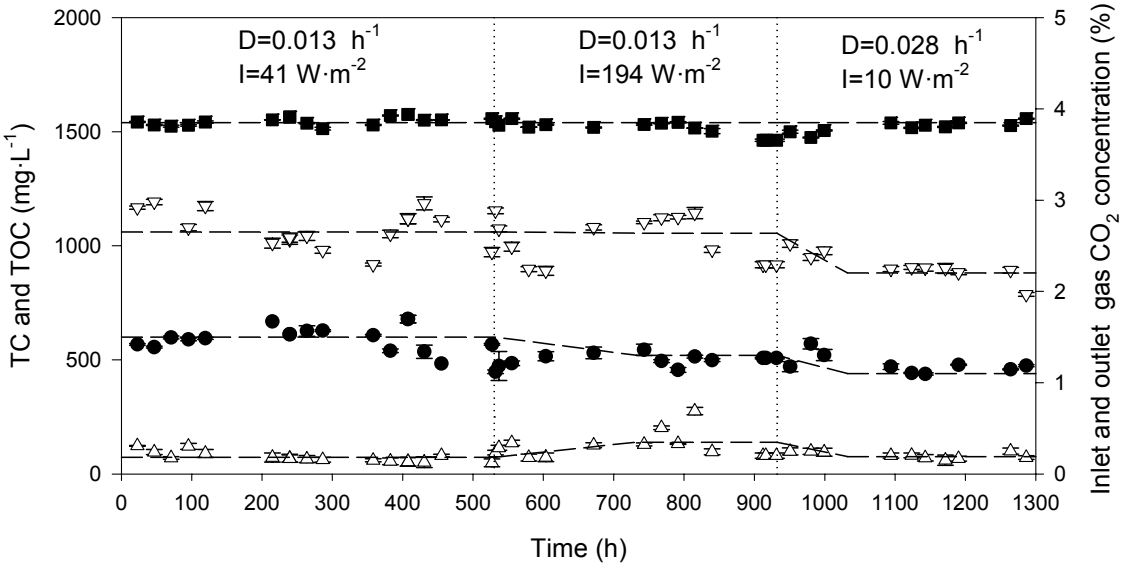

Figure 3.9 Evolution of total carbon (TC, empty ▼) and organic carbon (TOC, empty ▲) concentration ($mg \cdot L^{-1}$) in liquid output flow rate and CO_2 concentration (%) in of inlet (■) and outlet (●) gas flow rates during the continuous cultures carried out at different dilution rates (D) and illumination levels (I). The steady-state values attained at each of the 3 phases are reported in Table 3.11 and correspond to Run 1 (D=0.013 h^{-1}; I=41 $W \cdot m^{-2}$), Run 3 (D=0.013 h^{-1}; I=194 $W \cdot m^{-2}$) and Run 7 (D=0.028 h^{-1}; I=10 $W \cdot m^{-2}$).

In order to determine the CO_2 consumption the following parameters are calculated:

- Error (%): Ratio between carbon balance (mol $C \cdot d^{-1}$), determined as [CO_2 gas inflow - CO_2 gas outflow - TC liquid outflow- Biomass C content], and input carbon flow rate (mol $C \cdot d^{-1}$ in gas inflow).
- Daily CO_2 uptake (mol $C \cdot d^{-1}$): Determined as [CO_2 gas inflow - CO_2 gas outflow - TC liquid outflow]
- CO_2 volumetric consumption rate, r_{CO2} (mmol $C \cdot L^{-1} \cdot h^{-1}$): Ratio between daily CO_2 uptake and culture volume (V=77L).
- CO_2 specific consumption rate, q_{CO2} (mmol $C \cdot g^{-1} \cdot h^{-1}$): Ratio between r_{CO2} (mmol $C \cdot L^{-1} \cdot h^{-1}$) and biomass concentration (DW, $g \cdot L^{-1}$) as reported in Table 3.5.

Table 3.11 shows the above mentioned parameters for each steady-state of the continuous cultures planned with the CCD, except for run 6 (D=0.05 h^{-1}, I=118 $W \cdot m^{-2}$), where CO_2-O_2 analyzer was not working properly. Moreover for run 9, 10 and 11 the mean value is shown, since this 3 runs are replicates carried out in the same culture conditions.

Similarly as done for the biomass concentration (DW) and productivity (Px), [Eq. 3.5] was used to evaluate whether a response model of CO_2 consumption as a function of dilution rate and light intensity could be obtained. However, low values of regression coefficients indicated that such a simple relation cannot be used for predicting CO_2 uptake.

Table 3.11 Results of CO_2 concentration in the input and output gas flow (%), carbon composition of the output liquid flow (TC, TIC and TOC), daily CO_2 gas uptake, CO_2 volumetric consumption rate (r_{CO2}), CO_2 and specific consumption rate (q_{CO2}) for each of the *Arthrospira* cultures performed at different dilution rates (D) and intensity values (I).

Run	D	I	Error	$[CO_2]$ in	$[CO_2]$ out	TC	TIC	TOC	Daily CO_2 uptake	r_{CO2}	q_{CO2}
	(h^{-1})	($W \cdot m^{-2}$)	%	%	%	$g \cdot L^{-1}$	$g \cdot L^{-1}$	$g \cdot L^{-1}$	$mol \cdot d^{-1}$	$mmol \cdot L^{-1} \cdot h^{-1}$	$mmol \cdot g^{-1} h^{-1}$
1	0.0133	41	14	3.9	1.5	1.06	0.99	0.07	1.26	0.68	1.10
3	0.0133	194	2	3.8	1.3	1.06	0.92	0.14	1.26	0.68	0.52
4	0.0437	194	-15	4.5	1.5	0.52	0.38	0.14	0.92	0.50	0.80
5	0.0070	118	28	3.7	2.1	0.73	0.67	0.06	1.42	0.77	0.77
7	0.0285	10	-5	3.8	1.1	0.88	0.81	0.08	0.22	0.12	0.72
8	0.0285	225	0	3.7	1.3	0.45	0.37	0.08	1.61	0.87	0.95
M(9,10,11)	0.0285	118	8	3.8	1.4	0.48	0.39	0.09	1.83	0.99	1.24

3.3.1.3 OXYGEN PRODUCTION

Like in the previous sections, the evolution of oxygen production is depicted only for some of the tests, though the steady-state values of related O_2 parameters are reported in Table 3.12 for each of the continuous cultures.

Figure 3.10 depicts dissolved oxygen (%), O_2 concentration (%) in inlet and outlet gas flow during the continuous cultures performed at three different culture conditions, which correspond to the ones defined for runs 1 (D=0.013 h^{-1}, I=41 $W \cdot m^{-2}$), 3 (D=0.013 h^{-1}, I=194 $W \cdot m^{-2}$) and 7 (D=0.028 h^{-1}, I=10 $W \cdot m^{-2}$). Figure 3.10 does not include the measure of dissolved O_2 during the short time periods where the O_2 probe was not measuring properly. It can be seen that the oxygen production increases at higher illumination levels, where the biomass concentration is also higher (Figure 3.6).

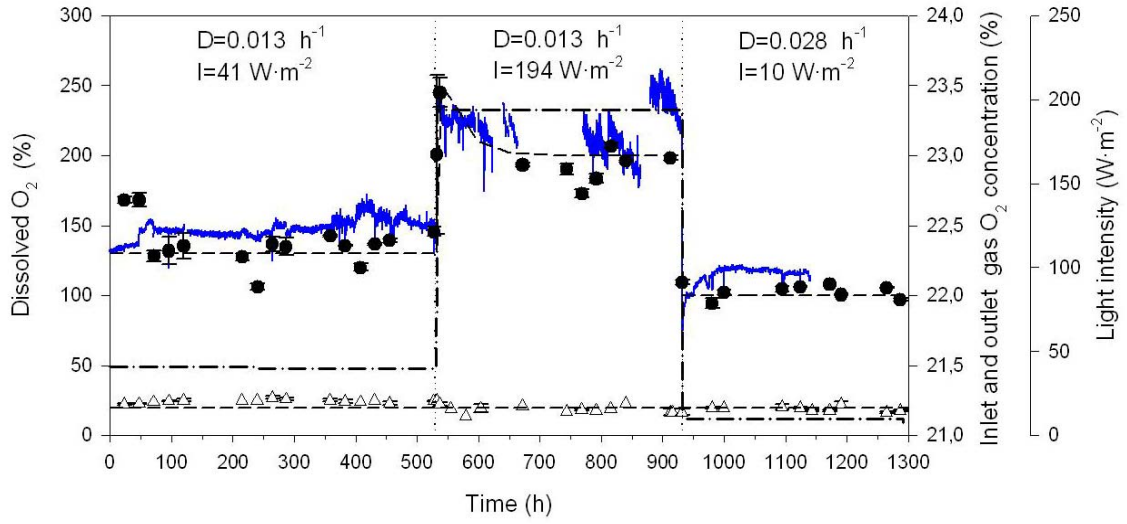

Figure 3.10 Evolution of dissolved oxygen (%, solid line) and O_2 concentration (%) in inlet (empty ▲) and outlet (●) gas flow rates during the continuous cultures carried out at different dilution rates (D) and illumination levels (I, dashed-dotted line). The steady-state values attained at each of the 3 phases are reported in Table 3.12 and correspond to Run 1 (D=0.013 h^{-1}; I=41 $W \cdot m^{-2}$), Run 3 (D=0.013 h^{-1}; I=194 $W \cdot m^{-2}$) and Run 7 (D=0.028 h^{-1}; I=10 $W \cdot m^{-2}$).

The parameters related to the oxygen production are calculated as indicated:

- Error (%): Ratio between oxygen balance (mol $O_2 \cdot d^{-1}$), determined as [O_2 gas outflow + O_2 liquid outflow + Biomass O_2 content - O_2 gas inflow], and input O_2 gas flow rate (mol $O_2 \cdot d^{-1}$ in gas inflow).
- Daily O_2 production (mol $O_2 \cdot d^{-1}$): Determined as [O_2 gas outflow + O_2 liquid outflow - O_2 gas inflow]
- O_2 volumetric production rate, r_{O2} (mmol $O_2 \cdot L^{-1} \cdot h^{-1}$): Ratio between daily O_2 production and culture volume (V=77L).
- O_2 specific production rate, q_{O2} (mmol $O_2 \cdot g^{-1} \cdot h^{-1}$): Ratio between r_{O2} (mmol $O_2 \cdot L^{-1} \cdot h^{-1}$) and biomass concentration (DW, $g \cdot L^{-1}$) as reported in Table 3.5.
- Photosynthetic quotient, PQ: Ratio of mols O_2 evolved to mols of CO_2 consumed, calculated as ratio between r_{O2} and r_{CO2}.

In Table 3.12 the above mentioned parameters are shown for each of the steady-state of the continuous cultures, except for run 6 (D=0.05 h^{-1}, I=118 $W \cdot m^{-2}$), since as mentioned in the previous section the CO_2-O_2 analyzer was not working properly. Also, the mean value of the 3 replicates performed at the center point of the CCD (run 9,10 and 11) is calculated.

Table 3.12 Results of O_2 concentration in the input and output gas flow (%), dissolved oxygen (%) and O_2 composition of the output liquid flow ($mg \cdot L^{-1}$), daily O_2 gas production, O_2 volumetric production rate (r_{O2}), O_2 specific production rate (q_{O2}) and photosynthetic quotient (PQ) for each of the *Arthrospira* cultures performed at different dilution rates (D) and intensity values (I).

Run	D	I	Error	$[O_2]$ gas-in	$[O_2]$ gas-out	Dissolved O_2	O_2 liq-out	Daily O_2 production	r_{O2}	q_{O2}	PQ
	(h^{-1})	($W \cdot m^{-2}$)	%	%	%	%	$mg \cdot L^{-1}$	$mol \cdot d^{-1}$	$mmol \cdot L^{-1} \cdot h^{-1}$	$mmol \cdot g^{-1} h^{-1}$	
1	0.0133	41	5	21.2	22.3	147	10.0	1.6	0.87	1.41	1.3
3	0.0133	194	7	21.2	23.0	216.7	14.9	2.0	1.11	0.85	1.6
4	0.0437	194	9	22.5	24.2	168	11.1	2.4	1.32	2.12	2.7
5	0.0070	118	6	22.6	23.9	167	10.7	2.1	1.16	0.97	1.5
7	0.0285	10	4	21.2	22.0	117	8.2	1.0	0.54	3.25	4.5
8	0.0285	225	8	21.2	22.9	231	15.2	2.4	1.32	1.45	1.5
M(9,10,11)	0.0285	118	9	21.2	23.1	156	10	2.8	1.52	1.89	1.5

Like for CO_2 consumption, no simple relation of oxygen production as function of dilution rate and illumination levels have been found. However, this values (Table 3.12) together with the biomass production rates obtained (Table 3.5, Figure 3.7, Figure 3.8) can be now used to define the operational conditions of this compartment, in respect to the rest of the MELiSSA loop, and in order to provide the necessary output for *Arthrospira* and O_2 production.

3.3.1.4 NITROGEN UPTAKE

As an example of the nitrogen evolution during the continuous cultures, Figure 3.11 shows the nitrogen concentration in the liquid inflow and outflow for *Arthrospira* cultures carried out at three different culture conditions, which correspond to the ones defined for runs 1 (D=0.013 h^{-1}, I=41 $W \cdot m^{-2}$), 3 (D=0.013 h^{-1}, I=194 $W \cdot m^{-2}$) and 7 (D=0.028 h^{-1}, I=10 $W \cdot m^{-2}$). Previous figures have depicted the corresponding biomass production (Figure 3.6), CO_2 consumption (Figure 3.9) and oxygen production (Figure 3.10) obtained in the same conditions.

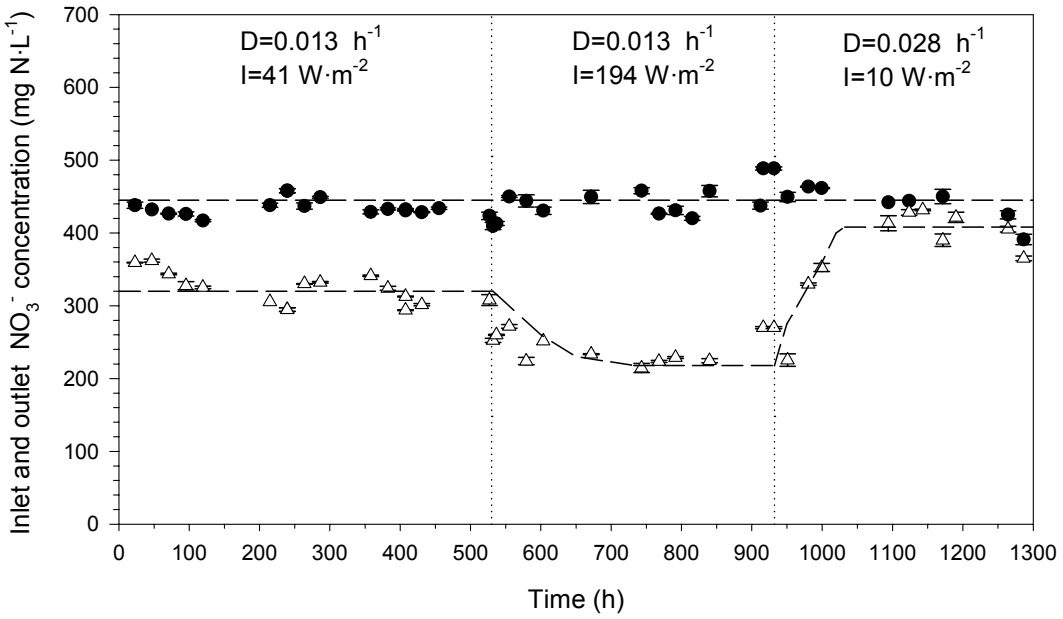

Figure 3.11 Evolution of nitrate concentration (mg $N \cdot L^{-1}$) in inlet (●) and outlet (empty ▲) liquid flow rates during the continuous cultures carried out at different dilution rates (D) and illumination levels (I). The steady-state values attained at each of the 3 phases are reported in Table 3.13 and correspond to Run 1 (D=0.013 h^{-1}; I=41 $W \cdot m^{-2}$), Run 3 (D=0.013 h^{-1}; I=194 $W \cdot m^{-2}$) and Run 7 (D=0.028 h^{-1}; I=10 $W \cdot m^{-2}$).

For the N consumption the following parameters are determined as described:

- Error (%): Ratio between nitrogen balance (mol $N \cdot d^{-1}$), determined as [N liquid inflow - N liquid outflow - Biomass N content], and input nitrogen flow rate (mol $N \cdot d^{-1}$ in liquid inflow).
- Daily N uptake (mol $N \cdot d^{-1}$): Determined as [N liquid inflow – N liquid outflow]
- N volumetric consumption rate, r_N (mmol $N \cdot L^{-1} \cdot h^{-1}$): Ratio between daily N uptake and culture volume (V=77L).
- N specific consumption rate, q_N (mmol $N \cdot g^{-1} \cdot h^{-1}$): Ratio between r_N (mmol $N \cdot L^{-1} \cdot h^{-1}$) and biomass concentration (DW, $g \cdot L^{-1}$) as reported in Table 3.5.
- Yield of nitrogen uptake to biomass, $Y_{N/X}$ (g $N \cdot g^{-1}$ biomass)

In Table 3.13 the nitrogen related parameters are shown for each of the cultures, except for the 3 replicates performed in the center point of the CCD (run 9, 10 and 11) where instead its mean is included.

Table 3.13 Results of nitrate concentration in the input and output liquid flow (mg $N\text{-}NO_3^-\cdot L^{-1}$), daily nitrate uptake (mol $N\cdot d^{-1}$), N volumetric consumption rate (r_N), N specific consumption rate (q_N) and yield of N uptake to biomass ($Y_{N/X}$) for each of the *Arthrospira* cultures performed at different dilution rates and intensity values. (CCD runs, repeated tests of the CCD runs and confirmation tests).

Run	D	I	Error	[N] liq-in	[N] liq-out	$N\text{-}NO_3^-$ uptake	r_N	q_N	$Y_{N/X}$
	(h^{-1})	($W\cdot m^{-2}$)	%	$mg\cdot L^{-1}$	$mg\cdot L^{-1}$	$mol\cdot d^{-1}$	$mmol\cdot L^{-1}\cdot h^{-1}$	$mmol\cdot g^{-1}h^{-1}$	$g\ N\cdot g^{-1}$
1	0.0133	41	12	435	320	0.20	0.11	0.18	0.19
3	0.0133	194	20	449	218	0.40	0.22	0.17	0.17
4	0.0437	194	8	419	323	0.55	0.28	0.48	0.15
5	0.0070	118	5	436	302	0.12	0.07	0.06	0.11
6	0.0500	118	-2	410	368	0.28	0.15	0.30	0.08
7	0.0285	10	6	452	408	0.17	0.09	0.54	0.27
8	0.0285	225	14	460	299	0.60	0.33	0.36	0.18
M(9,10,11)	0.0285	118	4	396	297	0.38	0.20	0.24	0.12

3.3.2 *ARTHROSPIRA* BIOMASS COMPOSITION

The elemental (C, H, N, S), macromolecular (proteins, carbohydrates, glycogen, fatty acid profile, nucleic acids) and pigment (chlorophyll and phycobilisomes) composition of *Arthrospira* biomass harvested at the steady state of each of the continuous cultures was analyzed.

Since the biomass of each of the runs defined by the Central Composite Design was grown under different dilution rates and light intensity values, the effect of these two factors on *Arthrospira* composition can be analyzed. Two different techniques were used for detecting any influence of dilution rate or light intensity on biomass composition. First, the response surface methodology was applied to each of the analyzed compounds of the biomass harvested at each steady state. Particularly, the averaged values of at least three replicates for each compound was considered the response variable of [Eq. 3.1]. The p-value associated to each of the parameters estimates was used to determine whether the independent variable significantly influenced the response. Secondly, the previous results were confirmed evaluating the effect of light intensity on biomass composition using data obtained at the dilution rate of 0.029 h^{-1} using the p-value associated to the slope of the linear regression.

Table 3.14 shows the elemental composition of *Arthrospira* biomass obtained in the different continuous cultures performed at different dilution rates and light intensity values selected with the CCD. The percentages of the elements (%DW biomass) do not sum up to 100%, since the determination of the oxygen, phosphorous and ashes content was not carried out. Last column contains the molecular formula of *Arthrospira* based on the analyzed elements (C, H, N and S).

Percentages of carbon (39 - 46%), hydrogen (5.5 - 6.6%) and nitrogen (8.3 - 10.6%) on *Arthrospira* biomass are in agreement with values reported by Marty (1997) and Vernerey (2000). Neither the RSM nor the linear regression approach detected any significant influence ($p>0.05$) of dilution rate and light intensity on percentage of C, H, N and S in *Arthrospira* biomass grown using CO_2 as carbon source.

Table 3.14 Elemental composition analysis (Mean± standard deviation of n samples analyzed) of *Arthrospira* biomass obtained at the steady state of each run. The dilution rate (D) and light intensity (I) levels used for each run were determined using a Central Composite Design (CCD) with 3 replicates in the center point. Percentages do not sum up to 100% due to the lack of determination of oxygen, phosphorous and ashes. Last column shows the corresponding molecular formula.

Run	D (h^{-1})	I ($W \cdot m^{-2}$)	n	C (%)	H (%)	N (%)	S (%)	Molecular formula
1	0.013	41	3	43.3±1	6.0±0.1	10.0±0.2	0.51±0.05	$CH_{1.65}N_{0.198}S_{0.004}$
3	0.013	194	6	46.7±0.7	6.5±0.1	10.8±0.2	0.60±0.02	$CH_{1.67}N_{0.199}S_{0.005}$
4	0.044	194	2	45.0±0.2	6.5±0.1	10.30±0.04	0.55±0.02	$CH_{1.74}N_{0.196}S_{0.005}$
5	0.007	118	2	39.2±0.7	5.5±0.1	9.4±0.2	1.05±0.01	$CH_{1.67}N_{0.206}S_{0.01}$
7	0.029	10	4	40±4	5.5±0.5	8.3±0.8	0.46±0.04	$CH_{1.67}N_{0.179}S_{0.004}$
8	0.029	225	3	43±2	6.1±0.3	9.7±0.5	0.50±0.05	$CH_{1.70}N_{0.194}S_{0.004}$
9	0.029	118	2	46.7±0.1	6.4±0.1	10.63±0.05	0.57±0.04	$CH_{1.64}N_{0.195}S_{0.005}$
10	0.029	118	2	45.3±0.2	6.3±0.1	10.2±0.1	0.53±0.01	$CH_{1.67}N_{0.193}S_{0.004}$
11	0.029	118	2	46.0±0.2	6.6±0.1	9.80	0.52	$CH_{1.72}N_{0.183}S_{0.004}$
Mean	-	-	26	44±3	6.1±0.5	9.8±0.9	0.5±0.1	$CH_{1.67}N_{0.192}S_{0.005}$

The macromolecular composition of the *Arthrospira* biomass at different culture conditions is reported in Table 3.15. The content of protein, carbohydrates, total fatty acids and nucleic acids (DNA and RNA) represent in all cases more than 82% of the total biomass dry weight, as shown in the last column.

Table 3.15 Protein, carbohydrates (CH), glycogen, total fatty acid (FA) and nucleic (DNA and RNA) content of *Arthrospira* biomass obtained at the steady state of each run. The dilution rate (D) and light intensity (I) levels used for each run were determined using a Central Composite Design (CCD) with 3 runs in the center point. Values represent the mean value (± standard deviation) of at least 3 samples analyzed per triplicate. Last column correspond to the addition of protein, CH, FA and nucleic acids percentages.

Run	D (h^{-1})	I ($W \cdot m^{-2}$)	Protein (%)	Carbohydrates (%)	Glycogen (%)	Fatty acids (%)	Nucleic acid (%)	Total (%)
1	0.013	41	76±7	11±1	5±1	4.75±0.06	7.1±0.9	99
3	0.013	194	70±5	10±1	6±1	5.40±0.02	4±2	89
4	0.044	194	64±5	-	16±2	3.80±0.04	5±1	-
5	0.007	118	57±3	7.4±0.1	3.9±0.3	5.03±0.03	2.1±0.7	71
7	0.029	10	75±8	15±1	5.7±0.3	4.1±0.3	3±1	97
8	0.029	225	58±6	12.8±0.3	7±1	5.29±0.06	6.2±0.8	82
9	0.029	118	59±2	12±1	8.43±0.03	5.24±0.01	6.3±0.5	82
10	0.029	118	60±4	18±1	8.3±0.3	4.90±0.04	7.1±0.9	90
11	0.029	118	68±2	16±5	11±1	4.4±0.1	2.3±0.8	90
Mean	-	-	65±7	13±3	8±4	5±1	5±2	90

Table 3.16 Fatty acid (FA) profile (mg·g^{-1} DW) of *Arthrospira* biomass obtained at the steady state of each run. The dilution rate (D) and light intensity (I) levels used for each run were determined using a Central Composite Design (CCD) with 3 runs replicates in the centre point of the experimental domain. Values represent the mean value of at least two samples. The total amount of fatty acids saturated (SFA), monounsaturated (MUFA) and polyunsaturated (PUFA) are also shown.

Run	D (h^{-1})	I ($W \cdot m^{-2}$)	C16:0 Palmitic	C16:1(t) Palmitelaidic	C16:1(c) Palmitoleic	C18:0 Stearic	C18:1(c) Oleic	C18:2(c) Linoleic	C18:3(c) γ-Linoleic	Total SFA	Total MUFA	Total PUFA	PUFA/SFA
1	0.013	41	23.8	0.5	1.1	0.7	4.9	7.7	8.9	24.5	6.5	16.6	0.67
3	0.013	194	27.3	0.5	1.3	0.9	4.9	9.2	10.0	28.1	6.7	19.2	0.68
4	0.044	194	19.6	-	0.6	0.6	2.4	7.0	7.9	20.2	3.0	14.8	0.73
5	0.007	118	25.8	0.6	1.5	0.6	3.8	9.5	8.7	26.4	5.9	18.1	0.68
7	0.029	10	20.5	-	0.9	0.9	4.1	6.7	7.9	21.3	5.0	14.6	0.68
8	0.029	225	26.0	-	0.8	1.0	5.2	9.8	10.2	27.0	6.0	20.0	0.74
9	0.029	118	26.6	-	0.8	1.1	5.0	9.1	9.8	27.7	5.8	18.9	0.68
10	0.029	118	24.4	-	0.8	1.1	4.6	8.6	9.5	25.5	5.4	18.1	0.71
11	0.029	118	22.8	-	0.8	0.7	2.6	7.8	9.5	23.4	3.4	17.2	0.73

Table 3.17 Fatty acid profile (% total FA) of *Arthrospira* biomass obtained at the steady state of each run. The dilution rate (D) and light intensity (I) levels used for each run were determined using a Central Composite Design (CCD) with 3 runs in the centre point of the experimental domain.

Run	D (h^{-1})	I ($W \cdot m^{-2}$)	C16:0 Palmitic	C16:1(t) Palmitelaidic	C16:1(c) Palmitoleic	C18:0 Stearic	C18:1(c) Oleic	C18:2(c) Linoleic	C18:3(c) γ-Linoleic
1	0.013	41	50	1	2	1	10	16	19
3	0.013	194	50	1	2	2	9	17	19
4	0.044	194	52	-	2	2	6	18	21
5	0.007	118	51	1	3	1	8	19	17
7	0.029	10	50	-	2	2	10	16	19
8	0.029	225	49	-	2	2	10	19	19
9	0.029	118	51	-	2	2	10	17	19
10	0.029	118	50	-	2	2	9	18	19
11	0.029	118	52	-	2	1	6	18	21

The protein content of *Arthrospira* biomass ranged from 57 to 76 %. Although some authors found lower protein contents, comprised between 38 and 59 % (Marty, 1997; Vernerey, 2000; Morist *et al.*, 2001), others found similar high protein levels (60-70%) in *Arthrospira* biomass (Ciferri, 1983). Moreover, the nutritional quality of this protein is of great value due to its amino acid profile, which includes all the essential amino acids (Ciferri and Tiboni ,1985; Babadzhanov *et al.*, 2004).

Carbohydrates represent between 7% and 18% of the *Arthrospira* biomass, which are similar to reference values (Ciferri and Tiboni, 1985; Becker and Venkataraman, 1984; Marty, 1997; de Oliveira *et al.*, 1999). The glycogen content of *Arthrospira* represent between a 37% and 70% of the total amount of carbohydrates.

The total fatty acid (FA) content oscillates between 4% and 5%, which represent the addition of all the FA acid identified in *Arthrospira* biomass. The fatty acid profile is presented in Table 3.16, as a percentage of biomass (mg FA·g^{-1} DW), and in Table 3.17, as percentage of total FA (%). Moreover, the subtotals corresponding to total fatty acids saturated (SFA), monounsaturated (MUFA) and polyunsaturated (PUFA) were also included.

The predominant fatty acids were palmitic acid (C16:0), γ-linoleic acid (C18:3) (GLA), linoleic acid (C18:2), oleic acid (C18:1), palmitoleic acid (C16:1), which are in agreement with the order of FA abundance found in several bibliographic studies (Morist *et al.*, 2001; de Oliveira *et al.*, 1999; Mühling *et al.*, 2005b; Babadzhanov *et al.,* 2004; Maslova *et al.*, 2004). The PUFA/SFA ratio was higher than the recommended ratio of 0.45 for the human diet in most of the test, similarly to results reported by Morist *et al*. (2001). However, the levels of GLA found are slightly lower than the GLA content (23-31%) found by Morist *et al.* (2001) and Olguín *et al.* (2001).

The nucleic acid content in *Arthrospira* is reported to be about 4-6% (Ortega *et al.*, 1993), which is in good agreement with values obtained in the biomass analyzed.

Table 3.18 includes the content of chlorophyll (Chl *a* and Chl*b*), phycocyanin (PC), allophycocyanin (APC) and phycoerythrins (PE) in *Arthrospira* biomass (% dw) for each of the continuous runs performed at different light intensities and dilution rates.

Chlorophyll content found in *Arthrospira* biomass harvested in some tests (run 5, 6 and 7) is similar to the 1% Chl *a* values reported in literature (Danesi *et al.*, 2004; Rangel-Yagui *et al.*, 2004; Bhattacharya and Shivaprakash, 2005). However, biomass from the other tests has lower chlorophyll amounts than usually found. Similarly, phycobilisomes content is lower than the bibliographic percentages of 7-17% for PC (Pervushkin *et al.*, 2001; Bhattacharya and Shivaprakash, 2005; Patel *et al.*, 2005) and 3.8 % for APC (Patel *et al.*, 2005; Bhattacharya and Shivaprakash, 2005), though similar to the range of 0.4 to 4% found by Morist *et al.* (2001) for PC.

Table 3.18 Pigment content (Mean± standard deviation of n samples analyzed) of *Arthrospira* biomass obtained at the steady state of each run. The dilution rate (D) and light intensity (I) levels used for each run were determined using a Central Composite Design (CCD) with 3 runs in the center point.

Test	D (h^{-1})	I ($W \cdot m^{-2}$)	n	Chl *a* (%)	Chl *b* (%)	PC (%)	APC (%)	PE (%)
1	0.013	41	3	0.19±0.03	0.13±0.02	2.6±0.7	1.8±0.2	0.61±0.03
3	0.013	194	6	0.8±0.2	0.11±0.02	3±1	2.1±0.6	0.7±0.1
4	0.044	194	3	0.36±0.04	0.02±0.01	0.36±0.08	0.5±0.1	-
5	0.007	118	3	1.02±0.08	0.15±0.01	6.9±0.8	4.5±0.4	0.8±0.2
7	0.029	10	6	0.8±0.2	0.10±0.02	1.8±0.3	1.7±0.3	0.6±0.1
8	0.029	225	3	0.16±0.01	0.10±0.01	2.3±0.6	2.3±0.6	0.8±0.3
9	0.029	118	3	0.14±0.02	0.12±0.02	1.8±0.2	1.7±0.1	0.55±0.06
10	0.029	118	3	0.16±0.02	0.13±0.02	2.4±0.4	2.1±0.3	0.69±0.09
11	0.029	118	3	0.45±0.06	0.02±0.01	0.32±0.01	0.46±0.003	-

Upon the results of the RSM and the linear regression approach, dilution rate has no statistically significant influence ($p>0.05$) on macromolecular and pigment composition of *Arthrospira* biomass. Regarding the effect of light intensity on biomass composition, only the protein and the chlorophyll content are affected. In both cases, an increase in light intensity produces a lower amount of proteins and chlorophylls in *Arthrospira*, which is in agreement with observations found by several authors (Tadros *et al.*, 1993; Tomaselli *et al.*, 1997; Olguín *et al.*, 2001; Danesi *et al.*, 2004), and reflects the Arthrospira adaptation of pigment at lower and high light intensities.

3.3.3 CULTURE RESPONSE TO DISTURBANCES OF NORMAL CULTURE CONDITIONS

During long term operation of a continuous culture, some hardware malfunctions or accidents may occur causing the deviation of the culture conditions from the corresponding set point value. When the deviation is high enough to jeopardize the *Arthrospira* culture, the control system activates the corresponding alarms and sets the pilot bioreactor into a safety operation mode. The reestablishment of normal operation usually takes place either after human actuation or once after the malfunctions are automatically restored. However, sometimes the effects of the disturbance on *Arthrospira* growth are irreversible and lead to cell lysis. Thus, in order to determine not only culture response to deviations from nominal conditions but also to evaluate whether consequences of disturbances are reversible, *Arthrospira* culture was subjected to several alterations of the normal operation conditions. Such information will also contribute to determine culture boundaries, particularly pH, liquid and gas (air and CO_2) flowrate.

3.3.3.1 DISTURBANCE OF PH

Arthrospira culture is maintained at pH 9.6. The measure of the pH sensor is used by the control system to activate the addition of base (1M NaOH) or the acid solution (1M H_2SO_4). Since *Arthrospira* grows photoautotrophically with a continuous input of CO_2 gas, usually only the addition of base is required to maintain pH, as shown in Figure 3.12.

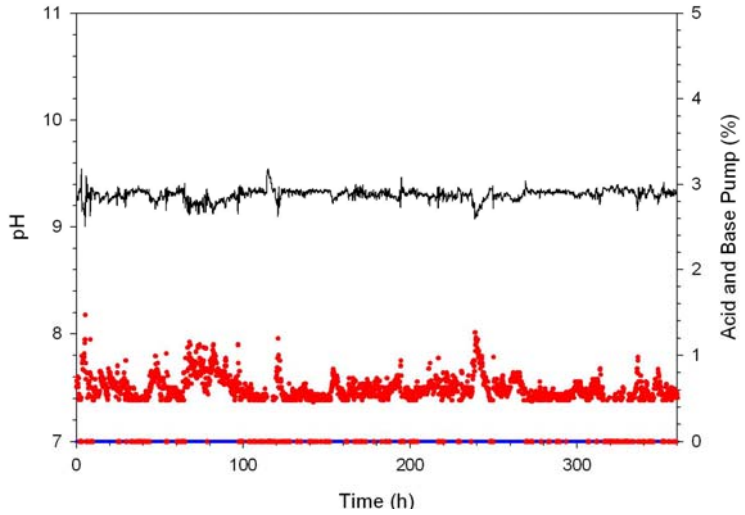

Figure 3.12 Typical pH profile (solid line) along *Arthrospira* continuous culture. Since there is a continuous CO_2 input that acidifies the culture media, only the addition of base (●) is required. Percentage of acid pump controller is always zero during the period shown.

Some of the possible malfunctions in the pH control loop could be the erroneous measure of pH during the culture or that the addition of the base solution was no possible due to a problem with the addition pump or the exhaustion of base solution. The second option was simulated. When the base solution tank is empty or the base pump is switched off, pH of the *Arthrospira* culture starts to decrease due to the continuous input of CO_2 gas, which acidifies the culture broth. In order to evaluate the response of *Arthrospira* to a decrease in pH, no addition of NaOH to maintain pH at 9.6 was allowed during one residence time.

Figure 3.13 shows the evolution of *Arthrospira* concentration measured with the biomass sensor and the CO_2 concentration in the gas outflow during the pH disturbance.

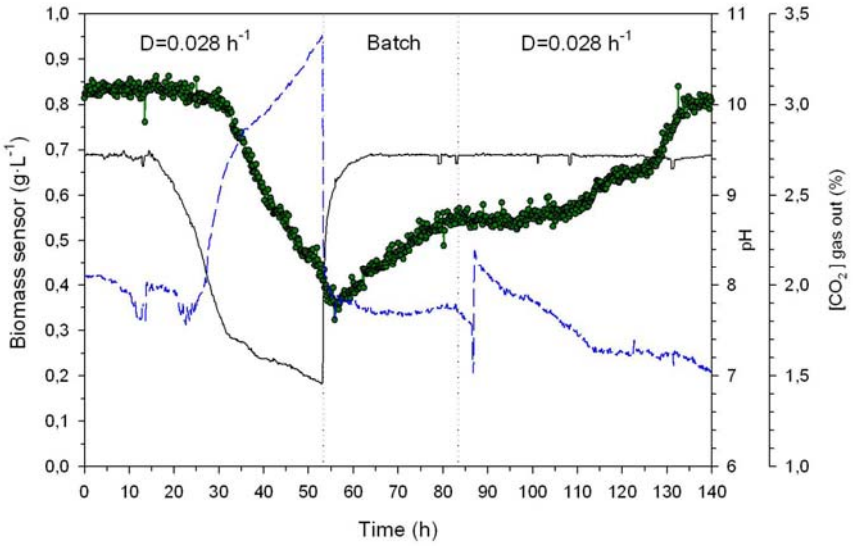

Figure 3.13 Evolution of *Arthrospira* concentration (●) measured with the biomass sensor and the CO_2 concentration (dashed line) in the output gas flow during a disturbance in pH (solid line) control. In the first phase at D=0.028 h^{-1} no addition of NaOH to maintain the pH at 9.6 is allowed and pH and biomass decrease. After around 40 hours, pH control is restarted and culture is first kept in batch and then continuous operation at D=0.028 h-1 is reestablished.

After one residence time without the addition of 1M NaOH to the culture, pH decreased to a value of 6.9 with the subsequent decrease in biomass levels from 0.85 $g \cdot L^{-1}$ to 0.35 $g \cdot L^{-1}$ and increase in CO_2 at the gas output of the bioreactor. In order to recover the initial biomass levels and pH values, the pH control system was restarted and the culture was kept in batch mode during one residence time of the previous continuous phase. Afterwards, the continuous culture was initiated at the same dilution rate that before the pH disturbance. As can be seen in Figure 3.13, pH and CO_2 composition returned to the set-point values after 8 hours of reinitiating the addition of the base solution. The biomass concentration began to increase during the batch phase and finally recover the initial values after restarting the continuous cultures.

The *Arthrospira* cells were examined microscopically before and after the pH disturbance a change in cells morphology was detected, as shown in Figure 3.14. As it can be observed, the normal cell morphology is lost in the low pH condition, and cells tend to form aggregates.

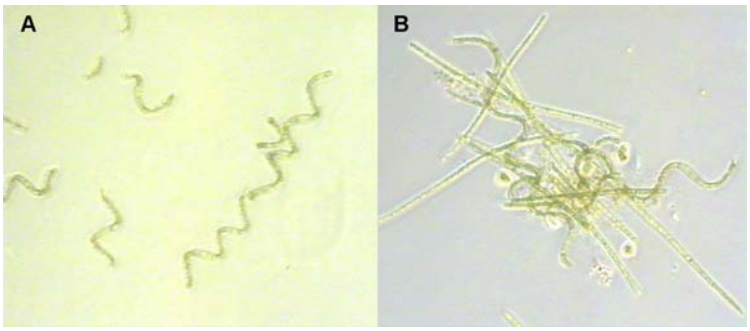

Figure 3.14 *Arthrospira* cells morphology at pH values of 9.6 (A) and 6.9 (B).

In conclusion, a pH decrease during the continuous culture of *Arthrospira* biomass produced a decrease in biomass concentration, an increase in CO_2 concentration in output gas flow and a change in cells morphology. Nonetheless, the former effects can be reversed after reestablishing the proper pH control and with a period where the *Arthrospira* culture is kept in batch mode.

3.3.3.2 DISTURBANCES OF LIQUID FLOWRATE

The bioreactor control system allows to control de liquid medium feed pumps to maintain a given flow-rate and therefore dilution rate in each operation conditions defined. Nonetheless, small oscillations of liquid flow rate around the set-point value are caused by (i) the liquid level decrease inside the buffer tank and (ii) the wear and tear of the pump tube along time.

Figure 3.15 shows a typical profile for the liquid input flow rate during a continuous *Arthrospira* culture at a dilution rate of 0.013 h^{-1}. The oscillations detected in the liquid flow rate influences the precision at which the dilution rate can be determined.

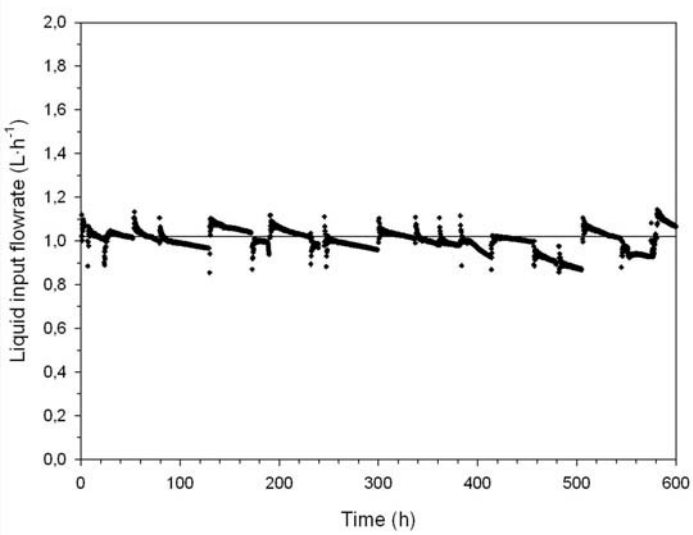

Figure 3.15 Typical liquid input flow rate profile during *Arthrospira* cultures. Input flow rate oscillates around 1.02 $L \cdot h^{-1}$ set point value, which corresponds to a dilution rate of 0.013 h^{-1}.

Besides the oscillations of liquid input flow rate around the set-point value, some major disturbances such as a malfunction in the pumps or the depletion of culture media in the liquid feed tanks or a choked liquid filter may force the culture to operate in batch mode.

In order to evaluate which variables were affected by such a disturbance, the continuous operation of the bioreactor at D=0.028 h^{-1} was manually changed from continuous to batch mode during 13 hours. As shown in Figure 3.16, biomass concentration increased during the batch phase, but no significant change was detected in pH or in output gas flow rate composition. After restarting the continuous mode operation of the photobioreactor, biomass levels decreased and returned to the cell concentrations observed before the disturbance.

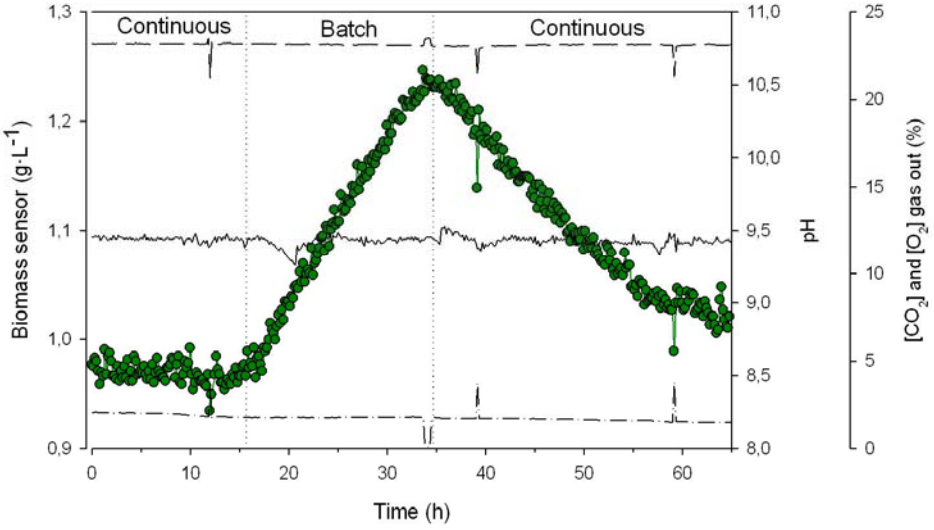

Figure 3.16 Evolution of *Arthrospira* concentration (●) measured with the biomass sensor at 118 $W \cdot m^{-2}$, pH (solid line) and CO_2 (dashed-dotted line) and O_2 (dashed line) concentration in the output gas flow rate during a disturbance in the liquid input flow rate. During the continuous operation dilution rate was set at 0.028 h^{-1}.

3.3.3.3 DISTURBANCES OF GAS FLOWRATE

Gas mass-flow meter-controllers located in the gas circuit measure and control the input and output gas flow rates continuously. In order to ensure a suitable mixing inside the bioreactor, input gas flow rate is maintained at 2.2 NL·min^{-1}, with a CO_2 concentration at 4-5%. The on-line CO_2 and O_2 analyzer measures continuously the composition of the output gas flow, whereas the input gas flow is measured on a daily basis. Due to the experimental set-up, when the composition of the inlet gas flow is measured, no gas flow is directed to the bioreactor. Consequently, the culture is not agitated and the control system automatically decreases light intensity values for safety reasons.

Figure 3.17 shows air, CO_2 and total gas flow rate together with CO_2 and O_2 composition of gas inlet and outlet respectively, in steady-state operation of the bioreactor, for one particular situation as example (D=0.028 h^{-1}, I=118 W·m^{-2}).

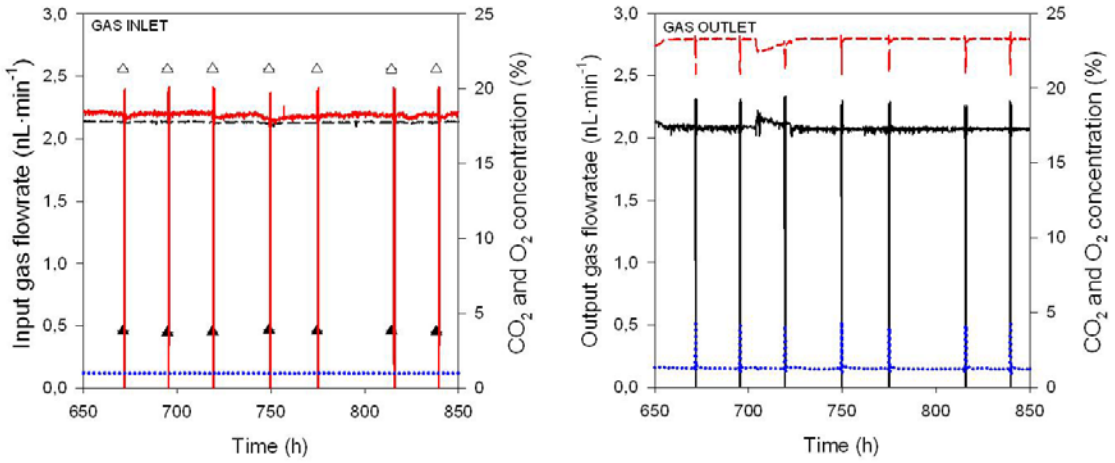

Figure 3.17 Evolution of gas flow-rate and composition in steady-state operation of the *Artrhrospira* culture (D=0.028 h^{-1}, I=118 h^{-1}) LEFT: CO_2 (dotted line), air (solid line) and total (dashed line) input gas flow rate (NL·min^{-1}) together with CO_2 (▲) and O_2 (empty ▲) concentration in total inlet gas. RIGHT: Total output gas flow rate (solid line) and their CO_2 (dotted line) and O_2 (dashed line) concentration (%).

Input gas flow rate can be disturbed by several reasons such as (i) a general power failure affecting the air compressor and the liquid input pumps or (ii) CO_2 bottle depletion. In the first case, as no air is introduced to the bioreactor, control system sets light intensity to lower values to avoid the increase of temperature in the culture broth. In the second situation, neither the mixing nor the light intensity are affected because the air flow is still entering the photobioreactor, but culture may be limited by carbon, since no carbon source is supplied in the liquid medium. Both situations were studied to evaluate the effects on *Arthrospira* biomass.

First, the bioreactor was operated in batch mode during 4 hours without liquid input media nor enriched CO_2 inlet gas flow due to a simulated power failure. Consequently, the control system set the light intensity to 0.4 W·m^{-2}. Figure 3.18 shows the evolution of biomass concentration, pH, outlet gas composition and dissolved oxygen inside the bioreactor during the disturbance of both the liquid and gas inlet flows.

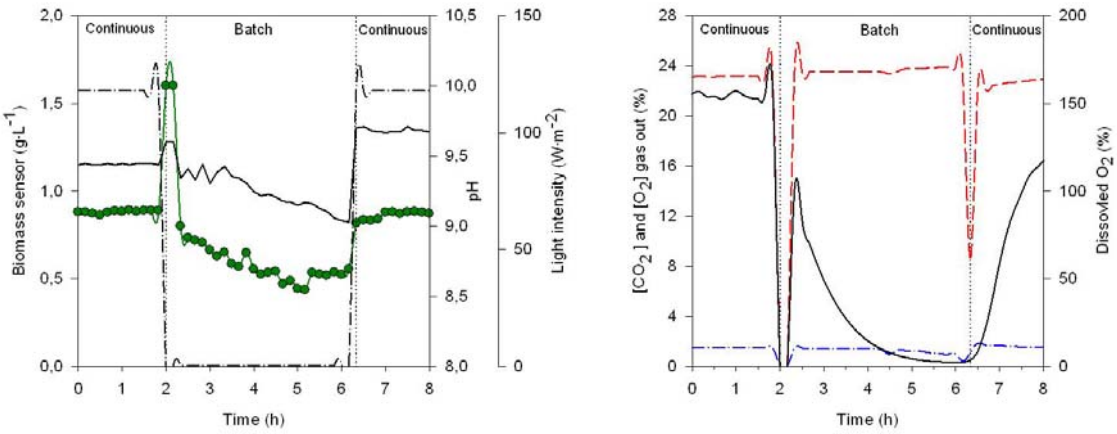

Figure 3.18 Culture evolution during a simulated power failure affecting liquid and gas input flows. LEFT: Biomass concentration measured by the sensor (●), pH (solid line) and light intensity (dashed-dotted line). RIGHT: CO_2 (dashed-dotted line) and O_2 (dashed line) concentration (%) in the gas outlet flow and dissolved oxygen (solid line) inside the bioreactor.

During the batch phase the biomass starts to diminish. A small decrease in pH and CO_2 concentration in the gas outflow and an increase in O_2 levels is observed. It is noteworthy the drastic decrease in dissolved oxygen concentration. Once the input liquid and gas flows are re-established, all the abovementioned parameters return satisfactorily to the levels observed before the disturbance.

Finally, CO_2 inlet flow gas was set to zero to evaluate the effect of a possible CO_2 bottle depletion during *Arthrospira* continuous culture. Figure 3.19 shows the evolution of biomass concentration, pH, the addition of acid or base solution, outlet gas composition and dissolved oxygen inside the bioreactor during the interruption in CO_2 supply.

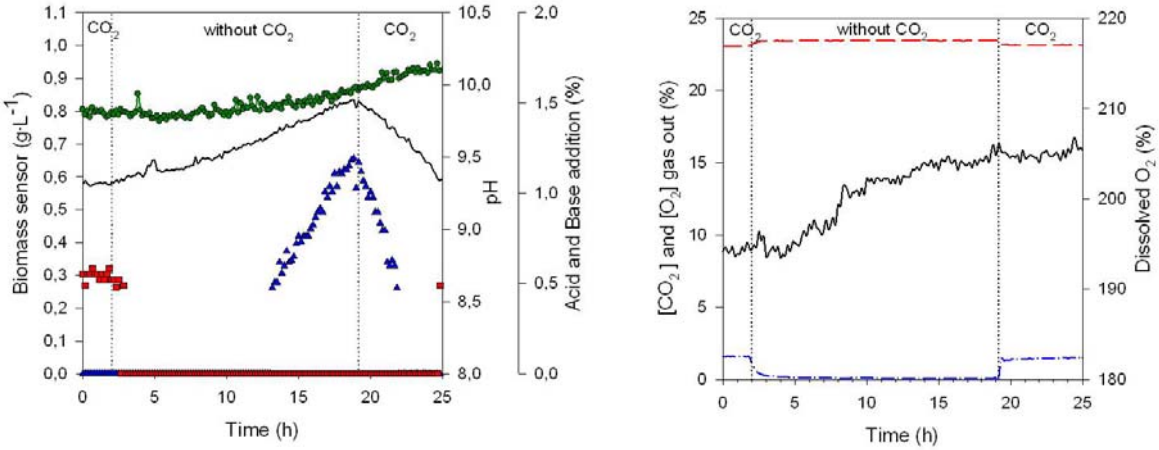

Figure 3.19 Culture evolution during an interruption of the CO_2 input flow for *Arthrospira* continuous culture at D=0.028 h^{-1} I=118 $W \cdot m^{-2}$. LEFT: Biomass concentration measured by the sensor (●), pH (solid line), base addition (■) and acid addition (▲). RIGHT: CO_2 (dashed-dotted line) and O_2 (dashed line) concentration (%) in the gas outlet flow and dissolved oxygen (solid line) inside the bioreactor.

When the CO_2 flow is interrupted, the pH starts to increase and consequently no more addition of base solution takes place and instead acid solution is added to the culture. In addition to this, gas phase composition changes significantly, since CO_2 decreases drastically and O_2 increases slightly. Nonetheless, when the supply of CO_2 is restored all the affected variables by the disturbances returned to the initial values, indicating the capability of *Arthrospira* culture to overcome the tested disturbances.

3.4 CONCLUSIONS

First, the operational limits operational limits and maximum productivity of *Arthrospira* photobioreactor of the MPP under normal culture conditions were studied. With this aim, several continuous cultures were carried out at different dilution rates (0.007-0.05 h^{-1}) and light intensities (10-225 $W \cdot m^{-2}$), planned using a Box-Wilson Central Composite Design (CCD). Although the main findings have been already discussed, the highlighted conclusions from this work are:

- The highest biomass concentration inside the bioreactor is obtained at the highest light intensity value and at low dilution rates.
- The highest productivity attained in the pilot plant photobioreactor is 27 $mg \cdot L^{-1} \cdot h^{-1}$ at a dilution rate of 0.044 h^{-1} and a light intensity of 194 $W \cdot m^{-2}$. Under these conditions the CO_2 volumetric consumption is 0.5 $mmol \cdot L^{-1} \cdot h^{-1}$, the O_2 volumetric production is 1.32 $mmol \cdot L^{-1} \cdot h^{-1}$ and the nitrogen volumetric uptake is 0.28 $mmol \cdot L^{-1} \cdot h^{-1}$. These values will be used in the mass balance model to evaluate the impact of integrating the photosynthetic compartments in the MPP (Chapter 8).
- Regarding the effect of light intensity on biomass composition, only the protein and the chlorophyll content are affected. In both cases, an increase in light intensity produces lower amount of proteins and chlorophyll in *Arthrospira* biomass, which reflects the cells adaptation of pigment at lower and high illumination levels.
- Disturbances of normal operation conditions affecting pH, liquid and gas flowrate affects *Arthrospira* growth, but all tested deviations allowed to recover the initial biomass values. However, a batch phase under normal culture conditions is required before the reestablishment of normal continuous operation.

Chapter 4

EFFECT OF AMMONIUM, LIGHT INTENSITY AND DILUTION RATE ON *ARTHROSPIRA* PRODUCTION: Determination of threshold values to avoid inhibitory conditions

4.1 INTRODUCTION

Nitrogen source is one of the main parameters influencing *Arthrospira* growth and composition. An extensive number of studies demonstrate the capability of this cyanobacteria to use a number of substrates as a nitrogen source including: (i) nitrate - $NaNO_3$, KNO_3, NH_4NO_3 - (Costa *et al*., 2001; Danesi *et al*., 2004; Liotenberg e*t al.*, 1996), (ii) ammonium - NH_4Cl, $(NH_4)_2SO_4$, $NH_4H_2PO_4$, NH_4NO_3 - (Azov and Goldman, 1982; Ciferri, 1983; Richmond, 1986; Boussiba and Gibson, 1991; Becker, 1994; Liotenberg *et al.*, 1996; Costa *et al*., 2001; Miller *et al*., 2002; Carvalho *et al*., 2004; Soletto *et al*., 2005; Converti *et al.*, 2006), (iii) urea - $CO(NH_2)_2$ - (Stanca and Popovici, 1996; Costa *et al.*, 2001; 2002; 2004; Danesi *et al.*, 2002; 2004; Rangel-Yagui *et al*., 2004; Soletto *et al.*, 2005; Converti *et al.*, 2006) and (iv) some amino acids such as glutamine and adenine (Filali *et al.*, 1997).

Among the possible nitrogen sources, nitrate (KNO_3 or $NaNO_3$) is the nitrogen form used in the conventional culture media described for *Arthrospira* (Zarrouk, 1966; Paoletti *et al*., 1975; Schlösser, 1982). Nonetheless, the use of cheaper nitrogen sources other than nitrate, such as ammonium and urea (Stanca and Popovici, 1996, Danesi *et al*., 2002, Sassano *et al*. 2004), is currently appealing from the economic point of view, since production costs would be decreased (Carvalho *et al*., 2004). Moreover, because these compounds are often present in wastewater, *Arthrospira* cultures could be a promising alternative for nitrogen removal from wastewater, as some preliminary studies using animal wastes and industrial effluents already show (Ayala and Vargas, 1987; Olguín *et al*., 2001, Converti *et al.*, 2006).

Also, urea addition to *Arthrospira* cultures seems to increase biomass production (Stanca and Popovici, 1996). Costa *et al*. (2004) determined that the addition of 1.125 $mg \cdot L^{-1}$ of urea to the Mangueira Lagoon water resulted in a 2.67-fold higher final biomass concentration of *Arthrospira*. Similarly, Danesi *et al*. (2002) reported that urea, added in exponentially increasing rates into fed-batch *Arthrospira* cultures at 30ºC, increased, not only biomass production, but also nitrogen-cell conversion yield ($Y_{X/N}$), when compared to cultures grown on KNO_3. Although the nitrogen source (urea or KNO_3) had no effect on the chlorophyll content (Danesi *et al*., 2002; Rangel-Yagui *et al*., 2004) and on lipid levels, protein content was higher when using urea (Danesi *et al*., 2004).

Some comparative cultures concluded that, using ammonium or urea as a nitrogen source, results in a higher maximum specific growth rate when compared to cultures using nitrate (Costa *et al*., 2001). Several authors have reported that when several nitrogen sources are supplied, ammonium is first consumed due to the lower energetic cost associated with its assimilation (Boussiba and Gibson, 1991; Guerrero and Lara, 1987; Converti *et al.*, 2006). As discussed in respect to the nitrogen assimilation mechanisms of *Arthrospira* presented in the general introduction, ammonium is directly incorporated, while other nitrogen sources must be first reduced to ammonium to be further metabolized.

4.1.1 REVIEW OF AMMONIUM INHIBITION EFFECT

Ammonium is toxic at high concentrations leading to growth inhibition or even cell death (Abeliovich and Azov, 1976; Belkin and Boussiba, 1991). Inhibitory and toxic ammonium concentration thresholds reported in literature for *Arthrospira* are: 1.7 mM (23.8 ppm $N\text{-}NH_4^+$) (Converti *et al*., 2006), 2 mM (28 ppm $N\text{-}NH_4^+$) (Abeliovich and Azov, 1976), 6 mM (84 ppm $N\text{-}NH_4^+$) (Carvalho *et al.* 2004), 7 mM (100 ppm $N\text{-}NH_4^+$) (Richmond, 1988) and 10 mM (140 ppm $N\text{-}NH_4^+$) (Belkin and Boussiba, 1991). Using nitrate as nitrogen source the apparent inhibition appears at a much higher nitrogen concentration (1.2 M; 16800 ppm $N\text{-}NO_3^-$) than that reported for ammonium (Ciferri, 1983).

Inhibitory nitrogen levels depend greatly on the individual cyanobacteria type and culture conditions (Tam and Wong, 1996). Particularly, Belkin and Boussiba (1991) reported that unlike other cyanobacteria such as *Anabaena, Arthrospira* withstood high ammonium concentration

(10 mM) at pH10 probably due to its relatively high internal pH ($pH_{cytoplasmic}$ = 8.3; $pH_{intrathylakoid}$ = 6.5), this would limit intracellular accumulation of ammonia. Nonetheless, as its maximal photosynthetic capacity was reduced by almost 70% with an ammonium concentration of 10 mM, such an amount was considered toxic to *Arthrospira* growth.

Moreover, pH is one of the culture conditions that significantly influences ammonium toxicity. Azov and Goldman (1982) demonstrated that the inhibiting molecule was free NH_3 instead of ammonium, observing a 50% reduction in photoassimilation at 1.2 mM NH_3. Since pH establishes the degree of dissociation of ammonium to ammonia (pKa=9.25), they suggested to use pH as control variable. Kallqvist and Svenson (2003) also reported the strong influence of pH on ammonium/ammonia toxicity. They determined the specific toxicity (EC50, 24 h exposure) of ammonia and ammonium ions to unicellular green alga, *Nephroselmis pyriformis*, and found that ammonia was more toxic than ammonium by a factor of 100.

In order to avoid ammonium concentrations in the medium reaching inhibitory levels, several ammonium feeding patterns are used. Successful results using fed-batch additions of ammonium prevented the ammonium accumulation in the culture, while ensuring final cell concentrations and productivities comparable with those obtained with nitrate (Danesi *et al*., 2002; Carvalho *et al*., 2004; Soletto *et al*., 2005; Converti *et al*., 2006).

4.1.2 AMMONIUM ROLE IN THE MELiSSA LOOP

As mentioned in the general introduction, the MELiSSA loop is based on the connection of five compartments, colonised respectively by thermophilic anoxygenic bacteria (CI), photoheterotrophic bacteria (CII), nitrifying bacteria (CIII), photoautotrophic bacteria (CIVa), higher plants (CIVb or HPC) and the crew (CV).

The nitrogen source for *Arthrospira* compartment (CIVa) is nitrate present in the outlet from the nitrifying compartment (CIII). Indeed, the nitrifying compartment was included in the MELiSSA loop design in order to convert ammonium to nitrate and avoid any potential inhibition in the photosynthetic compartments. However, a perturbation in the former compartment (CIII), such as a decrease in the oxygen supply, would increase the ammonium concentration in the liquid inlet of the *Arthrospira* compartment. Therefore, it is interesting to determine to which extent *Arthrospira* is able to assimilate ammonium. Such a study would also contribute to determining whether ammonium from the hydrolysis of urea generated in the crew compartment could be used as an additional nitrogen source for the *Arthrospira* compartment. With this aim and in within the MELiSSA consortium, some preliminary work was performed on *Arthrospira* growth using different nitrogen sources.

Filali *et al.* (1997) analyzed the capability of *Arthrospira* cells to grow on several nitrogen sources (nitrate, nitrite, ammonium, urea and amino acids - glutamine and adenine-) supplied to the cultures individually or in combination as pairs or triads. They confirmed the capability of *Arthrospira* to grow on all the abovementioned nitrogen compounds at pH 9.5. Concerning the cultures with a single nitrogen source, the tolerance to nitrogen concentration was high for

nitrate (up to 100 mM; 1400 ppm N-NO_3^-) but low for urea and ammonium (3 mM; 42 ppm N-NH_4^+). Moreover, the inhibition due to an increase of nitrogen concentration appeared at low light intensities, suggesting that nitrogen assimilation was related to photosynthesis.

In order to overcome the limitations of low light intensity (8 $W \cdot m^{-2}$) supplied to Erlenmeyer-flask cultures of the previous experiments (Filali *et al.*, 1997) and to better mimic the continuous operation of *Arthrospira* compartment within the MELiSSA loop, further batch and continuous cultures under higher light intensities were carried out (Lattenmayer, 2001). During a continuous culture carried out at pH 8.5 and 80 $W \cdot m^{-2}$, the *Arthrospira* productivity decreased from 0.0106 $g \cdot L^{-1} \cdot h^{-1}$ to 0.0086 $g \cdot L^{-1} \cdot h^{-1}$ when ammonium concentration inside the bioreactor increased from 38 ppm N-NH_4^+ (2.7 mM) to 80 ppm N-NH_4^+ (5.7 mM). From this continuous culture and various Erlenmeyer-flask cultures performed at 10 $W \cdot m^{-2}$, they determined 70 ppm N-NH_4^+ (5 mM) to be a critical ammonium concentration for *Arthrospira* cultures.

Nevertheless, the data from these two previous studies were not sufficient to get a deeper understanding of *Arthrospira* production when using ammonium as nitrogen source. Although they demonstrated the capability of *Arthrospira* to grow using ammonium, both the ammonium inhibitory concentrations and the role of light intensity were not clearly determined.

Therefore, the main objective of this study is to identify the effect of ammonium concentration and light intensity on *Arthrospira* production and biomass composition at different reference dilution rates. In this framework, several continuous culture tests were performed at different dilution rates, ranging from 0.016 h^{-1} to 0.035 h^{-1}, with one step of light intensity in each of the tests. The results will contribute to the future formulation of mathematical models of the response observed. These studies will allow prediction of the behaviour of the strain when ammonium increases at the input of the compartment.

4.2 MATERIALS AND METHODS

4.2.1 BENCH PHOTOBIOREACTOR

The bench scale photobioreactor used for *Arthrospira* cultures is shown in Figure 4.1. The working volume was 1.6 L with an internal diameter of 0.12 m and a liquid height of 0.14 m. In such conditions, the illuminated area of the culture was 0.053 m^2. The culture was stirred mechanically at 200 rpm by an agitation axis with two 6-blade Rushton turbines (RZR Heidolph Instruments, Schwabach, DE)

Illumination of the bioreactor was provided by 15 halogen lamps (Sylvania, 12V, 20W), which were distributed radially around the external wall, in 5 columns containing 3 lamps each. A power supply regulator (SM1540-d, 0-15V, 0-40A, Delta Elektronika, Zierikzee, NL) was used to modify light intensity supplied to the culture by means of changing the voltage of the lamps.

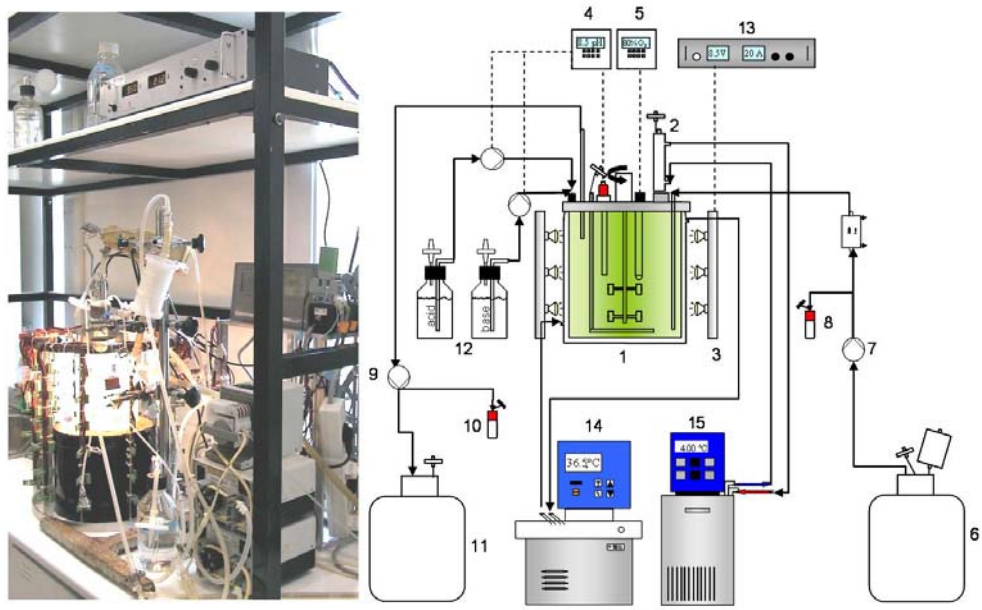

Figure 4.1 Bench scale photobioreactor used for *Arthrospira* cultures. The following parts are indicated in the scheme: (1) glass tank, (2) condenser, (3) halogen lamps, (4) pH 2100 controller connected to a pH probe, (5) O2 4100 controller connected to a dissolved oxygen sensor, (6) liquid inlet buffer tank, (7) liquid inlet peristaltic pump, (8) liquid inlet sample tube, (9) liquid outlet peristaltic pump, (10) liquid outlet sample tube, (11) liquid outlet buffer tank, (12) acid and base buffer bottle for pH control, (13) lamp power supply, (14) thermostatic bath and (15) refrigeration bath.

For the continuous operation, liquid input media was pumped by a peristaltic pump (Reglo-Analogue MS 4/8-100, tube ID 2.06 mm, Ismatec SA, Glattbrugg, CH) from a 10L polypropylene tank, through a liquid filter (0.22 µm Millipore, Billerica, MA, USA) and then to the top of the bioreactor. A 50 mL sampling tube, located before the photobioreactor inlet, was used for sampling the input liquid medium. In order to ensure a constant culture volume inside the photobioreactor, the bottom part of the outlet tube was fixed at the culture height corresponding to a culture volume of 1.6L and the outlet pump (Reglo-Analogue MS 4/8-100, tube ID 2.79 mm, Ismatec SA, Glattbrugg, CH) was set at higher rates than the input pump.

Instrumentation associated with the photobioreactor allowed for the in-line measurement of pH (pH 2100 controller connected to an InPro3000/120 Mettler Toledo pH probe), temperature and dissolved oxygen (O_2 4100 controller connected to an Ingold 73052 Mettler Toledo polarographic oxygen probe).

4.2.1.1 CONTROL SYSTEM

Temperature was kept at 36 ºC by means of a thermostatic bath (D8 Haake, Karlsruhe, DE), which circulated water through the external glass jacket of the photobioreactor.

An autonomous controller (pH 2100, Mettler Toledo, CH) regulated the pH of the culture media by addition of acid (1.5M HCl) or base (1M NaOH) solutions. The controller received the value measured by the pH sensor and accordingly activated the acid or the base pump.

4.2.1.2 PHOTOBIOREACTOR START-UP

Before describing the sequence for the photobioreactor start-up carried out for each of the different tests performed, the light intensity calibration procedure is detailed.

The light intensity at the bioreactor's surface was obtained by measuring the light intensity at the axis of the bioreactor, using a spherical light sensor (Li-Cor, LI-193SA, Lincoln, NE, USA) that integrated the light reaching its radial illuminated surface.

In order to apply the previously developed light transfer mathematical models for the photobioreactors within the MELiSSA group, it is necessary to convert the photosynthetic photon flux (PPF) units of the spherical sensor ($\mu mols \cdot m^{-2} \cdot s^{-2}$) to $W \cdot m^{-2}$ (Cornet *et al.*, 1992 a, b, 1998).

It is noteworthy to mention that for higher plant cultures presented later in this work (Chapter 5 and 6), light irradiance is expressed as $\mu mols \cdot m^{-2} \cdot s^{-2}$, since the corresponding light transfer mathematical models are still under development, and therefore it is still not required to convert the units of the spherical sensor.

The conversion coefficient for *Arthrospira* (0.291) was calculated integrating the spectra of the used lamps between 350 nm and 750 nm (Cornet *et al.*, 1998), which is the absorption range of *Arthrospira* cells. Conversion of the light intensity measured by the spherical sensor ($\mu mol \cdot m^{-2} \cdot s^{-1}$) to the light intensity at the surface of the bioreactor ($W \cdot m^{-2}$) was done using [Eq. 4.1].

$$I = 0.291 \cdot \frac{Eb \cdot rb}{\pi \cdot Rb} \qquad \text{[Eq. 4.1]}$$

In [Eq. 4.1], I ($W \cdot m^{-2}$) is the light flux at the bioreactor's surface, Eb ($\mu mol \cdot m^{-2} \cdot s^{-1}$) is the light intensity measured by the sensor, rb (mm) is the sensor's radius (30 mm) and Rb (mm) is the bioreactor's radius (60 mm).

Eb values were measured in the empty bench bioreactor with water circulating through the external jacket. Light intensity measurements were done at different vertical positions (assuming 0 at the bioreactor's base) and at different voltages supplied to the lamps (Figure 4.2, left).

Averaging the measurements obtained at different vertical positions, the mean light intensity value for each voltage supplied to the lamps was obtained. The light intensity values measured by the sensor Eb ($\mu mols \cdot m^{-2} \cdot s^{-2}$), were converted to I ($W \cdot m^{-2}$) values using [Eq. 4.1]. The adjusted equation between the light intensity at the surface of the bioreactor and the voltage supplied to the lamps (Figure 4.2, right), expressed as I ($W \cdot m^{-2}$) against voltage (V) was: $y=5.15 - 0.35\ x - 0.62\ x^2 - 0.12\ x^3$ ($r^2=0.999$, SE of I=0.36). This light calibration equation was used to calculate the light intensity ($W \cdot m^{-2}$) supplied to the culture at a determined voltage supplied to the lamps.

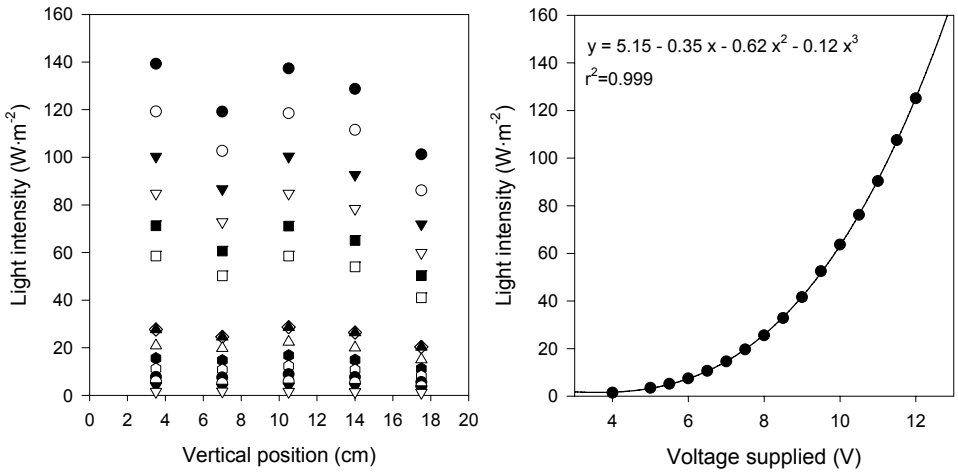

Figure 4.2 LEFT: Light intensity measured by the spherical light sensor, which was located in bioreactor's centre, at different vertical positions (assuming 0 cm the bottom part of the reactor) while supplying different voltages from 4V to 12 V in 0.5V steps. Each symbol type correspond to a given voltage level. RIGHT: Relation between average light intensity at bioreactor's surface and voltage supplied to lamps

Once the light intensity was calibrated, the following steps were carried out to start-up each of the *Arthrospira* cultures performed in the bench scale photobioreactor:

- Set-up of the bioreactor, instrumentation and liquid circuit.
- Calibration of the pH sensor using commercialized standard solutions at pH 4 and 7.
- Sterilization of the equipment in order to satisfy the axenicity of *Arthrospira* culture. Bench bioreactor filled with culture medium and associated instrumentation was sterilized in the autoclave (Varioklav 400, H+P Labortechnik AG, Oberschleissheim, DE) at 120 ºC for 30 minutes. The complete set of complementary equipment required for the culture (inlet/outlet medium tanks, acid/base bottles and liquid tubing) were also sterilized in the same way as the photobioreactor (120 ºC for 30 minutes) and connected to it following the corresponding sterility safety procedures.
- Calibration of the dissolved oxygen sensor with culture media saturated with bubbled air (100%).
- Inoculation of the photobioreactor with 200 mL *Arthrospira* inoculum.

4.2.2 STRAIN, CULTURE MEDIUM AND CULTURE CONDITIONS

The axenic strain used for this study was the cyanobacterium *Arthrospira sp*. (PCC 8005), also known as *Spirulina*, as mentioned in previous chapter. The inoculum was grown in Erlenmeyer-flasks containing modified Zarrouk's medium (Zarrouk, 1966) with constant illumination and periodically agitation. The modified Zarrouk medium (Table 3.1) was adjusted to pH 9.5 before its use.

For the continuous cultures performed in this study the Zarrouk medium was modified. As the goal of these tests was to evaluate the effects of ammonium on *Arthrospira*, the nitrogen source was changed from sodium nitrate $NaNO_3$ 2.5 $g \cdot L^{-1}$ (29 mM, 412 ppm $N\text{-}NO_3^-$) to ammonium sulphate $(NH_4)_2SO_4$.

However, the initial batch phase was done using nitrate as the nitrogen source in order to achieve the required biomass levels for starting the continuous culture, without being inhibited by any toxic effects such as those probably caused by the presence of ammonium. Once the continuous culture is started, no nitrate is provided and instead ammonium is used as the nitrogen source to evaluate its effects on *Arthrospira* growth.

Using ammonium as the nitrogen source, the nitrogen concentration of the Zarrouk medium (29 mM) had to be reduced to avoid toxic ammonium levels to *Arthrospira* growth. Therefore, ammonium concentration in the inlet medium was reduced to 8 mM (116 ppm $N\text{-}NH_4^+$) as an intermediary ammonium concentration. Such concentration is expected to be high enough to supply the nitrogen requirement of the cells and low enough to avoid high residual ammonium concentration, which could be toxic to *Arthrospira*.

In contrast to the previous chapter, carbon was supplied directly in the liquid medium, in the form of carbonates, following the initial Zarrouk formulation.

Moreover, pH was set at 8.5 to avoid both (i) high levels of ammonia inside the bioreactor since this form seems to be more toxic than ammonium (Azov and Goldman, 1982; Källqvist and Svenson, 2003) and (ii) losing part of the nitrogen through the gas phase in form of ammonia (Danesi *et al.*, 2002). The ammonia/ammonium equilibrium establishes that at 36 ºC and pH of 8.5, 28% of the total nitrogen is in the ammonia form and the remaining 72% in the ammonium form.

4.2.3 ANALYTICAL METHODS

The following analyses were carried out during the ammonium test:

- Determination of the biomass concentration (Dry Weight and Optical Density)
- Determination of nitrogen concentration (nitrate and ammonium).
- Determination of biomass composition (CHNS, protein, fatty acids profile, chlorophyll *a*, phycocyanin and allophycocyanin).

Except for the determination of ammonium composition, all the other analyses have been described in the previous chapter (Chapter 3). Thus, only the analytical procedure for the ammonium determination is include here.

- **Ammonium concentration (ppm $N\text{-}NH_4^+$)**

Ammonium was measured using UV measurement determinations by means of LCK 305 ammonium analysis kits (Dr. Lange Nitrax, calibration range 1-12 ppm $N\text{-}NH_4^+$). The analysis is

based on the reaction of ammonium ions with hypochloride and salicylate ions, in the presence of the catalyser nitroferrocyanide, forming iodophenol blue, which is quantified measuring the absorption at 694nm.

For the ammonium determination, 0.5 mL of filtered sample, previously diluted to be within the calibration range, was added to the ammonium analysis kit. After 15 min the absorbance at 694 nm was measured with the Dr. Lange Xion 500 spectrophotometer (Hach Lange GmbH, Düsseldorf, DE). Several standard solutions were prepared to verify the correct ammonium quantification by the Dr. Lange spectrophotometer. The ammonium concentration of the liquid input and output flows was determined in triplicate.

4.3 RESULTS AND DISCUSSION

4.3.1 CONTINUOUS CULTURES USING AMMONIUM AS NITROGEN SOURCE

The evolution of the continuous cultures performed using ammonium as a nitrogen source is shown in the subsequent sections. All the cultures were started with a batch phase using nitrate followed by the start-up of the ammonium continuous culture, where first a transient phase took place until reaching the first steady state (at a given dilution rate and light intensity level). The graphs presented in the figures of this section provide the results from the time when the continuous culture using ammonium as a nitrogen source is started and do not include the culture evolution corresponding to the batch phase. In the tests with high dilution rates, a gradual increase in input liquid flow rate was performed in order to allow a progressive adaptation of the cells to the continuous culture conditions. Once the first steady state was reached an illumination step up was performed and the culture was followed until the second steady state was reached. Tables included in this section provide average values of culture conditions and main parameters to evaluate *Arthrospira* culture only for the steady states without taking into account values from the transient phases.

The yield coefficient of nitrogen on biomass for continuous cultures ($Y_{N/X}$) was calculated as the difference between input and residual ammonium concentration divided by biomass dry weight. Light irradiance per biomass ($W \cdot g^{-1}$) was calculated dividing the product of light intensity ($W \cdot m^{-2}$) and the illuminated culture area (0.053 m^2) by the product of biomass dry weight ($g \cdot L^{-1}$) and total culture volume (1.6L).

As mentioned in the materials and methods section 4.2.2, the initial batch phase was performed using nitrate as a nitrogen source in order to achieve the required biomass levels for starting the continuous culture, without being inhibited by any toxic effects such as those probably caused by the presence of ammonium. Thus, at the beginning of the continuous phase nitrate remaining from the culture media of the batch phase was also measured to evaluate whether the outlet concentration was in agreement with the nitrate wash-out curve, as some authors already reported (Guerrero and Lara, 1987, Creus, 2003).

The nitrate wash out curve is calculated using [Eq. 4.2], where [NO_3^-] is the nitrate concentration (ppm N- NO_3^-) inside the bioreactor at time t (h), [NO_3^-]$_0$ is the initial nitrate concentration (ppm N- NO_3^-) inside the bioreactor , t_0 is the initial time and D (h^{-1}) is the dilution rate.

$$[NO_3^-] = [NO_3^-]_0 \cdot \exp^{-(t-t_0)\cdot D} \qquad \text{[Eq. 4.2]}$$

As an example, Figure 4.3 shows the nitrate wash out curve profile obtained for one of the cultures at the beginning of the continuous phase, where the ammonium was the only nitrogen source present in the inlet culture media.

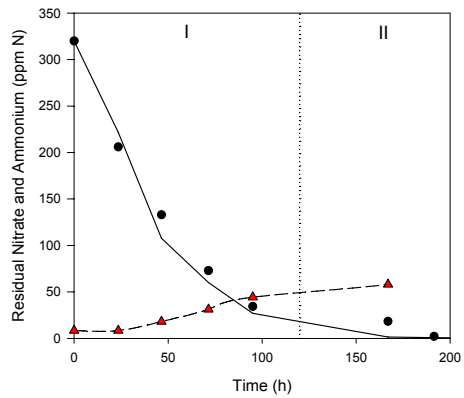

Figure 4.3 Evolution of nitrate (●, ppm N-NO_3^-) and ammonium (▲, ppm N-NH_4^+) concentration in the liquid outflow at the beginning of the *Arthrospira* continuous cultures at light intensity of 33 W·m^{-2}. In Phase I the input liquid flow rate is increased until the D=0.032 h^{-1} of Phase II is reached. Nitrate present in the outlet is the remaining from the culture medium used for the previous batch phase (not shown), which is in agreement with its wash-out curve (solid line) calculated using [Eq. 4.2]. Once the continuous culture is started (t=0), the inlet medium has no nitrate but 140 ppm N-NH_4^+ of ammonium.

In Figure 4.3, the outlet nitrate concentration (●) is in agreement with the wash-out curve (solid line), which was calculated using [Eq. 4.2] and the corresponding culture conditions of the test (Test 3, shown in section 4.3.1.3). In this culture in order to allow a progressive adaptation of the cells to the continuous culture conditions, a gradual increase in input liquid flow rate was performed (Phase I) until the desired dilution rate (D) of 0.032 h^{-1} was reached (Phase II). As a consequence, the value used for (D) in phase I changes accordingly to the increase in input flow rate. The value for [NO_3^-]$_0$ is the nitrate concentration at t=0, which correspond to 320 ppm N-NO_3^-.

Moreover, the ammonium concentration present in the outlet flow was lower than the inlet ammonium concentration of 140 ppm N-NH_4^+, which indicates that *Arthrospira* cells are consuming ammonium as nitrogen source.

Since in all the tests the nitrate outlet concentration matched the nitrate wash-out curve in a similar way as depicted in Figure 4.3, it was confirmed that *Arthrospira* cells have a higher affinity for ammonium and that ammonium is consumed first in front of other nitrogen sources (Guerrero and Lara, 1987, Creus, 2003).

4.3.1.1 TEST 1: D=0.016 h^{-1}

The first experiment of these series was carried out at a low dilution rate, D= 0.016 h^{-1}, and two illumination conditions 33 and 76 $W \cdot m^{-2}$.

Figure 4.4 shows the evolution of biomass concentration, residual ammonium concentration in the bioreactor and light irradiance per biomass for the continuous culture of Test I. Moreover, as the desired dilution rate had a low value (0.016 h^{-1}), it was not necessary to have an intermediary phase with a stepwise increase of input flow rate after the batch phase. Table 4.1 summarizes the operational conditions (light intensity, liquid input flow rate, residence time, dilution rate) and the averaged value of the main parameter values (optical density, biomass dry weight concentration, biomass productivity, input and residual ammonium concentration, nitrogen uptake per biomass and light irradiance per biomass) at each steady state.

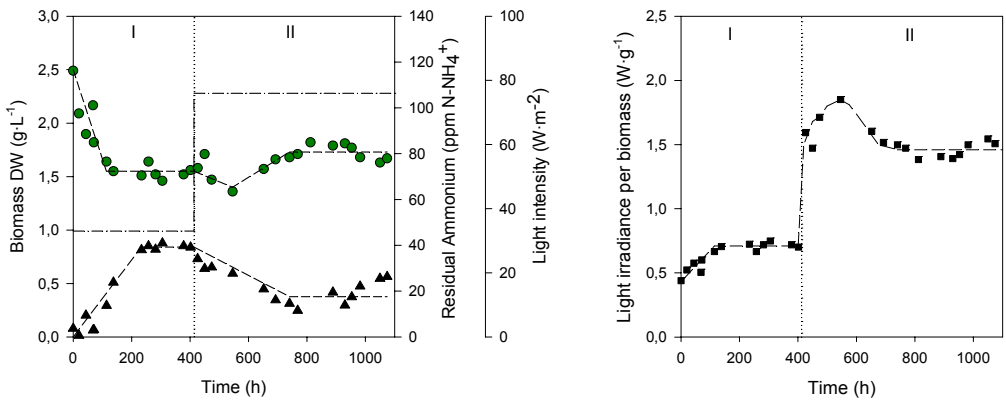

Figure 4.4 Evolution of *Arthrospira* continuous cultures using ammonium as nitrogen source (input ammonium concentration of 114 ppm $N\text{-}NH_4^+$) with changing light intensity levels (Phase I: 33 $W \cdot m^{-2}$, Phase II: 76 $W \cdot m^{-2}$) and at a fixed dilution rate of 0.016 h^{-1}. LEFT: ● Biomass concentration (g $dw \cdot L^{-1}$), ▲ residual ammonium concentration (ppm $N\text{-}NH_4^+$), dashed-dotted line: light intensity ($W \cdot m^{-2}$), dashed line: averaged values at steady state and transient light phases. RIGHT: ■ Light irradiance per biomass ($W \cdot g^{-1}$).

The initial biomass concentration of 2.5 $g \cdot L^{-1}$ from the end of batch phase began to decrease when the continuous mode was started up until it reached a stable value around 1.55 $g \cdot L^{-1}$ for more than 4.5 residence times. In order to determine where the initial transient phase ends and the steady state began, a least squares linear regression approach was used. The regression output is based on the null hypothesis that the slope of the data is zero, which would imply that the steady state is reached (Chung, 2004). Since the p-value associated with the slope of biomass concentration along time was higher than 0.05 (p=0.29) for Phase I, at an alpha (α) level of 0.05 it can be accepted that the slope of cell concentration along time is not significantly different from zero. This implies that biomass has reached a stable value corresponding to the steady-state phase. Thus, a first steady state was attained with success and the corresponding values are reported in Table 4.1.

Afterwards, when a light step up from 33 $W \cdot m^{-2}$ to 76 $W \cdot m^{-2}$ was performed, *Arthrospira* concentration increased (1.73 $g \cdot L^{-1}$) confirming that in these conditions, the biomass growth was limited by light intensity. The averaged values for the second steady state (p=0.36), kept for more than five residence times, are shown in Table 4.1.

Table 4.1 Mean values (± 95% interval confidence) of main parameters at each steady state reached in Test 1.

Parameter	Phase I	Phase II
Light intensity, I ($W \cdot m^{-2}$)	33	76
Liquid input flow rate, Q ($L \cdot d^{-1}$)	0.60	0.60
Residence time, ι (h)	64	64
Dilution rate, D (h^{-1})	0.016	0.016
Optical density at 750 nm	0.7±0.2	0.9±0.4
Biomass concentration, DW ($g \cdot L^{-1}$)	1.55±0.04	1.73±0.05
Productivity ($mg \cdot L^{-1} \cdot h^{-1}$)	24.2±0.7	27.0±0.7
Input ammonium concentration (ppm $N\text{-}NH_4^+$)	114±7	114±6
Residual ammonium (ppm $N\text{-}NH_4^+$)	39±7	17±4
Nitrogen uptake per biomass, $Y_{N/X}$ ($mg\ N \cdot g^{-1}$)	52±6	56±4
Light irradiance per biomass ($W \cdot g^{-1}$)	0.71±0.02	1.46±0.04

Due to the higher levels of biomass in Phase II and taking into account that the inlet flow ammonium concentration remained constant, the residual ammonium concentration in the outlet flow diminished from 39 to 17 ppm $N\text{-}NH_4^+$ (equivalent to 2.8 and 1.2 mM, respectively).

Although some bibliographic studies (Converti *et al*., 2006; Abeliovich and Azov, 1976) reported the ammonium concentration of 2 mM as inhibitory to *Arthrospira* growth, no adverse effect was observed during the present *Arthrospira* culture. Therefore, it can be confirmed the capability of *Arthrospira* to grow using ammonium as a nitrogen source and to withstand residual ammonium concentrations of 2.8 mM.

Under this operational conditions, a light step up produced an increase of biomass productivity (from 24 to 27 $mg \cdot L^{-1} \cdot h^{-1}$), but no statistically significant effect on nitrogen uptake per biomass. Moreover, as both steady states were reached successfully, the light irradiance received by biomass (Phase I: 0.71 $W \cdot g^{-1}$; Phase II: 1.46 $W \cdot g^{-1}$; Maximum value: 1.85 $W \cdot g^{-1}$) did not cause any apparent photoinhibition to the culture.

4.3.1.2 TEST 2: D=0.027 h^{-1}

The second test of this series was performed with a higher liquid input flow rate (D=0.027 h^{-1}) than Test I and at two different illumination levels, 33 and 125 $W \cdot m^{-2}$. Figure 4.5 depicts the evolution through time of biomass concentration, residual ammonium concentration and available irradiance per biomass for test 2.

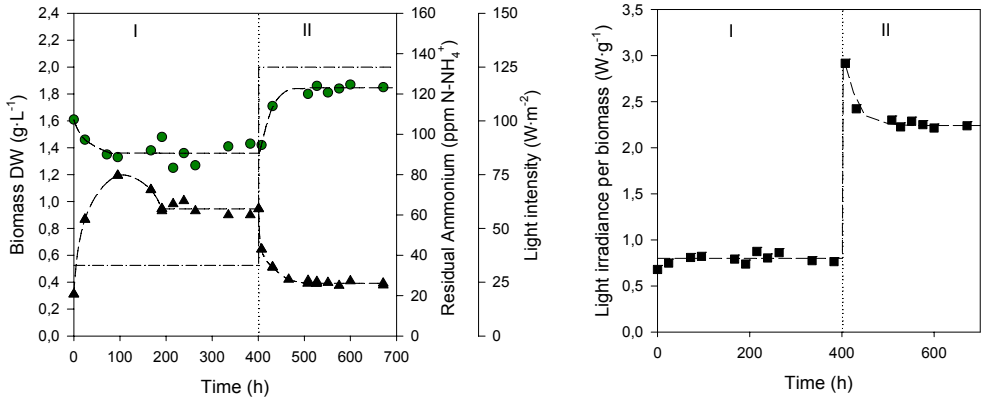

Figure 4.5 Evolution of *Arthrospira* continuous cultures using ammonium as nitrogen source (input ammonium concentration of 140 ppm $N\text{-}NH_4^+$) with changing light intensity levels (Phase I: 33 $W{\cdot}m^{-2}$, Phase II: 125 $W{\cdot}m^{-2}$) and at a fixed dilution rate of 0.027 h^{-1}. LEFT: ● Biomass concentration (g $dw{\cdot}L^{-1}$), ▲ residual ammonium concentration (ppm $N\text{-}NH_4^+$), dashed-dotted line: light intensity ($W{\cdot}m^{-2}$), dashed line: averaged values at steady state and transient light phases. RIGHT: ■ Light irradiance per biomass ($W{\cdot}g^{-1}$).

Initially, light intensity at the surface of the bioreactor was fixed at 33 $W{\cdot}m^{-2}$ and continuous operation of *Arthrospira* culture was started when biomass levels at the end of the batch phase were around 1.6 $g{\cdot}L^{-1}$. After 190 hours, a first steady state was achieved (p=0.64) with biomass values of 1.4 $g{\cdot}L^{-1}$. Five residence times later with established values, light intensity was increased from 33 $W{\cdot}m^{-2}$ to 125 $W{\cdot}m^{-2}$ and the new biomass steady state value (p=0.71) of 1.85 $g{\cdot}L^{-1}$ at 125 $W{\cdot}m^{-2}$ was maintained during four residences times. A summary of the operational conditions together with the mean values of each steady state reached for Test 2 are provided in Table 4.2.

Table 4.2 Mean values (± 95% interval confidence) of main parameters at each steady state reached in Test 2.

Parameter	Phase I	Phase II
Light intensity, I ($W{\cdot}m^{-2}$)	33	125
Liquid input rate, Q (L·d-1)	1.05	1.05
Residence time, ι (h)	37	37
Dilution rate, D (h^{-1})	0.027	0.027
Optical density at 750 nm	1.2±0.2	1.9±0.1
Biomass concentration, DW ($g{\cdot}L^{-1}$)	1.4±0.1	1.85±0.02
Productivity ($mg{\cdot}L^{-1}{\cdot}h^{-1}$)	37±2	50.5±0.5
Input ammonium concentration (ppm $N\text{-}NH_4^+$)	141±5	143±4
Residual ammonium (ppm $N\text{-}NH_4^+$)	63±2	26±1
Nitrogen uptake per biomass, $Y_{N/X}$ ($mg\ N{\cdot}g^{-1}$)	57±4	63±2
Light irradiance per biomass ($W{\cdot}g^{-1}$)	0.80±0.04	2.24±0.02

Similarly to the previous continuous culture (D=0.016 h^{-1}), light increase lead to a higher biomass concentration and productivity, and did not influence nitrogen uptake. The levels of ammonium remaining in the bioreactor, of around 63 ppm $N\text{-}NH_4^+$ (4.5 mM) at phase I and around 26 ppm $N\text{-}NH_4^+$ (1.9 mM) after light increase (Phase II), did not cause a measurable inhibition effect on the biomass growth in these conditions. In addition to this, although a high

light irradiance per biomass (2.92 $W \cdot g^{-1}$) was reached at the beginning of Phase II, no photoinhibition effect was observed.

4.3.1.3 TEST 3: D=0.032 h^{-1}

The third continuous culture was carried out at a higher dilution rate (D=0.032 h^{-1}) than the previous two cultures and at two different illumination levels (33 and 125 $W \cdot m^{-2}$). Figure 4.6 illustrates *Arthrospira* concentration, residual ammonium and light irradiance per biomass evolution through time.

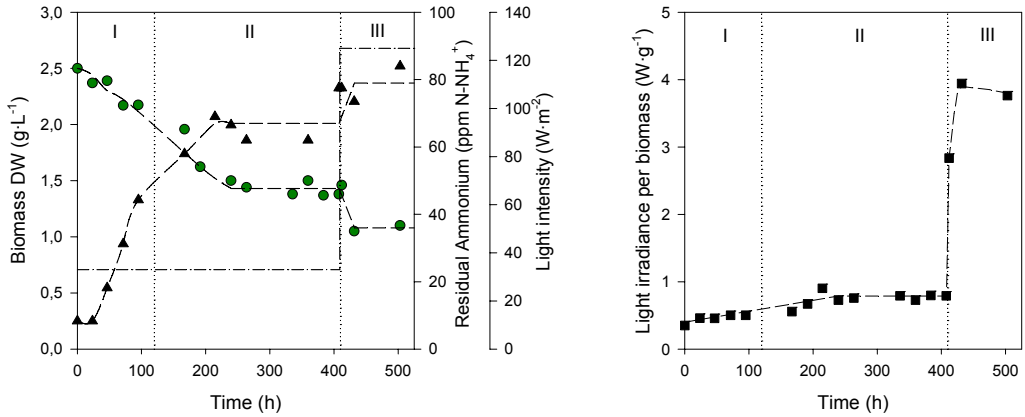

Figure 4.6 Evolution of *Arthrospira* continuous cultures using ammonium as nitrogen source (input ammonium concentration of 140 ppm $N\text{-}NH_4^+$) with changing light intensity levels (Phase I and II: 33 $W \cdot m^{-2}$, Phase III: 125 $W \cdot m^{-2}$) and at a fixed dilution rate (D) of 0.032 h^{-1} except in Phase I where the input liquid flowrate is increased until the D=0.032 h^{-1} is reached. LEFT: ● Biomass concentration (g $dw \cdot L^{-1}$), ▲ residual ammonium concentration (ppm $N\text{-}NH_4^+$), dashed-dotted line: light intensity ($W \cdot m^{-2}$), dashed line: averaged values at steady state and transient light phases. RIGHT: ■ Light irradiance per biomass ($W \cdot g^{-1}$).

Due to the fact that the desired dilution rate (D=0.032 h^{-1}) was higher than the abovementioned cultures (Test 1 and 2), in this test it was decided to perform a gradual increase in the input liquid flow rate during Phase I until 1.23 $L \cdot d^{-1}$ (D=0.032 h^{-1}) was reached (Phase II), so that cells could adapt progressively to the continuous culture conditions.

Biomass concentration of 2.5 $g \cdot L^{-1}$ reached at the end of batch phase started to decrease and 240 hours later a first steady state (p=0.11) was attained at biomass levels of 1.39 $g \cdot L^{-1}$. Five residence times of the first steady state later, light intensity was increased from 33 $W \cdot m^{-2}$ to 125 $W \cdot m^{-2}$ (Phase III). Operational conditions and averaged values for each phase of Test 3 are summarized in Table 4.3.

Based on the previous results, a higher biomass concentration and a subsequent lower residual ammonium concentration for a constant nitrogen culture media concentration were expected after the light increase. However, biomass concentration diminished from 1.39 $g \cdot L^{-1}$ to 1.08 $g \cdot L^{-1}$ and residual ammonium concentration increased from 67 ppm $N\text{-}NH_4^+$ (4.8 mM) to 79 ppm $N\text{-}NH_4^+$ (5.6 mM). In addition to this, although in Phase III biomass levels were quite stable,

optical density decreased from 0.8 to 0.2 and the culture turned to a yellowish colour forming aggregates. The presence of aggregates, also referred as clusters or clots, surely implied that the dry weight measured in the output flow no longer reflected the situation inside the bioreactor. This would explain why the dry weight value did not decrease as strongly as the optical density (Table 4.3).

Table 4.3 Mean values (± 95% interval confidence) of main parameters at each phase of Test 3.

Parameter	Phase II	Phase III
Light intensity, I ($W \cdot m^{-2}$)	33	125
Liquid input rate, Q (L·d-1)	1.23	1.23
Residence time, ι (h)	31	31
Dilution rate, D (h^{-1})	0.032	0.032
Optical density at 750 nm	0.7±0.1	0.39
Biomass concentration, DW ($g \cdot L^{-1}$)	1.39±0.05	1.08
Productivity ($mg \cdot L^{-1} \cdot h^{-1}$)	45±1	34.4
Input ammonium concentration (ppm $N\text{-}NH_4^+$)	133±6	131
Residual ammonium (ppm $N\text{-}NH_4^+$)	67±7	79
Nitrogen uptake per biomass, $Y_{N/X}$ ($mg\ N \cdot g^{-1}$)	49±4	49
Light irradiance per biomass ($W \cdot g^{-1}$)	0.79±0.02	3.85

The biomass aggregation and the change in pigment content observed in the culture indicated that either the residual ammonium concentration of 79 ppm $N\text{-}NH_4^+$ (5.6 mM) or the high local light intensity received by cells (3.94 $W \cdot g^{-1}$) or a combination of both inhibited *Arthrospira* growth and probably influenced protein synthesis.

The hypothesis that the ammonium concentration of 5.6 mM would be inhibitory to *Arthrospira* growth is supported by several authors that reported 6 mM (Carvalho *et al.*, 2004) or even lower ammonium levels (Abeliovich and Azov, 1976; Lattenmayer, 2001; Converti *et al*., 2006) to be inhibitory to *Arthrospira* growth.

Besides, previous experiments under conditions of nitrate limitation resulted in similar modifications of biomass aggregation and colour (Vernerey, 2000). It is possible that the metabolic alterations resulting from deficient nitrogen incorporation, either due to a limitation or due to an inhibition, have an effect on the photosynthetic system due to the limited nitrogen availability for synthesis of either the proteins or the pigments, like the phycocyanins, involved in the process. As a result, a different sensitivity to light intensity might result. In this case, light intensity would have an inhibiting effect at different nitrogen source levels for different nitrogen sources.

For all these reasons, it is highly likely that a combination of high ammonium concentration (5.6 mM) and high irradiance levels (3.94 $W \cdot g^{-1}$) inhibited *Arthrospira* growth and led cells to aggregate.

4.3.1.4 TEST 4: D=0.035 h^{-1}

In order to evaluate whether the inhibition to *Arthrospira* growth caused by a high residual ammonium concentration and high local light intensity was a reversible process and to verify previous results, another culture was carried out.

Focusing on this aim, a new *Arthrospira* culture was started at similar conditions than the previous one (D=0.035 h^{-1} and I=33 $W \cdot m^{-2}$) as shown in Figure 4.7.

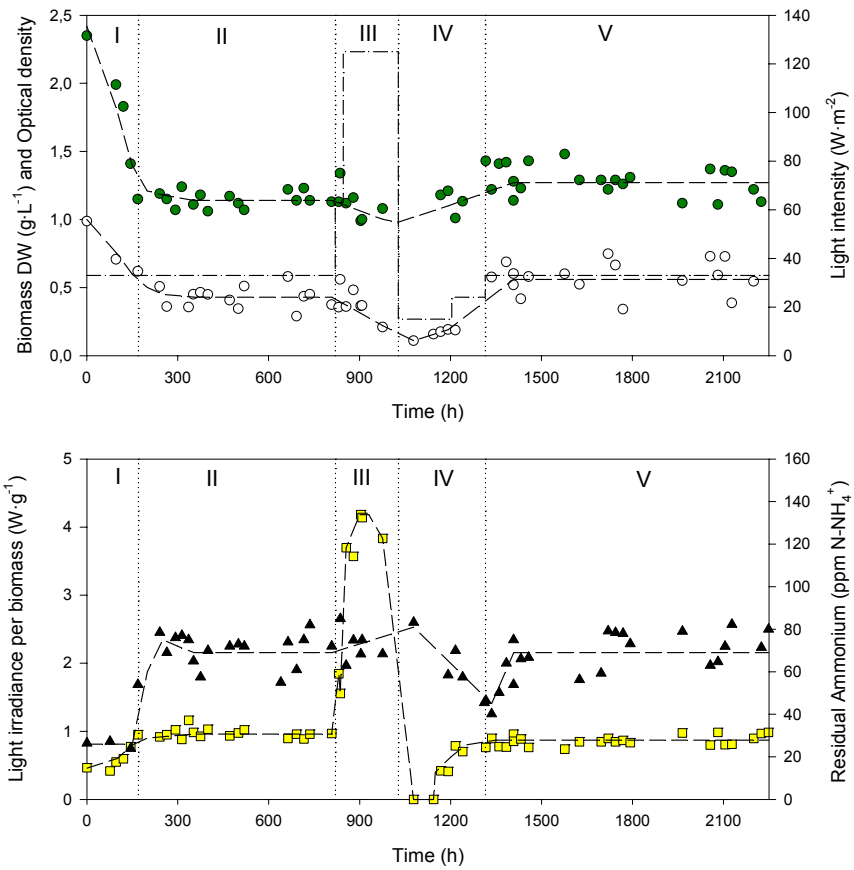

Figure 4.7 Evolution of *Arthrospira* continuous cultures using ammonium as nitrogen source (input ammonium concentration of 140 ppm $N\text{-}NH_4^+$) with changing light intensity levels (Phase I-II: 33 $W \cdot m^{-2}$, Phase III: 125 $W \cdot m^{-2}$, Phase IV: 15-24 $W \cdot m^{-2}$, Phase V: 33 $W \cdot m^{-2}$) and at a fixed dilution rate (D) of 0.035 h^{-1} except (i) in Phase I were the input flow rate is increased until the D=0.035 h^{-1} is reached and (ii) in Phase IV where culture is kept in batch mode for biomass recovery. TOP: ● Biomass concentration (g $dw \cdot L^{-1}$), ○ Optical density at 750 nm, dashed-dotted line: light intensity ($W \cdot m^{-2}$), dashed line: averaged values at steady state and transient light phases. BOTTOM: □ Light irradiance per biomass ($W \cdot g^{-1}$) ▲ residual ammonium concentration (ppm $N\text{-}NH_4^+$).

Like in the previous culture, a gradual increase in input liquid flow rate was performed until reaching the desired dilution rate (Phase I). After the establishment of the first steady state (Phase II), an increase of light would be performed to mimic the same inhibitory conditions that lead to cell death in the previous test (Phase III). After confirmation of cell inhibition in phase III, the culture would be turned into batch (Phase IV) to check the capacity of *Arthrospira* culture to

recover from the inhibition. If so, the culture would be turned into continuous mode (Phase V) to evaluate the capacity to reach a new steady state.

After 350 hours from the end of batch phase, a first steady state (p=0.26) was attained with a biomass concentration of 1.14 $g \cdot L^{-1}$ and a residual ammonium concentration of 69 ppm $N\text{-}NH_4^+$ (4.9 mM) for more than 16 residence times (Phase II Figure 4.7, Table 4.4). Values obtained in this first steady state were in agreement with values from the previous test under similar operational conditions (Phase II, Table 4.3), which were 1.39 $g \cdot L^{-1}$ and 67 ppm $N\text{-}NH_4^+$.

As mentioned, in order to lead *Arthrospira* culture into the inhibitory threshold values of ammonium concentration and of light irradiance supplied to cells, light intensity was increased from 33 $W \cdot m^{-2}$ to 125 $W \cdot m^{-2}$ (Phase III). In the same way as it was observed in test 3, biomass and optical density started to decrease (DW from 1.14 $g \cdot L^{-1}$ to 1 $g \cdot L^{-1}$ and OD from 0.43 to 0.11) with a subsequent increase in the residual ammonium concentration from 69 ppm $N\text{-}NH_4^+$ (4.9 mM) to 89 ppm $N\text{-}NH_4^+$ (6.3 mM) and in the local light irradiance (from 0.96 $W \cdot g^{-1}$ to 4.18 $W \cdot g^{-1}$). Under these conditions, *Arthrospira* turned into a yellowish colour and formed thick clusters indicating that its growth was inhibited (Figure 4.8).

Moreover, the number of clusters formed hindered the dry weight measure, since part of the biomass weighed correspond to aggregates instead of the active *Arthrospira* cells. As shown in Figure 4.8, some *Arthrospira* cells were alive, but trapped inside heterogeneous aggregates formed by cells.

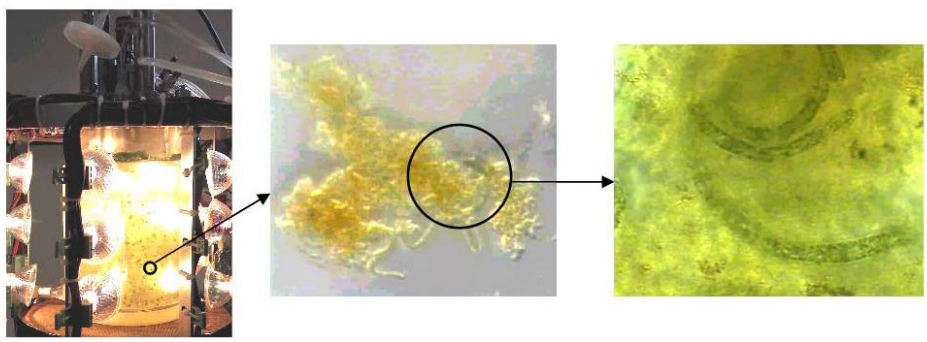

Figure 4.8 Culture and morphology of *Arthrospira* at Phase III where light intensity was 125 $W \cdot m^{-2}$ and residual ammonium concentration was around 89 ppm $N\text{-}NH_4^+$ (6.3 mM). The clusters formed under these inhibitory conditions trapped some *Arthrospira* cells as observed in the microscope. Photo magnification: middle 20x, right 100x.

Phase III lasted for five residence times and at this point it was decided to change the culture operation into a batch mode and to decrease the light intensity to 15 $W \cdot m^{-2}$ to evaluate the capability of biomass to recover (Phase IV). These conditions were kept for the equivalent of 4 residence times of the previous test phase, and since biomass concentration started to increase, light was increased to 24 $W \cdot m^{-2}$. The continuous culture at the same dilution rate and light intensity as in Phase II was started after 234 hours of batch operation (Phase V).

A new steady state (p=0.18) was successfully reached (Table 4.4) and was kept for more than 28 residences times, confirming the complete recovery of the culture.

Table 4.4 Mean values (± 95% interval confidence) of main parameters at each steady state reached in Test 4.

Parameter	Phase II	Phase V
Light intensity, I ($W \cdot m^{-2}$)	33	33
Liquid input rate, Q ($L \cdot d^{-1}$)	1.36	1.36
Residence time, ι (h)	28	28
Dilution rate, D (h^{-1})	0.035	0.035
Optical density at 750 nm	0.43±0.05	0.56±0.09
Biomass concentration, DW ($g \cdot L^{-1}$)	1.14±0.03	1.27±0.05
Productivity ($mg \cdot L^{-1} \cdot h^{-1}$)	40±2	48±3
Input ammonium concentration (ppm $N\text{-}NH_4^+$)	123±4	125±3
Residual ammonium (ppm $N\text{-}NH_4^+$)	69±4	69±5
Nitrogen uptake per biomass, $Y_{N/X}$ ($mg\ N \cdot g^{-1}$)	46±5	44±5
Light irradiance per biomass ($W \cdot g^{-1}$)	0.96±0.03	0.87±0.03

Nevertheless, the morphology of *Arthrospira* cells from this culture (Phase V) was still different from the one of the cells grown using nitrate as a nitrogen source in non limiting conditions but was similar to the ones previously found in nitrate limiting conditions (Vernerey, 2000). Therefore, it is possible that full recovery requires a longer period. For comparison purposes, Figure 4.9 shows *Arthrospira* grown using either ammonium (A) or nitrate under non limiting (B) and limiting conditions (C).

Figure 4.9 Morphology of *Arthrospira* using different nitrogen sources. (A) *Arthrospira* cells grown in the laboratory bioreactor (V=1.6L) using ammonium as nitrogen source. It corresponds to the Phase IV shown in Figure 4.7 (magnification x10). (B) *Arthrospira* cells grown in the pilot plant bioreactor (V=77L) using nitrate as a nitrogen source (magnification x10). (C) Picture of biomass in nitrate limitation. ($0.1\ kg \cdot m^{-3}$ NO_3^-) at $0.05\ h^{-1}$ dilution rate (I: $50\ W \cdot m^{-2}$, 7L bioreactor, magnification x5, from Vernerey, 2000).

From this culture it has been demonstrated the capability of *Arthrospira* to achieve a new steady state after being inhibited by high ammonium concentration and high irradiance levels. In order to overcome such inhibitory conditions the culture was kept in batch and under low illumination levels.

4.3.2 EFFECT OF DILUTION RATE ON PRODUCTIVITY AND RESIDUAL AMMONIUM

In order to evaluate the effect of dilution rate on biomass concentration, productivity and residual ammonium concentration, data from the ammonium cultures obtained at a light intensity of 33 $W \cdot m^{-2}$ were used.

As shown in Figure 4.10, biomass concentration decreases from 1.5 $g \cdot L^{-1}$ to 1.2 $g \cdot L^{-1}$ when dilution rate increasing from 0.016 h^{-1} to 0.036 h^{-1}. Productivity increases with increases dilution rates until reaching a value of 45 mg $dw \cdot L^{-1} \cdot h^{-1}$ at dilution rates between 0.032 h^{-1} and 0.036 h^{-1}.

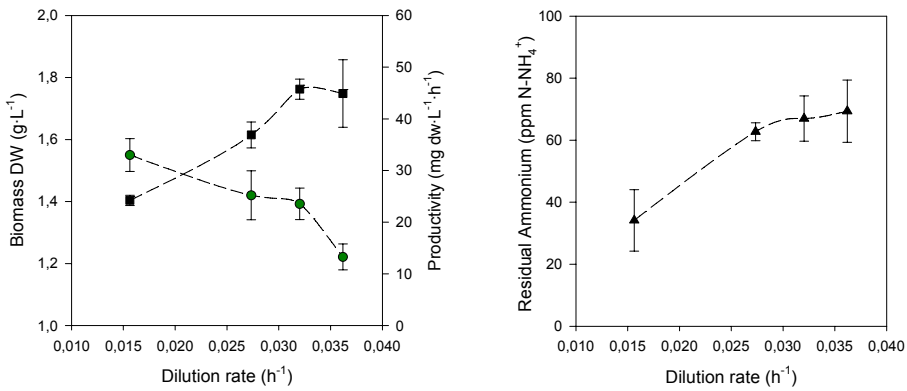

Figure 4.10 Steady state mean values (95% confidence intervals) at different dilution rates (h^{-1}) LEFT: ● Biomass concentration (g $dw \cdot L^{-1}$), ■ Biomass productivity (mg $dw \cdot L^{-1} \cdot h^{-1}$) RIGHT: ▲ Residual ammonium concentration (ppm $N\text{-}NH_4^+$).

At a fixed input ammonium concentration, the residual ammonium concentration increased from 34 ppm $N\text{-}NH_4^+$ to 69 ppm $N\text{-}NH_4^+$ with increasing dilution rates, caused by a decrease of biomass concentration.

4.3.3 *ARTHROSPIRA* BIOMASS COMPOSITION

The biomass harvested at each steady state reached in the previous experiments was analyzed for determining its elemental (C, H, N, S), macromolecular (proteins, carbohydrates, fatty acid profile) and pigment (chlorophyll and phycobilisomes) composition. Moreover, the composition of aggregates formed due to inhibitory conditions of light intensity and residual ammonium concentration was also determined (Test 4, Phase II, see Figure 4.7 and Figure 4.8). For each of the abovementioned compounds, its content in *Arthrospira* biomass is compared with composition values from literature. Besides, the effect of dilution rate, light intensity, aggregate formation and nitrogen source on biomass composition is evaluated as explained in the following paragraph.

The effect of dilution rate on cell composition was evaluated using data from steady states reached under a light intensity of 33 $W \cdot m^{-2}$ to minimize interferences of irradiance, in case illumination level should influence *Arthrospira* composition. Taking into account all the ammonium cultures at 33 $W \cdot m^{-2}$, four different levels of dilution rates ranging between 0.016 h^{-1} and 0.035 h^{-1} were used in the analysis.

The effect of light intensity on composition was evaluated for those tests where a steady state could be achieved at two different illumination levels (Test 1 and Test 2). As for dilution rate, p-values associated with the slope of the linear regression of composition against light intensity is used to conclude whether irradiance influences biomass composition.

Since composition of biomass aggregated was analyzed, changes in composition with respect to the first steady state of Test 4 (Phase I) were determined. In addition to this, biomass composition of the second steady state of Test 4 (Phase IV), where the biomass overcame satisfactorily the inhibitory conditions of Phase II, was used to evaluate whether biomass returned to the initial composition values obtained in the first steady state (Test 4, Phase I).

Finally, the effect of nitrogen source in biomass composition was also studied. For comparison purposes of *Arthrospira* composition, a culture using nitrate as nitrogen source was carried out with the same bench bioreactor as in the ammonium cultures at a dilution rate of 0.032 h^{-1} and a light intensity of 33 $W \cdot m^{-2}$. Since the main objective of this nitrate test was to obtain *Arthrospira* biomass grown using nitrate for comparing its composition with the one of cells grown using ammonium, it has been decided not to include the evolution of the nitrate culture in the results. The comparison of other culture variables, such as biomass concentration or nitrogen uptake, is out of the scope of the current series of experiments, and consequently nitrate culture evolution is not included.

Table 4.5 shows the elemental composition of *Arthrospira* biomass obtained in the test performed at different dilution rates and light intensity values.

Table 4.5 Elemental composition analysis (Mean± standard deviation of n samples analyzed) for each of the *Arthrospira* continuous test using ammonium as nitrogen source performed at different dilution rates (D) and light intensity (I). Percentages do not sum up to 100% due to the lack of determination of oxygen, phosphorous and ashes. Last column shows the corresponding molecular formula. An additional test using nitrate as nitrogen source is also included, for comparison purposes as discussed in the text.

Test (Phase)	D (h^{-1})	I ($W \cdot m^{-2}$)	n	C (%)	H (%)	N (%)	S (%)	Molecular formula
1 (I)	0.0016	33	4	40±3	6.0±0.6	9.3±0.7	0.7±0.1	$CH_{1.78}N_{0.196}S_{0.007}$
1 (II)	0.0016	76	2	25.7±0.6	3.8±0.1	5.5±0.1	0.8±0.2	$CH_{1.19}N_{0.183}S_{0.012}$
2 (I)	0.027	33	4	47.3±0.3	6.8±0.1	11.3±0.2	0.58±0.04	$CH_{1.73}N_{0.205}S_{0.005}$
2 (II)	0.027	125	5	48.0±0.6	7.1±0.2	10.1±0.3	0.52±0.07	$CH_{1.77}N_{0.181}S_{0.004}$
3 (II)	0.032	33	2	34.5±0.2	5.3±0.2	7.94±0.01	1.5±0.1	$CH_{1.84}N_{0.197}S_{0.016}$
4 (I)	0.035	33	4	44±2	6.5±0.2	10±1	0.6±0.3	$CH_{1.78}N_{0.202}S_{0.005}$
4 (II-Cluster)	0.035	125	6	18.4±0.3	3.55±0.08	2.0±0.04	0.70±0.08	$CH_{2.32}N_{0.093}S_{0.014}$
4 (IV)	0.035	33	2	35±0.7	5.3±0.1	8.0±0.1	0.94±0.06	$CH_{1.81}N_{0.196}S_{0.01}$
NO_3^-	0.032	33	4	44.4±0.5	6.7±0.2	11±0.4	0.6±0.2	$CH_{1.80}N_{0.206}S_{0.005}$

The percentages (% dw biomass) do not sum up to 100%, since it was not possible to determine the oxygen, phosphorous and ash content. In addition to this, the molecular formula is shown for each case based on the analyzed elements (C, H, N and S). The coefficients for C, H, N and S are in agreement with those of $CH_{1.65}O_{0.531}N_{0.170}S_{0.007}P_{0.006}$ and $CH_{1.74}O_{0.51}N_{0.196}S_{0.005}$ reported by Cornet *et a*l. (1992a,b) and Morist *et al*. (2001), respectively.

When evaluating the effects of culture conditions on elemental composition (C, N, H and S), it can be observed that:

- Dilution rate did not significantly influence the percentage of carbon (p=0.9), hydrogen (p=0.9), nitrogen (p=0.8) and sulphur (p=0.6) in *Arthrospira* biomass grown using ammonium as nitrogen source.
- Sulphur content was not influenced by light intensity (p>0.05) in any of the tests. In test 1 and 2, nitrogen content was significantly lower (p<0.05) at higher irradiance levels. No firm conclusion regarding the carbon and hydrogen at different illumination levels can be drawn, since in test 1 carbon (p=0.002) and hydrogen (p=0.009) content decreased when light increased, but in test 2 carbon content was not affected by light (p=0.06) and hydrogen increased with light (p=0.04).
- Carbon, hydrogen and nitrogen content of clusters were respectively 56%, 43% and 76% lower than normal culture conditions before the inhibitory phase. However, once biomass reached a new steady state after a batch phase with low light intensity, all the elements recovered to a level of around 80% their of initial levels observed in the first steady state, prior to inhibition.
- Elemental composition did not change significantly between nitrate and ammonium cultures at a 95% confidence interval.

Protein, carbohydrates and total fatty acid content of *Arthrospira* in the tests are provided in Table 4.6.

Table 4.6 Protein, carbohydrates and total fatty acid content (Mean± standard deviation of n samples analyzed) of *Arthrospira* biomass for each of the continuous test using ammonium as nitrogen source performed at different dilution rates (D) and light intensity (I). An additional test using nitrate as nitrogen source is also included, for comparison purposes.

Test	D	I	Protein		Carbohydrates		Total Fatty acids	
(Phase)	(h^{-1})	($W \cdot m^{-2}$)	n	(%)	n	(%)	n	(%)
1 (I)	0.0016	33	6	49±6	6	6±2	-	-
1 (II)	0.0016	76	3	35±9	3	4±1	-	-
2 (I)	0.027	33	2	39±1	2	10±1	3	8±3
2 (II)	0.027	125	2	34±0.8	2	8±1	2	14.2±0.7
3 (II)	0.032	33	2	28±0.1	2	6±2	5	6.7±0.6
4 (I)	0.035	33	4	33±6	3	8±2	4	5.5±0.2
4 (II-Clusters)	0.035	125	4	18±4	4	9±4	10	1.5±1.2
4 (IV)	0.035	33	2	40±8	3	8.1±0.4	2	2.9±0.1
NO_3^-	0.032	33	6	65±9	6	6.4±0.5	6	7±2

Protein levels (as % of DW of cells) for ammonium tests without considering aggregates ranged from 28 to 49%. Although some studies report protein levels in *Arthrospira* biomass around 65% (Ciferri and Tiboni, 1985; Babadzhanov *et al.* 2004), other authors have reported lower protein levels ranging form 38 to 59%, similar to levels obtained in our ammonium cultures (Cañizares-Villanueva *et al*., 1995; Marty, 1997; Vernerey, 2000).

Regarding the effect of dilution rate, light intensity, cluster formation and nitrogen source on protein content, the following conclusions can be drawn from the performed tests:

- Despite the fact that protein content seems to decrease with increasing liquid flow rates, when considering the confidence intervals at an alpha level of 0.05, no significant effect of dilution rate on protein content is found.
- Light intensity has a negative effect on protein content in both Test 1 and 2 in agreement with previously reported observations (Tadros *et al.*, 1993; Tomaselli *et al*., 1997; Olguín *et al*., 2001).
- Biomass aggregates formed in Test 4 (Phase II) had a 53% lower protein content than cells under non-inhibitory conditions such as Phase I. In the same experiment however, after cell recovery from inhibition (Test 4, Phase IV) biomass returned to its initial protein levels.
- Significant differences exist in protein levels among ammonium and nitrate cultures, being higher in the later ones. Olguín *et al*. (2001) already pointed out that *Arthrospira* biomass had lower protein levels when grown using ammonium than when using Zarrouk medium. Such an influence would explain the lower protein levels found in these cultures when compared to bibliographic studies, which frequently are carried out using nitrate as nitrogen source.

Carbohydrates content in *Arthrospira* biomass ranged between 4% and 10% (Table 4.6), in agreement with values found in literature (Ciferri and Tiboni, 1985; Becker and Venkataraman, 1984; Marty, 1997; de Oliveira *et al.*, 1999). Upon examination of the results, neither dilution rate (p=0.15) nor light intensity (p=0.27) had any significant influence on carbohydrates content in *Arthrospira* biomass. Besides, unlike the decrease observed in C, H, N and S and protein content during the formation of aggregates (Test 4, Phase II), carbohydrates increased 56% with respect to the first steady state (Phase I). However, after the batch phase carbohydrates returned to the initial levels. Moreover, when contrasting carbohydrates content in *Arthrospira* grown using either ammonium or nitrate, no significant difference was detected, though nitrogen deficiency seems to stimulate the synthesis of all the carbohydrate fractions (Olguín et al., 2001).

Total fatty acid (FA) content in *Arthrospira* biomass cultured in the ammonium tests oscillated from 4 to 14% (Table 4.6), which are similar to FA levels found by Babadzhanov *et al.* (2004). The fatty acid profile is presented in Table 4.7 (mg FA·g^{-1} dw biomass) and in Table 4.8 (% of total FA).

Table 4.7 Fatty acid profile ($mg \cdot g^{-1}$ dw, Mean± standard deviation of n samples analysed) of *Arthrospira* biomass for each of the continuous test using ammonium as nitrogen source performed at different dilution rates (D) and light intensity (I). An additional test using nitrate as nitrogen source is also included for comparison purposes as discussed in the text. Total amount of saturated fatty acids (SFA), monounsaturated (MUFA) and polyunsaturated (PUFA) are also shown.

Test (Phase)	n	C14:0 Myristic	C16:0 Palmitic	C16:1(t) Palmitelaidic	C16:1(c) Palmitoleic	C17:0 Margaric	C18:0 Stearic	C18:1(t) -	C18:1(c) Oleic	C18:1(c) Vaccenic	C18:2(c) Linoleic	C18:3(c) γ-Linoleic	Total SFA	Total MUFA	Total PUFA	PUFA/SFA
1 (II)	3	-	2.4±0.2	-	0.2±0.1	0.1±0.1	0.8	0.7±0.1	0.3±0.1	0.7±0.1	0.8±0.1	0.5±0.1	3.3±0.2	1.8±0.2	1.2±0.1	0.4±0.01
2 (I)	3	-	39.4±13.3	1.2	2.2±0.6	-	1.0±0.1	-	5.2±1.3	-	14.1±5.7	14.1±7.0	40.4±13	7.7±2.6	28±13	0.7±0.1
2 (II)	2	-	104.4±6.2	-	2.3±0.3	-	2.8±0.1	-	6.3±0.3	-	16.7±0.4	10.0±0.1	107±6	8.6	26.7±0.5	0.2±0.01
3 (II)	5	-	33.2±3.4	0.8±0.2	2.2±0.2	-	0.9	-	4.6±0.4	-	13.4±1.4	11.7±1.1	34.1±3.5	7.7±0.6	25.0±2	0.7±0.04
4 (I)	4	-	28.9±1.0	0.8±0.1	2.2±0.3	-	1.1±0.1	-	3.6±0.1	1.3±0.005	9.8±0.6	7.5±0.9	29.9±0.9	7.8±0.4	17±1	0.6±0.05
4 (II-C)	10	0.2±0.1	7.3±5.5	0.3±0.1	0.4±0.2	0.4±0.2	0.6±0.3	0.3±0.01	1.1±0.7	0.5±0.3	2.9±2.6	3.8±0.6	8.1±5.8	2.2±1.5	4.8±4.7	0.4±0.3
4 (IV)	2	-	13.1±0.4	-	1.3±0.1	-	1.0±0.2	-	2.0±0.0	0.9±0.2	6.0±0.6	5.1±0.6	14.0±0.1	4.2±0.1	11.0±1.3	0.8±0.1
NO_3^-	6	-	33.8±7.0	1.0±0.1	2.1±0.6	-	0.8±0.1	-	3.2±0.3	-	15.4±2.7	17.7±6.0	34.2±6.6	5.7±0.9	33.1±8.7	1.0±0.1

Table 4.8 Fatty acid profile (% total fatty acid, Mean± standard deviation of n samples analysed) of *Arthrospira* biomass for each of the continuous test using ammonium as nitrogen source performed at different dilution rates (D) and light intensity (I). An additional test using nitrate as nitrogen source is also included for comparison purposes as discussed in the text.

Test (Phase)	n	C14:0 Myristic	C16:0 Palmitic	C16:1(t) Palmitelaidic	C16:1(c) Palmitoleic	C17:0 Margaric	C18:0 Stearic	C18:1(t) -	C18:1(c) Oleic	C18:1(c) Vaccenic	C18:2(c) Linoleic	C18:3(c) γ-Linoleic
1 (II)	3	-	37.5	-	2.6	2.1	12.6	10.4	5.2	10.4	12.0	7.3
2 (I)	3	-	52.1	1.1	2.9	-	1.4	-	7.0	-	18.3	17.9
2 (II)	2	-	73.3	-	1.6	-	2.0	-	4.4	-	11.7	7.0
3 (II)	5	-	49.7	1.2	3.4	-	1.3	-	6.9	-	20.0	17.5
4 (I)	4	-	52.6	1.4	4.0	-	1.9	-	6.5	2.4	17.7	13.5
4 (II-Clots)	10	1.1	50.5	0.5	4.0	1.7	5.9	0.5	8.7	4.6	15.3	7.3
4 (IV)	2	-	44.8	-	4.5	-	3.3	-	6.9	2.9	20.4	17.3
NO_3^-	6	-	46.4	1.1	2.8	-	1.3	-	4.6	-	21.0	23.6

Arthrospira fatty acid composition can be found under different culture conditions in bibliography (Cañizares-Villanueva *et al*., 1995; Xue *et al*., 2002; Mühling *et al.*, 2005; Palmegiano *et al*., 2005). Taking into account the influence of several culture conditions factors on fatty acid composition of *Arthrospira* obtained in the present cultures, it was observed that:

- High illumination levels increased the content of total fatty acids (p=0.006), particularly of SFA (p=0.004) and MUFA (p=0.01), though no significant increment was detected on PUFA (p=0.1). Thus, PUFA/SFA diminished significantly (p=0.005) at higher illumination levels. Olguín *et al*. (2001) already detected an increase in MUFA content, particularly of palmitoleic acid (16:1) under higher light irradiances.
- The fatty acid content of biomass clots formed under inhibitory conditions, decreased drastically reaching values around 15% of the initial fatty acid composition (Test 4, Phase I). After the batch phase at low illumination intensities, biomass recovered partially its fatty acid composition (55% of the total FA, specifically 47% of SFA, 52% of MUFA and 69% of PUFA). It was noteworthy that the presence of myristic acid (C14:0), margaric acid (C17:0) and trans-9-octadecenoic acid (C18:1(9t)) were only detected in the biomass clusters.
- Regarding differences in fatty acid profiles due to nitrogen source, only a significant lower MUFA content in nitrate cultures than in ammonium were detected. Consequently, PUFA/SFA factor was higher when using nitrate. Piorreck *et al.* (1984) found no other significant changes in fatty acid compositions caused by different nitrate concentrations.

The predominant fatty acids were palmitic acid (C16:0), linoleic acid (C18:2) (LA), γ-linoleic acid (C18:3) (GLA), oleic acid (C18:1), palmitoleic acid (C16:1), which matches exactly with the order of FA abundance found by Babadzhanov *et al.* (2004) and Maslova *et al.* (2004). Palmitic acid was also the most predominantly FA found by Morist *et al.* (2001), de Oliveira *et al.* (1999) and Mühling *et al.* (2005), but they also found higher levels of GLA than in the present ammonium cultures. The PUFA/SFA ratio was higher than the recommended ratio of 0.45 for the human diet in most of the test, similarly to results reported by Morist *et al.* (2001).

The high content of GLA, ranging form 7 to 17% of total FA obtained in the ammonium cultures are similar to the GLA content reported by de Oliveira *et al.* (1999) and slightly lower than the GLA levels 23–24% 26% to 31% found by Morist *et al.* (2001) and Olguín *et al*. (2001). However, the former higher GLA compositions are in agreement with GLA content of 23% found in the nitrate culture. In any case, the high content of this essential FA is of great value since it has been found to have therapeutic effects on humans such as in the reduction of serum triglycerides and low density lipoproteins levels and the stimulation of the immune system (Ciferri and Tiboni, 1985; Ahlgren *et al.*, 1992; Mühling *et al.*, 2005).

As mentioned in the general introduction, the light-harvesting pigments of *Arthrospira* include chlorophyll *a* (Chl *a*) and phycobiliproteins, which can be classified into phycoerythrin (PE), phycocyanin (PC) and allophycocyanin (APC) (Siegelman and Kycia, 1982). Estrada *et al.* (2001) pointed out that PC was the component mainly responsible for the antioxidant activity of *Arthrospira*. Moreover, such pigments are used as nutrient ingredients and natural dyes for food and cosmetics (Ciferri and Tiboni, 1985).

Table 4.9 shows Chl *a*, PC and APC content of *Arthrospira* biomass (% dw) for each of the continuous tests using ammonium as nitrogen source, together with an additional test performed using nitrate.

Table 4.9 Pigment content (Mean± standard deviation of n samples analyzed) of *Arthrospira* biomass for each of the continuous test using ammonium as nitrogen source performed at different dilution rates (D) and light intensity (I). An additional test using nitrate as nitrogen source is also included, for comparison purposes as discussed in the text.

Test	D	I	Chl *a*		Chl *b*		PC		APC	
(Phase)	(h^{-1})	($W \cdot m^{-2}$)	n	(%)	n	(%)	n	(%)	n	(%)
1 (I)	0.016	33	6	0.9±0.2	6	0.2±0.2	6	0.3±0.2	6	0.2±0.2
1 (II)	0.016	76	3	0.3±0.1	3	0.2±0.3	3	0.15±0.08	3	0.11±0.06
2 (I)	0.027	33	2	0.78±0.02	2	0.06±0.01	2	1.7±0.1	2	0.54±0.07
2 (II)	0.027	125	2	0.63±0.01	2	0.065±0.002	NA	NA	NA	NA
3 (II)	0.032	33	2	0.45±0.01	2	0.024±0.002	2	1.22±0.04	2	0.44±0.03
4 (I)	0.035	33	4	0.80±0.09	4	0.03±0.01	4	0.9±0.5	4	0.6±0.8
4 (II-Clots)	0.035	125	4	0.11±0.03	1	0.037	2	0.06±0.03	2	0.10±0.06
4 (IV)	0.035	33	4	1.0±0.3	4	0.3±0.5	2	0.7±0. 8	2	1±1
NO_3^-	0.032	33	6	1.0±0.1	6	0.1±0.1	6	0.4±0.3	6	0.3±0.1

The results indicate that chlorophyll *a* content of *Arthrospira* biomass was not influenced by the dilution rate used for the continuous cultures ($p=0.6$). However, an increase of illumination produces a significant decrease in Chl *a* levels ($p<0.05$), also in agreement with previous results reported by several authors (Tomaselli *et al.*, 1997; Danesi *et al*., 2004).

Biomass clusters had 84% less chlorophyll *a* content than biomass of the first steady state, but after the recovery phase, chlorophyll levels reached again the initial ones. No significant differences among nitrate and ammonium tests were detected.

Results obtained for chlorophyll *a* content had similar values to the 1% Chl *a* reported in literature (Danesi *et al*., 2004; Rangel-Yagui *et al*., 2004; Bhattacharya and Shivaprakash, 2005). Both PC and APC levels were much lower than the ones found in bibliography, which ranged from 7 to 17% (Pervushkin *et al*., 2001; Bhattacharya and Shivaprakash, 2005; Patel *et al*., 2005) for PC and around 3.8% (Patel *et al*., 2005; Bhattacharya and Shivaprakash, 2005). However, Morist *et al*. (2001) also obtained low percentages of PC in *Arthrospira* biomass ranging from 0.4 to 4%.

4.4 CONCLUSIONS

Several continuous culture tests were performed using ammonium as nitrogen source at different dilution rates, ranging from 0.016 h^{-1} to 0.035 h^{-1}, with at least one step of light at each test. The main conclusions drawn from this study are summarized next.

- The capability of *Arthrospira* to grow using ammonium as a nitrogen source is confirmed. Moreover, when nitrate is present in the outlet due to the fact that initial batch culture phase is done with nitrate instead of ammonium, the evolution of nitrate concentration follows the nitrate wash-out curve. Therefore, it can also be confirmed that the biomass shows a higher affinity for ammonium than for other nitrogen sources.

- In order to avoid inhibition of the *Arthrospira* growth, the steady-state ammonium concentration and the light irradiance per biomass have to be lower than 5.6 mM and 3.94 $W \cdot g^{-1}$, respectively. Such a conclusion was reached after observing that:

    - A steady state of the continuous culture was successfully reached with a steady-state ammonium concentration of 4.5 mM and a light irradiance per biomass of 2.92 $W \cdot g^{-1}$.
    - *Arthrospira* biomass aggregation and inhibition observed in test 3 was caused by either the high residual ammonium concentration of 79 ppm $N\text{-}NH_4^+$ (5.6 mM) or the high local light intensity received by cells (3.94 $W \cdot g^{-1}$) or a combination of both.

- *Arthrospira* is able to recover from inhibitory conditions resulting from high ammonium concentration and high irradiance levels. Full recovery is attained after keeping the culture in batch mode and under reduced illumination levels.

- Light intensity has no effect on sulphur and carbohydrate content in *Arthrospira* biomass. However, an increase of illumination produces a decrease in nitrogen, protein and chlorophyll content and an increase in total fatty acid content, mainly caused by the increases of SFA and MUFA.

- Biomass aggregates formed under inhibitory conditions of ammonium or light have a lower content of carbon, hydrogen, nitrogen, protein, fatty acids and chlorophyll, but a higher amount of carbohydrates than biomass which has not been inhibited.

- Nitrogen source (nitrate or ammonium) has no significant effect on biomass composition, except for protein content, which is higher under nitrate sources.

The obtained results provide an increased knowledge of *Arthrospira* behaviour using ammonium as nitrogen source, which can result from an unstable operation of compartment III. As a result, it can be proposed to design a control strategy maintaining ammonium levels below 5.6 mM in the bioreactor. In case the combination of ammonium and illumination levels achieved result in the modification of the cells behaviour as observed and described above, the effect is reversible and can be easily reversed by introducing a recovery period in batch operation of the culture at low illumination levels.

Unit II

Higher Plant Compartment

Chapter **5**

Baseline data of yield, tissue composition and nutrient uptake from beet and lettuce trials in sealed environment chambers

Chapter **6**

Carbon dynamics in batch and staged cultures of beet and lettuce

Chapter 5

BASELINE DATA OF YIELD, TISSUE COMPOSITION AND NUTRIENT UPTAKE FROM BEET AND LETTUCE TRIALS IN SEALED ENVIRONMENT CHAMBER

5.1 INTRODUCTION

As mentioned in the general introduction, only three plants from a complete optimized menu (designed to supply the dietary requirements of the crew with a 10 day menu cycle) (Waters *et al.*, 2002), would be initially considered for production trials within the MELiSSA loop. The selected species - wheat (*Triticum aestivum* L.), lettuce (*Lactuca sativa* L.) and red beet (*Beta vulgaris* L.) - are representatives of plants with a predominant nutritional value in seed, leaves and hypocotyls respectively. In particular, beet and lettuce have been selected as the first crops to be cultivated in the closed loop demonstration at the MELiSSA Pilot Plant (MPP) located at Universitat Autònoma de Barcelona (UAB). Once these initial closed loop experiments have been performed satisfactorily wheat will be the next crop to be considered. Thus, historical efforts in empirical data collection within the MELiSSA consortium have been focused on beet and lettuce crops.

Data sourced from bibliographic review of beet growth and yield provide insight into its growth characteristics in controlled environment conditions and the required culture conditions for their successful growth in sealed spaces.

The influence of different artificial lighting technologies on beet was evaluated by Goins (2002). In this study, they used High Pressure Sodium (HPS) lamps and Light Emitting Diodes (LEDs), which are semiconductor diodes that when charged with electricity emit a single wavelength of light. Beets grown under HPS lamps produced significantly more biomass (10.4 g dw·plant^{-1}) than beets illuminated with different LEDs configurations (ranging 5.4 to 7.4 g dw·plant^{-1} for 690 + 470nm LEDs and 660 + 470nm LEDs respectively). However, other parameters remained unaffected, such as: beet leaf area (HPS: 1045 cm^2·plant^{-1}; LEDs: 985 to 1270 cm^2·plant^{-1}), net photosynthesis (HPS: 10.2 μmol CO_2·m^{-2}·s^{-1}; LEDs: 7 to 10.8 μmol CO_2·m^{-2}·s^{-1}) and transpiration (HPS: 2.5 mmol H_2O·m^{-2}·s^{-1}; LEDs: 1.5 to 2.5 mmol H_2O·m^{-2}·s^{-1}).

The effect of CO_2 influence has been widely studied and in general, high CO_2 levels increase photosynthetic capacity, daily carbon gain, stomatal conductance and crop yield (Wheeler *et al.*, 1999; Mackowiak and Wheeler, 1996; Demmers-Derks *et al.*, 1998; Monje and Bugbee, 1998; Drake *et al.*, 1997). Similarly, Demmers-Derks *et al.* (1998) studied the impacts of CO_2 and temperature on the growth and yield of beet. An elevated CO_2 level of 1000 μL CO_2·L^{-1} Air (1000 ppm) produced an increase in total dry biomass. Although warm temperatures accelerated the early growth of beet, they had a negative effect on final biomass, probably due to canopy senescence and increased maintenance respiration.

In addition to this, several studies addressed the effects of nutrient stresses on beet growth. An example is a study in which a decrease in plant biomass dry weight and leaf area was observed in five different beet varieties grown under salinity stress (0 to 200 mM NaCl) (Ghoulam *et al.*, 2002). However, another study showed that chlorophyll levels and photosynthetic rates were not affected by different sodium concentrations (0-50 mM NaCl) (Subbarao *et al.*, 2001). Moreover, the use of red beet in closed life support systems is interesting for its enormous capability to uptake sodium. On one hand, beet would be able to tolerate high sodium levels for sources such as urine. On the other side, the sodium accumulation in beet tissue may contribute to continual sodium recycling within the loop (Subbarao *et al.*, 1999, 2000, 2003). Another study showed a reduction in leaf area (80%), total dry biomass (70%) and net photosynthesis (32%) detected in beets grown under a low P (0.025 mM) concentration in the culture medium compared to the control values (0.05 mM), where LA=2269 cm^2·plant^{-1}; total biomass=23.5 g dw·plant^{-1} and Pn 30.3 μmol CO_2·m^{-2}·s^{-1} (Abadia *et al.*, 1987).

Lettuce harvest data collected under different culture conditions within closed environments have also been reported widely in the literature. The effect of different lighting systems was initially studied with HPS and metal halide (MH) lamps. Lettuce grown in NASA's Biomass Production Chamber (BPC) under CO_2 levels of 1200 μL CO_2·L^{-1} Air and a Photosynthetic Photon Flux (PPF) of 186 to 194 μmol PAR·m^{-2}·s^{-1} produced an average total dry

biomass productivity of 5.8 g $m^{-2}\cdot d^{-1}$ with HPS lighting and 7.7g $m^{-2}\cdot d^{-1}$ with MH lighting. Both treatments resulted in a harvest index of 93% and an evapo-transpiration rate of 4 L H_2O m^{-2} d^{-1}(Wheeler *et al.*, 1994, 1995a). Afterwards, the influence of LEDs on lettuce growth was compared to HPS and fluorescent lamps. HPS produced the highest average total dry biomass increment (5.4 $g\cdot m^{-2}\cdot d^{-1}$), followed by; the 5.0 $g\cdot m^{-2}\cdot d^{-1}$ obtained with LEDs (Snap-Lite™ arrays filled with red (660-725 nm) and blue (470nm LEDs) and, the 4.28 $g\cdot m^{-2}\cdot d^{-1}$ with fluorescent lamps under CO_2 concentrations of 1200 μL $CO_2\cdot L^{-1}$ Air and PPF of 187 μmol $PAR\cdot m^{-2}\cdot s^{-1}$(Goins *et al.*, 2001, Berkovich *et al.,* 2004). This study also contributes to confirm that normal growth for lettuce can be achieved using only red and blue photons (Kim *et al.*, 2004; Yorio *et al.*, 2001). However, the work of Goins *et al.* (2001) illustrates that higher yields may be expected using conventional HPS lighting systems.

Regarding salinity stress studies for lettuce, Bie *et al.* (2004) studied the effects of Na_2SO_4 and $NaHCO_3$ salinity on the growth, gas exchange and mineral composition. Results showed that increasing salinity stress (Na_2SO_4: 0 to 60 mM; $NaHCO_3$: 0 to 7.5 mM) diminishes leaf area, plant biomass, net photosynthesis and water uptake.

Beet and lettuce tissue composition allows evaluating the nutritional quality of the crew diet. A detailed literature review of mineral and proximate composition for the selected crops is done in the general introduction (Chapter 1). However, most of the data available corresponds to crops grown in field, where water, nutrient or temperature stresses may exist. Since such stresses may influence crop composition, mineral and proximate content should be determined under controlled environmental conditions in the absence of any limiting environmental factors.

After considering the bibliographic availability of beet and lettuce culture data, it was decided that it is necessary to quantify harvest production, tissue composition, nutrient uptake rate and carbon gain dynamics for the selected crops grown under nominal environment conditions, as expected in the MPP. Therefore, several beet and lettuce cultures were performed in sealed environment chambers (SEC) located at the University of Guelph (UoG) Controlled Environment Systems Research Facility (CESRF). These studies collected baseline growth and tissue composition data of the selected crops under culture conditions anticipated for the MPP. For each crop, batch and staggered cultures were carried out to evaluate effects on biomass productivity and gas exchange dynamics.

The objective of this work is to obtain baseline data relating to harvest biomass, plant mineral and proximate composition and nutrient uptake dynamics for beet and lettuce. Such empirical data from batch and staggered cultures not only will contribute to the proper sizing and design of the Higher Plant Chamber (HPC) prototype to be included at the MPP, but also will be used in growth and yield modeling to support development of the higher level HPC control law.

Initially, destructive analysis performed on the harvested biomass allows for the determination of plant characteristics, such as weight per plant, water content, leaf area and harvest index.

Secondly, mineral, macromolecular (protein, fat, ash and carbohydrates,), fiber and energy content in different plant parts is determined. The nutrient composition of the crops cultivated in a CO_2 enriched environment is of great value for future estimations of diet quality supplied to the crew compartment of the MELiSSA loop.

Lastly, nutrient uptake rates from the hydroponic solution are necessary for evaluating the impact on mass balances of HPC when integrated into the loop. Moreover, the feasibility of estimating the crop proximate composition from the nutrient content is considered.

5.2 MATERIALS AND METHODS

5.2.1 SEALED ENVIRONMENT CHAMBER DESCRIPTION

All crop production experiments were conducted in ambient pressure sealed environment chambers (SEC) located at the UoG CESRF. These two identical plant growth chambers (Figure 5.1), measuring 4.5 m x 2.8 m x 2.3 m (LxWxH) internally, have a 5 m^2 growing culture area. This production area is the same as originally envisioned for the experimental culture chambers of the MPP, although it is the subject of subsequent chapters to finalize this production size estimate (Chapter 7) and to evaluate its integration on the mass balances of the MPP, using the data presented in this chapter.

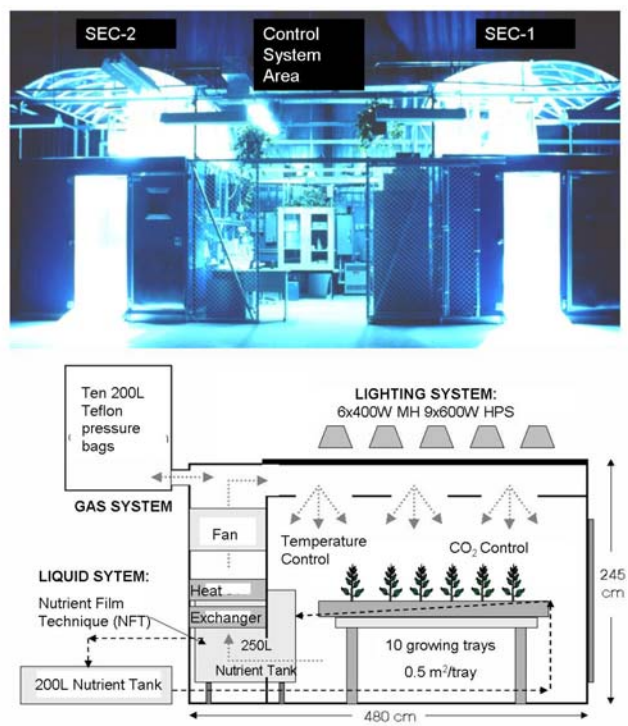

Figure 5.1 Picture (Top) and sketch (Bottom) of Sealed Environment Chambers (SEC).

A detailed description of the chamber is included here to reflect changes in the initial configuration described by Dixon *et al.* (1999).

5.2.1.1 LIGHTING SYSTEM

Overhead irradiation was provided by 400 Watt MH and 600 Watt HPS lamps (PL Light Systems, Grimsby, ON, CA), positioned over each chamber and mounted externally to the chambers. Cooling of the lamp loft, positioned externally to the chamber, was accomplished with forced air venting.

Photosynthetically photon flux (PPF), measured at bench height using a LI-COR LI191SA Quantum Sensor (LICOR Inc, Lincoln, NE, USA), ranged between 400-450 µmol $PAR \cdot m^{-2} \cdot s^{-1}$. All crops were growing under conditions of a 14/10 hour light/dark (06:00-20:00) photoperiod.

5.2.1.2 LIQUID SYSTEM

Plants were watered using the Nutrient Film Technique (NFT). The nutrient solution was stored in a 200 L stainless steel tank located inside the chamber, was continuously pumped (Model OM-3435: Setcho, Hauppage, NY, USA) and was distributed to the heads of 10 stainless steel growing trays. The hydroponic solution flowed by gravity along the 2.5 m long trays (pitched at 2% grade) back to the stainless steel tank. Evapo-transpired water was condensed using a cooling coil and collected in a stainless steel tray positioned under the coil. The condensed water then flowed by gravity into an outside storage tank. A floating level sensor activated a metering pump (Model HD; Barnant Co., MA, USA), which returned condensed water to the nutrient solution reservoir.

5.2.1.3 GAS SYSTEM

Both chambers were atmospherically isolated from the exterior. All the major variables in the aerial environment, such as temperature, humidity, CO_2 and O_2 composition and pressure were monitored and controlled.

- **Temperature Control**

Two fans mounted inside the chamber distribute the air past heat exchange coils and through the growing area. Air temperature was controlled by modulated steam and chilled water valves (M100 Motor Activator, Johnson Controls) feeding a single heat exchange coil mounted in the chamber plenum. Temperature control range was 10-40 ºC ± 0.2 ºC and set point values were 26/20 ºC day/night coupled to the photoperiod.

- **Pressure Control**

Atmospheric pressure inside the chamber was passively controlled by ten 200L double sealed Teflon TM liners (Now Technologies Inc., Minneapolis, MN, USA) manifolded on a 50 mm diameter stainless steel tube, which protruded through the rear wall of the chamber. This provided a total expansion volume potential of 2 m^3 ± 1 m^3, which represented about 7% ± 3% volume expansion/contraction capability. During the day period, the Teflon bags would passively expand to maintain constant chamber pressure at ambient levels. During the dark

period reduced chamber volume, brought about by temperature reduction, would result in the passive contraction of the Teflon bags to maintain constant pressure.

- **Atmospheric Composition Control**

Both O_2 and CO_2 concentration in the chamber growing volume were monitored continuously using an Infrared Gas Analyzer (IRGA) for CO_2 (LiCor LI6262, Li-Cor Inc. Lincoln, NE, USA) and a Paramagnetic Analyzer for O_2 (Model 200, California Analytical Instruments, Orange, CA, USA). The computer controller maintained atmospheric CO_2 at fixed concentrations (1000 µL $CO_2 \cdot L^{-1}$ Air) during day-light hours using a compensatory system drawn from bottled CO_2. During the dark period, no provision was made to scrub CO_2 accumulations resulting from canopy respiration. Relative humidity inside growing area was measured and excess water vapour was removed through condensation on the cooling coil. Addition of water vapour was not required since evapo-transpiration rates were sufficient to maintain humidity level near 70%.

5.2.1.4 COMPUTER CONTROL SYSTEM

Chamber environment control and data acquisition was achieved using software customized by L.W. Anderson Software Consultant Ltd. (Leamington ON, CA).

5.2.2 EXPERIMENTAL DESIGN

Empirical production trials were performed to collect baseline data sets for two of the three MELiSSA candidate crops: beet (*Beta vulgaris* L., Betterave Detroit Medium Top, 70 days) and lettuce (*Lactuca sativa* L., Grand Rapids, 45 days). Batch cultures, with a single seeding date, and staggered (or staged) cultures, with multiple seeding dates, were the two different production regimes used for each crop. In the staged cropping scenario, seeding and harvesting occurred at 10 day intervals. This resulted in multiple age classes represented in the chamber once full stocking was achieved.

For beet, three batch (BB1, BB2 and BB3) and two staggered (BS1 and BS2) independent trials were completed. Equally, three batch (LB1, LB2 and LB3) and two staged (LS1 and LS2) independent trials were carried out with lettuce. Whenever possible trials were completed simultaneously using both SEC chambers.

5.2.3 EXPERIMENTAL PROCEDURE

5.2.3.1 LEAKAGE TEST

Following equipment start verification and before starting the plant cultures, a 48 hour leak test was completed using CO_2 as a marker gas. The chamber was operated at the temperature and humidity conditions of the culture and the CO_2 demand was set to 1200 ppm.

The CO_2 injection system remained on during equilibration and once demand levels were reached, shut-off. The leakage rate was determined from the slope of the decay profile in CO_2 over time bracketing the intended CO_2 concentration for the experiment.

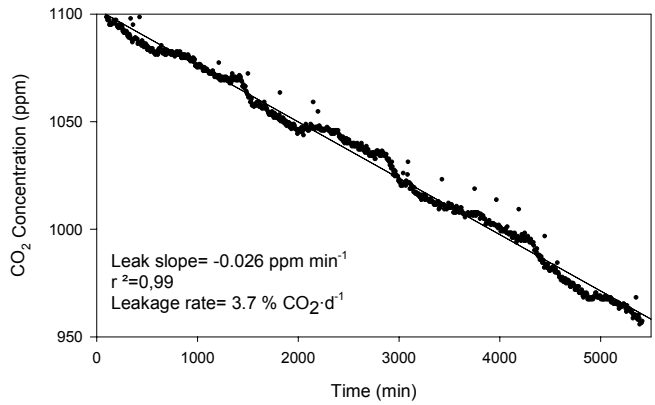

Figure 5.2 Typical leakage rate profile

The leakage rate is used as a correction term in the calculation of net carbon exchange rate (as in Chapter 6).

5.2.3.2 SOWING AND HARVEST

Beet and lettuce seeds were initially germinated in a research greenhouse using Rockwool© cubes. During the germination and true leaf emergence period, seedlings were watered regularly with distilled water and once weekly with a dilute fertilizer solution (20-8-20 $mg \cdot L^{-1}$ N-P-K commercial). After 30 days for beet and 20 days for lettuce, the Rockwool© cubes containing seedlings were positioned in larger cubes (4" x 4" x 2.5", 625 cm^3) to improve water distribution in the hydroponics channels and were transferred to the chamber growing trays. Trays were covered once the blocks were in position so as to minimize the growth of algae on the surface of the Rockwool©.

In batch cultures a total of 120 seedlings (12 plants per stainless steel trough) were planted at once and harvested on the same day after their growing period.

In staggered cultures a 10 day cycle between planting was used. Figure 5.3 shows the procedure for staggered production from the initial sowing to the harvest of the mature plants.

For beet staged experiments 24 seedlings were transferred inside the chamber after 30 days of germination and seedling growth. Following the initial planting, the chamber was planted with 24 additional plants at 10 day intervals. This procedure continued until full chamber stocking (age classes of 40, 50, 60 and 70 days were represented).Thus, after 40 days in chamber, the first plants reached the mature age of 70 days and were harvested. On the same day, 24 new seedlings were transferred from the germination area to the vacant growing trays. On the final day of the experiment all plants from each of the four age classes were harvested and analyzed.

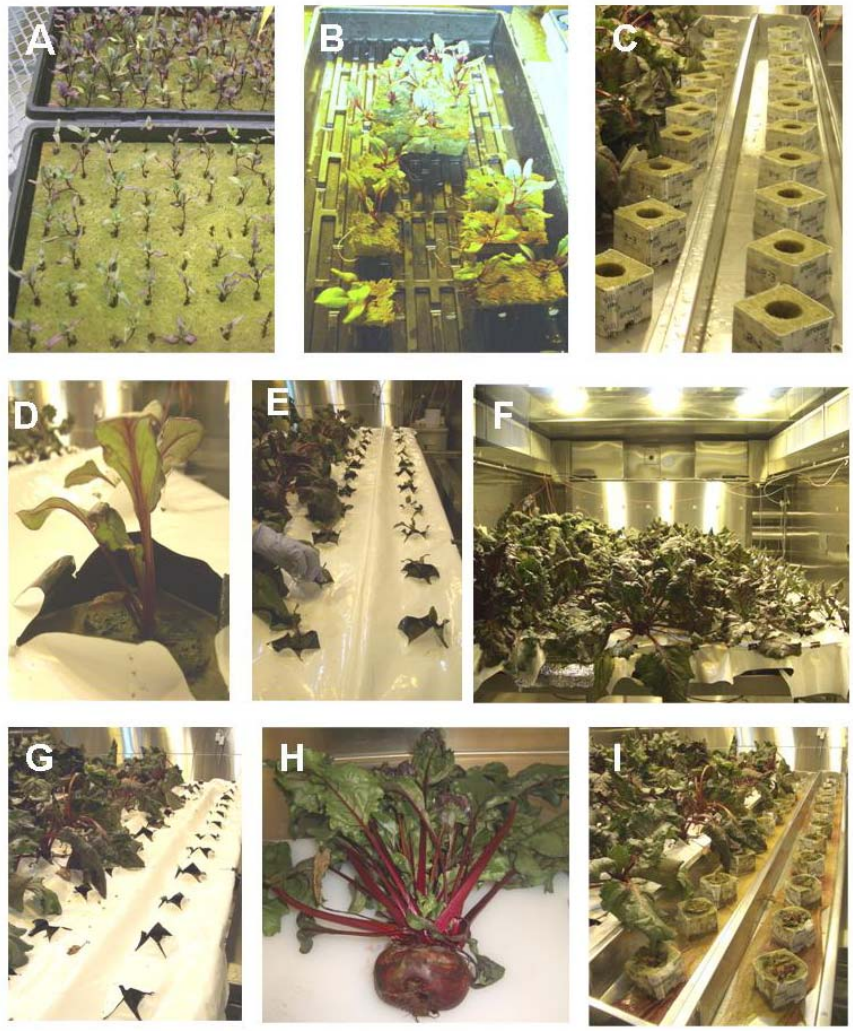

Figure 5.3 Experimental procedure for staged cultures inside the SEC chambers from the initial sowing to the harvest of mature beets: (A) initial germination in a research greenhouse, (B) selection of 24 germinated seedlings for transfer to the SEC chamber, (C) large Rockwool© cubes inside the SEC trays, where the germinated seedlings are introduced, (D) seedling already transferred into the chamber with the tray covered, (E) watering the 24 sowed with nutrient solution just before closing the SEC chamber, (F) view of a beet staggered production trial with plants of different ages at full chamber stocking, (G) harvest of 24 mature plants after 10 days from last sowing, (H) mature beet plant harvested, (I) harvest of beet roots and removal of old Rockwool© cubes before introducing another 24 young seedlings.

For lettuce staged experiments, 36 seedlings were transferred inside the chamber after 20 days of germination and seedling growth. Following the initial planting, the chamber was planted with 36 additional lettuce seedlings at 10 day intervals. This procedure continued until full chamber stocking (age classes of 30, 40 and 50 were represented). Thus, after 30 days in chamber, the first plants reached the mature age of 50 days and were harvested. On the same day as harvest, 36 new seedlings were transferred from the germination area to the vacant growing tray. On the final day of the experiment all plants from each of the 3 age classes were harvested and analyzed.

5.2.3.3 NUTRIENT SOLUTION REPLACEMENT

The nutrient solution used in all experiments had the composition shown in Table 5.1. The pH of the solution is adjusted to 6 with the addition of 1 M $NaHCO_3$ solution at a rate of approximately 25 mL per 100 L solution total volume. At the initial transplant of the seedlings, 160 L of nutrient solution was pumped to the internal nutrient solution reservoir. This solution was re-circulated within the growing system for five subsequent days without any amendments to the solution composition. Every seven days after initial planting for batch cultures and every five days after initial planting for staged cultures, the used solution is pumped out the reservoir and replaced with 160 L of fresh nutrient solution.

Solution volumes were measured at the start and end of the change-over periods to allow for the correction of nutrient uptake results due to evapotranspiration. This was completed using pumping to (fresh solution) or from (used solution) large graduate tanks. Three 25 mL samples were taken for each of the fresh and used nutrient solutions on every solution change-over day. These samples were then stored in a dark refrigerator (3°C) until analyzed with off-line HPLC (high performance liquid chromatography) for nutritionally important anions and cations.

Table 5.1 Nutrient solution composition used for beet and lettuce cultures (Hoagland, 1950). Concentrated stocks were made (100x reservoir strength solution) by separating calcium nitrate from the rest of the solution salts. This prevented precipitation of calcium salts that would otherwise occur in a concentrated mix. The reservoir solution was made by dilution of Stock A with the remaining components and distilled water in a large graduated tank.

Stock Solution	Solution Components	Reservoir Solution Concentration ($mmol \cdot L^{-1}$)
A	$Ca(NO_3)_2.4H_2O$	3.62
	$FeCl_3$	0.025
B	$MgSO_4.7H_2O$	1.00
	KNO_3	5.00
	$NH_4H_2PO_4$	1.50
	$(NH_4)_2SO_4$	1.00
Micronutrients	H_3BO_4	0.020
	$MnSO_4.H_2O$	0.005
	$ZnSO_4.7H_2O$	0.0035
	$CuSO_4.5H_2O$	0.0008
	$H_2MoO_4(85\%MoO_3)$	0.0005

5.2.4 ANALYTICAL METHODS

5.2.4.1 BIOMASS ANALYSIS

After harvesting, plant parts were sampled at the individual plant scale with the exception of roots, since in some cultures harvested root material was pooled by each trough in the chamber. Biomass data were collected for leaves, roots and in the case of beet, hypocotyls. The following data were collected;

- **Fresh Weight (FW)**

  Plant weight, by part, obtained just after harvesting, expressed as g $fw \cdot plant^{-1}$.

- **Dry Weight (DW)**

Plant weight, by part, obtained after at least four days in a drying oven at 60ºC, expressed as g dw·plant^{-1}.

- **Harvest index (HI)**

Harvest Index corresponds to the percentage of edible material in plant tissue (g edible dw·(g total dw)$^{-1}$). For beet, hypocotyl and leaves are the edible fractions and roots the inedible fraction. For lettuce, leaves are the edible part and root the inedible.

- **Total Plant Productivity**

Total plant productivity (g dw·m^{-2}·DIC^{-1}) was calculated as the total biomass harvested divided by the production area and by the total days in chamber (DIC).

- **Leaf Area (LA)**

Leaf area (cm^2·plant^{-1}) was measured on a representative sub-sample of the harvested plants using a LiCOR 3100 Leaf Area Meter (Li-Cor Inc., Lincoln, NE, USA). Initial leaf area was also determined on a sub-sample of the remaining and representative (un-planted) seedlings.

- **Mineral Analysis**

Harvested tissue was pooled for mineral (Ca, K, Mg, P, N and C) analysis. Edible and inedible fractions of each crop were analyzed by the UoG Laboratory Services.

The concentration of Ca, K, Mg, and P in plant materials was determined using a high temperature dry oxidation of the organic matter and the dissolution of the ash with hydrochloric acid. Mineral concentrations are determined using a Varian atomic absorption spectrometer and a Technicon auto analyzer.

The method used to quantify the total N in plant samples is based on the Dumas Method. This method involves the conversion all the forms of N into gaseous nitrogen oxides (NOx) by combustion in an oxygen-rich atmosphere at about 1000ºC, reducing the NOx gases catalytically (metallic copper, tungsten) to N_2 and quantifying the amount of nitrogen gas by a thermal conductivity cell (Nollet, 2004).

The total carbon content in plant samples were measured using the combustion method E1019, approved by the American Society for Testing and Material, using a LECO SC-444 Carbon Analyzer (LECO Instrument Limited, Mississauga, ON, CA). Plant samples were combusted at 135 ºC and the CO_2 produced was measured by an infrared detector.

- **Proximate Analysis**

The proximate analysis includes the determination of the macromolecular composition (fat, protein, ash, carbohydrates and moisture) and calorie content. Methods used for proximate tissue analysis were developed by UoG Laboratory Services and accredited by the Standards Council of Canada.

Fat content was measured using the Soxhlet extraction procedure described in FC-LP-203 UoG procedure based on AOAC-920.39 (1990). Protein content was determined as detailed in FC-PR-109 UoG procedure (‘Crude protein in Food & Feed products by

Combustion') based on AOAC 990.03, 992.15, 992.23 (1990) and LECO corporation. Ash determination was done in accordance with AOAC Method 930.05 (1990). Moisture content was obtained according to AOAC Method 930.04 (1990). After determining ash, fat, protein and moisture content, carbohydrates were calculated by difference. Energy content ($kcal \cdot g^{-1}$) of plants was obtained by completely combustion of dry biomass in a bomb calorimeter.

- **Fiber Analysis**

The analyses of Neutral Detergent Fiber (NDF), Acid Detergent Fiber (ADF) and lignin from plant samples were carried out by Agri-Food Laboratories (AgTest, Guelph, ON, CA).

NDF was measured using a gravimetric determination of amylase treated ADF in feeds (Merters, 2002). In addition to the components which make up ADF, NDF contains hemicelluloses, which are a more digestible fiber fraction. NDF values are good predictors of dry matter intake.

Lignin and ADF content were determined simultaneously using a titration method as described in AOAC-973.18 (1990). ADF consists of cellulose, lignin, bound protein, and acid insoluble ash portions. Since these constituents are quite indigestible, ADF is a negative indicator of energy level in grains, i.e., as ADF increases, digestible energy is decreased.

5.2.4.2 NUTRIENT SOLUTION COMPOSITION ANALYSIS

Nutrient solution samples are analyzed using the Dionex HPLC Model DX500 (Sunnyvale, CA, USA) for the ions of interest which included NO_3-, PO_4^{3-}, SO_4^{2-}, NH_4^+, Na^+, K^+, Ca^{2+}, Mg^{2+}. Nutrient uptake rates were determined over change-over period (by concentration difference in solution samples) and integrated to generate a profile of the accumulated nutrient uptake for NO_3-, PO_4^{3-}, SO_4^{2-}, NH_4^+, Na^+, K^+, Ca^{2+}, Mg^{2+} over the period of crop growth.

5.2.4.3 ATMOSPHERIC COMPOSITION ANALYSIS

SEC chambers are equipped with a CO_2 gas analyzer IRGA LiCor LI6262 (Li-Cor Inc. Lincoln, NE, USA) which measured, online, the CO_2 composition in samples actively drawn from the growing volume by vacuum pump every 3 minutes. Oxygen was measured on the same sample with an O_2 analyzer Model 100P (California Analytical Instruments, Orange, CA, USA).

5.2.5 DATA ANALYSIS

All data analyses were completed using the Sigmaplot® statistical software (SPSS Inc.) or the S-PLUS® software (Insightful Corp.) with libraries for non-linear and linear models described in Venables and Ripley (2002).

Analysis of variance (one-way ANOVA) was performed to test significant variation in response to replications. In order to determine significant differences the Fisher least significant difference test was used with a significance level of $p<0.05$.

5.2.6 PLANT GROWTH CURVES

In classical plant growth analysis, defined functional approaches are fitted crop to biomass accumulation obtained from the dry weight increment between successive harvests (Hunt, 1982). Although generally these empirical models use time as independent variable, other parameters such as accumulated day degrees can be employed.

Empirical growth functions are used mainly as description of experimental data or as part of a larger model. Two of the most frequently used empirical models for plant growth are the exponential growth function and the Gompertz function (Gompertz, 1825).

Simple exponential growth is the most basic growth function, which assumes that the quantity of growth machinery is proportional to dry mass (W), that works at a constant rate and that growth is irreversible. This model considers that growth is independent of substrate availability, implying that either nutrient supply is proportional to biomass growth or nutrient components are in excess. Consequently, the model can apply when sources are much stronger than sinks or in the early stages of growth when there is negligible shading so that substrate supply is approximately proportional to plant dry mass and the plant is vegetative (Thornley and Johnson, 2000). In the exponential equation [Eq.5.1] , μ corresponds to the specific growth rate and W_0 to the initial DW.

$$W = W_0 \exp[\mu \cdot t] \qquad \text{[Eq. 5.1]}$$

The Gompertz growth equation assumes that the substrate is non-limiting so that the growth is always saturated with substrate, the quantity of growth is proportional to the dry biomass with a constant proportionality and the effectiveness of the growth decays with time according to first-order kinetics, giving exponential decay. This decay can be viewed as due to degradation, or senescence, or development and differentiation (Thornley and Johnson, 2000). In the Gompertz function [Eq. 5.2], W_0 corresponds to the initial biomass dry weight, μ_0 to the value of specific growth rate at t=0 and D_r is a parameter describing the decay in the specific growth rate.

$$W = W_0 \exp\left[\frac{\mu_0(1-e^{-D_r t})}{D_r}\right] \qquad \text{[Eq. 5.2]}$$

5.2.7 CULTURE CONDITIONS

Table 5.2 and Table 5.3 show a summary of the main operational conditions for beet and lettuce cultures respectively.

Table 5.2 Experiment summary sheet for beet (*Beta vulgaris* cv. Detroit Medium Red) batch (3 replicates) and staged (2 replicates) cultures. NA: Not available, NFT: Nutrient Film Technique.

Parameter	Batch Cultures			Staggered Cultures	
	BB1	BB2	BB3	BS1	BS2
Chamber used	SEC-1	SEC-1	SEC-1	SEC-1	SEC-1
Photoperiod (h day/night)	14/10	14/10	14/10	14/10	14/10
Demand Temperature (ºC day/night)	25/20	25/20	25/20	25/20	25/20
Relative Humidity average (% day/night)	69/73	67/72	NA	56/59	57/66
PPF average ($\mu mol \cdot m^{-2} \cdot s^{-1}$)	476	444	400	NA	407
Demand CO_2 ($\mu L\ CO_2 \cdot L^{-1}$)	1000	1000	1000	1000	1000
Daily leakage rate at CO_2 level of 1000 $\mu L\ CO_2 \cdot L^{-1}$ Air (% $CO_2\ d^{-1}$)	14	NA used 3.9	3.9	NA used 6.7	6.7
Hydroponic system	NFT	NFT	NFT	NFT	NFT
Number of plants inside full chamber	120	120	120	96	96
Number of plants harvested at end culture	120	120	120	384	192
Production area (m^2)	5	5	5	4	4
Planting density (number plants$\cdot m^{-2}$)	24	24	24	24	24
Total days in chamber (DIC) or length of experiment (d)	42	35	36	160	80
DIC of plants (d)	42	35	36	10,20,30,40	
Days after planting (DAP) or crop age (d)	72	67	66	40,50,60,70	

Table 5.3 Experiment summary sheet for lettuce (*Lactuca sativa* L. cv. Grand Rapids) batch (3 replicates) and staged (2 replicates) cultures. NA: Not available, NFT: Nutrient Film Technique.

Parameter	Batch Cultures			Staggered Cultures	
	LB1	LB2	LB3	LS1	LS2
Chamber used	SEC-2	SEC-2	SEC-1	SEC-1	SEC-1
Photoperiod (h day/night)	14/10	14/10	14/10	14/10	14/10
Temperature (ºC day/night)	25/20	25/20	25/20	25/20	25/20
Relative Humidity average (% day/night)	67/73	70/73	56/65	47/62	54/63
PPF average ($\mu mol \cdot m^{-2} \cdot s^{-1}$)	380	431	456	450	NA
Demand CO_2 ($\mu L\ CO_2 \cdot L^{-1}$)	1000	1000	1000	1000	1000
Daily leakage rate at CO_2 level of 1000 $\mu L\ CO_2 \cdot L^{-1}$ Air (% $CO_2\ d^{-1}$)	NA used 6.7	6.7	3.7	NA used 6.7	4.4
Hydroponic system	NFT	NFT	NFT	NFT	NFT
Number of plants inside full chamber	120	120	120	108	108
Number of plants harvested at end culture	120	120	120	288	228
Production area (m^2)	5	5	5	4.5	4.5
Planting density (number plants$\cdot m^{-2}$)	24	24	24	24	24
Total DIC or length of experiment (d)	33	37	35	80	70
DIC (days in chamber)	33	37	35	10,20,30	
Days after planting (DAP) or crop age (d)	53	57	64	30, 40, 50	

Figure 5.4 shows a typical temperature and humidity profile inside one of the sealed chambers during a 5 day period. Temperature evolution matches the temperature demanded by the control system (25/20 ºC day/night) only with a 0.5 ºC offset. Relative humidity, which is only partially controlled inside the chamber, presents higher values during night periods than during day hours.

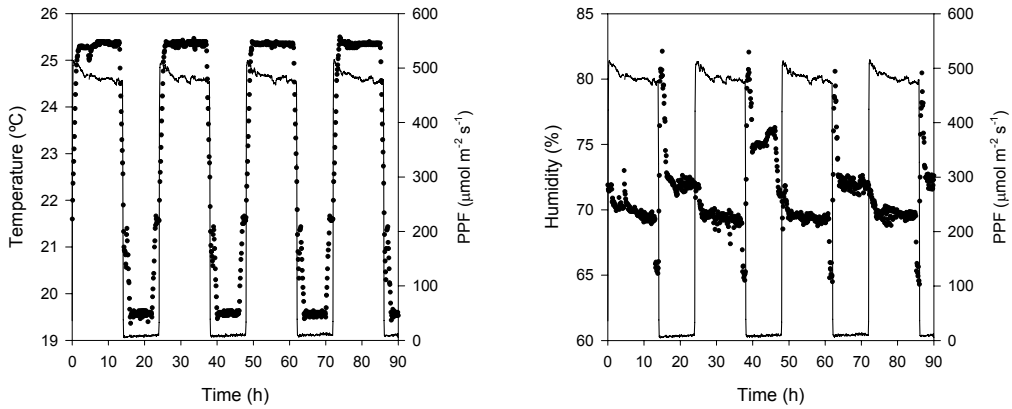

Figure 5.4 Typical temperature (ºC) and humidity (%) profile inside the SEC chambers (●) with a 14/10 h day/night photoperiod (solid line: photosynthetic photon flux, PPF in µmol PAR·m^{-2}·s^{-1} during a 5 day period of a beet batch culture.

Photosynthetic photon flux (PPF) values (Table 5.2 and Table 5.3) differ slightly between experiments due to several factors such as lamp depreciation or short-term light curves performed in some experiments, where light was attenuated with neutral density screens.

In staggered cultures beet plants were grown for a period of 30 days in a research greenhouse and 40 days inside the chamber (DIC). Therefore, the crop age of a mature plant was 70 days (days after planting, DAP=70). However, in the final harvest 4 different beet ages are collected (DAP=40, 50, 60 and 70). Similarly, lettuce plants were transferred after 20 days of sowing into the chamber, where they resided for 30 days. The final harvest included 3 different lettuce ages (DAP=30, 40 and 50).

5.3 RESULTS AND DISCUSSION

5.3.1 BIOMASS PRODUCTION

The following tables provide a summary of harvest and yield data collected for both the beet and lettuce batch and staggered experiments conducted using NFT.

5.3.1.1 BEET HARVEST DATA

The first series of beet trials started with 3 batch cultures (BB1, BB2 and BB3) at the culture conditions reported at Table 5.2.

At the end of each beet batch culture, 120 plants were destructively analyzed by plant part in order to determine biomass productivity. Results are summarized in Table 5.4 for each beet batch culture together with the average value calculated among replications. In addition to this, Figure 5.5 shows the edible dry weight and growth rate per plant part (leaves and hypocotyl), total plant water content and harvest index for each trial.

Table 5.4 Harvest data for beet grown in batch cultures. Values represent the mean (± 95% confidence interval) of 120 plants in each of the BB1, BB2 and BB3 cultures and of 360 plants for the mean column, except for leaf area where:(1) n=15 (2) n=30 (3) n=13 (4) n=21 (5) n=20 (6) n=54 .

Beet Batch Harvest Data	BB1	BB2	BB3	Mean
Leaves				
Fresh Weight, FW (g fw·plant^{-1})	126±10	77±6	81±8	95±5
Dry Weight, DW (g dw·plant^{-1})	12.28±1.95	10.03±0.66	9.49±0.73	10.60±0.47
Growth rate (g dw·plant^{-1}·DIC^{-1})	0.29±0.02	0.29±0.02	0.26±0.02	0.28±0.01
Initital Leaf Area, LA_o (cm^2·plant^{-1})	NA	25±4(1)	17±2(1)	21±3(2)
Leaf Area, LA (cm^2·plant^{-1})	1375±380(3)	754±75(4)	1140±167(5)	1046±124(6)
Total DW (g dw)	1474	1203	1138	1272
Hypocotyl				
FW (g fw·plant^{-1})	100±9	63±5	87±8	83±5
DW (g dw·plant^{-1})	12.06±0.98	7.54±0.69	11.84±1.02	10.48±0.56
Growth rate (g dw·plant^{-1}·DIC^{-1})	0.29±0.02	0.21±0.02	0.33±0.03	0.28±0.01
Total DW (gdw)	1447	904	1421	1257
Roots				
FW (g fw·plant^{-1})	11.0±1.1	7.4±0.5	7.7±0.3	8.7±0.4
DW (g dw·plant^{-1})	1.05±0.09	1.04±0.08	1.14±0.05	1.08±0.04
Growth rate (g dw·plant^{-1}·DIC^{-1})	0.025	0.03	0.03	0.03
Total DW (g dw)	127	125	137	130
Total				
Initial DW (g dw·plant^{-1})	NA	0.11	0.09	0.10
DW (g dw·plant^{-1})	25.40±1.85	18.60±1.22	22.47±1.64	22.16±0.95
Growth rate (g dw·plant^{-1}·DIC^{-1})	0.60±0.04	0.53±0.03	0.62±0.05	0.59±0.02
Total DW (g dw)	3048	2232	2696	2659
Water content (%)	89.0±0.3	87.2±0.3	86.9±0.32	87.7±0.2
Harvest Index (%)	95.9±0.2	93.8±0.6	94.2±0.46	94.6±0.28
Total productivity (g dw·m^{-2}·DIC^{-1})	14.51	12.75	14.97	14.07

The fresh (FW) and dry weight (DW) per plant, averaged over 120 samples, present significant differences among trials ($p<0.05$). Differences in fresh weight are known to be attributed to variability in plant water status during the harvest and weighing procedures, so plant dry weight is the parameter which is investigated more closely. As days in chamber (DIC) are different between cultures (Table 5.2), dry weight values were normalized by DIC to determine whether the average growth rate (g dw·plant^{-1}·DIC^{-1}) of each plant part was significantly different among replications. A comparison of confidence intervals of the mean plant part growth rate for each trial indicates that hypocotyl growth rate is significantly lower in BB2 when compared to that obtained in BB1 and BB3 (Figure 5.5). No significant differences could be identified in beet leaf growth rate among batch culture replicates. It is difficult to assess whether significant differences among replications occurred in total plant biomass growth rate since roots could not be harvested at the individual plant scale. For the purposes of subsequent mass balance calculations, the mean value of total plant growth rate (including roots) calculated across replications is used under the assumption that no significant differences in growth occurred among replications.

Total productivity for the present beet batch cultures ranged between 12.75 and 14.97 g dw·m^{-2}·DIC^{-1}. This productivity is 20 to 50% higher than the values of 10 g dw·m^{-2}·d^{-1} reported in Hanford and Ewert (2006). Similarly, the average dry weight of beets obtained in the present replicates (ranging from 19 to 25 g dw·plant^{-1}) is higher than the values of 10.4 g dw·plant^{-1}, grown also under HPS lamps, obtained by Goings (2002).

The mean harvest index indicates that roughly 95% of the produced biomass is edible. This value is high when compared to the lower HI of 65% reported in some studies (Wheeler *et al.*, 2003), where beet leaves were not considered an edible part. However, beet leaves were used as part of the Biosphere-2 food system reported by Silverstone and Nelson (1996) and so for the purposes of subsequent mass balance studies presented in this work, it is assumed that beet leaves would be eaten.

The total water content of beet plants ranges between 87-89 %, in agreement to the 80% obtained by Wheeler *et al.* (2003).

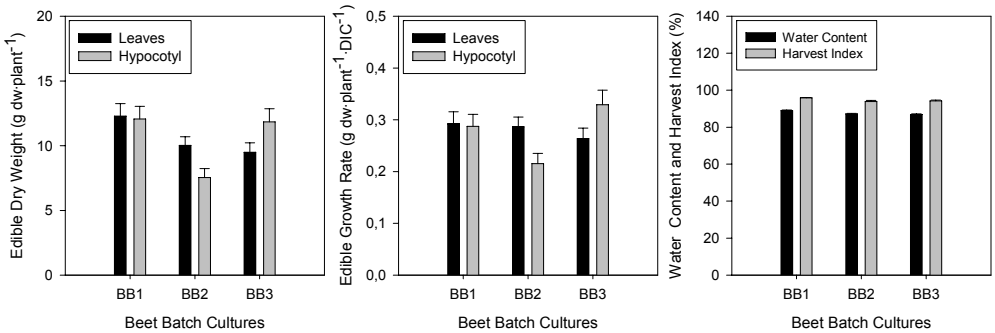

Figure 5.5 Beet batch harvest data (mean value with 95% confidence interval error) per plant part (leaves and hypocotyl) obtained in batch cultures. LEFT: Edible dry weight (g dw·plant^{-1}), MIDDLE: Edible growth rate (g dw·plant^{-1}·DIC^{-1}), RIGHT: Total plant water content (%) and harvest index (%).

In addition to the 3 replicates of batch cultures, 2 staggered cultures of beet were carried out. At the final harvest of each staggered trial, 24 plants at different growth ages (40, 50, 60 and 70 days) are collected. However, throughout the staged culture multiple harvest of the most mature age class (70 days) are performed. Therefore, a high number of mature plants are collected through the culture, specifically 431 beets considering both replications. Such data collected at different plant ages allows evaluating beet growth along time.

Figure 5.6 shows the evolution of plant fresh weight and dry weight, also plotted per each plant part (leaves, hypocotyl and roots), leaf area and harvest index along beet growth. Values for the hypocotyl and root of the youngest plants (30 d) are not available, since they were not enlarged enough to obtain a reliable measure.

As it can be seen in Figure 5.6, in the last growth stages of beet hypocotyl increases its weight while leaves slow down its growth, indicating that beets develop first the leafy part and then the storage root part.

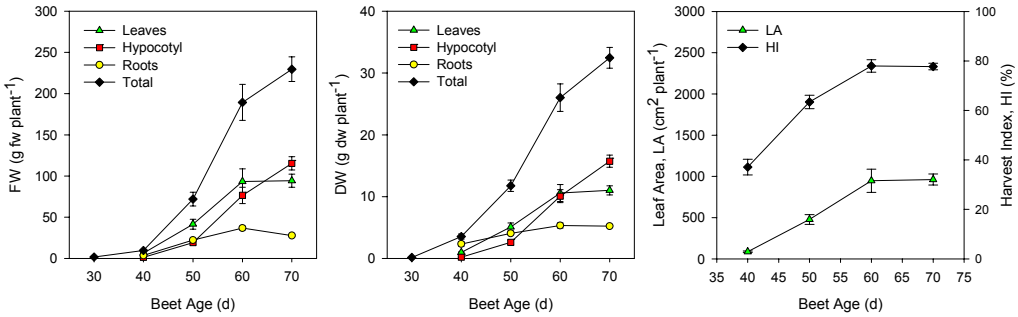

Figure 5.6 Beet harvest data per plat part (▲ leaves, ■ hypocotyl, ● roots; ♦ total) along beet development obtained in staggered cultures. LEFT: Fresh weight (FW, g fw·plant^{-1}), MIDDLE: Dry weight (DW, g dw·plant^{-1}), RIGHT: Leaf area (▲ LA, cm^2·plant^{-1}) and total harvest index (♦ HI, %). Values are calculated as the mean value (± 95% confidence interval) of all the plants harvested at different growth stages throughout beet staged cultures (BS1 and BS2). Numbers of plants harvested at different growth ages are: 24 beets at 30 days, 48 beets at 40 days, 48 beets at 50 days, 46 beets at 60 days and 431 beets at 70 days.

Data shown in Figure 5.6 can be used to adjust typical curves for classical plant growth analysis, such as the exponential and the Gompertz equation (Hunt, 1982; Thornley and Johnson, 2000), as mentioned in the plant growth curves section 5.2.6. Increase of beet biomass along crop age follows the Gompertz equation profile described by [Eq. 5.2].

Using the non linear least squares regression (nls) procedure, Gompertz model was fitted to DW (g dw·plant^{-1}) from BS1 and BS2 cultures to obtain estimates of W_0, μ_0, and D_r together with r^2, standard error (SE) of estimate and degrees of freedom (df) [Eq. 5.3]. Figure 5.7 shows the Gompertz equation fitted to DW harvested in staggered cultures, wich agrees with beet growth patterns reported in Tei *et al.* (1993b).

$$W = 1.26 \cdot 10^{-40} \exp\left[\frac{8.514 \cdot \left(1 - e^{-0.089 \cdot [\text{BeetAge}]}\right)}{0.089}\right] \quad \text{[Eq. 5.3]}$$

$r^2 = 0.67$
SE of W = 15.26
df =594

Figure 5.7 Beet total dry weight (DW) as a function of crop age (d). Values are calculated as the mean value of BS1 and BS2. The adjusted parameters of Gompertz equation (solid line) and the corresponding statistical values are included in [Eq. 5.3].

Statistical values of Gompertz equation fitted to beet staged data show the high dispersion of beet weight harvested. Thus, it is difficult to obtain good growth curves using a destructive analysis such as harvesting the plant at different ages, due to the high variability in biomass produced per plant. Consequently, it is advisable to use a non-destructive analysis, such as Net Carbon Exchange Rate (NCER) (Dutton *et al.*, 1988), for growth modeling and for being integrated within the control laws of the whole compartment. NCER data of the present beet cultures is presented in Chapter 6.

Regarding the operation mode for plant cultures, staggered production is preferred for long operations of life support systems, since the technique provides more stabilized atmospheric conditions than in batch cultures (Stasiak *et al.*, 2003; Wheeler, 1996c; Stutte *et al.* 1997). However, the method's effects on biomass production and productivity are still unclear (Stutte *et al.* 1997).

Beets grown in the presently discussed batch cultures have a mean value (± 95% CI) of 22±0.9 g dw·plant^{-1} slightly lower than the 32±1.7 g dw·plant^{-1} averaged for 431 mature plants of the staged cultures BS1 and BS2. As a consequence, the average total productivity in staged cultures (14.78 g dw·m^{-2}·DIC^{-1} for BS1 and 19.52 g dw·m^{-2}·DIC^{-1} for BS2) is also higher than the one observed in batch cultures. Nonetheless, harvest index observed in batch trials (95%) is higher than the values of 83% of mature plants in staged cultures. As no firm conclusion about the effect of the operational regime on biomass production can be drawn it is decided to use for the subsequent chapters the averaged value among all the batch and staged cultures.

Thus, beet productivity of 15.31 g dw·m^{-2}·DIC^{-1} and harvest index of 89% is used for the sizing of the HPC (Chapter 7) and for the mass balance analysis of the MPP (Chapter 8).

5.3.1.2 LETTUCE HARVEST DATA

Like for beet cultures, 3 replicates of lettuce batch cultures were carried out. Destructive analysis were used to obtain lettuce productivity parameters per each plant part of the 120 plants harvested at the end of each replication. Results are summarized in Table 5.5 for each lettuce batch culture (LB1, LB2, LB3) together with the average value calculated among trials.

Lettuce total DW obtained in batch cultures (averaging 21.86 g dw·plant^{-1} are lower to values described in Tei *et al.* (1996a) of 28.3 g dw·plant^{-1} obtained for a different cultivar (*Lactuca sativa* L. var. Crispa, Saladin R100) grown on a sandy soil under solar irradiation. However, the average total productivity (14.92 g dw·m^{-2}·d^{-1}) is higher than the 7.3 g dw·m^{-2}·d^{-1} reported by Hanford and Ewert (2006), which represents an average value from different tests performed in NASA's BPC under similar culture condition as ones used in the present batch trials (Wheeler *et al.* 2003).

Table 5.5 Harvest data for lettuce grown in batch cultures. Values represent the mean (± 95% confidence interval) of 120 plants for LB1, LB2 and LB3 cultures and of 360 plants for mean column, except for leaf area where:(1) n=20 (2) n=60.

Lettuce Batch Harvest Data	LB1	LB2	LB3	Mean
Leaves				
Fresh Weight, FW (g fw·plant^{-1})	273±4	265±6	259±8	266±3
Dry Weight, DW (g dw·plant^{-1})	14.75±0.42	18.77±0.49	14.57±0.52	16.03±0.34
Growth rate (g dw·plant^{-1}·DIC^{-1})	0.45±0.13	0.51±0.01	0.42±0.01	0.46±0.01
Initital Leaf Area, LA_o (cm^2·plant^{-1})	33	58±6	18±4	37±8
Leaf Area, LA (cm^2·plant^{-1})	3246±444(1)	3763±207(1)	3916±185(1)	3641±180(2)
Total DW (gdw)	1770	2253	1748	1924
Roots				
FW (g fw·plant^{-1})	26.4±0.3	41.4±0.5	47.5±1.1	38.4±1.01
DW (g dw·plant^{-1})	2.68±0.06	6.12±0.09	8.69±0.21	5.83±0.27
Growth rate (g dw·plant^{-1}·DIC^{-1})	0.08±0.001	0.16±0.002	0.25±0.01	0.16±0.01
Total DW (g dw)	321	735	1043	700
Total				
Initial DW (g dw·plant^{-1})	0.02	0.1	0.03	0.05
DW (g dw·plant^{-1})	17.43±0.44	24.90±0.51	23.26±0.63	21.86±0.45
Growth rate (g dw·plant^{-1}·DIC^{-1})	0.53±0.01	0.67±0.01	0.66±0.02	0.62±0.01
Total DW (g dw)	2091	2988	2791	2623
Water content (%)	94.2±0.1	91.8±0.1	92.3±0.2	92.8±0.1
Harvest Index (%)	84.4±0.4	75.2±0.5	62.6±0.7	74.1±1.0
Total productivity (g dw·m^{-2}·DIC^{-1})	12.67	16.15	15.95	14.92

The performance of two replicates of staggered production of lettuce allows collecting at the final harvest, 36 plants at different growth ages (30, 40 and 50 days). Nonetheless, multiple harvests of the most mature age class (50 days) are carried out through culture length. Thus, 396 mature lettuces were collected trough the trial taking into account both replications. Such data collected at different plant ages allows evaluating lettuce growth along time. Figure 5.8 shows the evolution of plant fresh weight (FW) and dry weight (DW), also plotted per each plant part (leaves and roots), leaf area and total harvest index along lettuce growth. Values for youngest plants (30 d) were measured on a plant basis.

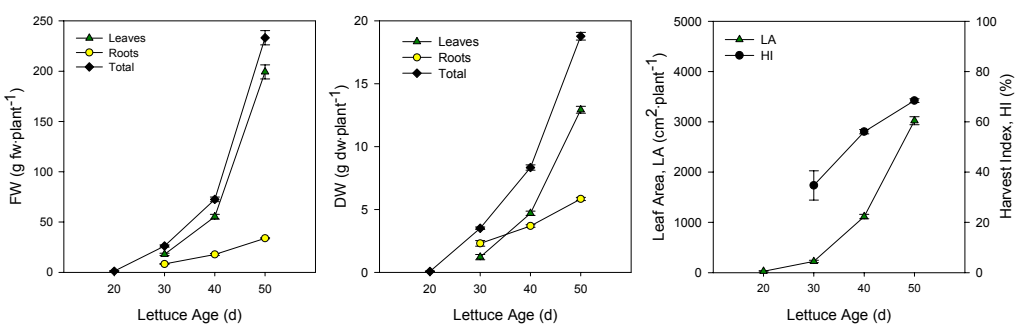

Figure 5.8 Lettuce harvest data per plant part (▲ leaves, ● roots; ♦ total) along lettuce development. LEFT: Fresh weight (FW, g fw·plant^{-1}), MIDDLE: Dry weight (DW, g dw·plant^{-1}), RIGHT: Leaf area (▲ LA, cm^2·plant^{-1}) and total harvest index (♦ HI, %). Values are calculated as the mean value (± 95% confidence interval) of all the plants harvested at different growth stages throughout lettuce staged cultures (LS1 and LS2). Numbers of plants harvested at different growth ages are: 15 lettuces at 20 days, 72 lettuces at 30 days, 72 lettuces at 40 days and 396 lettuces at 50 days.

Upon examination of the results, in the present staged cultures the averaged weight of a mature lettuce is 18.77±0.30 g dw·plant^{-1} with a harest index of 68%, while the mean total productivity obtained range from 11.67 to 12.81 g dw·m^{-2}·DIC^{-1} for LS2 and LS1 cultures respectively. Leaf area development matches with the increase in dry weight of lettuces leaves. In contrast to beet cultures, where a slow down in leaves growth of beets was observed at the final growth stages (Figure 5.8), lettuce leaves growth exponentially at leas until 50 days after planting.

Lettuce biomass harvested at different growth stages is used to build a lettuce growth curve, which follows an exponential profile [Eq.5.1]. Figure 5.9 shows the evolution of lettuce dry weight as a function of age with the adjusted exponential equation line. The corresponding estimates and statistical parameters are presented in [Eq. 5.4].

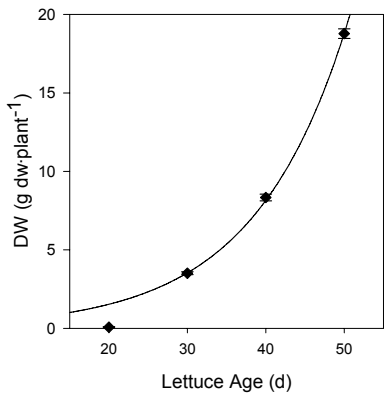

$$W=0.288\ e^{0.0836[\text{ Beet Age}]} \qquad \text{[Eq. 5.4]}$$

$r^2 = 0.92$
SE of W= 2.67
df= 553

Figure 5.9 Lettuce total dry weight (DW) as a function of crop age (d). Values are calculated as the mean value of LS1 and LS2. The adjusted parameters of exponential equation (solid line) and the corresponding statistical values are included in [Eq. 5.4].

Taking into account the parameters of the regression, the exponential adjustment to empirical data is better than the one obtained with the Gompertz regression of beet biomass. Lettuce growth and the corresponding leaf area development present the same profile as the one presented by Tei *et al.* (1993b). Although for lettuce, classical growth analysis performed may provide more reliable results than for beet, it seems more advisable to use a non-destructive analysis technique based on monitoring net CO_2 exchange rate (NCER) for determining plant growth along time. Such an approach would reduce the thinning effects associated with a partial harvest of the canopy for destructive growth analysis. NCER data of the present lettuce cultures is presented in Chapter 6.

Water content in lettuce from batch and staged cultures varies from 91% to 94%, which are within the range (90-95%) found in Wheeler *et al.* (2003). Owing to that all parameter values obtained in staged cultures are similar to the ones obtained in batch cultures, it may be concluded that biomass production is not affected by the type of culture regime (batch or staged) for lettuce.

Therefore, for the sizing of the HPC (Chapter 7) and for the mass balance analysis of the MPP (Chapter 8), the averaged values among batch and staged lettuce cultures for productivity (13.85 g dw·m^{-2}·DIC^{-1}) and harvest index (72%) are used.

5.3.2 PLANT TISSUE COMPOSITION

A detailed review on biomass composition and quality under different operational conditions for the selected crops (beet, lettuce and wheat) has been included in the general introduction (Chapter 1). Values found in the literature are compared to tissue composition of beet and lettuce batch and staged trials.

Due to the fact that plants were dissected at harvest and the different parts grouped into similar types, tissue composition is quantified in a dry weight basis for each plant part (roots, hypocotyl and leaves). Therefore, if a composition on a total plant biomass basis is desired, productivity data per plant part at harvest should be multiplied by the compound content in the corresponding part.

Moreover, for staggered cultures tissue composition was not only analyzed by plant part but also by plant age, so that any composition change along growth could be detected.

For each crop of lettuce and beet, the results are presented using the same following structure. First, data from the staggered cultures contributes to an evaluation of whether mineral content varies along plant growth.

Afterwards, a table summarizes the mean tissue mineral composition (Ca, K, Mg, N, P and C) for each culture. Proximate composition (carbohydrates, protein, fat, ash, moisture and fiber) and energy content is discussed in the same way.

5.3.2.1 BEET MINERAL AND PROXIMATE COMPOSITION

Mineral composition for each part of beet at different growth stages is depicted in Figure 5.10 for each staged replication (BS1 and BS2). Results indicate that mineral content of beets is similar between replications.

Linear regression analysis was done to evaluate whether the mineral composition significantly changes among the plant growth. Table 5.6 summarizes the statistics parameters values of this analysis, which include the linear regression slope, its standard error, t- statistics (t), p-value (p) and degrees of freedom (df). Under the null hypothesis that no significant age effect on mineral composition occurs, the slope of the regression line should not be significantly different from zero. Thus, when p-value is lower than 0.05, at an alpha (α) level of confidence, it can be stated that composition changes significantly along crop growth.

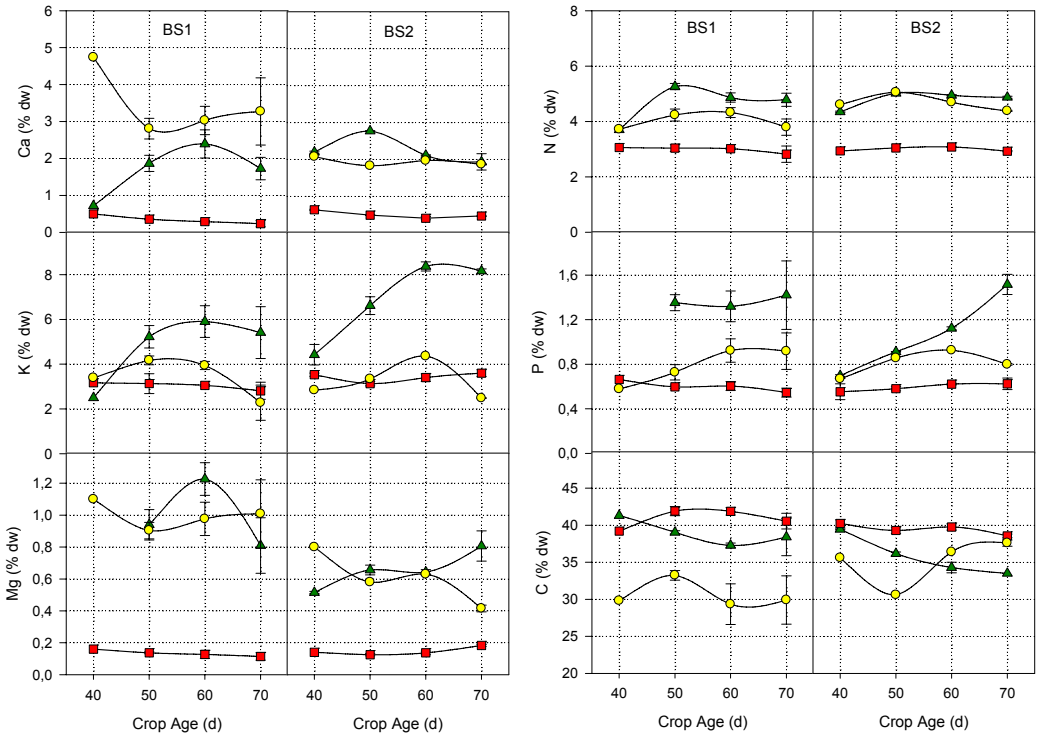

Figure 5.10 Beet mineral composition (Ca, K, Mg, N, P, C) for experiment BS1 and BS2 on a percent dry weight basis (% dw) for each part (▲ leaves; ■ hypocotyl, ○ roots). Represented values correspond to the mean value and the associated standard deviation.

In BS1, mineral content in leaves remain constant for the elements analysed ($p>0.05$). However, in BS2 leaves seems to increase significantly its K, Mg and P content and decrease its percentage of carbon.

Similar discrepancies between replications are found when analysing mineral content in the other beet parts. On one side, in BS1 magnesium content in hypocotyl decreases significantly, whereas in BS2 presents a statistically significant increase along beet maturity. On the other side, in BS1 phosphorous content in hypocotyl diminishes through plant age, while its content in roots increases. However, no change of P-content in hypocotyl and root part is detected in BS2 beet. Calcium content in hypocotyl diminishes along growth in both cultures.

Results of composition variation through plant development are not robust enough to obtain a reliable model to describe mineral reallocation through beet growth, since some differences between replication exist. Although changes by age for certain minerals are evident, an average mineral composition among age will be calculated and assumed for model purposes and subsequent calculations. A summary of mineral content (% dw) in beet tissues for each of the batch and staged cultures is in shown Table 5.7.

Table 5.6 Linear regression parameters (slope and standard error, SE) for beet mineral content versus crop age. Statistic analysis was applied for each beet part and replication (BS1 and BS2). (*) Significant differences exist among the crop age at an alpha level of 0.05.

Mineral	BS1 regression parameters					BS2 regression parameters				
	Slope	SE	t	p	df	Slope	SE	t	p	df
Leaves										
Ca	0.004	0.009	0.46	0.65	24	-0.018	0.009	-2.07	0.07	9
K	0.040	0.027	1.51	0.14	24	0.123	0.021	5.86	$2{\cdot}10^{-4}$*	9
Mg	-0.001	0.005	-0.21	0.83	24	0.008	0.002	4.68	$1{\cdot}10^{-3}$*	9
N	0.002	0.008	0.28	0.78	24	0.012	0.006	1.94	0.08	9
P	0.011	0.007	1.68	0.10	24	0.027	0.002	13.69	$2{\cdot}10^{-7}$*	9
C	-0.046	0.053	-0.87	0.39	24	-0.189	0.022	-8.76	$1{\cdot}10^{-5}$*	9
Hypocotyl										
Ca	-0.007	0.009	-3.94	$6{\cdot}10^{-4}$*	24	-0.005	0.002	-2.99	0.01*	8
K	-0.015	0.008	-1.83	0.08	24	0.006	0.006	0.95	0.37	8
Mg	-0.001	0.0005	-2.60	0.01*	24	0.001	0.0005	2.87	0.02*	8
N	-0.010	0.006	-1.73	0.10	24	-0.001	0.002	-0.24	0.82	8
P	-0.003	0.001	-3.82	$8{\cdot}10^{-4}$*	24	0.002	0.001	2.26	0.05	8
C	-0.027	0.026	-1.02	0.31	24	-0.047	0.015	-3.11	0.01*	8
Roots										
Ca	0.023	0.032	0.73	0.47	24	-0.005	0.003	-1.35	0.27	3
K	-0.077	0.018	-4.16	$2{\cdot}10^{-4}$*	24	-0.014	0.034	-0.41	0.71	3
Mg	-0.003	0.006	-0.49	0.63	24	-0.011	0.003	-4.22	0.02*	3
N	-0.014	0.007	-1.95	0.06	24	-0.013	0.009	-1.32	0.28	3
P	0.016	0.007	2.44	0.02*	24	0.003	0.003	0.84	0.46	3
C	-0.126	0.093	-1.36	0.19	24	0.132	0.104	1.27	0.29	3

Table 5.7 Beet mineral composition for all experiments on a percent dry weight basis (% dw) for each part (leaves, hypocotyl and roots). Mean values ± 95% confidence interval for number of samples specified for each part (n). Values in staggered cultures are the mean composition among all ages.

Mineral content (%dw)	BB1	BB2	BB3	BS1	BS2
Leaves	n=3	n=3	n=3	n=26	n=11
Ca	1.90± 0.45	1.87±0.55	1.63±0.21	1.78±0.16	2.26±0.21
K	5.88±0.55	6.57±0.29	6.11±0.36	5.34±0.45	7.12±0.91
Mg	0.47±0.24	0.28±0.05	0.28±0.07	0.86±0.09	0.67±0.07
N	5.40±0.05	4.56±0.24	4.62±0.23	4.81±0.13	4.84±0.15
P	1.30±0.12	1.56±0.16	1.50±0.12	1.38±0.11	1.10±0.18
C	35.40±1.14	35.20±0.75	36.23±0.62	38.45±0.87	35.53±1.32
Hypocotyl	n=3	n=3	n=3	n=26	n=10
Ca	0.26±0.1	0.25±0.03	0.19±0.07	0.27±0.04	0.49±0.05
K	3.33±0.16	3.52±0.24	2.92±0.88	2.89±0.14	3.43±0.13
Mg	0.07	0.08±0.06	0.06	0.12±0.01	0.15±0.02
N	3.31±0.15	3.69±0.18	3.08±0.31	2.88±0.10	3.00±0.05
P	0.59±0.01	0.72±0.02	0.57±0.02	0.56±0.02	0.60±0.03
C	39.20±1.63	39.03±1.65	39.13±1.61	40.80±0.44	39.41±0.45
Roots	n=1	n=1	n=1	n=26	n=5
Ca	2.19	1.04	1.83	3.70±0.52	1.92±0.09
K	1.54	1.2	1.32	2.73±0.39	3.10±0.69
Mg	0.48	0.16	0.38	0.92±0.10	0.57±0.14
N	4.45	4	4.03	3.90±0.13	4.63±0.24
P	0.48	0.74	0.50	0.99±0.12	0.81±0.08
C	37.50	39.4	38.40	29.45±1.57	35.56±2.55

Despite samples were taken from pooled tissues among all the harvested plants, the low number of samples analyzed for mineral content is likely responsible of finding statistically significant differences among the 3 replicates of batch cultures for some mineral content. This may be also the cause of finding discrepancies in mineral allocation through beet growth detected in staggered cultures. Beet hypocotyl and leaves has a higher mineral content that the values of beets grown in field (Mahn *et al.*, 2002; Ghoulam *et al.*, 2002; USDA, 2005). However, as it can be seen in Table 5.7, mineral content have similar values among all plant cultues.

The proximate composition of beets was only analyzed for the staggered cultures (BS1 and BS2). Figure 5.11 shows fat, protein, ash, carbohydrate, energy and moisture content in each beet part at different beet ages for BS1 and BS2.

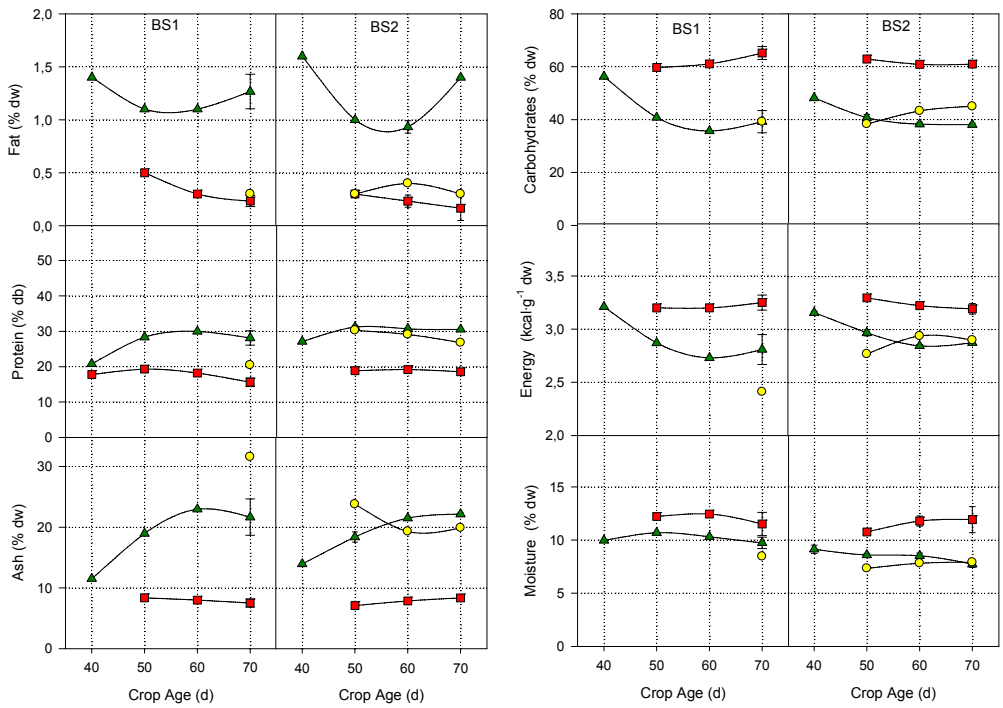

Figure 5.11 Beet macromolecular composition (fat, protein, ash, carbohydrates and moisture) on a percent dry weight basis (% dw) and energy content (cal·g^{-1} dw) for experiment BS1 and BS2 for each part (▲ leaves; ■ hypocotyl, ○ roots).

A linear regression analysis was preformed to detect any variation of composition along crop growth. The corresponding results are shown in Table 5.8 and the p-value is used to determine that proximate content is significantly different along beet development ($p>0.05$).

In beet leaves the content of fat and protein has no significant variation along plant growth, whereas ash composition increases along plant maturity. Discrepancies between cultures exist in carbohydrates, energy (kcal·g^{-1}) and moisture content evolution. In regard to beet hypocotyl composition, only energy and moisture content are not significantly affected by

plant age ($p<0.05$). No linear regression analysis in roots proximate content was performed, since its value was only available for the oldest plants.

Table 5.8 Linear regression parameters (slope and standard error SE) for beet proximate composition versus crop age. Statistics parameters include t-statistics, p-values and degrees of freedom (df). Analysis was applied for each beet part and each replication (BS1 and BS2).
(*) Significant differences exist among the crop age, considering an alpha level of 0.05.

Proximate	BS1 regression parameters					BS2 regression parameters				
	Slope	SE	t	p	df	Slope	SE	t	p	df
Leaves										
Fat	$-3{\cdot}10^{-4}$	0.005	-0.06	0.95	7	-0.004	0.009	-0.52	0.67	8
Protein	0.161	0.083	1.93	0.09	7	0.413	0.261	1.58	0.15	8
Ash	0.268	0.100	2.68	0.03*	7	0269	0.033	8.20	$3{\cdot}10^{-5}$*	8
Carbohydrates	-0.407	0.171	-2.39	0.05*	7	-0.635	0.261	-2.43	0.04	8
Energy	-0.993	0.470	-2.11	0.07	7	-0.926	0.190	-4.87	$1{\cdot}10^{-3}$*	8
Moisture	-0.020	0.017	-1.21	0.27	7	-0.044	0.009	-5.00	$1{\cdot}10^{-3}$*	8
Hypocotyl										
Fat	-0.012	0.003	-4.56	$3{\cdot}10^{-3}$*	6	0.007	0.004	-1.51	0.19	5
Protein	-0.109	0.043	-2.53	0.04*	7	-0.027	0.016	-1.62	0.16	5
Ash	-0.044	0.031	-1.40	0.21	6	0.060	0.011	5.30	$3{\cdot}10^{-3}$*	5
Carbohydrates	0.295	0.116	2.54	0.04*	6	-0.071	0.056	-1.26	0.26	5
Energy	0.290	0.331	0.88	0.41	6	-0.462	0.208	-2.22	0.08	5
Moisture	-0.045	0.051	-0.87	0.42	6	0.047	0.047	1.00	0.36	5

The Neutral Detergent Fiber (NDF), Acid Detergent Fiber (ADF) and lignin content were determined only for BS2 culture. As can be seen in Figure 5.12, the higher fiber content within beet parts is found in roots, followed by leaves and hypocotyl. The NDF refers to the total cell wall, which is comprised of the ADF fraction and hemicelluloses, and ADF fraction refers basically to the cell wall portions containing mainly lignin and cellulose.

Upon the results of the linear regression analysis fiber content has no significant dependency on beet age with p-values of 0.1, 0.2, 0.3, 0.1, 0.5, 0.7 for ADF, NDF and lignin in leaves (df=6) and hypocotyl (df=5) respectively.

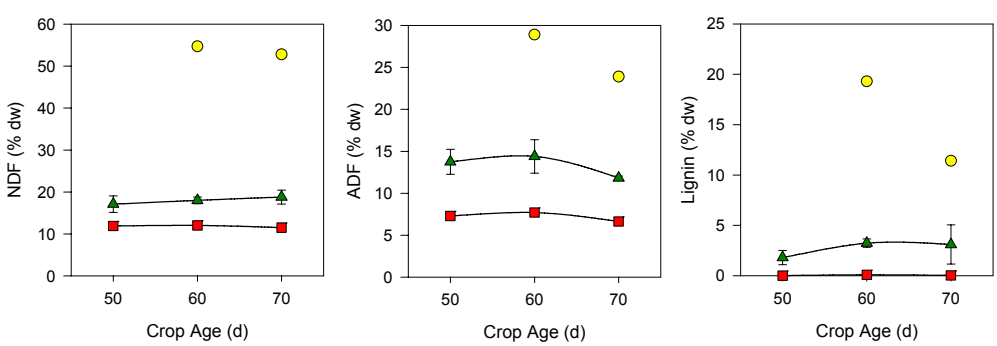

Figure 5.12 Beet fiber composition (NDF, ADF, Lignin) for experiment BS2 on a percent dry weight (% dw) basis for each part (▲ leaves; ■ hypocotyl, ○ roots).

Due to differences between replications, macromolecular composition (protein, fat, ash, carbohydrates and moisture), energy and fiber content are presented separately for each age in Table 5.9.

Table 5.9 Beet Proximate Composition (Mean ± 95% confidence interval) on a percent dry weight basis for each part (leaves, hypocotyl and roots) and for each beet age collected at the final harvest of BS1 and BS2. Number of samples, drawn from pooled tissues, are: (1)n=2 (2) n=3 (3) n=1

Proximate content	Beet Age (d)			
	40	50	60	70
Leaves	n=3	n=3	n=4	n=9
Protein (%)	25.03±4.15	30.27±1.93	30.55±0.5	32.27±7.06
Fat (%)	1.53±0.13	1.03±0.07	0.98±0.09	1.31±0.01
Ash (%)	13.14±1.59	18.59±0.77	21.87±0.75	21.83±1.56
Carbohydrates (%)	50.90±5.30	40.77±0.96	37.65±1.39	35.52±7.18
Moisture (%)	9.41±0.63	9.30±1.37	8.97±0.9	9.07±0.72
Energy (kcal·g^{-1})	3.18±0.03	2.94±0.07	2.82±0.06	2.83±0.08
NDF (%)	NA	17.10±2.74(1)	18.00±0.93(2)	18.80±1.88(2)
ADF (%)	NA	13.75±2.06(1)	14.40±2.25(2)	11.83±0.24(2)
Lignin (%)	NA	1.80±0.98(1)	3.23±0.47(2)	3.10±2.20(2)
Hypocotyl		n=2	n=4	n=9
Protein (%)	NA	19.09±0.41	18.96±0.53	16.60±1.17
Fat (%)	NA	0.40±0.20	0.25±0.06	0.21±0.05
Ash (%)	NA	7.74±1.24	7.90±0.24	7.80±0.45
Carbohydrates (%)	NA	61.30±3.14	60.95±0.5	63.77±1.91
Moisture (%)	NA	11.49±1.43	11.95±0.5	11.65±0.70
Energy (kcal·g^{-1})	NA	3.25±0.9	3.22 ±0.03	3.23±0.04
NDF (%)	NA	11.90(3)	12.03±0.53(2)	11.50±1.20(2)
ADF (%)	NA	7.30(3)	7.70±0.45(2)	6.63±0.35(2)
Lignin (%)	NA	0.01(3)	0.09±0.02(2)	0.03±0.02(2)
Roots		n=1	n=1	n=2
Protein (%)	NA	30.31	29.14	23.63±6.26
Fat (%)	NA	0.30	0.40	0.30
Ash (%)	NA	23.80	19.30	25.75±11.46
Carbohydrates (%)	NA	38.30	43.30	42.10±5.68
Moisture (%)	NA	7.34	7.82	8.19±0.54
Energy (kcal·g^{-1})	NA	2.77	2.94	2.65±0.5
NDF (%)	NA	NA	54.70	52.80(3)
ADF (%)	NA	NA	28.90	23.90(3)
Lignin (%)	NA	NA	19.30	11.40(3)

Beet leaves have higher content of proteins (25-32%), fat (0.9-1.5%) and ash (13-21%) than those found in hypocotyl (17-19% proteins, 0.2-0.4% fat and 8% ash). As carbohydrate content is determined by difference, its content is higher in hypocotyl (61-64%) than in leaves (36-51%). The highest fiber content is found in roots, followed by leaves and hypocotyl.

Moreover, protein and ash content in beet is higher than the one reported in USDA (2005) (13% proteins and 9% ash). However, the percentage of carbohydrates is lower, while the percentage of fat (1.4%) and energy content (3.5 kcal·g^{-1}) present similar values.

5.3.2.2 LETTUCE MINERAL AND PROXIMATE COMPOSITION

In lettuce staggered cultures, during the full chamber stocking 36 plants were harvested every 10 days until the final harvest, whereas 36 plants of each plant age inside chamber (30, 40 and 50 days old) were collected during the final harvest.

Figure 5.13 shows mineral content in lettuce leaves and roots at different growth ages for LS1 and LS2.

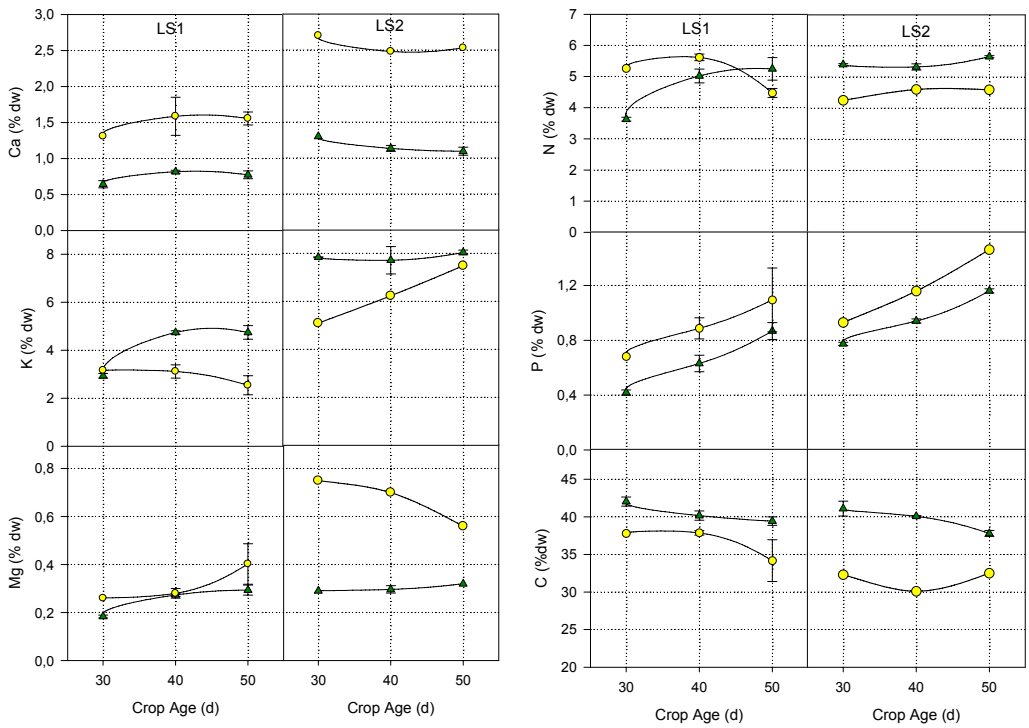

Figure 5.13 Lettuce mineral composition (Ca, K, Mg, N, P, C) for experiment LS1 and LS2 on a percent dry weight basis (%dw) for each part (▲ leaves; ○ roots).

Upon the results from the ANOVA analysis, no significant differences exist between replications (LS1 and LS2), except for Ca, K and P, where its content is higher in LS2.

In order to determine whether mineral content changes through lettuce development, linear regression analyses were performed on the LS1 and LS2 data. Similar to beet results, in some cases, p-values of each replication for a specific mineral lead to opposite conclusions (Table 5.10).

Table 5.10 Linear regression parameters (slope and standard error SE) for lettuce mineral content versus crop age. Statistics parameters include t-statistics, p-values and degrees of freedom (df). Analysis was applied for each lettuce part and each replication (LS1 and LS2).

(*) Significant differences exist among the crop age

Mineral	LS1 regression parameters					LS2 regression parameters				
	Slope	SE	t	p	df	Slope	SE	t	p	df
Leaves										
Ca	0.005	0.002	2.41	0.03*	12	-0.01	0.002	-4.2	$6 \cdot 10^{-3}$*	6
K	0.080	0.015	5.40	$2 \cdot 10^{-4}$*	12	0.012	0.016	0.73	0.49	6
Mg	0.005	0.001	7.05	$1 \cdot 10^{-5}$*	12	0.002	$5 \cdot 10^{-4}$	3.47	0.01*	6
N	0.074	0.013	5.82	$1 \cdot 10^{-4}$*	12	0.014	0.006	2.44	0.05	6
P	0.023	0.002	12.66	$3 \cdot 10^{-8}$*	12	0.019	0.001	21.9	$5 \cdot 10^{-7}$*	6
C	-0.124	0.020	-6.18	$5 \cdot 10^{-5}$*	12	-0.170	0.026	-6.44	$7 \cdot 10^{-4}$*	6
Roots										
Ca	0.007	0.007	0.99	0.34	10	-0.008	0.008	-1.09	0.47	1
K	-0.041	0.017	-2.44	0.03*	10	0.119	0.003	37.6	0.02*	1
Mg	0.009	0.003	2.67	0.02*	10	-0.009	0.003	-3.65	0.17	1
N	-0.066	0.015	-4.44	$1 \cdot 10^{-3}$*	10	0.017	0.010	1.63	0.35	1
P	0.021	0.009	2.32	0.04*	10	0.026	0.002	12.6	0.05	1
C	-0.248	0.110	-2.25	0.05*	10	0.010	0.133	0.07	0.95	1

In LS1 cultures, all minerals content quantified in leaf tissue depend significantly on lettuce age. In contrast, statistics shows that N and K content remain constant in LS2 leaves. Moreover in some particular cases, such as Ca in leaves and K in roots, mineral content has a statistically significant dependency on age for both replications, but the tendency differs between them. As for the beet results, these differences between replications suggest that more empirical data is required to conclude which minerals content change in plant tissue during its growth. Therefore, for the moment a constant lettuce mineral content will be assumed for the purposes of the preliminary mass balance calculations performed in later chapters. Table 5.11 includes mineral contents averaged per plant part for each one of the lettuce trials.

Table 5.11 Lettuce mineral composition for all cultures on a percent dry weight basis (% dw) for each part (leaves and roots). Mean values ± 95% confidence interval for number of samples specified for each part (n). Values in staged cultures are the mean composition among all ages.

Mineral content (%dw)	LB1	LB2	LB3	LS1	LS2
Leaves	n=3	n=3	n=3	n=14	n=8
Ca	0.94±0.15	0.61±0.17	0.70±0.2	0.76±0.04	1.16±0.07
K	5.85±0.52	5.29±0.16	6.02±0.95	4.35±0.42	7.87±0.24
Mg	0.16±0.01	0.14±0.01	0.15±0.01	0.27±0.03	0.30±0.01
N	4.83±0.98	3.89±0.14	4.67±0.39	4.85±0.38	5.47±0.12
P	0.95±0.05	0.70±0.18	0.84±0.25	0.72±0.10	0.98±0.11
C	38.10±0.99	39.40±1.24	38.03±0.87	40.14±0.63	39.48±1.05
Roots	n=1	n=1	n=1	n=14	n=3
Ca	1.72	1.35	1.31	1.54±0.09	2.57±0.13
K	1.27	1.74	1.99	2.74±0.25	6.27±1.35
Mg	0.21	0.12	0.18	0.36±0.05	0.67±0.11
N	3.82	4.00	3.80	4.83±0.31	4.48±0.23
P	1.21	1.58	1.32	1.01±0.13	1.18±0.30
C	35.00	35.10	37.30	35.40±1.62	31.63±1.51

Calcium, potassium and nitrogen average content in lettuce leaves among all the cultures is higher than percentage of these elements in lettuces grown in field (Ca: 0.34 to 0.63%, K: 1.31 to 3.12%; N: 3%) reported by Watt and Merril (1975) and McKeehen (1994).

However, results obtained are similar to elemental composition of lettuce grown in hydroponics (Ca: 0.63 to 0.72%; K: 7.02 to 8.48%; N: 4.1 to 4.7%; Mg: 0.20-0.23%) (McKeehen, 1994). Potassium percentage of lettuce grown in the present batch and staged trials is higher than the one reported for lettuce cultivated in field or hydroponics, ranging from 0.12 to 0.68% (Watt and Merril, 1975; McKeehen, 1994, USDA, 2005).

Lettuce proximate content at different crop ages is shown in Figure 5.14. Since not enough data for root parts are available to evaluate changes in composition through plant growth, linear regression was only applied for the proximate content of leaves (Table 5.12).

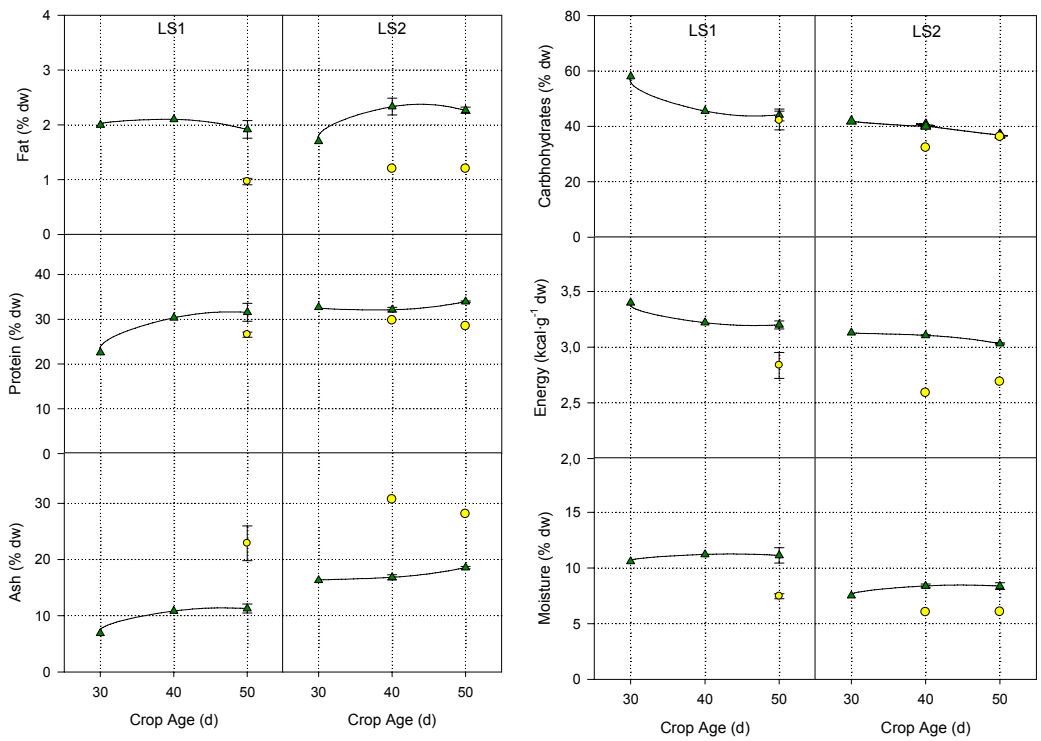

Figure 5.14 Lettuce macromolecular composition (fat, protein, ash, carbohydrates and moisture) on a percent dry weight basis (% dw) and energy content (kcal·g^{-1} dw) for experiment LS1 and LS2 for each part (▲ leaves; ○ roots).

Table 5.12 Linear regression parameters (slope and standard error, SE) for lettuce proximate composition versus crop age. Statistics parameters include t-statistics, p-values and degrees of freedom (df). Analysis was applied for each lettuce part and each replication (LS1 and LS2). (*) Significant differences exist among the crop age.

Proximate	LS1 regression parameters					LS2 regression parameters				
	Slope	SE	t	p	df	Slope	SE	t	p	df
Leaves										
Fat	-0.006	0.008	-0.82	0.44	6	0.020	0.012	1.66	0.15	5
Protein	0.397	0.110	3.59	0.01*	6	0.092	0039	2.35	0.06	5
Ash	0.191	0.049	3.92	$7{\cdot}10^{-3}$*	6	0.127	0.025	5.20	$3{\cdot}10^{-3}$*	5
CH	-0.604	0.142	-4.27	$5{\cdot}10^{-3}$*	6	-0.271	0.031	-8.63	$3{\cdot}10^{-4}$*	5
Energy	-0.871	0.221	-3.94	$7{\cdot}10^{-3}$*	6	-0.546	0.079	-6.91	$1{\cdot}10^{-3}$*	5
Moisture	0.021	0.033	0.64	0.54	6	0.032	0.018	1.80	0.13	5

In both staggered trials, carbohydrates and energy content present in leaves decrease significantly through lettuce growth, while ash percentages increase. Fiber content (ADF, NDF and Lignin) in leaves remains constant between 40 and a 50 days old lettuce (p-values of 0.7, 0.07, 0.3 for ADF, NDF and Lignin respectively, df=3). Table 5.13 summarizes mean proximate percentages in lettuce determined for each age and plant part.

Table 5.13 Lettuce Proximate Composition (Mean±95% confidence interval) on a percent dry weight basis (% dw) for each part (leaves and roots) and for each lettuce age (30, 40 and 50 days) collected at the final harvest of LS1 and LS2. Number of plants analyzed are: (1)n=2 (2) n=4 (3) n=9 (4) n=3 (5) n=1

Proximate (%dw)	Leaves			Roots	
	30(1)	40(2)	50(3)	40(5)	50(2)
Protein	27.63	31.69±1.57	32.37±1.52	29.76	27.06±1.7
Fat	1.85	2.28±0.27	2.03±0.16	1.20	1.03±0.2
Ash	11.59	15.34±4.80	13.70±2.84	30.70	24.19±5.78
CH	49.90	41.60±4.16	41.70±3.07	32.30	40.63±6.42
Moisture	9.05	9.10±2.26	10.21±1.15	6.03	7.11±1.15
Energy ($kcal{\cdot}g^{-1}$)	3.26	3.13±0.09	3.14±0.07	2.59	2.80±0.2
NDF (%)	NA	21.05(1)	22.90±1.97(4)	NA	43.70(5)
ADF (%)	NA	20.35(1)	20.73±2.88(4)	NA	26.60(5)
Lignin (%)	NA	4.10(1)	5.10±2.86(4)	NA	10.50(5)

As for beet, fiber content is higher in roots than n leaves. In comparison with field grown plants, lettuce leaves have higher protein and ash levels. In hydroponics cultures, nutrients are available in higher levels than in soil. Wheeler *et al.* (2005b) suggest that this fact may have lead to excess uptake of some nutrients (particularly K and N), which might increase ash and protein levels in plant tissue. Accordingly, Davis *et al.* (1988) found enhanced leaf protein content (27-36%) compared to the field caused by all N nutrition treatments applied under controlled environments.

Under a CO_2 enriched atmosphere higher lettuce productivity is obtained (Knecht and O'Leary, 1983; Knight and Mitchell, 1988). High CO_2 concentrations produce not only a lower protein and fat content, but also a decrease in the nitrate accumulation in lettuce. Due to this fact, manipulation of atmospheric CO_2 concentrations is proposed to be an interesting strategy for controlling nitrate accumulation in tissue other than diminishing nitrate composition in solution (McKeehen, 1994).

5.3.3 NUTRIENT UPTAKE RATES

5.3.3.1 BEET NUTRIENT UPTAKE

As mentioned in the method section, nutrient solution samples, taken for each of the fresh and used nutrient solutions on every solution change-over day, are analyzed for the ions of interest (NO_3-, PO_4^{3-}, SO_4^{2-}, NH_4^+, Na^+, K^+, Ca^{2+}, Mg^{2+}). Nutrient uptake rates were determined over change-over period by concentration difference in solution samples and integrated to generate a profile of the accumulated nutrient uptake for nitrogen, phosphate, sulphates, sodium, potassium, calcium and magnesium over the period of crop growth. Figure 5.15 and Figure 5.16 depicts the accumulated nutrient uptake profiles for batch and staggered cultures respectively.

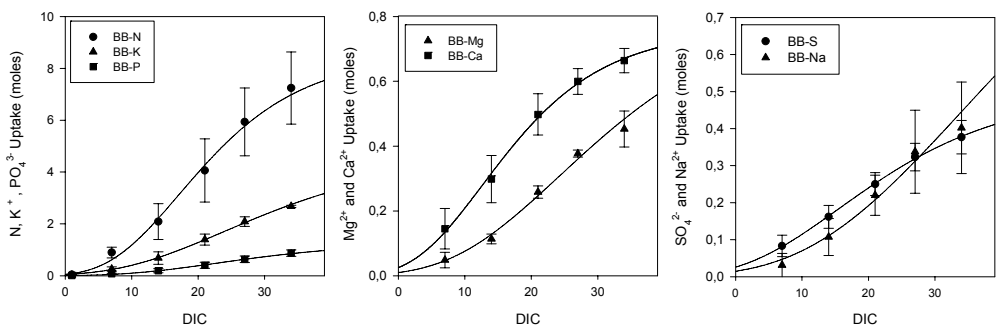

Figure 5.15 Beet accumulated nutrient uptake for batch cultures (Mean±SD)

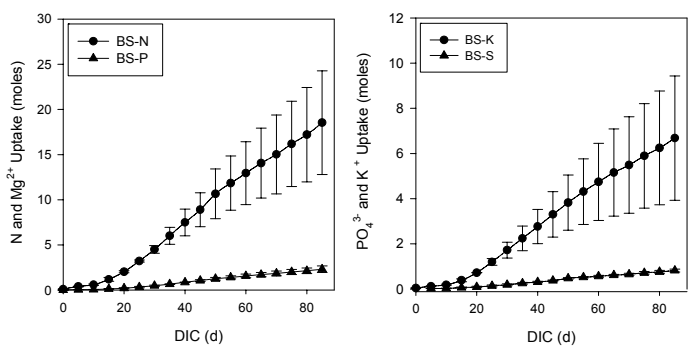

Figure 5.16 Beet accumulated nutrient uptake for staged cultures (Mean±SD).

In order to compare consumption rates between replications, values are normalised by DIC and growing area (Table 5.14).

Table 5.14 Nutrient uptake for beet batch and staged cultures. Mean values ± SD. Days in chamber are (DIC): 42 (BB1), 35 (BB2), 34 (BB3), 160 (BS1) and 80 (BS2).

Nutrient uptake rate ($mmol \cdot m^{-2} \cdot DIC^{-1}$)	BB1	BB2	BB3	Mean BB	BS1	BS2	Mean BS	Mean All
N (NO_3^-; NH_4^+)	34.1	43.9	49.2	42±8	40.6	66.4	54±18	47±12
PO_4^{3-}	4.7	5.2	5.7	5.2±0.5	5.5	7.5	7±1	6±1
SO_4^{2-}	NA	2.0	2.4	2.2±0.3	2.0	2.5	2.3±0.4	2.2±0.3
Na^+	3.1	1.5	2.7	2.4±0.8	2.8	1.0	2±1.3	2.2±0.9
K^+	16.7	15.2	16.0	16.0±0.7	13.7	25.4	20±8	17±5
Mg^{2+}	3.1	2.4	2.5	2.6±0.4	1.2	4.0	3±2	3±1
Ca^{2+}	NA	3.6	4.1	3.9±0.3	3.0	5.3	4±2	4±1

Beets grown in batch and staged cultures have similar nutrient uptake rates. Nitrogen uptake rate has the highest value (between 34 to 66 mmol m^{-2} DIC^{-1}), followed by potassium (from 14 to 25 mmol m^{-2} DIC^{-1}). All the other nutrient uptakes rates ranged between 1.2 and 7.5 mmol m^{-2} DIC^{-1}.

Nitrogen uptake used for the mass balance analysis presented in Chapter 8 is the average value (47 mmol m^{-2} DIC^{-1}) among all cultures.

5.3.3.2 LETTUCE NUTRIENT UPTAKE

Similar to beet data, lettuce nutrient uptake rates were obtained over change-over period by concentration difference in solution samples and integrated to generate a profile of the accumulated nutrient uptake over the period of crop growth. Accumulated nutrient uptake from the hydroponic solution is shown in Figure 5.17 and Figure 5.18 for batch and staggered cultures, respectively.

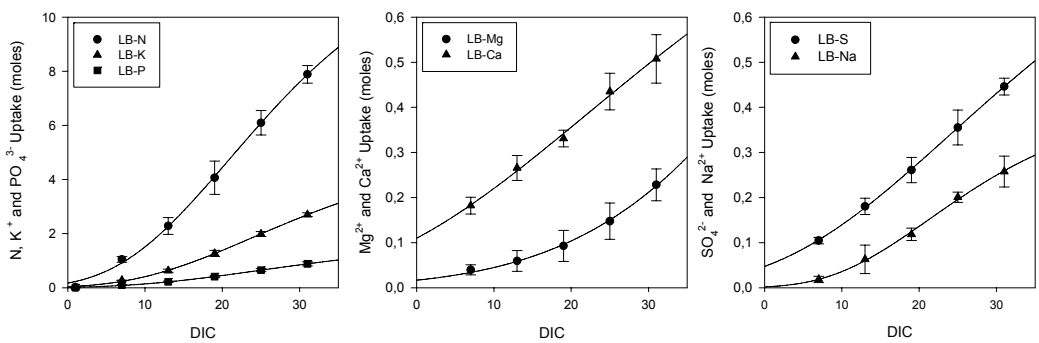

Figure 5.17 Lettuce accumulated nutrient uptake for batch cultures (Mean±SD).

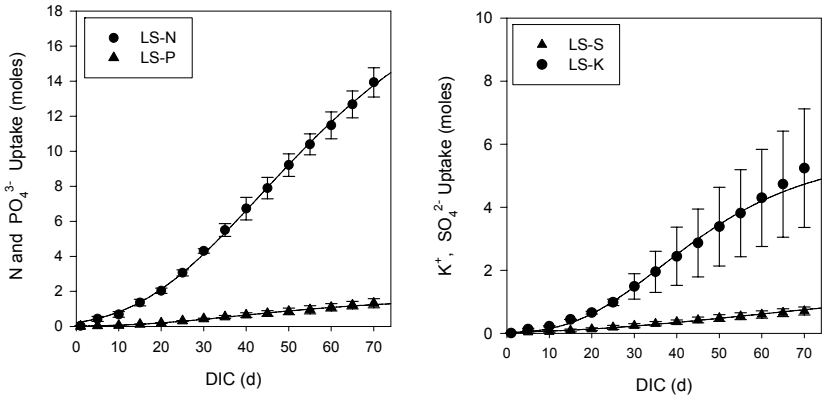

Figure 5.18 Lettuce accumulated nutrient uptake for staged cultures (Mean±SD).

As for the beet nutrient uptake data, accumulated profiles are normalized by DIC and growing area (Table 5.15).

Table 5.15 Nutrient uptake for lettuce batch and staged cultures. Mean values ± SD. Days in chamber are (DIC): 331 (LB1), 37 (LB2), 35 (LB3), 80 (LS1) and 70 (LS2).

Nutrient uptake rate ($mmol \cdot m^{-2} \cdot DIC^{-1}$)	LB1	LB2	LB3	Mean LB	LS1	LS2	Mean LS	Mean All
N (NO_3^-; NH_4^+)	50.7	53.0	48.8	51±2	43.6	46.1	45±2	48±4
PO_4^{3-}	5.6	6.3	5.3	5.7±0.5	3.6	4.8	4.2±0.8	5±1
SO_4^{2-}	2.9	3.0	2.8	2.9±0.1	2.6	2.0	2.3±0.4	2.7±0.4
Na^+	1.9	1.6	1.5	1.7±0.2	0.8	0.8	0.8±0.01	1.3±0.5
K^+	17.5	17.8	16.9	17.4±0.5	12.8	20.9	17±6	17±3
Mg^{2+}	1.6	1.6	1.2	1.5±0.2	0.1	1.4	0.7±0.9	1.2±0.6
Ca^{2+}	3.7	3.0	3.2	3.3±0.3	1.4	4.2	2.8±2.0	3±1

As observed in beet cultures, lettuce grown in batch and staged cultures has similar nutrient uptake rates. Moreover, nitrogen is consumed by lettuce at the highest rate, followed by potassium, equally as in beet cultures.

Nitrogen uptake used for the mass balance analysis presented in Chapter 8 is the average value (48 mmol m^{-2} DIC^{-1}) among all cultures.

5.3.4 NUTRIENT MASS BALANCES

Nutrient mass balances were determined by comparing the accumulated nutrient uptake as obtained through analysis of the hydroponics solution with the total nutrient content in biomass obtained from tissue analysis.

Accumulated nutrient uptake in moles was calculated from differences in mineral concentrations of the hydroponic solution at every change over period. Total accumulated uptake corresponds to the last value of the accumulation profile shown in Figure 5.15 (BB), Figure 5.16 (BS) Figure 5.17, (LB) and Figure 5.18 (LS).

Total nutrient content in biomass is obtained as [Eq. 5.5] indicates.

$$\text{Biomass Content} = (\Sigma \text{ Total } DW_i \cdot [A]_i)/MW\ A \qquad \text{[Eq. 5.5]}$$

where:

i: sub-index representing plant part. For beet values are leaves, hypocotyl or roots and for lettuce leaves or roots.

Total DW_i (g dw): Total plant biomass for each part (leaves, hypocotyl or root) collected at final harvest. Values for batch cultures are reported in Table 5.4 (BB) and in Table 5.5 (LB). For staggered cultures values are detailed next. BS1: 2968 g dw leaves, 4480 g dw hypocotyl, 2014 g dw roots; BS2: 2561 g dw leaves, 2900 g dw hypocotyl, 785 g dw roots; LS1: 2947 g dw leaves, 1665 g dw roots; LS2: 2599 g dw leaves, 1078 g dw roots.

$[A]_i$ (% dwb): Mineral (A=Ca, K, Mg, N, P and C) content in each plant part. Values reported in Table 5.7 for beet cultures and in Table 5.11 for lettuce cultures.

MW A: Molecular weight of mineral A.

Figure 5.19 and Figure 5.20 compare nutrient uptake from the hydroponic solution with the nutrient content present in the harvested biomass for each of the five experiments performed with beet and lettuce.

When empirical values are near the 1:1, mineral uptake could be used with the estimated biomass (using growth curves or NCER data) for predicting the mineral composition of the whole plant tissue using the concept of steady state nutrition (Ingestad and Agren, 1988). This approach implies that relative nutrient uptake rate (RUR) is equivalent to relative growth rate (RGR), when assuming a constant nutrient concentration in plant tissue regardless of its physiological stage.

Previous studies concluded that the relationship between RGR and RUR was strong in beet but substantially weaker in the lettuce data, all grown in batch hydroponics cultures in SEC chambers (Waters, 2002). However, composition results of beet and lettuce tissues, presented in the above section, show the difficulty to determine whether the mineral content remains constant throughout plant growth. Therefore, more detailed studies are required to asses whether the adherence to steady state nutrition is confirmed.

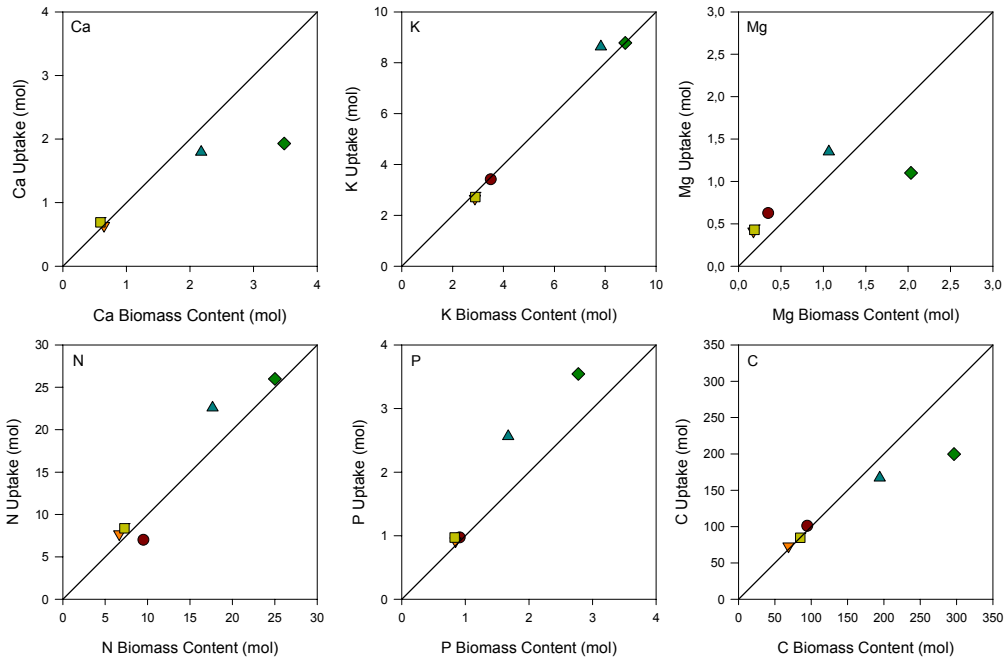

Figure 5.19 Accumulated nutrient uptake (mol), calculated using nutrient concentration in hydroponic solution at every solution change-over, plotted against total nutrient content in beet (mol), estimated from the total biomass harvested and mineral composition of each part (● BB1;▼ BB2; ■BB3; ♦BS1; ▲ BS2, 1:1 line).

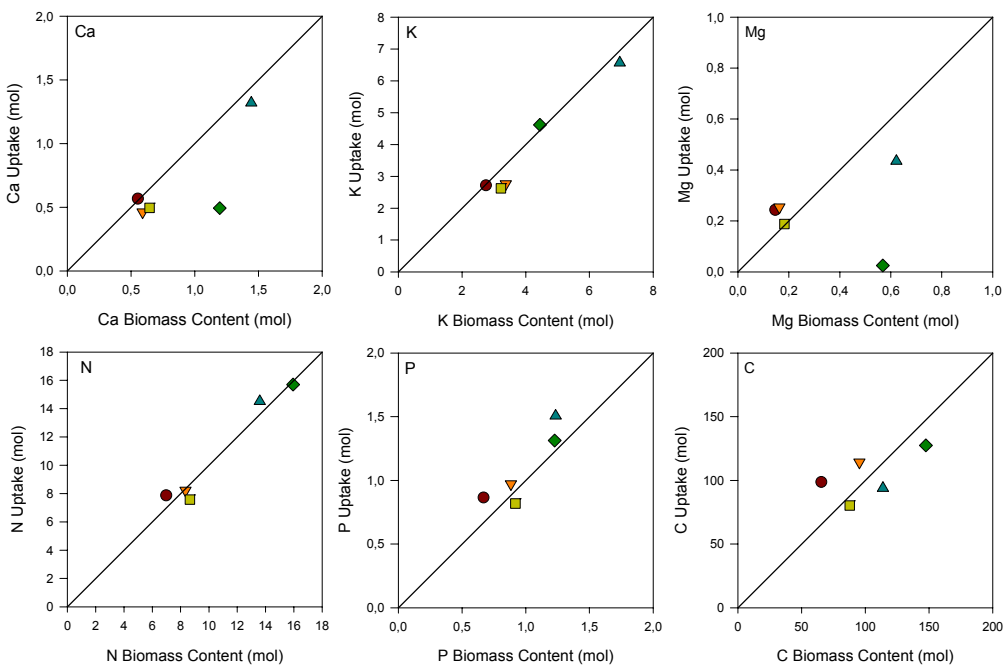

Figure 5.20 Accumulated nutrient uptake (mol), calculated using nutrient concentration in hydroponic solution at every solution change-over, plotted against total nutrient content in beet (mol), estimated from the total biomass harvested and mineral composition of each part (● LB1;▼ LB2; ■LB3; ♦LS1; ▲ S2, 1:1 line).

Deviation from 1:1 line indicates unbalances caused by several factors, such as:

- The presence of microbial communities in the hydroponics culture may consume some of the nutrients. In this case, microbial communities should be eliminated or profiled (Dent *et al.*, 2004).
- Errors in analytical systems for determining nutrient composition in hydroponics or mineral content in plant tissue can lead to non-exact results.

However, as can be seen in Figure 5.19 and Figure 5.20, in most of the cases deviation from 1:1 line is small, which indicates that mineral uptake could be use with the estimated biomass for predicting the mineral composition of the whole plant tissue. Thus, the ionic uptake of the nutrient solution is a good predictor of total canopy mineral content.

5.4 CONCLUSIONS

Three batch cultures and two staggered cultures were performed for beet and lettuce. Harvest production, growth analysis, mineral and proximate content in plant tissue, nutrient uptake dynamics and nutrient mass balances were studied.

The main conclusions obtained from this study are:

- For beet, the mean total plant productivity among batch and staggered cultures are 15.31 g dw $m^{-2} \cdot d^{-1}$ with a harvest index of 89% and a nitrogen uptake of 0.047 mol m^{-2} d^{-1}. For lettuce, total plant productivity averaged is 13.85 g dw $m^{-2} \cdot d^{-1}$ and percentage of edible biomass is 72% and a nitrogen uptake of 0.048 mol m^{-2} d^{-1}. Such values will be used for the sizing of the HPC to be incorporated in the MPP and for assessing the N, CO_2 and O_2 balances in the MPP to evaluate the impact of the photosynthetic compartments integration.
- Classical growth analysis based on dry weight of destructively harvested plant at different growth stages does not provide reliable growth rate curves. Instead, it is proposed to use non-destructive analysis techniques based on monitoring net CO_2 exchange rate (NCER) for determining plant growth along time.
- Mineral and proximate content of each crop collected at different growth stages were compared in order to have first hand values of biomass composition and to evaluate composition dependency on age. Nevertheless, differences between replications, probably due to the low number of plants analyzed, suggest that more detailed studies are required to assess whether the concept of steady state nutrition holds or if reallocation of nutrient in plant tissue warrant a more complicated model than relating relative growth rate (RGR) and nutrient relative uptake rate (RUR). Studies which investigate RGR and RUR relations at the full canopy level will be required to further develop control algorithms for nutrient management when the HPC is connected to the MPP.

- Beet and lettuce grown in these hydroponics cultures has usually higher mineral content than beet and lettuce grown in field reported in the literature. Moreover, protein and ash levels found in crops cultivated using hydroponics are higher in comparison with field grown plants. This is probably caused by a luxuriant uptake of some nutrients.
- Nutrient uptake dynamics showed that nitrogen is the nutrient with the highest consumption rate, followed by potassium. All the other nutrients analyzed (PO_4^{3-}, SO_4^{2-}, Na^+, Mg^{2+} and Ca^{2+}) present similar uptake rate values.
- Mineral uptake could be used with the estimated biomass (using growth curves or NCER data) for predicting the mineral composition of the whole plant tissue, since good nutrient mass balances were obtained when comparing nutrient uptake rate from the hydroponic solution with the nutrient content present in the harvested biomass. Therefore, the ionic uptake of the nutrient solution is a good predictor of total canopy mineral content.

Chapter 6

CARBON DYNAMICS IN BATCH AND STAGED CULTURES OF BEET AND LETTUCE

6.1 INTRODUCTION

The process of integrating a Higher Plant Chamber (HPC) in the MELiSSA Pilop Plant (MPP) demands reliable data on crop photosynthetic responses. Such data will contribute to the development of a first principle dynamic photosynthetic model necessary for the predictive control strategy of carbon exchange, foreseen when the HPC is connected to the MELiSSA loop.

The aim of this chapter is to evaluate the canopy photosynthetic data corresponding to beet and lettuce cultures, for which biomass production, tissue composition and nutrient dynamic data have been presented in chapter 5. In addition, atmospheric evolution of batch and staggered trials is compared to identify the most desirable method of production, from an atmospheric management perspective, under long term operation of the prototype chamber. Moreover, so-called “light curves,” relating leaf photosynthetic responses to varying light intensity are used to estimate parameters of a full canopy photosynthesis model. The predictions of the full canopy model are compared to observed carbon gain of beet and lettuce

cultures. The photosynthetic model used in this study is described after a brief review in crop modelling.

6.1.1 CROP MODELLING REVIEW

Two main types of models used to predict crop growth and yield include (i) descriptive models (also called statistical, regression or empirical), which reflect few or none of the mechanisms involved in the system; and (ii) explanatory models (also known as mechanistic or process based), which contain sub-models at least one hierarchical level deeper than the response (van Oijen, 2002). These explanatory models are based on an understanding of specific photosynthetic processes and to predict carbon exchange in plant canopies.

Descriptive models for plant growth use mathematical functions to relate crop development rate to environmental factors, such as heat sum (accumulated day-degrees), light intensity, temperature or photoperiod. Some examples are the use of linear and logistic models to describe leaf unfolding rate given a set of environmental conditions (Larsen and Hiden,1995) or a model for greenhouse lighting control based on the empirical relation between dry mass accumulation and light integral (Albright *et al.* 2000; Ferentinos *et al.* 2000).

Explanatory models for plant growth are usually based on photosynthesis. Tubiello and Ewert (2002) reviewed the most common approaches in productivity modelling to simulate growth, light interception, leaf area development, photosynthesis and respiration.

Plant growth is either calculated using radiation use efficiency (RUE), which is the approximate constancy of energy conversion into dry matter, or from canopy gross assimilation and respiration (Ewert, 2004).

Light interception is modeled frequently with the Monsi-Saeki equation (Monsi and Saeki, 1953), which is equivalent to the law of Lambert-Beer.

For leaf area (LA) development, two approaches are predominantly considered: either LA is calculated as a function of plant development stage or is predicted from simulated leaf dry weight using a knowledge of biomass allocation to leaf mass and the mass of leaves per unit of leaf area (or its inverse), typically known as Specific Leaf Area (SLA) (Marcelis *et al.*, 1998). Recently, Ewert (2004) provided some clarification about the relative importance of Leaf Area Index (LAI) for canopy assimilation and growth in biomass under increasing CO_2 levels and discussed its implication in process-based modelling (Tubiello and Ewert, 2002). Ewert (2004) concluded that improving in LAI modelling is necessary to progress in estimating plant productivity under conditions of rising CO_2, particularly for vegetation types with large variability in LAI. This improvement in LAI modelling depends on better knowledge of several processes such as substrate allocation, LA development and senescence and LAI adaptation to environmental changes. Usually, descriptive allometry models, which study the relative growth of a plant part in relation to the growth of the whole plant, are based on empirical ratios used to simulate dry matter partitioning (Marcelis *et al.*, 1998).

Different approaches for modelling leaf photosynthesis are used. On one hand, empirical functions, such as the non-linear hyperbolic model (Thornley and Johnson, 2000) reproduce satisfactorily leaf photosynthetic responses for different environmental conditions. On the other side, the biochemical model describing photosynthetic CO_2 assimilation developed by Farquhar (1980) considers that photosynthesis rate, limited by either light intensity or enzyme Rubisco concentrations, is based on the underlying biochemical relationships of the photosynthetic pathway (Collatz *et al.*, 1990; Farquhar *et al.*, 2001). However, mechanistic biochemical models are not always advantageous over the simpler leaf photosynthesis model, especially for developing control algorithms in controlled environments (Gao *et al.*, 2004). This is because instrumentation existing allow for direct empirical measurement of key parameters of the more mechanistic models. As such, it is possible to use semi-empirical models derived from data at the leaf scale to infer the carbon exchange behaviour of the full canopy.

Canopy photosynthesis can be simulated considering light absorption of different leaf layers together with a leaf photosynthesis model. Respiration models usually are subdivided into growth and maintenance respiration (Thornley and Johnson, 2000).

Specific models for lettuce are described in the literature. Van Henten (1994) validated a photosynthesis-based model for dynamic lettuce growth as function of photosynthetic photon flux (PPF), temperature and CO_2 levels. Currently, a model called NiCoLet (Nitrate Control in Lettuce) for predicting growth and nitrate content of lettuce is under development. The original NiCoLet was first developed under non-limiting environmental conditions. Then, the model was extended to N stress conditions (Seginer, 2003), fitted to data, examined for its dynamic behaviour (Linker *et al.* 2004) and modified for root mass prediction (Linker and Johnson-Rutzke, 2005). Mathieu *et al.* (2006) confirmed that the NiCoLet model simulated accurately lettuce crop growth and nitrate uptake for rapid fault detection in hydroponic systems.

Detailed reviews of models relating plant growth and yield to nutrition (Le Bot *et al.*, 1998), water relations (Jones and Tardieu, 1998) and to LA, light interception, dry matter production and partitioning (Marcelis *et al.*, 1998) are provided for further exploration in plant models.

6.1.2 PHOTOSYNTHETIC MODEL DESCRIPTION

The photosynthetic canopy model considered in this study, known as the Non-Rectangular Hyperbola (NRH) model, was developed by Thornley and Johnson (2000). The original NRH has been further modified, first to respond dynamically to light and nitrogen (Thornley, 1998) and then different plant respiration approaches were considered (Cannell and Thornley, 2000; Thornley and Cannell, 2000). Also, Thornley (2002) developed a model for instantaneous canopy photosynthesis based on the NRH leaf model, which allowed for sun/shade illumination and photosynthetic acclimation.

Thornley's original model (as used in this study) is based on the leaf photosynthetic response to light intensity and CO_2, which is then scaled up to the full canopy photosynthetic model by integrating light attenuation through the canopy. A brief description of the original model and the corresponding parameters is presented next.

6.1.2.1 LEAF PHOTOSYNTHESIS NON-RECTAGULAR HYPERBOLA MODEL

The Non-Rectangular Hyperbola (NRH) model for single leaf gross photosynthesis is described in [Eq. 6.1] (Thornley and Johnson, 2000).

$$P = \frac{1}{2\theta}\left\{\alpha I + P_{\max} - \left[\left(\alpha I + P_{\max}\right)^2 - 4\theta\alpha I P_{\max}\right]^{\frac{1}{2}}\right\} \qquad \text{[Eq. 6.1]}$$

where P (μmol $CO_2 \cdot m^{-2} \cdot s^{-1}$) is the gross photosynthetic rate, θ is the convexity term defined by [Eq. 6.2], α (μmol $CO_2 \cdot \mu mol^{-1}$ PAR) is the quantum yield, I (μmol $PAR \cdot m^{-2} \cdot s^{-1}$) is the leaf irradiance and P_{max} (μmol $CO_2 \cdot m^{-2} \cdot s^{-1}$) is the maximum gross photosynthetic rate at saturating irradiance [Eq. 6.3]

$$\theta = \frac{r_d}{r_d + r_x} \qquad 0 \le \theta \le 1 \qquad \text{[Eq. 6.2]}$$

$$P_{\max} = \frac{R_d r_d + C_a}{r_d + r_x} \qquad \text{[Eq. 6.3]}$$

In [Eq. 6.2] and [Eq. 6.3], r_d ($s \cdot m^{-1}$) is the diffusion resistance of CO_2 from the atmosphere into the leaf, r_x ($s \cdot m^{-1}$) is the carboxylation resistance, R_d (μmol $CO_2 \cdot m^{-2} \cdot s^{-1}$) is the dark respiration rate and C_a is the atmospheric CO_2 concentration (μL $CO_2 \cdot L^{-1} \cdot$).

The special cases where the convexity term equals its extreme values, although physiologically unlikely, deserve a brief explanation. When θ=1, it is assumed that r_x=0, in which case the gross photosynthetic rate increases linearly as irradiance increases, until photosynthesis is limited by CO_2 diffusion from the air. The derived equation, known as the Blackman response, presents some analytical problems caused by the discontinuity in the derivative at $I = P_{max} \cdot \alpha^{-1}$. Under the case of θ=0, one considers that diffusion resistance between the environment and the sites of photosynthesis is negligible (r_d=0). In this situation, P_{max} is defined as the ratio between the atmospheric CO_2 concentration and the carboxylation resistance, r_x. The advantage of this assumption is that [Eq. 6.1] reduces to a simpler rectangular hyperbola (RH) model [Eq. 6.4] and enables the direct, empirical estimation of P_{max} from the use of hand-held leaf photosynthetic systems.

$$P = \frac{\alpha I P_{max}}{\alpha I + P_{max}} \qquad \text{[Eq. 6.4]}$$

Since the net photosynthetic rate P_n is defined as the difference between the gross photosynthetic rate P and the dark respiration rate R_d, [Eq. 6.5] defines the leaf net photosynthetic rate for the rectangular hyperbola model.

$$P_n = \frac{\alpha I P_{max}}{\alpha I + P_{max}} - R_d \qquad \text{[Eq. 6.5]}$$

The NRH model of leaf photosynthesis has been demonstrated satisfactorily to describe observed leaf photosynthetic responses to environmental variables (Pachepsky *et al.*, 1996; Rodriguez *et al.*, 2001; Thornley and Johnson, 2000). As described above, this model has three parameters: the quantum yield (α), corresponding to the slope of the curve relating CO_2 uptake to incident light (I), the light saturated photosynthetic rate (P_{max}) and the dark leaf respiration rate(R_d).

Several studies conclude that quantum yield values (α) are independent of CO_2 atmospheric levels (Pachepsky and Acock, 1996; Waters *et al.*, 2005), but Peri *et al.* (2005) found α dependency on other environmental conditions such as temperature, nitrogen concentration or water status. This is in agreement with results reported by Cannell and Thornley (1998), where α was found to be constant at saturated CO_2 atmospheres within a temperature range of 10-40 ºC, but declined with increasing temperatures in elevated but non-saturating CO_2 levels such as at 700 ppm.

P_{max} varies among species and is affected by temperature and CO_2 levels (Cannell and Thornley, 1998a,b; Pachepsky and Acock, 1996; Waters *et al.*, 2005). This is consistent with the mathematical dependency of P_{max} on the atmospheric CO_2 concentration, as in [Eq. 6.3].

The convexity factor (θ), which can vary between a value of 0 and 1, is unaffected by the range of temperature, water status and nitrogen content (Peri *et al.*, 2005). However, θ is inversely related to external CO_2 partial pressures (Akhkha *et al.*, 2001).

The ambiguity surrounding the functional significance of θ, lead several authors to discuss whether the convexity term should be considered. Akhkha *et al.* (2001) concluded that the convexity term (θ), describes significantly better the photosynthetic light response curve than the frequently used RH model, except for high CO_2 levels (>10 KPa) where results are fairly the same. Nonetheless, Gomes *et al.* (2006) demonstrated that RH is quantitatively adequate for describing the irradiance-response of photosynthesis and for predictive

calculations in productivity models either isolated or as part of a model. In addition to this, they found that NRH is less adequate for P_{max} and R_d estimations, but can be integrated to larger models to study the mechanisms of photosynthesis, as convexity term refers to resistances to CO_2 diffusion. Similar conclusions are achieved by Pachepsky *et al.* (1996) after evaluating RH and the Farquhar biochemical modelling approach. Therefore, due to the adequacy and simplicity of RH model, it was decided in this study to use RH model for estimating light parameters at leaf scale and then scaling up to the full canopy case.

6.1.2.2 LIGHT RELATIONS IN PLANT CANOPIES

In plant canopies, light attenuation is usually described with the Monsi-Saeki equation [Eq. 6.6] (Monsi and Saeki, 1953).

$$I(l) = I_0 \cdot e^{-k \cdot l} \qquad \text{[Eq. 6.6]}$$

In [Eq. 6.6], I(*l*) (μmol PAR·m^{-2}·s^{-1}) is the light intensity at cumulative leaf area index *l* (m^2 leaf·m^{-2} ground), I_0 (μmol PAR·m^{-2}·s^{-1}) is the light intensity at leaf area index 0 (canopy top) and k (m^2 ground·m^{-2} leaf) is the light extinction coefficient through the canopy.

6.1.2.3 CANOPY PHOTOSYNTHESIS MODEL

The canopy gross photosynthetic rate (μmol CO_2·m^{-2}·s^{-1}) incorporates the RH model of leaf photosynthesis and light attenuation equation (Cannell and Thornley, 1998). The approach used is the multilayer model where leaf photosynthesis, obtained with the hyperbola model, is integrated (downwards) through canopy with accomodation for light attenutation through the canopy and increasing accumulated LAI. [Eq. 6.7] presents the full canopy model used to calculate instantaneous carbon exchange. To derive daily carbon gain estimates, the results of the equation are integrated over the photoperiod.

$$P = \int_{l=0}^{l} \frac{\alpha I_o e^{-k \cdot l} P_{\max}}{\alpha I_o e^{-k \cdot l} + P_{\max}} - R_d \cdot dl \qquad \text{[Eq. 6.7]}$$

In [Eq. 6.7], *l* is the cumulative LAI (m^2 leaf·m^{-2} ground), I_0 (μmol PAR·m^{-2}·s^{-1}) is the light intensity at leaf area index 0 (canopy top) and k (m^2 ground·m^{-2} leaf) is the light extinction coefficient through the canopy. The quantum yield (α), corresponding to the slope of the curve relating CO_2 uptake to incident light (I), the light saturated photosynthetic rate (P_{max}) and the dark leaf respiration rate, R_d are parameters as defined above and are estimated from leaf photosynthetic curves (described below).

$$\frac{dl}{dt} = \frac{P \cdot L_{plant} \cdot SLA}{C_{leaf}} \quad \text{[Eq. 6.8]}$$

In [Eq. 6.8], *l* (m^2 leaf·m^{-2} ground) is the cumulative LAI, P the photosynthesis rate, L_{plant} (% dw) is the leaf content of the plant, SLA (m^2 leaf·g^{-1} leaf) is the specific leaf area and C_{leaf} (% dw) corresponds to the carbon content of leaf.

6.2 MATERIALS AND METHODS

Results presented in this chapter correspond to the atmospheric data and light curves of the same batch and staggered cultures with beet and lettuce explained in the previous chapter. Thus, materials and methods of the plant trials are not repeated here and the reader is referred to Chapter 5, where a description of the sealed environment chambers is provided and the experimental design, procedure, analytical methods and cultural conditions are explained in detail.

Consequently, this section describes only specific materials and data analysis related to the atmospheric results and to the generation of light curves.

6.2.1 CANOPY PHOTOSYNTHESIS

As mentioned in the previous chapter, both of the SEC plant growth chambers operate isolated from the exterior. All the major variables in the aerial environment, such as temperature, humidity, CO_2 and O_2 composition and pressure are monitored.

Oxygen concentration is monitored continuously, but not controlled. Figure 6.1 (right) shows a typical profile of O_2 evolution inside the chamber for a 5 day period. Since plant photosynthetic rate is higher than the respiration rate, where O_2 is consumed, oxygen accumulates inside the chamber.

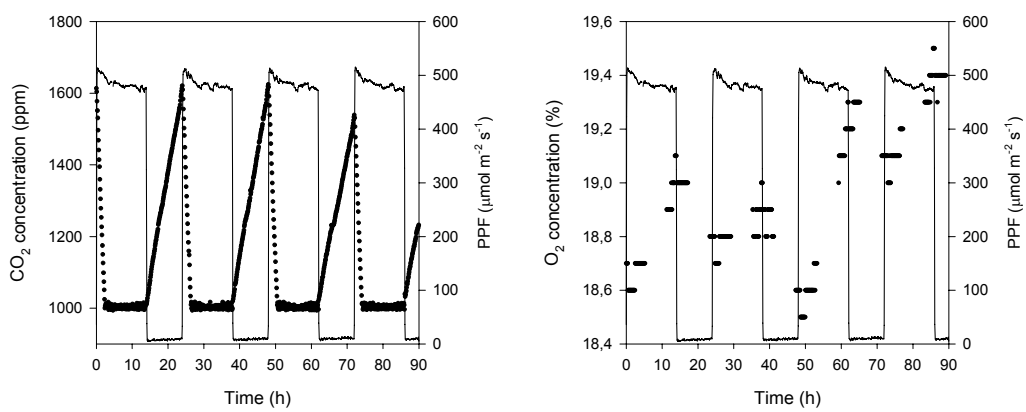

Figure 6.1 CO_2 (ppm) and O_2 (%) profile inside the SEC chambers (●) with a 14/10 h day/night photoperiod (solid line: photosynthetic photon flux density, PPF in μmol $m^{-2}s^{-1}$) during a 5 day period of a beet batch culture.

Atmospheric CO_2 concentration (Figure 6.1, left) is maintained at fixed concentrations (1000 $\mu L \cdot L^{-1}$ CO_2) during day-light hours (14 h, from 6:00 to 20:00) by a computer regulated compensatory system using bottled CO_2 (Dutton *et al.*, 1988). In this way, any net carbon gain by the stand through photosynthetic activity was compensated by injections from the external tank. During the dark period (10 h, from 20:00 to 6:00) CO_2 concentration increases due to respiration process, since was not possible to remove CO_2 from the chamber to achieve static conditions.

Daytime Net Photosynthesis (Pn, μmole $CO_2 \cdot m^{-2} \cdot s^{-1}$) is determined non-destructively using a gas compensation technique (Dutton *et al.*, 1988) and calculated from recorded chamber data on a daily basis as in [Eq. 6.9].

$$Pn = \frac{(CO_{2,t=5:55} - CO_{2,daylight}) \cdot V_{air} + CO_{2,injected} - Leakage_{day}}{Photoperiod_{Daylight} \cdot Area \cdot 3600} \qquad [Eq.\ 6.9]$$

In [Eq. 6.9] $CO_{2,\ t=5:55}$ is the CO_2 (μmol CO_2 ·mol air $^{-1}$) concentration at the end of dark period (t=5:55), $CO_{2,\ daylight}$ is the fixed concentration of 1000 μmol CO_2 ·mol air $^{-1}$ during daylight time, V_{air} (mol air) is the inside air volume of SEC chamber, $CO_{2,\ injected}$ (μmol CO_2) is the daylight CO_2 injected to maintain $CO_{2,\ daylight}$ measured with a metered flow, leakage rate (μmol CO_2) during daylight time is shown in the cultural condition tables in chapter 5 , $Photoperiod_{daylight}$ is 14 h, Area correspond to growing area and 3600 is a conversion factor from seconds to hours.

Dark Net Respiration Rate (Rr, μmole $CO_2 \cdot m^{-2} \cdot s^{-1}$) is obtained from the difference in accumulated CO_2 during dark period and CO_2 demand, corrected for the chamber leakage rate. Parameters involved in Rr [Eq. 6.10] have been already explained for Pn equation.

$$Rr = \frac{(CO_{2,t=5:55} - CO_{2,daylight}) \cdot V_{air} + Leakage_{night}}{Photoperiod_{night} \cdot Area \cdot 3600} \qquad [Eq.\ 6.10]$$

Net Carbon Exchange Rate (NCER, μmole CO_2 m^{-2} s^{-1}), defined as the difference between Pn and Rr [Eq. 6.11].

$$NCER = \frac{Pn \cdot Photoperiod_{day} - Rr \cdot Photoperiod_{night}}{24} \qquad [Eq.\ 6.11]$$

NCER over a 24 hour period is also known as Daily Carbon Gain (DCG). Integrated Daily Carbon Gain (IDCG, mol CO_2), which is the accumulated DCG at the end of each culture, contributes to estimated biomass production (DW) with knowledge of the carbon content. The relative error (RE) between the estimated DW and the DW harvested allows checking if NCER may be used as a reliable estimator of DW yield.

6.2.2 LEAF LIGHT PHOTOSYNTHETIC RESPONSE

Photosynthetic response to light at the leaf scale was determined at the end of the grow-out period in order to estimate the quantum yield (α), corresponding to the slope of the curve relating CO_2 uptake to incident light (I), the light saturated photosynthetic rate (P_{max}) and the dark leaf respiration rate, $R_{d.}$. A LiCOR LI-6400 portable photosynthetic analysis system (Figure 6.2) was used for generation of these light response curves, usually one day prior to final harvest. The system employs a flow-through gas analysis-system which determines Pn on the basis of metered flow rates and CO_2 concentrations in incoming and out-going air streams of a cuvette.

Figure 6.2 LI-6400 used for photosynthetic response to light at leaf scale.

Response curves were collected on the youngest fully expanded leaf of the six sample plants for batch cultures and of three plants of each age class for staged trials. Light response curves were generated at 5 different CO_2 concentrations in the cuvette ranging from 350 to 2000 $\mu L \cdot L^{-1}$ in batch cultures. Under staged production, light curves were performed at each of the different crop ages represented inside the culture. For lettuce data, this corresponds to three ages at a CO_2 concentration of 1000 ppm and for beet, four ages (40, 50, 60 and 70 days) at different CO_2 levels (350, 700, 1000 and 1300 $\mu L \cdot L^{-1}$).

The resulting data were fitted to the rectangular hyperbola model [Eq. 6.5] using the non-linear least squares regression (nls) procedure. Estimates for α, P_{max}, and R_d along with their standard errors were determined from the output of the nls analysis. Initial parameter estimates were derived from visual inspection of raw data. Significant differences in parameter estimates among CO_2 concentrations was assessed using a t-test at p=0.05.

6.3 RESULTS AND DISCUSSION

Initially, empirical canopy photosynthesis data for beet and lettuce is presented in terms of net photosynthesis (Pn), dark net respiration rate (Rr) and net carbon exchange rate (NCER). The integrated daily carbon gain (IDCG) allow for an estimation of dry weight (DW), which is compared with the harvested values.

Secondly, light parameter estimates are generated applying the Thornley model to the leaf light curves at leaf scale at different drop ages and CO_2 levels. The dependency of light estimates on these two factors is also evaluated.

Finally, leaf parameters estimates together with other harvest parameters are used in the full canopy model, for comparing with empirical values of harvested biomass.

6.3.1 EMPIRICAL CANOPY PHOTOSYNTHESIS

6.3.1.1 BEET CARBON EXCHANGE DATA

Figure 6.3 shows daytime net photosynthesis (Pn), dark net respiration rate (Rr), net carbon exchange rate and photosynthetic photon flux (PPF) profile through canopy development (days in chamber, DIC) of beet batch cultures (BB1, BB2 and BB3).

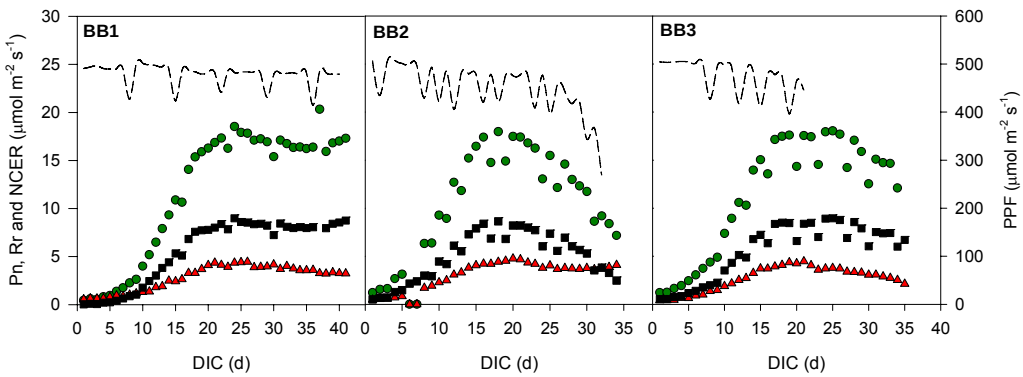

Figure 6.3 Daytime Net Photosynthesis (● Pn), Dark Net Respiration Rate (▲ Rr) and Net Carbon Exchange Rate (■ NCER) and photosynthetic photon flux (dashed line, PPF) for beet batch cultures (BB1, BB2 and BB3). Oscillations in PPF values correspond to short-term light curves, where light was attenuated with screens (data not presented).

The integrated carbon gain (IDCG) profile of beet batch replications is depicted in Figure 6.4.

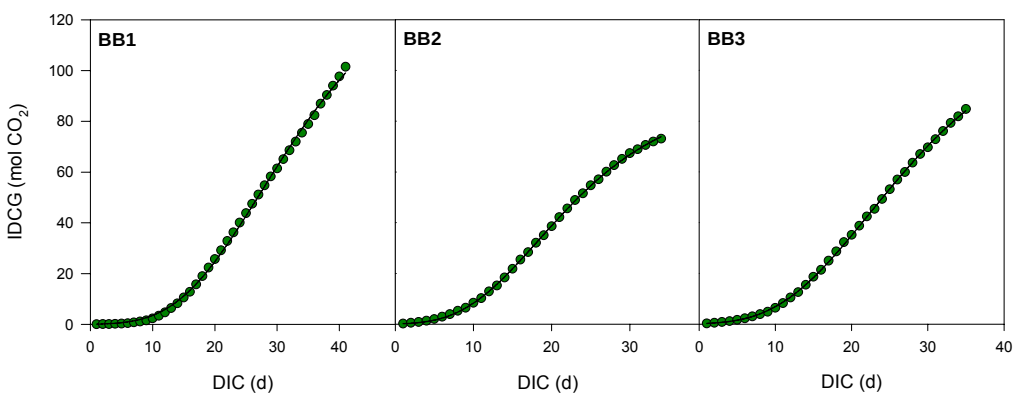

Figure 6.4 Integrated Daily Carbon Gain (IDCG) for beet batch cultures (BB1, BB2 and BB3).

In staggered cultures Pn, Rr and NCER oscillates periodically coinciding with the intermediate harvests performed every 10 days (Figure 6.5).

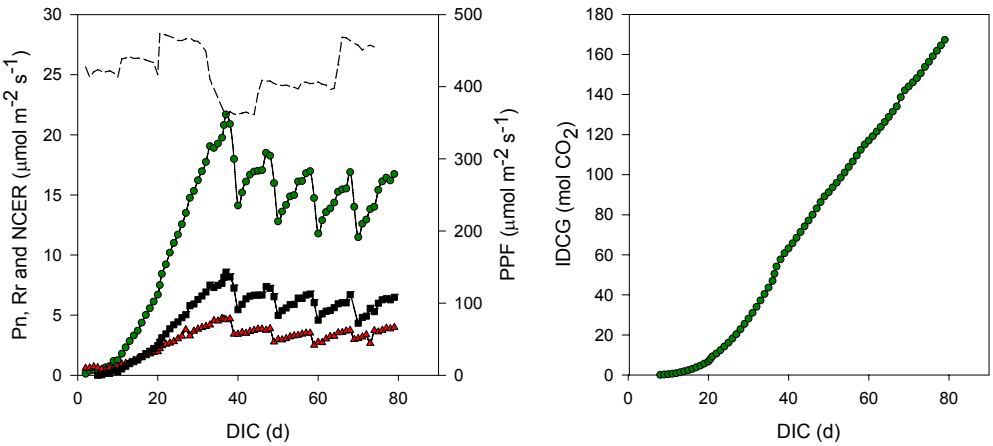

Figure 6.5 LEFT: Daytime Net Photosynthesis (● Pn), Dark Net Respiration Rate (▲ Rr), Net Carbon Exchange Rate (■ NCER) and photosynthetic photon flux (dashed line, PPF) for beet staged culture BS2. RIGHT: Integrated Daily Carbon Gain (IDCG) for BS2. Values are not shown for BS1 due to problems with the computer data acquisition.

The total amount of CO_2 injected can be used to estimate the DW production. Table 6.1 compares the estimated biomass from the last value of IDCG and the carbon content obtained with mineral analyses of harvested biomass (Chapter 5) with the total DW harvested at the end of each trial. Low relative errors (0.4<%RE<13) obtained suggests that non-destructive NCER technique is in close agreement with DW biomass determined by conventional destructive analyses.

Table 6.1 Comparison between estimated biomass estimated from CO_2 injected and carbon content and biomass harvested for beet cultures.

Parameter	BB1	BB2	BB3	BS2
CO_2 injected (moles)	101	73	85	167
Carbon Content (%)	37	38	38	36.8
Estimated DW from CO_2 injection (g)	3259	2315	2685	5460
DW at Harvest (g)	3048	2232	2696	6246
Relative Error (%)	-7	-4	0.4	13

Therefore, the NCER technique is deemed to be a good alternative for estimating plant growth inside the chamber without using destructive analyses. This finding provides empirical confirmation of the adequacy of employing the NCER technique for biomass estimation as suggested by other authors (Dutton *et al.*, 1988; Monje and Bugbee ,1998).

6.3.1.2 LETTUCE CARBON EXCHANGE DATA

Lettuce results for canopy photosynthesis are presented following the same structure as in beet.

Figure 6.6 depicts the Pn, Rr, NCER and PPF evolution through batch cultures (LB1, LB2 and LB3) and Figure 6.7 shows the corresponding IDCG for each of the 3 replications.

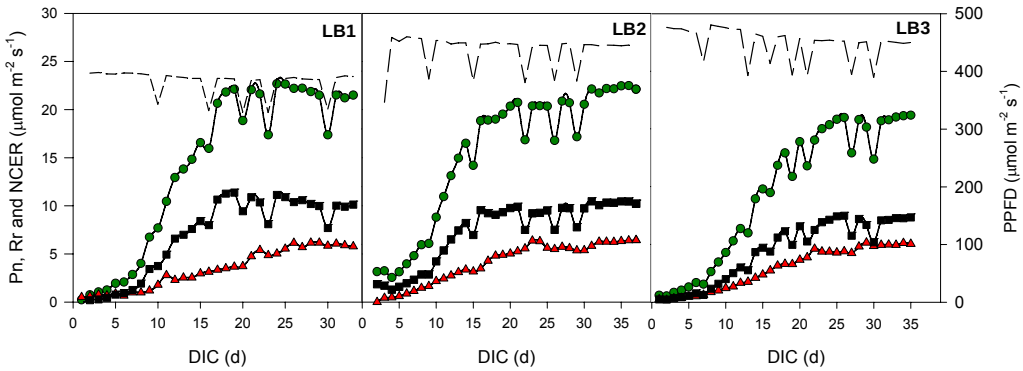

Figure 6.6 Daytime Net Photosynthesis (● Pn), Dark Net Respiration Rate (▲ Rr), Net Carbon Exchange Rate (■ NCER) and photosynthetic photon flux (dashed line, PPF) for lettuce batch cultures (LB1, LB2 and LB3). Oscillations in PPF values correspond to short-term light curves, where light was attenuated with screens.

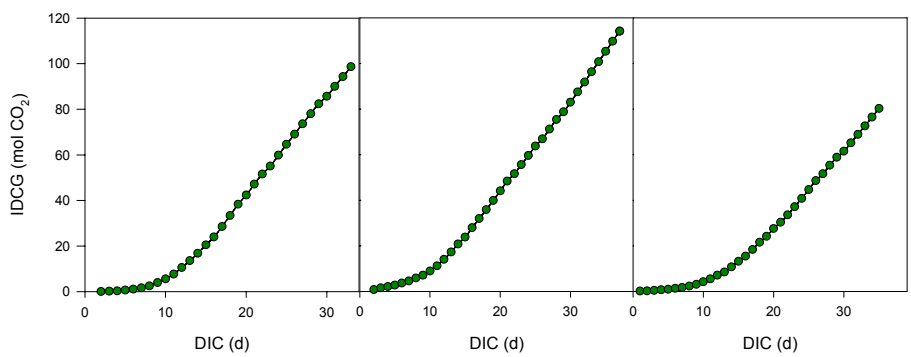

Figure 6.7 Integrated Daily Carbon Gain for lettuce batch cultures.

Staggered cultures at full chamber stock has a 10 day period oscillation of Pn, Rr and NCER values caused by the intermediary collection of the mature plants, as shown in Figure 6.8.

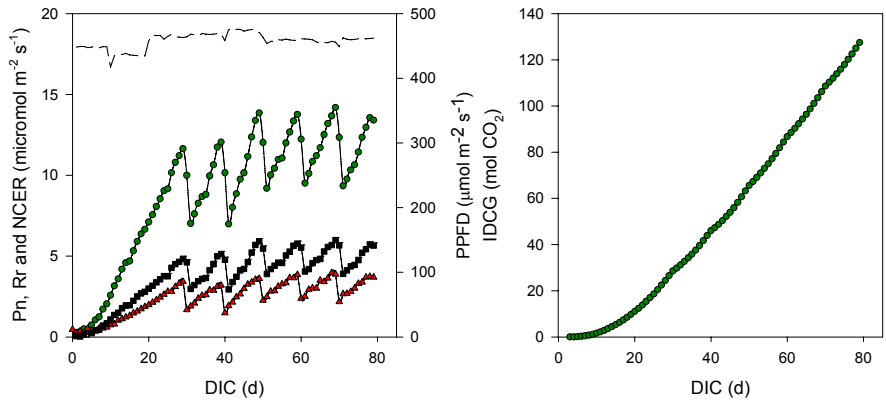

Figure 6.8 LEFT: Daytime Net Photosynthesis (● Pn), Dark Net Respiration Rate (▲ Rr), Net Carbon Exchange Rate (■ NCER) and photosynthetic photon flux (dashed line, PPF) for lettuce staged culture LS1. RIGHT: Integrated Daily Carbon Gain (IDCG) for lettuce staged culture LS1. Values are not shown for LS2 due to some problems with the computer data acquisition.

Similarly to beet cultures, estimated DW biomass from the total CO_2 injected together with the carbon content in lettuce is compared with the DW gathered at the end of each culture (Table 6.2).

Table 6.2 Comparison between biomass estimated from CO_2 injected and carbon content and biomass harvested for lettuce cultures.

Parameter	LB1	LB2	LB3	LS1	LS2
CO_2 injected (moles)	99	114	80	127	94
Carbon Content (%)	37	37	38	37	35
Estimated DW from CO_2 injection (g)	3239	3682	2587	4160	3210
DW at Harvest (g)	2091	2988	2791	4611	3677
Relative Error (%)	-55	-23	7	10	13

All relative errors are reasonably low except for LB1 and LB2 cultures, where harvested biomass is less than the potential DW production based on the CO_2 injected. Some of the possible reasons for this discrepancy are either a greater leakage rate in the chamber than the measured one or a lack of accuracy in calibration of the CO_2 metered injection. Since these two cultures are the only ones among all beet and lettuce trials performed in SEC-2 instead of SEC-1, it may be concluded that any of the mentioned causes related to hardware calibration are highly likely.

With improvements in calibration (flow meters, IRGA) and measurement procedures (C content in biomass), daily carbon gain data can be converted into a daily increase in biomass and crop growth rate with the non-destructive NCER technique. Monje and Bugbee (1998) reported that estimated biomass from CO_2 data was usually within 5% of the dry mass harvested. Therefore, during the construction and start up of the new HPC for the MPP, it is important to have good instruments calibration and leakage rate determination in order to achieve such accurate estimations of biomass from CO_2 data.

6.3.1.3 BATCH AND STAGGERED NCER COMPARISON

Atmospheric stabilization is essential for long term dynamic operation inside the MELiSSA loop. In order to compare the gas dynamic evolution between different methods of production, Figure 6.9 depicts for each crop the NCER obtained in a staggered culture together with successive NCER from a batch culture.

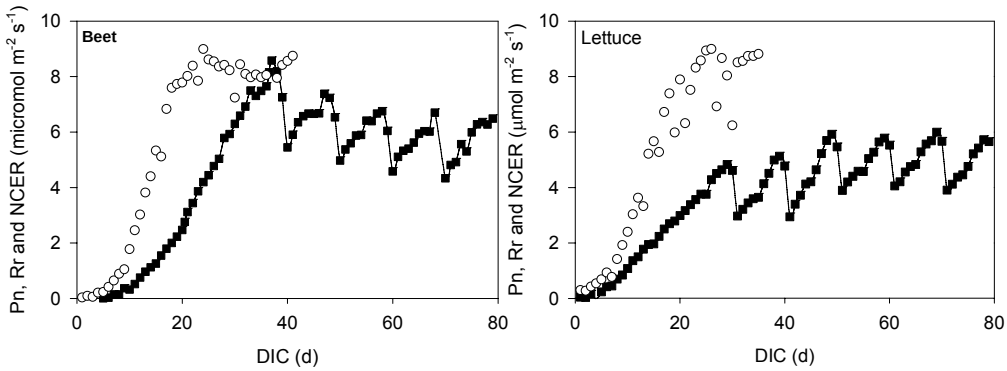

Figure 6.9 Comparison of NCER between batch (○) and staggered (■) cultures for beet (BB1, BS2) and lettuce (LB3, LS1).

Clearly, staggered cultures dampen the long term oscillation in gas exchange rates obtained in batch culture. Moreover, staggered planting provides a uniform supply of O_2, food and water than batch planting, while reducing the size of storages buffers (Wheeler 1996). Besides, Stutte *et al.* (1997) obtained higher yield in water, O_2 and food in staggered than batch planting for potatoes. They attribute the increase in yield to the more open canopy system of staggered plantings, where additional leaf area is exposed to light resulting in a higher photosynthetic surface.

In conclusion, as NCER evolution in staggered operation is more stable through DIC than in batch operation, staged cultures are preferred. This choice in type of culture will have implication in the design of HPC for the MPP (Chapter 7).

6.3.2 EMPIRICAL LEAF PHOTOSYNTHESIS

The rectangular hyperbola model, as defined in [Eq. 6.5], is fitted to leaf light photosynthetic responses to estimate the quantum yield (α, µmol $CO_2 \cdot \mu mol^{-1}PAR$), the maximum photosynthetic rate (P_{max}, µmol $CO_2 \cdot m^{-2} \cdot s^{-1}$) and the dark respiration rate (R_d, µmol $CO_2 \cdot m^{-2} \cdot s^{-1}$) at a determined CO_2 level for beet and lettuce.

6.3.2.1 BEET LEAF LIGHT PHOTOSYNTHETIC RESPONSE

Initially, leaf photosynthetic response of beet at different growth stages was measured to determine whether light parameters estimates depend on age. With this aim, [Eq. 6.5] was fitted to the light photosynthetic response data at four CO_2 levels for beets of four different ages cultivated in the staged culture BS2 (Figure 6.10).

Points represent the observed mean (±SE) of the net photosynthetic rate, Pn (μmol $CO_2 \cdot m^{-2} \cdot s^{-1}$) at each light level of the six sampled plants. The solid lines represent the fitted rectangular hyperbola model [Eq. 6.5].

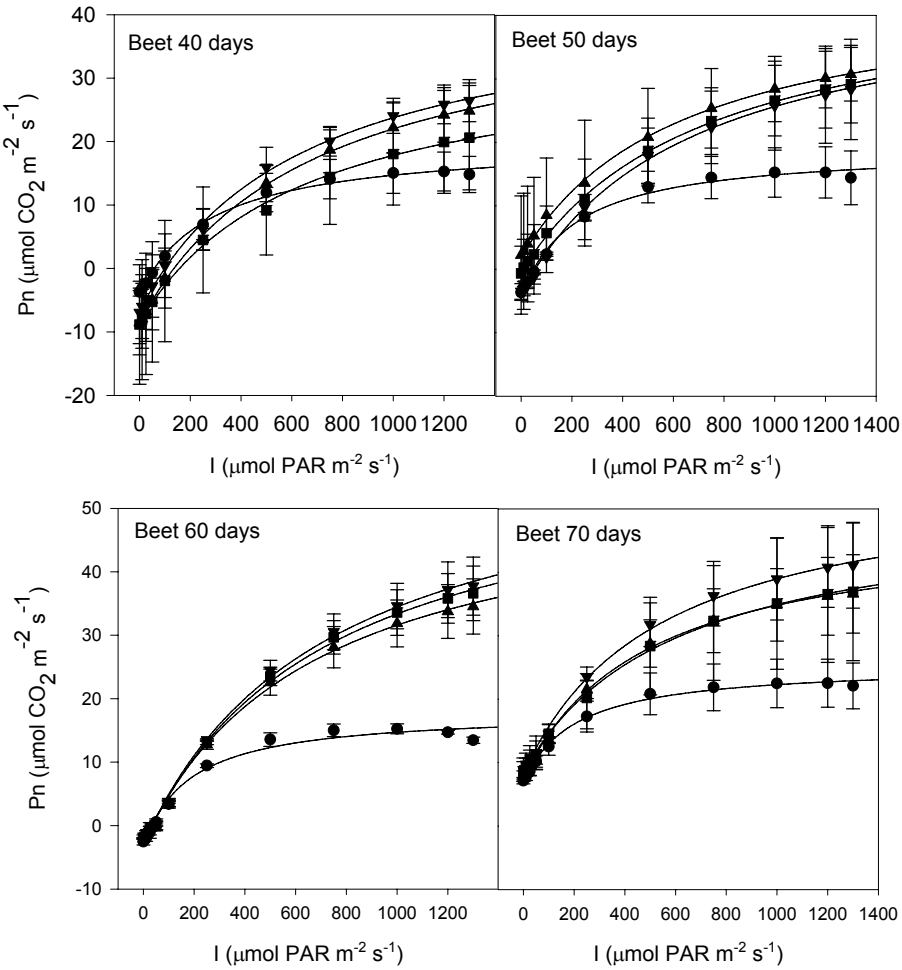

Figure 6.10 Beet leaf light response curve at different CO_2 levels (● 350 ppm▲ 700 ppm ■ 1000 ppm▼1300 ppm) and at different crop ages (40, 50, 60 and 70 days) for beet staggered culture (BS2).

Table 6.3 summarizes the parameter estimates for α, P_{max} and R_d at different CO_2 levels and beet ages along with the standard error of the residuals (RSE) and degrees of freedom (df) for beet staged cultures (BS2).

Upon anlysis of the data, no significant differences (p=0.05) were observed at each CO_2 level (C_a= 350, 700, 1000 and 1300 μL $CO_2 \cdot L^{-1}$) for the quantum yield (p=0.7, 0.3, 0.5, 0.2), maximum photosynthetic rate (0.02*, 0.7, 0.8, 0.9) and dark respiration rate (p=0.1, 0.6, 0.3, 0.05) among beet ages, except for one case (*). As a consequence, it may be conclude that α, P_{max} and R_d values remain constant through crop development.

Table 6.3 Parameter estimates for leaf response curves of beet staggered culture BS2 with the standard errors. Units are: Age (d), C_a (µL $CO_2 \cdot L^{-1}$), α (µmol $CO_2 \cdot \mu mol^{-1}$ PAR), P_{max} (µmol $CO_2 \cdot m^{-2} \cdot s^{-1}$) and R_d (µmol $CO_2 \cdot m^{-2} \cdot s^{-1}$).

Age	C_a	α	P_{max}	R_d	RSE	df
40	350	0.09±0.02	24.11±1.46	4.09±0.74	1.98	30
	700	0.08±0.02	51.23±6.60	8.53±1.18	3.61	30
	1000	0.07±0.04	43.2±12.6	8.53±2.46	7.43	30
	1300	0.08±0.02	50.10±6.72	6.70±1.17	3.53	26
50	350	0.11±0.03	23.30±1.63	4.30±1.27	2.11	17
	700	0.07±0.03	42.88±11.0	1.87±2.12	6.70	31
	1000	0.06±0.02	45.96±8.63	0.44±1.45	4.44	30
	1300	0.07±0.02	48.67±6.94	3.74±1.30	3.94	30
60	350	0.12±0.02	21.25±0.76	3.28±0.54	1.09	19
	700	0.09±0.01	57.03±3.91	2.77±0.73	2.21	30
	1000	0.09±0.01	62.16±4.10	2.87±0.68	2.10	30
	1300	0.09±0.01	64.47±4.57	2.79±0.74	2.28	30
70	350	0.09±0.03	18.64±1.35	3.24±0.90	2.29	30
	700	0.08±0.02	40.40±3.99	2.43±1.11	3.22	30
	1000	0.07±0.03	42.16±9.26	1.52±1.98	5.93	30
	1300	0.09±0.02	47.13±4.93	1.71±1.20	3.55	30

In beet batch culture BB2, photosynthetic response to light intensity was determined at four different CO_2 levels ranging from 350 to 2000 µL $CO_2 \cdot L^{-1}$ (Figure 1.11).

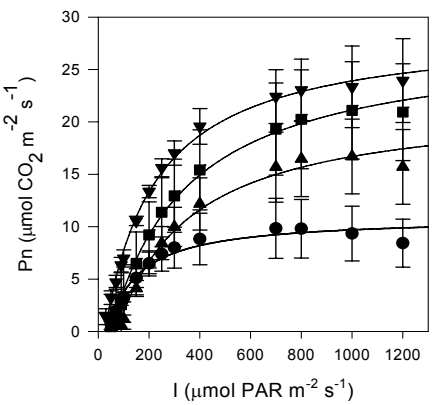

Figure 6.11 Beet leaf light curve at different CO_2 levels (● 350 ppm▲ 700 ppm ■ 1000 ppm ▼2000 ppm) for beet batch culture BB2.

Table 6.4 summarizes the corresponding estimates for the quantum yield (α), the maximum photosynthetic rate (P_{max}) and dark respiration rate (R_d) along with the standard error of the residuals (RSE) and degrees of freedom (df).

Using all the parameters estimated from the beet batch and staged cultures, no significant differences (p=0.725, 0.85) were observed for α and R_d estimated among CO_2 levels, which is consistent with results found in literature (Pachepsky and Acock, 1996; Waters *et al.*, 2005).

Table 6.4 Parameter estimates for leaf response curves of beet batch culture BB2 with the standard errors. Units are: C_a (μL $CO_2 \cdot L^{-1}$), α (μmol $CO_2 \cdot \mu mol^{-1}$ PAR), P_{max} (μmol $CO_2 \cdot m^{-2} \cdot s^{-1}$) and R_d (μmol $CO_2 \cdot m^{-2} \cdot s^{-1}$).

Rep.	C_a	α	P_{max}	R_d	RSE	df
BB2	350	0.20±0.08	16.10±1.57	5.20±1.83	1.74	81
	700	0.14±0.02	29.35±1.01	7.43±1.16	2.21	81
	1000	0.13±0.03	33.36±1.64	5.44±1.66	3.46	81
	1300	0.14±0.03	34.91±1.28	6.98±1.30	2.70	81
	2000	0.19±0.03	33.13±1.09	4.21±1.35	1.85	81

However, α dependency on temperature has been identified (Cannell and Thornley, 1998; Peri *et al.*, 2005). Since temperature was constant for all the experiments and any age or CO_2 influence is detected, a mean value of all parameter estimates at different CO_2 levels and crop ages can be used for quantum yield (0.10±0.01 with n=21) and for dark respiration rate (4.02±0.57 with n=21).

In contrast, P_{max} changes significantly ($p=0.018<0.05$) on CO_2 levels. As shown in Figure 6.12 where P_{max} estimates for beet in batch and staged cultures are plotted against the different CO_2 concentrations, the greater the CO_2 level the greater the P_{max}. This finding is consistent with the dependency of P_{max} on C_a for the case of $\theta=0$ (Cannell and Thornley, 1998a,b; Pachepsky and Acock, 1996; Waters *et al.*, 2005). Thus, although P_{max} is not influenced by crop age, one must derive new estimates for each operational CO_2 level.

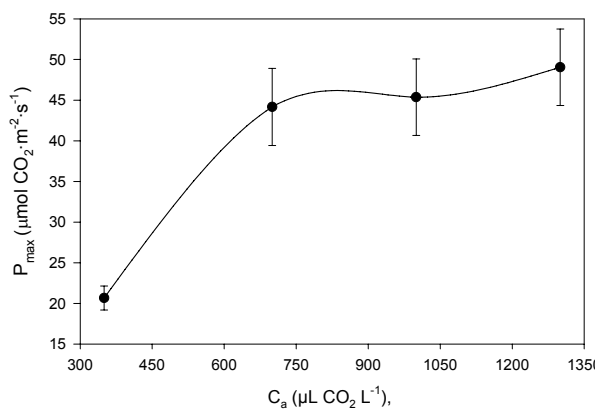

Figure 6.12 P_{max} estimate for beet at different CO_2 levels.

6.3.2.2 LETTUCE LEAF LIGHT PHOTOSYNTHETIC RESPONSE

First, light parameters are estimated in staggered culture to check whether α, P_{max} and R_d values are independent from lettuce age as concluded for beet. Figure 6.13 depicts photosynthetic response to light intensity (I) for lettuce leaves at CO_2 concentration of 1000 $\mu L \cdot L^{-1}$ for each crop age.

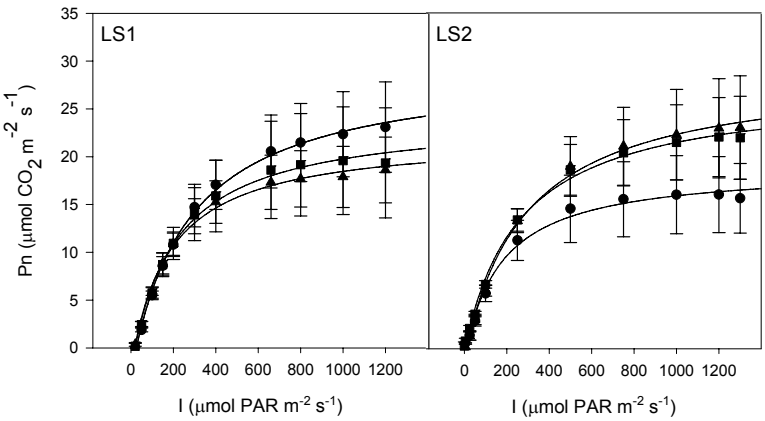

Figure 6.13 Lettuce leaf light response curve at different crop ages levels (● 30 days, ▲ 40 days ■ 50 days) for staged culture (LS1 and LS2).

The parameter estimates for α, P_{max} and R_d are presented in Table 6.5 along with their corresponding standard errors (SE), the residuals SE (RSE) and the degrees of freedom of the RSE estimate (df).

Table 6.5 Parameter estimates for leaf response curves of lettuce staggered cultures (LS1 and LS2) with the stardard errors at C_a =1000 µL $CO_2 \cdot L^{-1}$. Units are: age (d), α (µmol $CO_2 \cdot µmol^{-1}$ PAR), P_{max} (µmol $CO_2 \cdot m^{-2} \cdot s^{-1}$), R_d (µmol $CO_2 \cdot m^{-2} \cdot s^{-1}$)

Rep.	Age	α	P_{max}	R_d	RSE	df
LS1	30	0.12±0.02	32.21±1.32	2.77±0.78	2.55	69
	40	0.13±0.02	24.20±0.85	2.04±0.64	1.97	69
	50	0.13±0.03	26.49±0.85	2.23±1.05	3.31	69
LS2	30	0.11±0.02	19.89±0.94	0.95±0.67	2.60	74
	40	0.10±0.02	29.96±1.58	0.82±0.76	2.96	63
	50	0.10±0.02	27.45±1.22	0.11c0.64	2.44	63

For lettuce, no significant differences (p=0.05) were observed for the quantum yield, maximum photosynthetic rate and dark respiration rate among beet ages at a fixed CO_2 level of 1000 ppm (LS1: p=0.53, 0.51, 0.49; LS2: 0.32, 0.48, 0.23). Mean values among ages and replications for alpha, P_{max} and R_d are 0.12±0.005 µmol $CO_2 \cdot µmol^{-1}$ PAR, 26.7±1.8 µmol $CO_2 \cdot m^{-2} \cdot s^{-1}$ and 1.48±0.4 µmol $CO_2 \cdot m^{-2}$ s^{-1}, respectively.

In lettuce batch culture LB2 and LB3, although light curves were performed at 5 CO_2 levels, Figure 6.14 shows only the photosynthetic response for 3 different CO_2 concentrations.

The parameter estimates for α, P_{max} and R_d are presented in Table 6.6 along with their corresponding SE, RSE and the degrees of freedom of the RSE estimate (df).

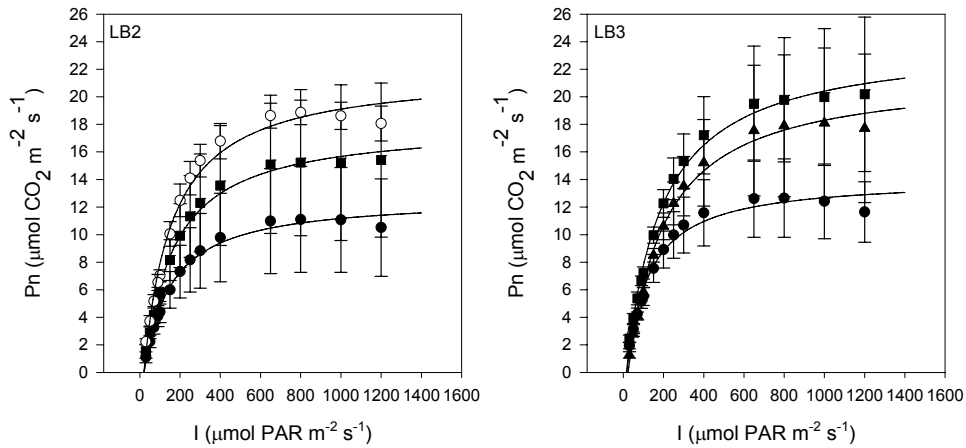

Figure 6.14 Lettuce leaf light response curve at different CO_2 levels (● 350 ppm▲ 700 ppm ■ 1000 ppm▼1300 ○2000 ppm) for batch cultures (LB2, LB3)

Table 6.6 Parameter estimates for leaf response curves of lettuce batch cultures (LB2 and LB3) with the stardard errors. Units are: C_a (μL $CO_2 \cdot L^{-1}$), α (μmol $CO_2 \cdot \mu mol^{-1} \cdot PAR$), P_{max} (μmol $CO_2 \cdot m^{-2} \cdot s^{-1}$), R_d (μmol $CO_2 \cdot m^{-2} \cdot s^{-1}$)

Rep.	C_a	α	P_{max}	R_d	RSE	df
LB2	350	0.13±0.06	15.11±1.57	2.41±1.92	2.34	81
	700	0.15±0.04	24.84±1.14	2.79±1.42	2.31	81
	1000	0.17±0.07	21.09±1.95	3.07±2.44	3.23	81
	1300	0.19±0.07	22.91±1.69	3.79±2.10	2.75	81
	2000	0.21±0.03	25.59±0.70	3.73±0.87	1.13	81
LB3	350	0.18±0.06	16.79±1.40	2.70±1.67	1.74	81
	700	0.16±0.05	25.01±1.44	3.29±1.81	2.83	81
	1000	0.16±0.04	26.43±1.33	2.35±1.67	2.65	81
	1300	0.20±0.05	21.67±1.29	3.52±1.58	1.88	81
	2000	0.16±0.06	30.28±2.13	0.83±2.62	4.49	81

No statistically significant difference (p=0.13, 0.9) were observed for α and R_d estimated among CO_2 levels among all the parameters estimated from the lettuce batch and staged cultures. Similar results are obtained for beet and are in agreement with bibliographic sources (Pachepsky and Acock, 1996; Waters *et al.*, 2005).

Therefore, a mean value of all parameters estimates at different CO_2 levels and crop ages can be used for quantum yield (0.15±0.01 with n=16) and for dark respiration rate (2.34±0.28 with n=16).

However, significant differences (p=0.04) are observed for P_{max} estimated among CO_2 levels, as shown in Figure 6.15.

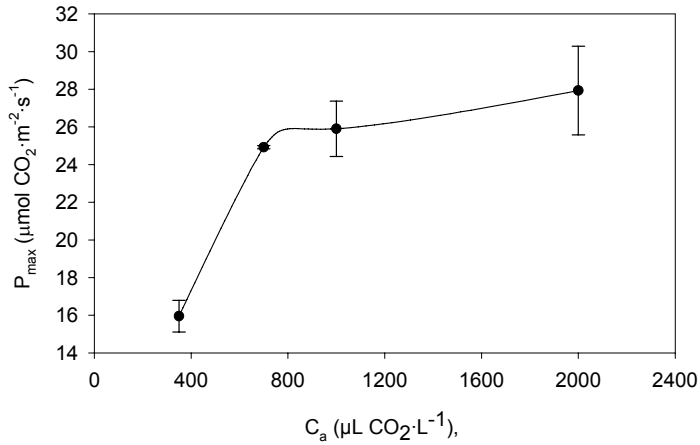

Figure 6.15 P_{max} estimate for lettuce at different CO_2 levels

6.3.3 CANOPY PHOTOSYNTHETIC MODEL

6.3.3.1 EMPIRICAL HARVEST PARAMETERS AND LEAF LIGHT ESTIMATES

Some of the beet and lettuce empirical data obtained in batch and staggered cultures are used as input variables for the full canopy photosynthetic model. Before presenting Table 6.7 and Table 6.8, where beet and lettuce input values for the model are summarized, a brief description of the parameters is presented:

- C_a (µL $CO_2 \cdot L^{-1}$): CO_2 concentration
- α (µmol $CO_2 \cdot$µmol^{-1} PAR): Quantum yield is calculated as the mean of α values at different CO_2 levels, since it was concluded that this parameters is independent of CO_2 concentration.
- P_{max} (µmol $CO_2 \cdot m^{-2} \cdot s^{-1}$): Maximum gross photosynthetic rate
- R_d (µmol $CO_2 \cdot m^{-2} \cdot s^{-1}$): Dark respiration rate is calculated as the mean of R_d values at different CO_2 levels, since R_d is independent of CO_2 concentration.
- LAI_o (%): Initial Leaf Area Index corresponds to the initial total canopy leaf area (m^2) over production area (m^2)
- LAI (%): Leaf Area Index is the total canopy leaf area (m^2) over production area (m^2)
- Lh_{plant} (% dwb): Plant Leaf Content at harvest
- SLA ($cm^2 \cdot g^{-1}$ dw plant^{-1}): Specific Leaf Area
- Ch_{leaf} (% dwb): Carbon content of leaves harvested

For BS2 the leaf light response was performed only at CO_2 levels of 350, 700, 1000 and 1300 µL $CO_2 \cdot L^{-1}$. As no significant differences has been found among ages and among CO_2 levels, α and R_d has been averaged over all ages and CO_2 concentrations, whereas P_{max} is the averaged value over all ages only at 1000 µL $CO_2 \cdot L^{-1}$.

For LS1 and LS2 the leaf light response was carried out only at CO_2 of 1000 ppm. Because no influence of age on parameters was identified, α, P_{max} and R_d have been averaged over all age classes.

Table 6.7 Beet parameters for Thornley model. Mean values ± 95% confidence interval

Variable	Units	BB1	BB2	BB3	BS1	BS2
C_a	µL $CO_2 \cdot L^{-1}$	1000	1000	1000	1000	1000
α	µmol $CO_2 \cdot \mu mol^{-1}$ PAR	NA	0.16±0.03	NA	NA	0.08±0.01
P_{max}	µmol $CO_2 \cdot m^{-2} \cdot s^{-1}$	NA	33.36±3.26	NA	NA	48.37±9.15
R_d	µmol $CO_2 \cdot m^{-2} \cdot s^{-1}$	NA	5.85±1.16	NA	NA	3.44±1.33
LAI_o	%	NA	0.06±0.01	0.041±0.005	0.068±0.016	0.043±0.019
LAI	%	3.3±0.9	1.81±0.18	2.74±0.4	1.54±0.11	3.03±0.29
Lh_{plant}	%	48.7±1.6	54.8±1.7	42.6±1.4	30.5±0.9	39.2±1.33
SLA	$cm^2 \cdot g^{-1}$ dw $plant^{-1}$	84±9	85±17	83±5	92±15	96±4
Ch_{leaf}	%	35.40±1.14	35.20±0.75	36.23±0.62	38.45±0.87	35.53±1.32

Table 6.8 Lettuce parameters for Thornley model. Mean values ± 95% confidence interval

Variable	Units	LB1	LB2	LB3	LS1	LS2
Ca	µL $CO_2 \cdot L^{-1}$	1000	1000	1000	1000	1000
α	µmol $CO_2 \cdot \mu mol^{-1}$ PAR	NA	0.17±0.03	0.17±0.01	0.13±0.01	0.11±0.01
P_{max}	µmol $CO_2 \cdot m^{-2} \cdot s^{-1}$	NA	21.09±3.89	26.43±2,65	27.63±4.67	25.76±5.93
R_d	µmol $CO_2 \cdot m^{-2} \cdot s^{-1}$	NA	3.16±0.53	2.54±0.93	2.35±0.43	0.62±0.51
LAI_o	%	0.079	0.139±0.014	0.043±0.009	0.065±0.031	0.046±0.02
LAI	%	7.79±1.07	9.02±0.49	9.40±0.44	5.11±0.3	6.48±0.4
Lh_{plant}	%	84.4±0.4	75.2±0.5	62.6±0.7	62.04±0.7	62.58±2.7
SLA	$cm^2 \cdot g^{-1}$ dw $plant^{-1}$	227±25	219±12	250±12	205±4	289±23
Ch_{leaf}	%	38.10±0.99	39.40±1.24	38.03±0.87	40.14±0.63	39.48±1.05

6.3.3.2 FULL CANOPY GROWTH PREDICTION AND VALIDATION

The estimates of leaf quantum yield, leaf dark respiration and maximum leaf photosynthetic rate were applied to the full canopy photosynthesis model presented in [Eq. 6.7]. The statistical package R was used to program the iterative calculations of canopy carbon gain and the model's predictions of biomass at harvest were compared to observed values.

Figure 6.16 depicts the observed and model predicted canopy harvest for each of the batch experiments.

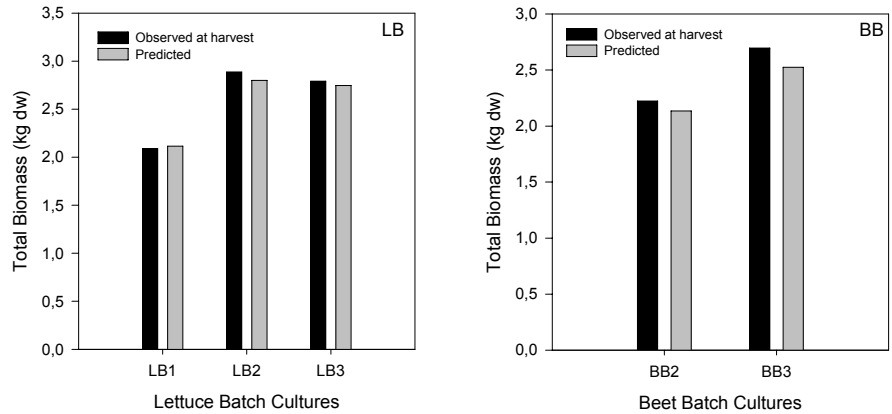

Figure 6.16 Observed and model predicted canopy harvest for each of the batch experiments of lettuce (LB) and beet (BB).

Generally the results are in good agreement and the Thornely model can be deemed an acceptable first approach for predicting biomass gain. It is important to note that direct comparison of yield estimates integrates any errors in model prediction over the crop grow out period. As such, this approach of comparison is justified. As part of future, more investigative efforts of the model's utility in HPC control are required, such as a detailed sensitivity analysis of model performance against initial values derived from the leaf light curve approach, a provision of error propagation and a comparision of model performance against staged culture data.

6.4 CONCLUSIONS

The canopy photosynthetic data corresponding to the beet and lettuce cultures, presented in the previous chapter is evaluated. In addition, atmospheric evolution of batch and staggered trials is compared to identify the most desirable method of production for a long term operation. Moreover, light photosynthetic curves performed at leaf level are used for estimating light parameters for the canopy model, which is validated against the integrated empirical net carbon exchange rates, expressed as predicted yield.

The main conclusions obtained from this study are:

- The NCER technique is a good alternative for estimating plant growth and dry weight production inside the chamber without using destructive analyses. It is important to have a good calibration of instruments and measurement techniques and leakage rate determination in order to achieve such accurate estimations of biomass from CO_2 data.
- Staggered cultures damp oscillation in gas exchange rates obtained in batch cultures. Therefore, staged cultures are rather preferred for long-term operation, such as the continuous operation of the MELiSSA loop. This choice in type of culture will have implication in the design of HPC for the MPP (Chapter 7).

- The rectangular hyperbola model was suitable in defining the leaf photosynthetic response to light at different CO_2 levels and crop ages.
- No significant differences are observed at each CO_2 level for the quantum yield (α), maximum photosynthetic rate (P_{max}) and dark respiration rate (R_d) among beet and lettuce ages. As a consequence, it may be concluded that α, P_{max} and R_d values remain constant through crop development.
- Using all the parameters estimated from batch and staged cultures for each crop, no significant differences were detected for α and R_d estimated among CO_2 levels. In contrast, P_{max} depends significantly on CO_2 levels.
- The full canopy NCER model adequately predicted biomass accumulation for the batch cultures of beet and lettuce. More detailed work will be required to assess the sensitivity of the model to parameter estimates and to assess the performance of the full canopy model in staged cultures. It is concluded that the Thornley model coupled with direct estimation of the quantum yield, dark respiration and maximum photosynthetic rate from leaf light curve studies is an appropriate first step in the development of an HPC control law for managing gas exchange.

Unit III

Photosynthetic Compartments Integration

Chapter **7**

Detailed design of the higher plant chamber for the MELiSSA Pilot Plant (MPP)

Chapter **8**

Integration of the photosynthetic compartments within the MPP: Mass balance analysis

Chapter 7

DETAILED DESIGN OF THE HIGHER PLANT CHAMBER FOR THE MELiSSA PILOT PLANT

7.1 INTRODUCTION

The integration of the Higher Plant Chamber (HPC) into the selected MELiSSA Pilot Plant (MPP) facility, located at Universitat Autònoma de Barcelona (UAB), is one of the key next steps to achieve the closure of the MELiSSA loop and to prove the viability of the MELiSSA concept at terrestrial level. Therefore, an immediate goal is the design and construction of an HPC prototype capable of operating in connection with the other MELiSSA compartments and also in autonomous mode.

The aim of this chapter is to describe the design of this HPC prototype. Initially, the HPC sizing is done using the empirical productivity data presented in Chapter 5 and taking into account several constraints and requirements decided within the MELiSSA consortium.

Afterwards, the main functional areas of the HPC prototype are identified in the selected basic configuration. The basic design section includes a brief discussion about the construction materials and the location of the HPC prototype at the MPP, considering its dimensions.

The design of the chamber is described in detail for each of the main functional systems, which include lighting, liquid, gas and access systems. Each section begins with a description of the subsystem, indicating the hardware involved and the method of operation. The associated control loops are explained and the corresponding instrumentation and signals are depicted schematically.

Finally, a functional description of the HPC prototype is included for each of the two possible operation modes: autonomously or interconnected to the rest of the MELiSSA compartments.

7.2 HPC SIZING

The HPC sizing was based on a previous study defining the crop growing area necessary to satisfy dietary requirements of the crew. As mentioned in the general introduction, initially, an optimized menu was designed to supply the dietary requirements of a 6 member crew for a 10 day menu cycle (Waters *et al.*, 2002). A list of 25 crops, suitable to meet the dietary requirements of the crew, while offering some variety, were selected for their nutritional values, adaptability to closed environment culture, processing requirements, crop yield and psychological value. From this study, it was estimated that in order to feed six crew members over a 10 day menu cycle, about 67 kg of dry edible biomass is required, equating to 1.1 kg of dry edible biomass per person per day.

The data obtained in beet and lettuce trials (Chapter 5) have been used to work in the design of the HPC for the MPP, taking into account the main guidelines defined as:

- Only three plants from the complete menu would be initially considered for production trials within the MPP. The selected species - wheat (*Triticum aestivum* L.), lettuce (*Lactuca sativa* L. cv. Grand Rapids) and beet (*Beta vulgaris* cv. Detroit Medium Red) - are representatives of plants with a predominant nutritional value in seeds, leaves and hypocotyls respectively.
- Each crop would be grown in separate chambers if their unique culture requirements would not allow for integrated production.
- Biomass productivity among plant chambers should provide 20% of the daily crew diet of one person. Thus, considering that the optimized menu determined the value of 1.1 kg dw·person^{-1}·d^{-1} as the daily requirement of food, biomass production in the chamber should achieve 222.3 g dw edible·d^{-1}.

Beet and lettuce empirical harvest data used for the sizing correspond to results obtained in batch and staggered cultures of each crop presented in Chapter 5. Total productivity averaged among batch and staged cultures was 15.31 g dw total·m^{-2}·d^{-1} for beet and 13.85 g dw total·m^{-2}·d^{-1} for lettuce, with a mean harvest index of 89% and 72% respectively. Wheat total productivity (50 g dw total·m^{-2}·d^{-1}) and harvest index (40%) used for the HPC sizing are the averaged values of several tests performed in NASA's Biomass Production Chamber (BPC). In

these cultures, wheat was grown during 79 days under a photosynthetic photon flux of 115 mol PAR·m^{-2}·d^{-1}, a photoperiod ranging from 20 to 24 h light day^{-1} and an air temperature of 20ºC (Hanford, 2006).

Under the assumption of providing 222 g dw edible·d^{-1} with wheat, lettuce and beet, several scenarios with different crop distributions may be considered.

First, an even distribution of produced edible biomass among three chambers can be assumed. Each chamber is devoted to each crop and should produce 74 g dw edible·d^{-1}. Table 7.1 shows the production areas required to meet this biomass demand as calculated from total productivity and harvest index values of each crop. Total and inedible biomass produced is also calculated. Results indicate that if an equal edible distribution is desired, the chambers' growing areas should be 3.7 m^2 for wheat, 7.4 m^2 for lettuce and 5.4 m^2 for beet.

Table 7.1 HPC sizing with even distribution of edible biomass of wheat lettuce and beet.
(1) Assumption of even edible distribution.
(2) Empirical data. Beet and lettuce values correspond to results presented in Chapter 5. Wheat values are derived from tests performed in NASA's BPC (Hanford, 2006).
(3) Calculated values.

Parameter	Wheat	Lettuce	Beet	Total
(1)Edible Production (g dw edible·d^{-1})	74	74	74	222
(2)Harvest Index (g dw edible·g^{-1} dw total)	0.40	0.72	0.89	-
(3)Total Production (g dw total·d^{-1})	185.0	100.0	83.1	370.9
(3)Inedible Production (g dw inedible·d^{-1})	111.0	28.8	9.1	148.9
(2)Total Productivity (g dw total·m^{-2}·d^{-1})	50.0	13.9	15.3	-
(3)Production Area (m^2)	3.7	7.4	5.4	16.6

However, from the economical point of view it is more advantageous to build three identical chambers than three different ones. Consequently, the assumption of even growing area distribution is evaluated in Table 7.2.

Table 7.2 HPC sizing with even production area distribution for wheat, lettuce and wheat.
(1) Assumption of even area distribution.
(2) Empirical data. Beet and lettuce values correspond to results presented in Chapter 5. Wheat values are derived from tests performed in NASA's BPC (Hanford, 2006).
(3) Calculated values

Parameter	Wheat	Lettuce	Beet	Total
(1)Production Area (m^2)	5.1	5.1	5.1	15.3
(2)Total Productivity (g dw total·m^{-2}·d^{-1})	50.0	13.9	15.3	-
(3)Total Production (g dw total·d^{-1})	255.0	70.6	78.1	403.7
(2)Harvest Index (g dw edible·g^{-1} dw total)	0.40	0.72	0.89	-
(3)Edible Production (g dw edible·d^{-1})	102	50.9	69.5	222.3
(3)Inedible Production (g dw inedible·d^{-1})	153.0	19.8	8.6	181.4

According to results obtained, three chambers of 5 m^2 each one devoted to one crop would provide the target edible biomass production. Analyzing these different approaches, it was concluded that 3 HPC prototype with 5 m^2 each one would be constructed.

7.3 HPC BASIC DESIGN

Several factors have to be considered for the HPC design. On one hand, a determining parameter for the HPC design is the operational mode (batch or staged) selected for biomass production. In the specific case of the MELiSSA loop, the continuous operation of the different compartments requires a periodic production of plant biomass as obtained with staggered cultures. Unlike in batch cultures, in staggered trials plant biomass is produced in a semi-continuous mode at the same periodic intervals as sowing. In addition to this, staggered cultures dampen oscillations in gas exchange rates observed in batch cultures, as shown in Chapter 6. Such an atmospheric stabilization is essential for long term dynamic operation of the MELiSSA loop, since it not only provides a more uniform exchange of CO_2 and O_2 with the other compartments, but also reduces the size of storage buffers required (Wheeler, 1996). Because of the advantages of the staggered cultures, this would be the operational mode selected for plant biomass production.

On the other hand, the plant chamber has to guarantee gas closure of the MELiSSA loop. Therefore, any gas exchange between the exterior and the plant growing area must not take place, even during harvest and sowing.

After considering different chamber designs, it was decided that an elongated chamber would fulfill the above mentioned requirements. In such a configuration, seeds can be transferred periodically at one chamber end, while mature plants can be harvested simultaneously at the opposite chamber end. The gas environment isolation during sowing and harvest is ensured with two air-locks located at each end of the chamber. A depiction of the HPC designed for its integration into the MPP is shown in Figure 7.1 and Figure 7.2.

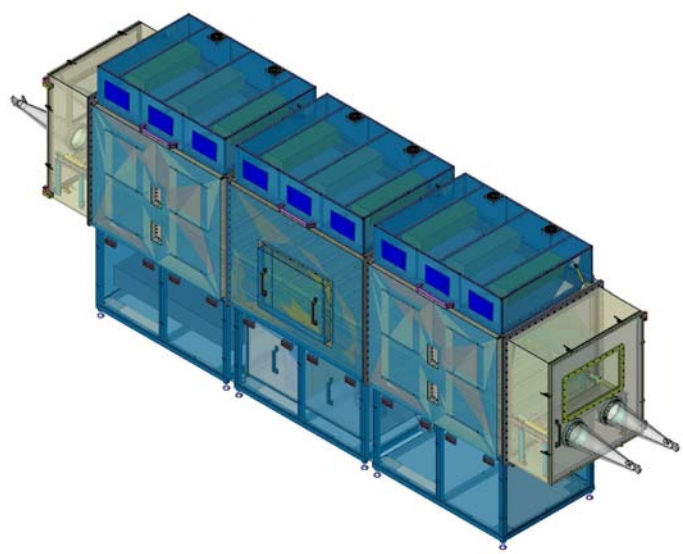

Figure 7.1 Diagrammatic representation of the higher plant chamber for integration into the MPP. Diagram provided by Angstrom Engineering (Cambridge, ON, CA). The chamber is modular in design with three growing modules and two air locks.

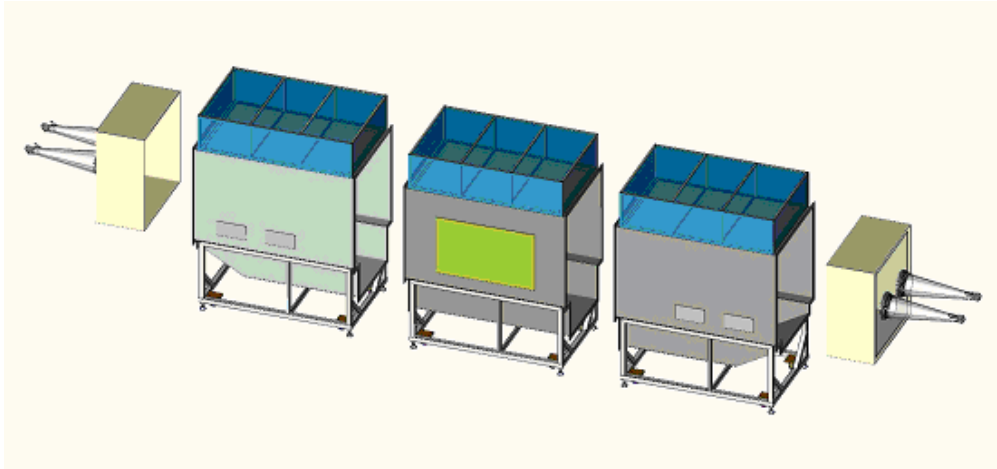

Figure 7.2 Modular design of HPC prototype drawn by Angstrom Engineering Inc. (Cambridge, ON, CA)

The design description of the HPC prototype is based on 5 main functional areas. These five subsystems of the HPC correspond to the lighting system (A100), the liquid system (A200), the air handling volume or gas system (A300), the chamber access areas (A400) and the crop growing volume (A500). Figure 7.3 shows the schematic distribution of the areas within the HPC.

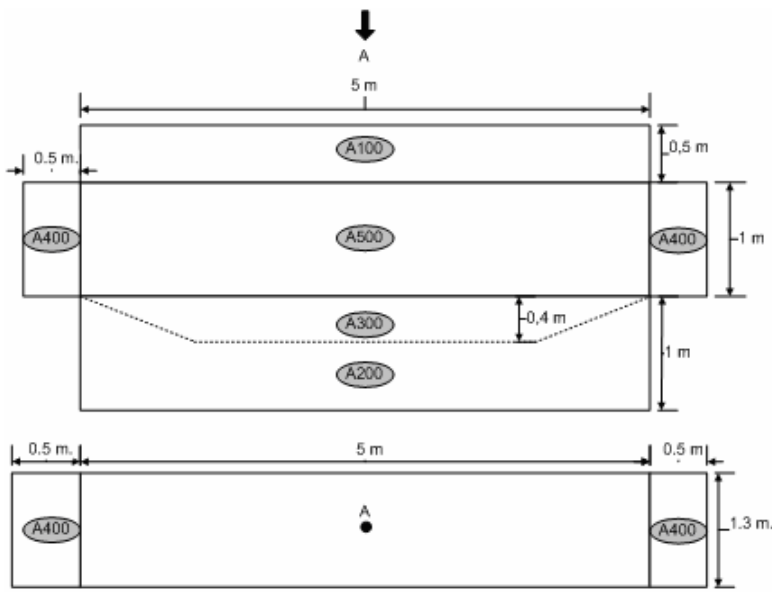

Figure 7.3 Schematic distribution of the HPC functional areas: lighting area (A100), liquid system (A200), air handling system (A300), access areas (A400) and plant growing areas (A500)(side and top view).

First, the lighting system (A100) corresponds to the lamps and the associated equipment situated in the top part of the chamber above the growing area.

Secondly, the liquid system (A200) includes all the solution tanks (such as nutrients, acid/base solutions and condensed water), pumps, plumbing and associated instrumentation required for crop cultures. Such hardware equipment would be situated in an isolated area

below the growing area for improving space utilization in the MPP and decreasing the air volume to be controlled inside the HPC.

The gas system (A300) comprises all hardware required for atmospheric control and for air handling. This area exchanges air with the growing area (A500), but both are kept isolated from the exterior.

The access area (A400) refers to air-locks located at each of HPC ends. One air lock would be used in the seeding procedure and the other in harvesting the mature plants without affecting the atmospheric conditions. As mentioned, this configuration allows for a staged culture strategy, while maintaining gas loop closure.

Finally, the growing area (A500) concerns the plant cultivation area.

7.3.1 MATERIALS

Several studies have determined the effect of plant chamber materials on plant growth. Batten *et al.* (1995) quantified volatile organic compound (VOCs) emissions by materials in NASA's BPC materials during a lettuce and wheat culture. Although levels toxic to plants where not reached, the authors advised minimizing the use of off gassing materials to avoid VOC accumulation inside the closed chamber (Stutte and Wheeler, 1997).

For the HPC prototype the following materials, which do not emit VOCs toxic to plants are proposed: (i) stainless steel 316 for walls, floors, valves and gas plumbing; (ii) tempered glass for lighting loft roof and windows; (iii) polypropylene for liquid buffer tanks and tubing; (iv) Heresite® - a pure phenolic thermosetting resinous coating- for heat exchanger and motor parts; (v) Viton® - a fluoroelastomer heat resistant – for O-rings and solenoid seats.

7.3.2 PROTOTYPE DIMENSIONS AND LOCATION AT MPP

As concluded in the HPC sizing section, a growing area of 5 m^2 per chamber satisfies the requirements of plant biomass production. The main dimensions of the chamber are therefore determined as reported in Table 7.3.

Table 7.3 HPC prototype main dimensions (L x W x H = Length x Width x Height).

HPC area	Dimensions (m)
Growing Area, A500 (L x W x H)	5 x 1 x1
Air-lock Area, A400 (L x W x H)	0.5 x 1 x1
Lighting Area, A100 (L x W x H)	5 x 1 x 0.5
Air handling envelope for each chamber side (W)	0.05
Chamber insulation with aesthetic covering for each chamber side (W)	0.2
Exterior chamber (L x W x H)	6x1.5x2.5

The laboratory space devoted to the HPCs within the MPP has a footprint area of 12 x 6 m and a height of 4 m. In the final proposed configuration (Figure 7.4, Section 9D), one long side of the chamber is exposed to promote logistical tasks and the other positioned against the

facility wall or an adjacent HPC. These dimensions would allow for a total clearance of 6 m on extremes and of 1.5 m on sides.

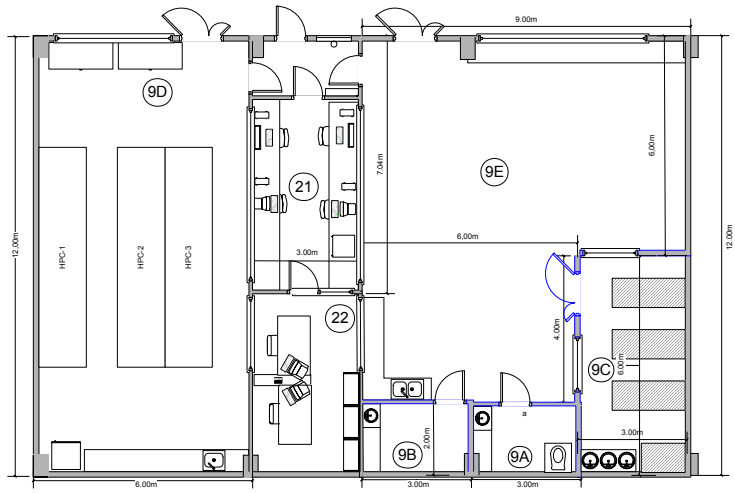

Figure 7.4 Higher Plant Compartment distribution in the MPP located at UAB. The HPC will be housed in Section 9D with a bay for analytical equipment located at the bottom end of the room.

7.4 HPC DETAILED DESIGN

7.4.1 LIGHTING SYSTEM (A100)

Radiation is the sole source of energy for plant growth and development. An important challenge in plant cultures is to provide radiation with an intensity and quality appropriate for ensuring a high efficiency in the photosynthetic process. Therefore, the selection of the artificial lighting system for the HPC is based on a number of factors including (i) emission spectral quality (photosynthetically active radiation, PAR, situated between 400 and 700 nm), (ii) light intensity (photosynthetic photon flux, PPF, expressed as µmol PAR s^{-1} m^{-2}), (iii) photosynthetic efficiency (PPF per unit of input electricity), (iv) rated life, (v) output loss and (vi) characteristics of the reflector.

7.4.1.1 LAMP TYPE SELECTION

A detailed study of different sources of radiation was performed by Masot (2004) for selecting the lamp type for the HPC lighting system. The types of lamps considered comprised incandescent lamps, fluorescent lamps, high intensity discharge lamps (HID) - such as metal halide (MH), high pressure sodium (HPS) and mercury lamps -, light emitting diodes (LEDs) and microwave lamps. After an initial comparison, incandescent, fluorescent and mercury lamps were ruled out for their low photosynthetic efficiency and short rated life compared to microwave, MH and HPS lamps and LEDs. Subsequently, a deeper study of these other options was performed taking into account the specific characteristics of commercial lamps.

A brief discussion of their general advantages and disadvantages is included before determining the final selection.

- **LEDs**

LEDs are small in mass and volume, safe and have a long life (Barta *et al.*, 1992). Several studies evaluated the use of LEDs as a light source for growing plants (Goins *et al.*, 2001; Yorio *et al*., 2001; Goins, 2002; Kim *et al.*, 2004). Although they confirmed that normal plant growth was achieved using only red and blue photons emitted by LEDs (Kim *et al.*, 2004, Yorio *et al.*, 2001), biomass production was higher when using a more conventional lighting, such as HPS (Goins *et al.*, 2001; 2002). In addition to this, when one considers the reduced delivery capacity of LEDs and the inefficiency of their lighting system ballasts, it is recommended to use MH or HPS lamps.

- **Microwave Lamps**

A mercury free, low infrared, microwave lamp using benign sulfur-based fill has achieved conversion efficiencies exceeding HPS lamps. However, the low efficiency of the microwave source, a magnetron, leads to an overall efficiency less than that of high intensity discharge lamps (Langhans *et al.*, 1997). Besides, experimental research with microwave lighting systems within the SEC chambers in UoG, determined that the microwave lamp system will be too unreliable for inclusion in the MPP HPC prototype.

- **Metal Halide (MH) Lamps**

MH radiation is produced by arcing electricity through a tube containing vapors of various metal salts of halogens (such as fluorine, chlorine, bromine and iodine) and mercury. Metal halides are vaporized and produce an emission spectrum almost continuous over the 400 and 700 nm waveband, which resembles the spectrum of daylight. MH lamps are less energy efficient and have a shorter rated life than HPS lamps.

- **High Pressure Sodium (HPS) Lamps**

Radiation from HPS lamps is produced by arcing electricity through high concentrations of sodium vapor and small amount of mercury vapor. This produces an emission concentrated between 550 and 650 nm but low between 400 and 500 nm. Thus, it is recommended to be used in conjunction with MH for satisfying the blue-absorbing pigments of plants (Langhans *et al.*, 1997). The ballast is required to limit and stabilize the current passing through the lamp, greatly reducing the loss of energy in the form of heat. The ballast also prevents overdriving of the lamp, resulting in longer lamp life.

HPS lamps are particularly useful for plant growth because of their high PAR efficiency compared to incandescent lamps. Moreover, HPS lamps have a long rated life and light intensity drops off slowly as the lamp ages.

Goins (2002) studied the influence of different light sources on plant growth, concluding that a higher plant yield and transpiration rate is obtained with HPS lamps than with incandescent or LEDs.

- **Selected lamp type**

After a comparison between several lamp types, it is recommended to use a combination of HPS and MH lamps for the HPC prototype. The selected lamps are PL2000 600 W HPS Remote and PL2000 400 W MH Remote with reflectors Hortilux Maxima Reflector (Figure 7.5), provided by P.L. Lighting System Inc.(ON, CA).

As the LEDs technology improves, it may be possible to remove the conventional lighting systems from the HPC and replace them with panels of LED arrays. This step should be considered only after experience has been gained in operation of the prototype under conventional lighting systems.

Figure 7.5 Selected lamp with attached ballast for HPC prototype.

7.4.1.2 LIGHTING SYSTEM DESCRIPTION

Due to the power availability within the MPP, the lighting system may accommodate, six 600 W HPS fixtures and three 400 W MH lamps. Power requirement for lighting will be therefore up to 5.3 kW per single 5 m^2 chamber, assuming 10% security factor for possible power peaks.

The lighting loft may be covered with a steel box lid with hinges or a lightweight reflective canopy to facilitate access. The full complement of ballasts will be positioned on the upper and outer side of the lamp loft cover. Only the lamps themselves, equipped with reflectors, are suspended externally over the chamber. The absence of the ballast over the crop results in reduced shading and heat load to the chamber. This configuration also minimizes the infrastructure required to support the lighting system over the growing area. The external mounting of the lamps (i) reduces heat load into the growing area, (ii) allows for the incorporation of a lighting loft cooling system and (iii) facilitates lamp and reflector change-out and re-distribution. Fans with appropriate ducting leading to the air cooling system of the MPP are positioned in the loft to prevent lamp over-heating. Air exchange may freely occur in the loft to promote cooling.

An anticipated light intensity distribution inside the HPC, using the P.L. Lighting System lamps PL2000 600 W HPS Remote and PL2000 400 W MH Remote, is shown in Figure 7.6. The calculations of uniformity in the illumination field were conducted using software designed and operated by P.L. Lighting Systems and is specific to their lamp and reflector combination.

Given the light uniformity projections, an average light intensity of 44147 lux inside the HPC is predicted. Considering that conversion factors from lux to PPF(µmol PAR $m^{-2} \cdot s^{-1}$) are 0.0122 for HPS lamps and 0.0141 for MH lamps, the weighted conversion factor from lux to PPF for a combination of 600W HPS and 400W MH may be determined as follows: 60% · 0.0122 + 40% · 0.0141 = 0.01296 (weightings based on the relative power). Therefore, the average light intensity inside the HPC prototype is calculated to be 572 µmol PAR m^{-2} s^{-1}.

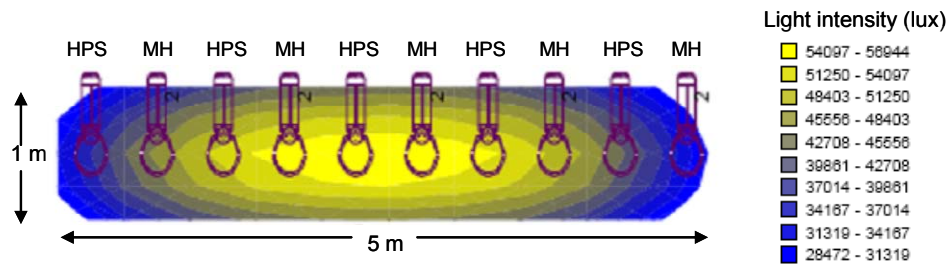

Figure 7.6 HPC light intensity distribution study performed by P.L. Lighting Systems Inc.

7.4.1.3 LIGHTING SYSTEM CONTROL

Control sections for all the different HPC subsystems are structured in the same way. First, the control group identifier and the objective of the control loop are detailed. Secondly, a description of the control loop with a schematic with the hardware and signals involved is included. Finally, a table shows all the instrumentation used in the control loop. Nomenclature used for equipment, control loops and instrumentation is explained in Annexes section (Nomenclature). The control system for the MPP should be based on a Schneider PLC.

- **Light Intensity Control**

Control Group Identifier: A_{IL} LC L1011

Objective: Turn on/off lamps positioned above chamber.

Description of the Control Loop:

Either neutral density screening or variable intensity lamps could be used to control light intensity for the purpose of controlling gas exchange in the HPC prototype. Due to the lack of available commercial dimmable HPS and MH lamps, it is proposed a combination of binary (on/off) control and manually introduced neutral density screening to attenuate light intensity when needed.

In the case of fixed ballasts, which are not dimmable, control of the lighting system intensity is limited. It is proposed that lamps would be wired in 3 control strings designated as strings A through C (Figure 7.7) and that a relay would switch each lamp string on or off, depending on the desired intensity. The chamber will be divided in 3 modules, each one equipped with 2 HPS and 1 MH lamps. One of the lamps strings (A) would connect one HPS lamp from each chamber module, B string would connect the MH from each module and C string would connect the next three HPS lamps. Thus, discrete changes in light intensity results in 33% increments from off to maximum intensity.

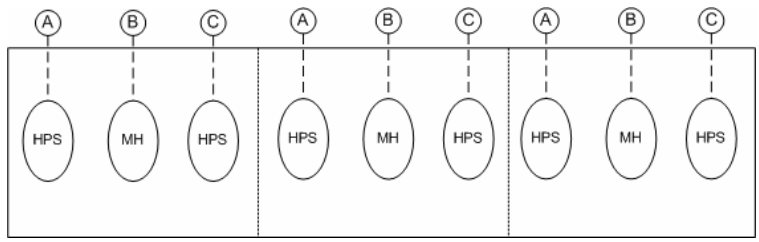

Figure 7.7 Lamp distribution in the lighting loft with the control rings.

The proposed control scenario for the lighting system is depicted diagrammatically in Figure 7.8. Output from PAR sensors ($A_{IL}T$ L1011A-E) positioned in the chamber is directed to the PLC through AI interfaces. If the light intensity is at desired levels, no action is taken by the controller ($A_{IL}IC$ L1011). If illumination levels are too high, additional lamp strings (A to C) may be turned off through outputs to relays XY L1011A-C.

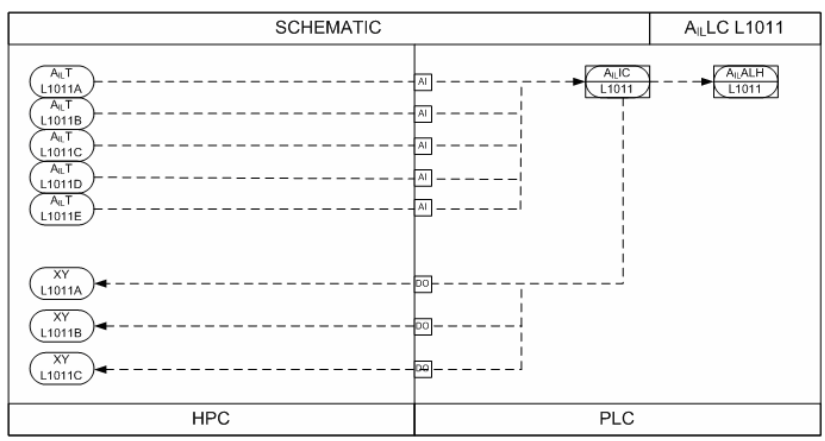

Figure 7.8 Control loop schematic for light intensity.

Instrumentation and Signals:

Instrument	Reference	Signal
PAR Sensors	$A_{IL}T$ L1011A-E	5 x AI
Relays	XY L1011A-C	3 x DO

- **Lighting Loft Temperature Control**

Control Group Identifier: TLC A1001

Objective: Maintain the temperature in the lighting loft at set point values (25ºC during day and 20°C during night).

Description of the Control Loop: An optimal cooling of the lamp loft will be required so that temperature increases in the plant culture area are minimized.

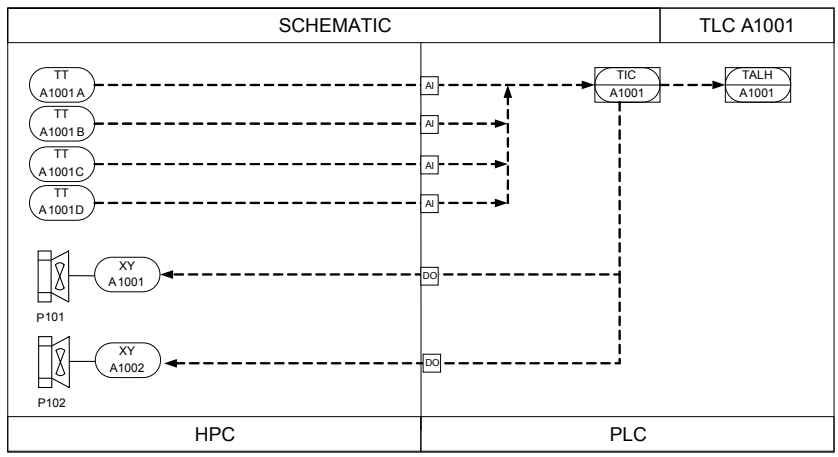

Figure 7.9 Control loop schematic for lighting loft temperature.

For this purpose, four temperature sensors (TT A1001A-D) will be positioned in the lighting loft (A100) to measure air temperature (Figure 7.9). The sensor signal is sent to the controller, which will turn on/off the exchange fans (P101, P102). The air introduced into the loft (A100) comes directly from the air input into the laboratory and circulated using two two-speed fans running at half speed.

Proposed air exchange rates are around 1 $m^3 \cdot s^{-1}$. In most operational scenarios, where light intensity is set at the maximum level, the air circulation will be continuous. An alarm is indicated (TALH A1001) when temperatures in the lighting loft exceed 35 °C.

Instrumentation and Signals:

Instrument	Reference	Signal
Temperature thermocouples	TT A1001A-D	4xAI
2 x Fan Relays	XY A1001, XY A1002	2 x DO

7.4.2 LIQUID SYSTEM (A200)

Water, oxygen, mineral nutrients and support for plants in growth chamber can be supplied by a wide range of root-zone media. Although solid media demand less maintenance, liquid cultures allow for consistent and immediate control of the root-zone environment, while

providing better water and mineral supply. For these reasons, only hydroponic culture types were considered in the selection of irrigation system type for HPC prototype.

After comparison of the main characteristics of several solution systems, including static aerated technique (SAT), nutrient film technique (NFT), intermittent irrigation and root misting technique (RMT), it was proposed to grown plants in the HPC prototype using a NFT (Masot, 2004).

7.4.2.1 LIQUID SYSTEM DESCRIPTION

In a NFT culture, a thin film of nutrient solution flows through the channels, where the plants are located. Nutrient solution circulation is described next in detail, referring to HPC liquid loop schematic depicted in Figure 7.10.

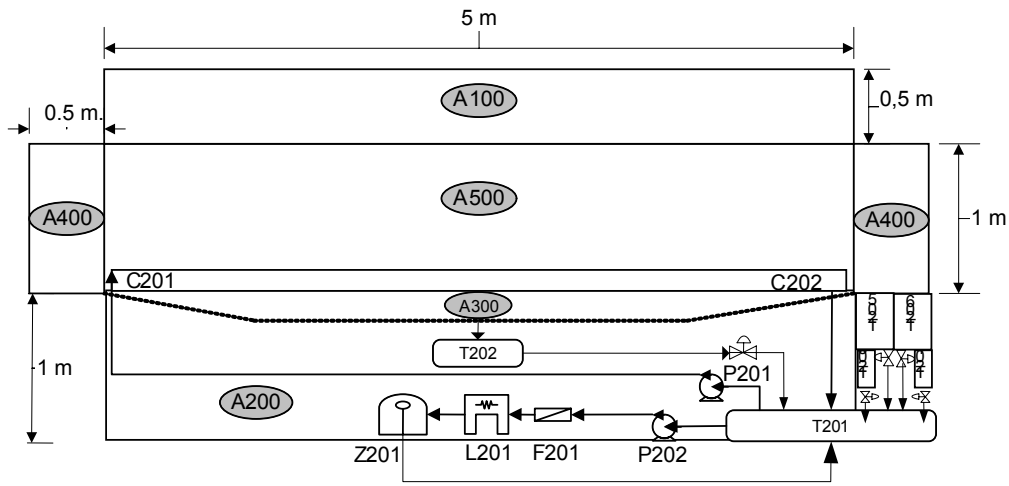

Figure 7.10 Schematics of the HPC liquid sub-system (side view). The following hardware is depicted in the figure: Nutrient solution external buffer tank (T201), nutrient reservoir pump (P201), growing troughs (C201), collecting trough (C202), condensed water tank (T202), acid stock solution tank (T203), base stock solution tank (T204), nutrient stock solution tanks (T205, T206), sterilization loop bypass pump (P202), UV lamp system (L201), liquid filter (F201) and ozonation system (Z201).

The nutrient solution will be pumped (P201) from the 200 L external buffer tank (T201) into the chamber through steel tubing to the head of sloped, one meter long, troughs (C201) spanning the width of the chamber. Nutrient solution delivery at the tray heads will be made using a water cascade system, which consists of a single solution distribution line spanning the 5 m length of the chamber. At distances along this main line, corresponding to the heads of the stainless steel troughs, will be mounted a t-fitting having an open top.

The troughs (C201) will be 0.20 m in width (outer edge) and will rest on a support rack with wheels (conveyer).

The trays are connected on their lateral side and will be moved manually down the length of the chamber during the harvesting and seeding procedures. The direction of tray movement on the conveyer is perpendicular to the direction of solution flow, (i.e. along the long axis of the chamber) as Figure 7.11 shows.

The throughs may accommodate a variety of root media as a substrate for the hydroponics solution. These include Rockwool©, Lecca© (expanded clay particles), silica sand, and glass beads. Gravity assists the return of the solution to the external reservoir via a separate collecting trough (C202) which runs the length of the chamber (5 m). The individual hydroponics trays feed into this common 5 m length collection trough.

A 20 L condensed water tank (T202) is used to collect condensate from the air handling system. When the chiller is activated for chamber temperature control, atmospheric water vapor will condense on the coil and be collected in a trough positioned underneath. Gravity assists the feed of condensed water to the condensate collection tank. This condensate water may then be pumped from the collection tank into the nutrient reservoir or out of the HPC to the compartments of the MELiSSA loop requiring fresh water.

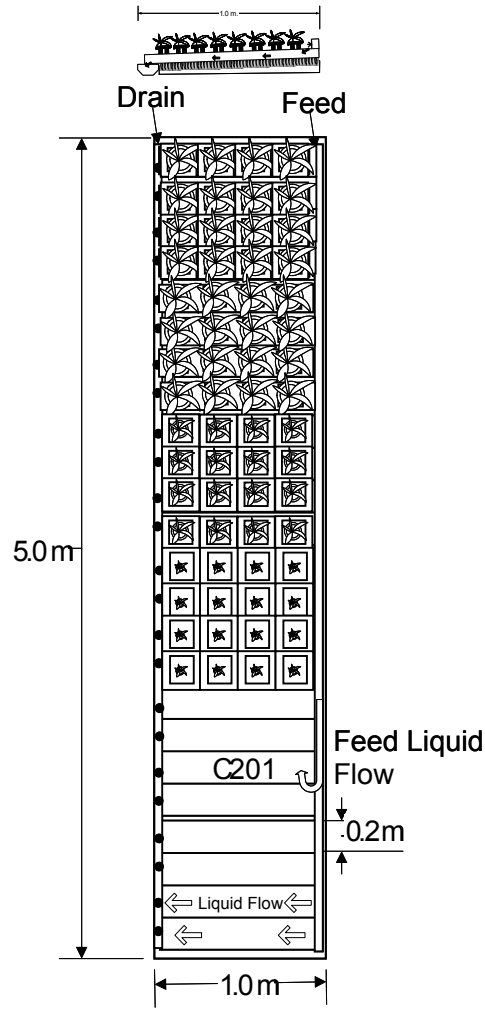

Figure 7.11 Growing trough distribution (frontal and top view) of the HPC prototype.

7.4.2.2 LIQUID SYSTEM CONTROL

- **Nutrient Reservoir Pump Control**

Control Group Identifier: XLC P2011

Objective: Switch on the nutrient reservoir pump (P201).

Description of the Control Loop: In the case of this control loop the main irrigation pump (P201) will be operated continuously.

Two flow sensors, one (FT P2011A) located between the reservoir pump (P201) and the growing trays (C201) and another one (FT P2011B) between the collecting tray (C202) and the input to the reservoir tank will indicate a tray overflow if the difference between input and drain flows is positive. In this case the reservoir pump (P201) will be deactivated.

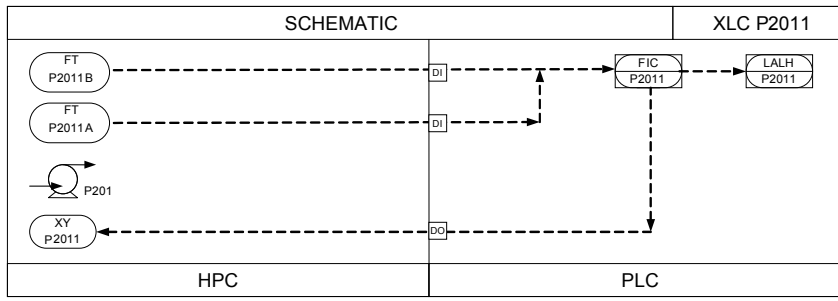

Figure 7.12 Control loop schematic for hydroponics plumbing and pumps.

Instrumentation and Signals:

Instrument	Reference	Signal
Flow sensor	FT P2011A-B	2xDI
Main Irrigation Pump Relay and Motor	XY P2011	DO

- **Nutrient Solution pH control**

Control Group Identifier: A_{pH}LC T2011

Objective: Control the nutrient solution pH in the reservoir to a set point within the range of 4.5 and 6.0.

Description of the Control Loop:

An pH sensor (A_{pH}T T2011) located in the nutrient buffer tank (T201) send the pH value to the controller (A_{pH}IC T2011). When this value deviates from the set point the controller sends a signal to regulate pH. Acid and base stock solutions reside in tanks resting above the nutrient solution reservoir (T203 and T204).

In the case of a solution that is too basic, the controller directs a solenoid valve (A_{pH}V T2011A) located at the bottom part of the acid stock solution tank (T203) and acid solution drains (H_3PO_4) by gravity into the reservoir.

Likewise, if the solution is too acid, solenoid valve (A_{pH}V T2011B) connected to base stock solution tank (T204) regulates base (usually KOH) to drain into the reservoir. Gravity drives fluid flow through the valves and the controller records how much time the valve is open, in order to calculate the amount of acid or basic solution added with a previous calibration of the drain.

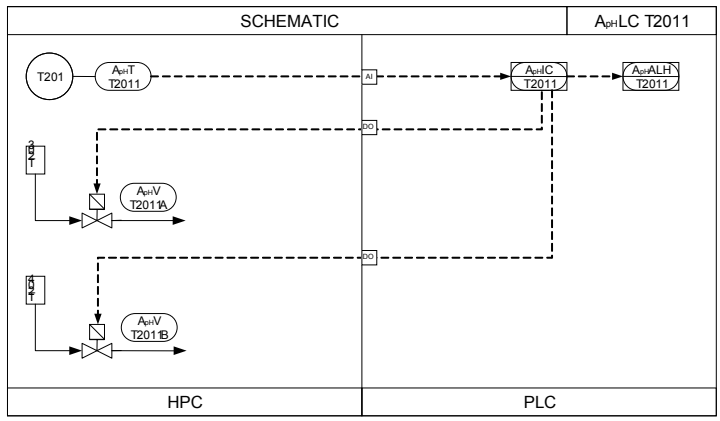

Figure 7.13 Control loop schematic for control of pH in the hydroponics solution.

Instrumentation and Signals:

Instrument	Reference	Signal
pH Sensor	A_{pH}T T2011	AI
Acid Stock solenoid valve	A_{pH}V T2011A	DO
Base Stock solenoid valve	A_{pH}V T2011B	DO

- **Nutrient Solution Electrical Conductivity Control**

The following section describes the control loop required to keep hydroponics solution at electrical conductivity (EC) levels appropriate for plants. The EC setpoint will depend on the solution composition/formulation used.

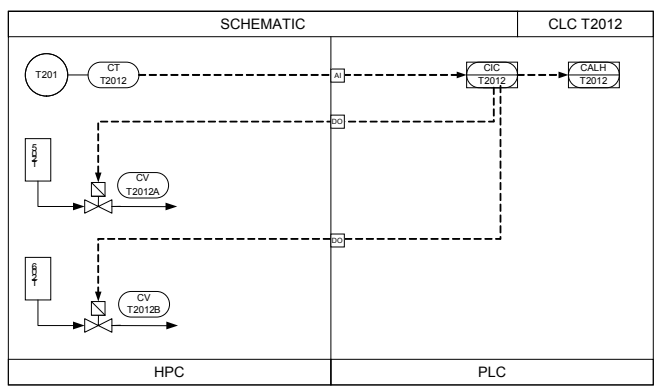

Figure 7.14 Control loop schematic for electrical conductivity control in the hydroponics reservoir.

Control Group Identifier: CLC T2012

Objective: Control of the nutrient solution electrical conductivity with the injection of nutrient stock solutions into the nutrient reservoir.

Description of the Control Loop: Output of the EC sensor (CT T2012) is used to control the solution nutrient concentration through the injection of stock solutions (A and B) when EC

levels fall below demand. The injection of the stock solutions is done in proportion to each other to maintain the desired composition. If EC is outside the acceptable range an alarm (CALH T2012) is indicated. Injections of concentrated stocks from tanks T205 and T206 (A and B) is by gravity assist and is regulated by metered solenoid valves (CV T2012A-B).

Instrumentation and Signals:

Instrument	Reference	Signal
EC Sensor	CT T2012	AI
Stock A solenoid valves	CV T2012A	DO
Stock B solenoid valves	CV T2012B	DO

- **Nutrient Solution and Condensate Water Levels control**

Control Group Identifier: LLC T2013, LLC T2021

Objective: Maintain the volume of nutrient solution inside the buffer tank (T201) between 20 L and 180 L, which correspond to it 10 % and 90% of T201 capacity. Similarly, water volume inside condensate buffer tank (T202) is kept within a range of 10% to 90% of its total volume (20 L).

Description of the Control Loop: Nutrient solution levels in the tanks are measured with float sensors positioned at 10% and 90% of the tanks' volume. The level sensor for the main hydroponics reservoir is identified as LT T2013. The level sensor for the condensate collection reservoir is identified as LT T2021.

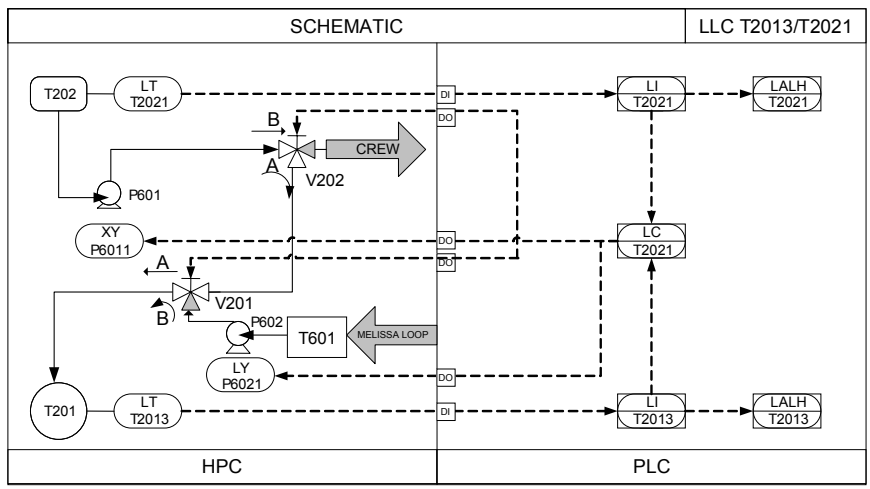

Figure 7.15 Control loop schematic for nutrient solution and condensate water levels.

Under autonomous HPC operation, the condensate collection tank (T202) is used as a source for water replenishment to the nutrient solution reservoir (T201). When the condensate tank volume is greater than 90% capacity or the volume of the nutrient solution reservoir is less 10% capacity (as indicated by output from sensors LT T2013 and/or LT T2021) a metering pump (P601) is activated and water is transferred to the nutrient solution reservoir (V201 and

V202 in position A). The metering pump (P601) is shut off when the volume of condensate water is less than 10% of the tank's capacity (level sensor off) or when the nutrient solution reservoir is at 90% capacity.

When the chamber is operating interconnected the other MELiSSA compartments, water from the loop (or from the MPP de-ionized water supply) is passed to the nutrient solution reservoir using a pump designated as P602 and through valve V201 in position B. The output from the condensate tank is passed to the crew compartment using pump P601 and valve V202 in position B. When the chamber is operating in interconnected mode, the shadowed arrows are in operation as described above. A description of the liquid interfaces between the MPP and the HPC is found in the HPC functional description section .

Instrumentation and Signals:

Instrument	Reference	Signal
Level sensor for reservoir	LT T2013	DI
Level sensor for condensate	LT T2021	DI
Condensate pump relay	XY P6011	DO
Loop to reservoir pump relay	XY P6011	DO
Flow valves	V201, V202	2xDO

- **Ultraviolet and Ozone System for Solution Contaminant Control**

Ultraviolet radiation is to be used as a germicidal agent in the HPC prototype. The dosing of the nutrient solution with wavelengths of UV radiation between 200 and 300 nm is effective at inactivating microorganisms by altering key metabolic enzymes and nucleic acids. Care must be taken to replace the UV lamps on a regular basis since the bulbs tend to degrade, resulting in a lowered dose. Chelating agents also tend to be susceptible to UV destruction and as such, iron, manganese, magnesium and calcium may precipitate from solution. Proper replacement of the precipitated ions and cleaning of residues on the lamp are prescribed. Additionally, an ozone system will be employed on the same by-pass loop to further aid in solution disinfection. The ozone system will target residual concentrations of ozone in solution of between 0 and 2 $mg \cdot L^{-1}$. A feedback control system will be required to maintain ozone concentrations in the hydroponics reservoir at acceptable levels.

Control Group Identifier: AO_3LC T2014

Objective: Turn on sterilization loop bypass pump (P202), ozonation system (Z201) and UV lamp system (L201).

Description of the Control Loop: This is not formally a control loop but is a relay for the on/off operation of a UV situated in the nutrient pump lines.

In the case of the control loop ($A_{O3}LC$ T2014) for the operation of the O_3/UV sterilization system by-pass pump (P202), an ozone sensor ($A_{O3}T$ T2014) will regulate the on/off operation of the by-pass pump and the ozone generator (Z201) if solution ozone levels in the hydroponics reservoir are low.

An alarm is also indicated if ozone levels are low or high (A_{O3}ALH T2014). The controller will also turn on the UV lamp system (L201) for concurrent disinfection.

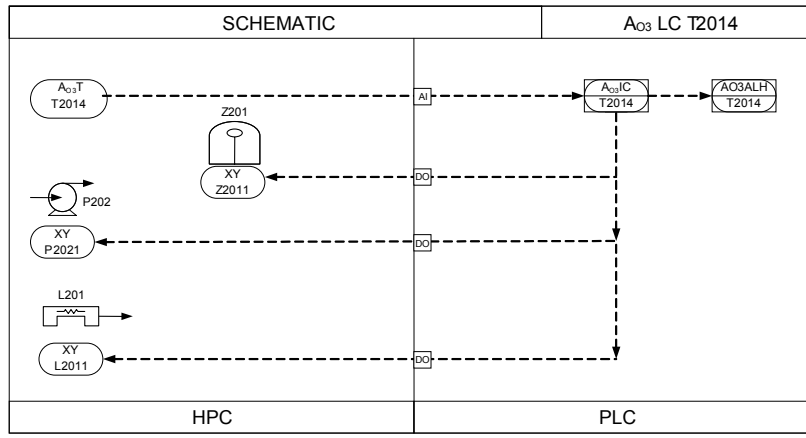

Figure 7.16 Control loop schematic for the ultraviolet and ozonation sterilization system.

Instrumentation and Signals:

Instrument	Reference	Signal
Ozone Sensor	A_{O3}T T2014	AI
Ozone generator relay	XY Z2011	DO
UV lamp relay	XY L2011	DO
Sterilization loop by-pass pump relay	XY P2021	DO

7.4.3 GAS SYSTEM (A300)

In order to supply CO_2 to the plants, to maintain a minimum vertical or horizontal temperature gradient and to evacuate heat from the chamber, an air circulation system is required. Thus, air should be conditioned for temperature and humidity and re-circulated inside the chamber.

7.4.3.1 GAS SYSTEM DESCRIPTION

Forced air movement in a closed plant chamber is essential for enhancing plant canopy photosynthesis. In order to obtain maximal gas exchange rates, the air velocity inside the plant canopy should be above 0.2 $m \cdot s^{-1}$ (Kitaya *et al.*, 2004).

One fan (P301) located in the sub-chamber bay will provide Internal air circulation of one air exchange per minute. Heresite coated fan and fan motor with silicone covered wiring will distribute the air through ducts running the length and height of the chamber walls and into the chamber growing interior from outlets mounted an the upper interior wall. The volume of the chamber considered includes 5 m^3 of growing area (A500) and volume of mechanical plenum (A300), leading to a required air exchange capacity higher than 5 $m^3 \cdot min^{-1}$.

A basic representation of the airflow direction inside the chamber is depicted in Figure 7.17 and in Figure 7.18.

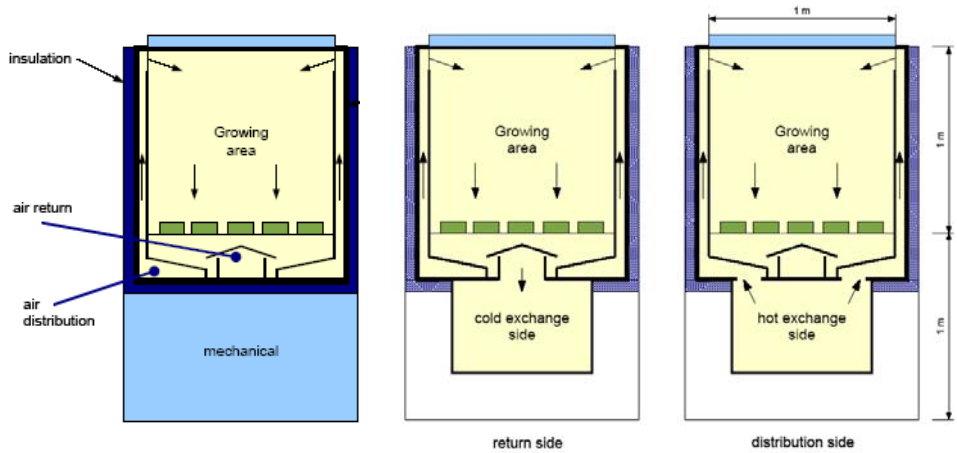

Figure 7.17 Air circulation patterns and air handling system for HPC prototype (cross sectional view).

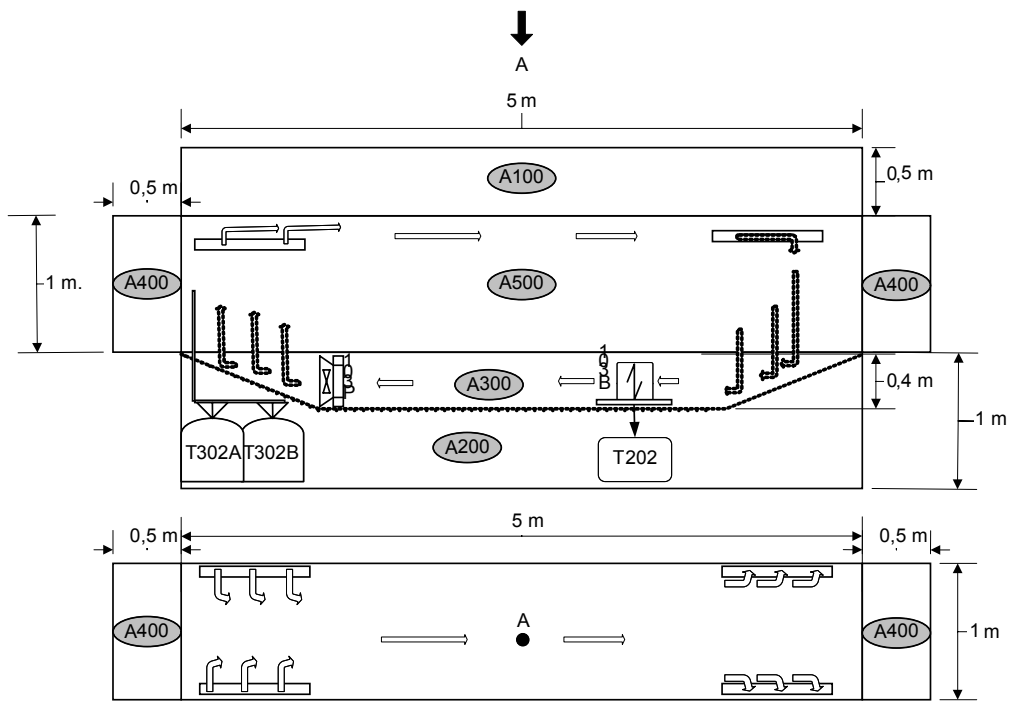

Figure 7.18 Air circulation patterns and air handling system for HPC prototype (side and top view). The following hardware is identified in the diagram: Internal circulation fans (P301, P302), heat exchange coil (B301), condensate water tank (T202), Teflon expansion bag for passive pressure control (T302A-B).

Several samples for analysis are automatically taken from different parts of the chamber. In this way the air composition (O_2, CO_2, N_2, VOCs such as ethylene and other compounds) is measured and controlled.

7.4.3.2 GAS SYSTEM CONTROL

- **Control of Air Handling Circulation fan**

Control Group Identifier: XLC P3011

Objective: Maintain internal air circulation of the plant chamber and minimize internal gradients in atmospheric conditions.

Description of the Control Loop: The internal air circulation fan (P301) is in continuous operation in the chamber and as such, no formal feedback control loop is defined.

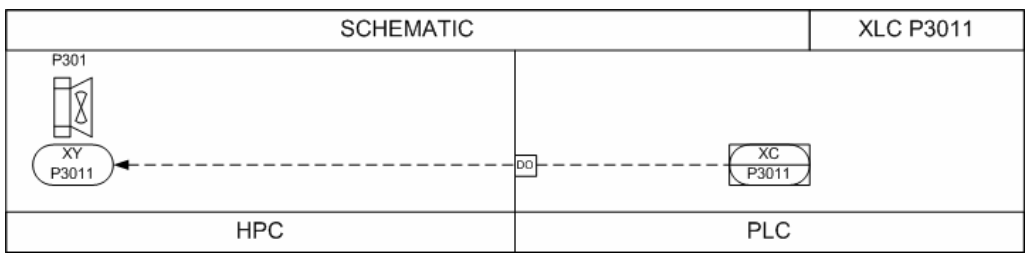

Figure 7.19 Control loop schematic for air circulation fan.

Instrumentation and Signals:

Instrument	Reference	Signal
Fan relays and motor	XY P3011	DO

- **Temperature Control**

Control Group Identifier: TLC A3001

Objective: Maintain internal chamber temperature and humidity at desired set points. The set points for temperature are within the range of 10-30°C.

Description of the Control Loop:

Temperature control in the higher plant chambers is maintained with the use of a heat exchange coil (B301) connected to hot water and chilled water lines. Five temperature sensors positioned in the interior of the chamber growing area are used (TT A3001A-E), 3 measuring the atmosphere and 2 in the hydroponics channels. If chamber temperature is above demanded set points, chilled water (c) is passed through the coil. In the event that the chamber temperature is below set points, hot water (s) is passed through the coil. The entry of hot water or chilled water into the heat exchange coils is regulated by valves (V301 and V302) mounted on each line.

Instrumentation and Signals:

Instrument	Reference	Signal
Temperature sensor	TT A3001A-E	5x AI
Regulating valves	TVA3001A-B	2xAO

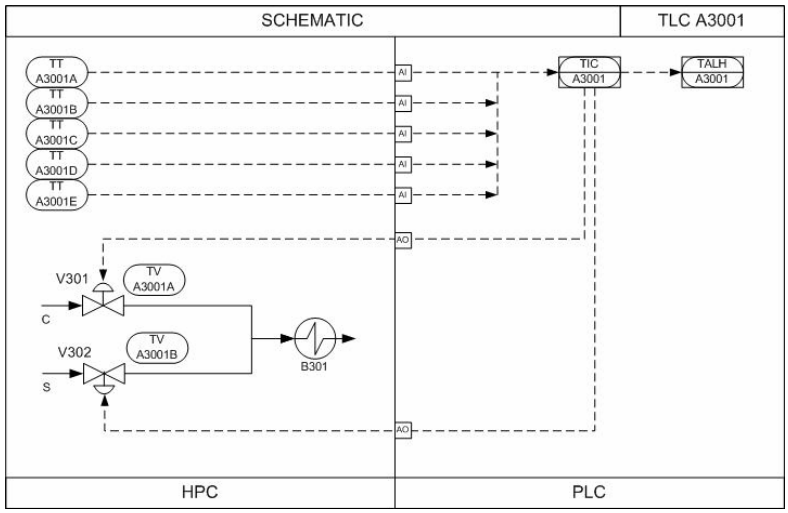

Figure 7.20 Control loop schematic for air temperature control.

- **Humidity Control**

Control Group Identifier: A_HLC A3002

Objective: Maintain internal chamber humidity at desired set points. The set points for humidity are within the range of 50-85% RH. Control may also be achieved using vapor pressure deficit as the input signal.

Description of the Control Loop: Three aspirated humidity sensors (A_HT A3002A-C) are positioned throughout the interior of the chamber. Atmospheric water vapor is condensed at the heat exchange coil (B301) whenever chilled water is passed through the coil by means of regulating V301 valve. Based on experimental experience, it is assumed that transpiration from the developing plant canopy is mostly sufficient in keeping the atmospheric humidity at levels near 70%, so no injection of de-ionized water is foreseen.

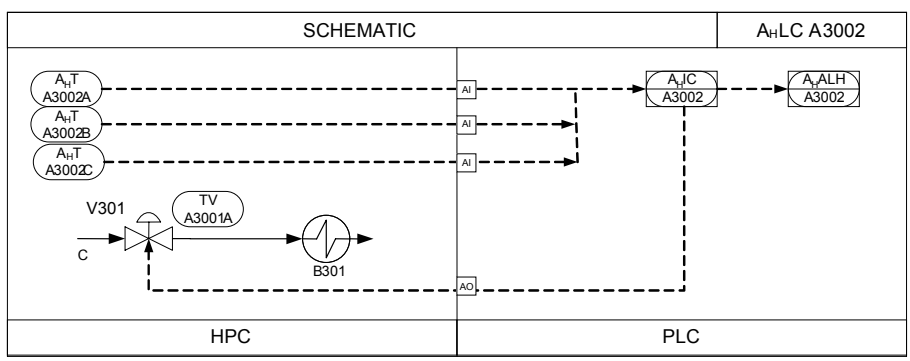

Figure 7.21 Representation of the control loop for chamber humidity control.

Instrumentation and Signals:

Instrument	Reference	Signal
Humidity sensor	A_HT A3002A-C	3x AI

- **CO_2 Control**

Control Group Identifier : A_{CO2}LC A3003

Objective: Maintain CO_2 concentration in the higher plant chamber at demand levels (typically at concentrations of 1000 µL L^{-1}).

Description of the Control Loop: A CO_2 (A_{CO2}T A3003) and O_2 (A_{O2}T A3003) analyzer (Infra-red gas analyzer and paramagnetic analyzer, respectively) are used to determine the atmospheric concentrations of these gases inside the plant chamber and pass their signal to the controller. The controller, in turn, responds by opening a mass flow controller having a programmable/controllable flow rates (FTC A3003A-B). The photosynthetic rate is determined from CO_2 injection rate into the plant chamber during daylight hours. If the CO_2 concentration is above demand levels no action is taken since the plant canopy will remove the excess CO_2 in time during daylight. During dark hours, the CO_2 concentration is not controlled and due to plant respiration CO_2 levels increase.

If the chamber is operating in autonomous mode, the source of the CO_2 is a pressurized bottle (T301) and so a pump is not required on the injection line. In integrated operation CO_2 is provided by the MELiSSA loop via a gas mixing tank (T601) fed by a pump (P603). A second pump (P604) is required to inject CO_2 enriched air into the plant chamber from the mixing tank if it is not under pressure. O_2 concentration in the chamber is not controlled but measured.

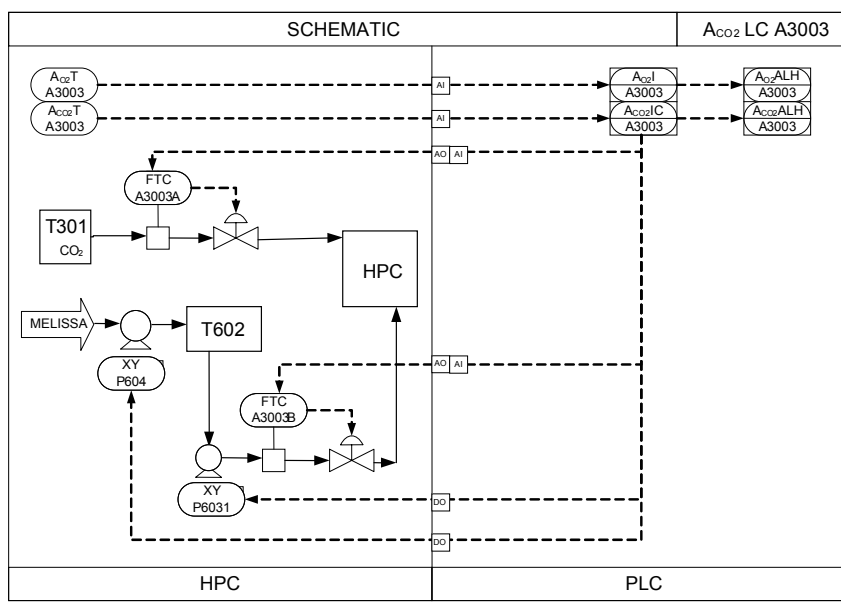

Figure 7.22 Control loop schematic for CO_2 levels.

Instrumentation and Signals:

Instrument	Reference	Signal
CO_2 mass flow/sensor controller (autonomous operation)	FTC A3003A	AI/AO
CO_2 mass flow sensor/controller (operation with the MELiSSA loop)	FTC A3003B	AI/AO
Infrared Gas Analyzer (IRGA) calibrated for CO_2	$A_{CO2}T$ A3003	AI
Paramagnetic Analyzer calibrated for O_2	$A_{O2}T$ A3003	AI
2 Pump relays (operation with the MELiSSA loop)	XY P603, XY P604	2xDO

- **Pressure Control**

Pressure control in the chamber is passive. Two Teflon expansion bags are required. These bladders (T302A-B) will expand and contract with changing chamber volumes precipitated by programmed diurnal temperature fluctuations. The expansion bags are connected to the interior chamber volume via a manifold.

Additionally, to prevent air accumulation in the headspace of the hydroponics reservoir, associated with growing tray drainage, a pressure equilibration line must be connected to the chamber interior.

7.4.4 CHAMBER ACCESS SYSTEM (A400)

Although the HPC prototype is an isolated environmental controlled chamber, some access doors has to be included to facilitate plant sowing and harvesting, chamber cleaning, diseased plant removal and other logistical tasks.

7.4.4.1 CHAMBER ACCESS SYSTEM DESCRIPTION

Access to the chamber growing area is gained through airlocks positioned at both chamber ends and hinged doors positioned along the length of exposed side on the chamber. The airlocks are designed to reduce atmospheric leakage or cross contamination between the chamber interior and exterior during seeding and harvesting procedures.

On the interior side of the airlock is proposed a Teflon coated fabric door (O402A-B). The door is manually opened or closed with glove box access, once the exterior air-lock door (O401A-B) is closed. The steps to be taken in the seeding and harvesting procedure are outlined in the section below, including a description of a manual procedure involving the purge of the air lock with nitrogen gas or calibrated air. During periodic cleaning of the HPC, the side doors (O403 A-C) may be opened to access the depths of the chamber interior. The exterior and side doors will be opened manually and will be fitted with Viton® gaskets and bolts/wing nuts to ensure a seal against the exterior chamber wall when not in use. The dimension of each side door is proposed to be 0.6x0.6 m, where width does not exceed clearance between chambers within the MPP. The chamber access system is represented in Figure 7.23.

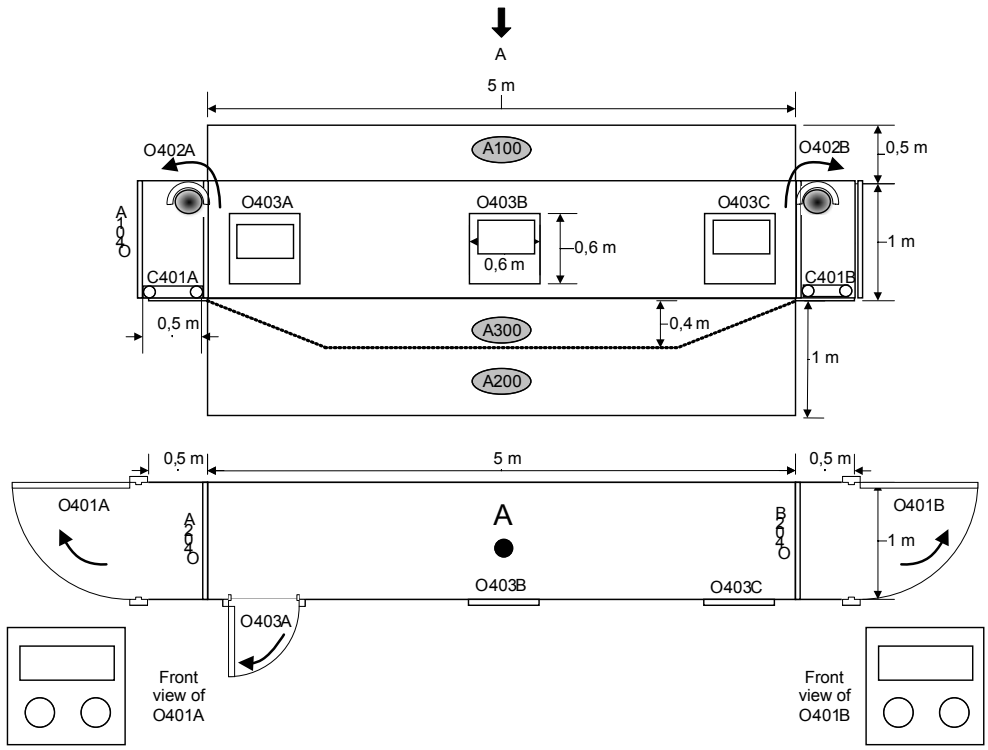

Figure 7.23 Schematic of the HPC access air locks. Parts identified are: exterior air-lock doors (O401A-B), interior air-lock doors (O402A-B), side doors (O403A-C).

The end air locks of the chamber are also fitted with glove boxes allowing access into the air lock interior when its external doors are closed. The glove boxes should be positioned on the air lock access door so that the operator may easily reach across the air lock length (0,5 m).

7.4.4.2 CHAMBER ACCESS SYSTEM CONTROL

- **Air Lock Purge Control**

Control Group Identifier: XLC V4011, XLC V4021, XLC V4031, XLC V4041

Objective: Purge the air locks after the seeding and harvesting procedures.

Description of the Control Loop: Once the exterior air locks doors (A401A and A401B) has been closed, after the sowing or harvesting procedures, a relay is activated (XYV4011) to allow for the injection of calibrated air mixture equal to the chamber interior control values (1000 ppm CO_2, 21% O_2, balance N_2) (T401) through a metering valve (V401 for planting /V402 for harvesting).

Simultaneously, the valve allowing venting of the air lock atmosphere is opened (V403 for planting /V404 for harvesting).

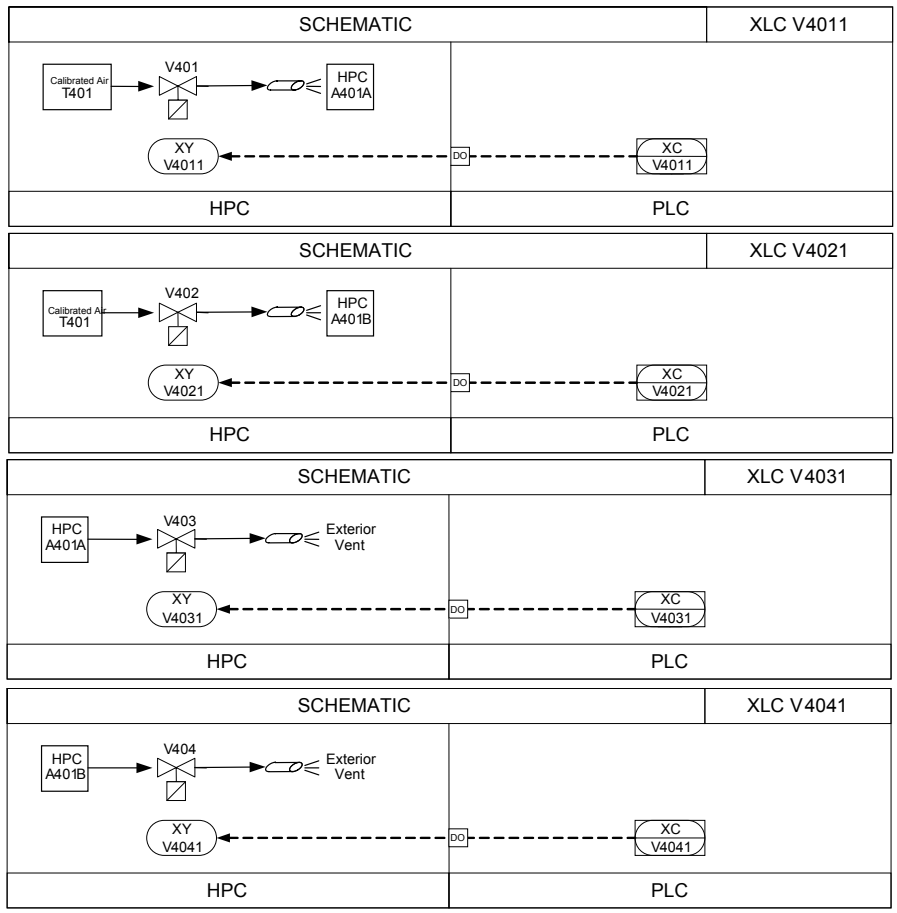

Figure 7.24 Control loop schematic for gas purge of the air locks.

Instrumentation and Signals:

Instrument	Reference	Signal
Valve Relay	XY V4011	DO
Valve Relay	XY V4021	DO
Valve Relay	XY V4031	DO
Valve Relay	XY V4041	DO

7.5 HPC FUNCTIONAL DESCRIPTION

As mentioned in the introduction, the HPC prototype can operate either autonomously or interconnected with the other compartments of the MELiSSA loop.

In this section, the functional description of each HPC subsystem is described for both types of operation. Some of the interfaces with the MELiSSA loop have been already described in the HPC detailed design section.

7.5.1 AUTONOMOUS OPERATION

7.5.1.1 LIGHTING SYSTEM

HPC prototype will be equipped with six 600W HPS and tree 400W MH lamps externally mounted overhead to provide illumination through a 10 mm tempered glass roof. Initially static ballasts will be used, which means that light intensity can not be attenuated through power supply regulation to the ballasts. Therefore, light intensity control will be discrete with binary (on/off) operation of the lamps to achieve desired illumination levels. More details on the lighting system operation area provided in the design section. The HPC lighting system will be hardwired to tri-phasic supply of the MPP at 50Hz and 380V. All other equipment will be wired to the wall supply.

7.5.1.2 LIQUID SYSTEM

Under autonomous operation the nutrient solution used for the hydroponics will be prepared in the laboratory. The nutrient solution used by plants is similar for the three species selected and is a modified half-strength Hoagland with nitrate as the primary N source.

The nutrient solution is pumped from the nutrient reservoir tank (T201) to the head of sloped troughs (C201) spanning the one meter width of the chamber. The solution drains from each tray into a common collection trough (C202) via gravity. The collection trough, 5m in length, then returns the solution back to the nutrient reservoir.

The condition of the solution with respect to pH and electrical conductivity is monitored and adjusted continuously through measured injections of acid, base and/or various nutrient mixes. An Electrical Conductivity (EC) sensor is positioned in the nutrient tank (T201) and the controller regulates the metered gravity feed of concentrated stock to the hydroponics reservoir to meet EC demand levels. Two stock reservoirs (T205 and T206) are used to prevent precipitation of salts. Stock reservoir A contains, most commonly, calcium nitrate and reservoir B contains the balance of solution salts. Since both stock reservoirs are at the same concentration relative to the reservoir, a low EC reading will indicate the equal volume injection from both stock reservoirs. In the same way pH is measured with a pH meter positioned in the tank T201 and is controlled by the metered gravity drain of acid or base (T203 and T204). The nutrient solution tank will have also a dissolved O_2 sensor ($A_{O2}T$ T201). An ultraviolet lamp and an ozone system will be used for contaminant control of the nutrient solution.

7.5.1.3 GAS SYSTEM

Internal air circulation will be provided by a fan with motor, which will distribute the air through ducts running the length and height of the chamber walls and into the chamber growing interior from outlets mounted an the upper interior wall (Figure 7.17).

Air temperature control inside the growing area is maintained with the use of a heat exchange coil (B301) connected to hot water and chilled water lines, supplied from services at

the MPP. Modulated chilled water valves effect dehumidification of the aerial environment, since atmospheric water vapor is condensed at the heat exchange coil. Experimental experience show that plant transpiration is enough for humidification of the air, then injection of water is not envisioned at this moment. Condensate from the chilled water coil will be collected and measured in a condensate collection reservoir (20 L reservoir volume). The condensate water may then be pumped back into the hydroponics reservoir. For a passive pressure control two double sealed Teflon bags, which can expand or contract with variable atmospheric volume associated with temperature fluctuations, will be used.

When the chamber is working in isolation/autonomous mode the air composition is regulated with injections of gases from laboratory lines (CO_2 O_2, N_2, air). In the case of CO_2 management, the computer controller will maintain internal chamber CO_2 concentrations during the day-light hours so that any net carbon gain by the stand through photosynthetic activity is compensated for by injections from an external CO_2 (either from the CO_2 laboratory line or a bottled CO_2). The net carbon exchange rate (NCER) of the developing crop will be determined using a compensation technique, as explained in Chapter 6.

7.5.1.4 SOLID SYSTEM

The following procedure is carried out to move seedlings, after leaf emergence, into the chamber and to harvest mature plants:

1. Ensure interior air lock door seal at both chamber ends.
2. Open the exterior air lock door of sowing side.
3. Place up to two growing troughs with seedlings placed at the proper density into the air lock, with the tray and chamber long dimensions perpendicular to each other.
4. Slide the troughs onto the air lock conveyer.
5. Close the exterior air lock door of sowing side and ensure seal.
6. Purge the air lock volume with nitrogen gas or a calibrated air stream by activating a solenoid valve connected to the gas tank regulator.
7. Open the interior air lock doors.
8. Using the glove box of the sowing air-lock, fasten the newly introduced troughs to those already on the conveyer and using the winch and pulley system, move the connected troughs along the conveyer into the harvest air lock.
9. Using the glove box of the harvest air lock, disconnect the harvested troughs from the conveyer line.
10. Close the interior doors of air locks and ensure seal.
11. Open the exterior door of the harvesting air lock and remove troughs and plants.
12. Prepare plants for tissue analysis (part separation, leaf area, drying and grinding).

7.5.2 INTEGRATED OPERATION

7.5.2.1 LIQUID INTERFACE

Under integrated operation the HPC will receive a liquid solution pumped (P602) from an interface buffer tank (T601) of the MELiSSA loop, as shown in Figure 7.15. This tank will contain a mix of effluents from different MELiSSA compartments, which basically would be the liquid outflow from compartment III and, possibly, the effluent from the crew urine degradation. This nutrient solution, as a mix of outflows from upstream compartments, will be pumped to the trays and returned back to the nutrient solution tank as in the autonomous operation mode. The control of the pH and nutrient composition of the hydroponics tank can be controlled either with this effluent, which is rich in nitrogen and minerals, or with the addition of acid, base or concentrated nutrient solution as described for the operation of the HPC in isolation, as noted above.

Condensate water, stored in T202, is pumped (P601) to MELiSSA compartments requiring fresh potable-condensate water. Therefore, the condensate collection reservoir serves as a direct interface point between the HPC and the MEliSSA loop.

7.5.2.2 GAS INTERFACE

In the case of HPC operation integrated with the rest of the MELiSSA loop, air circulation inside the chamber, air temperature control, humidity control and pressure control remains the same as described for autonomous operation of the HPC prototype. Nonetheless, the gas inlet originates from other MELiSSA compartments instead of the laboratory gas lines and the gas outlet of the HPC is sent to the aerobic compartments. In such an integrated operation, two different gas handling configurations of the MELiSSA gas loop can be additionally considered.

In the first case, the O_2 and CO_2 from the HPC are separated and stored independently in buffer tanks. In this way, mixing of gas compositions among compartments is minimized. This leads to a greater flexibility of atmospheric control in each compartment.

In the second case, it is assumed that there is no gas separation device and so the gas line from other compartment flows directly to the HPC and then from the chamber directly to the consumer compartments (C-III, crew compartment).

Both possible configurations are still under study, but it likely that the first option will be the final selection. Thus, it has been foreseen a connection of the MPP to the HPC through an intermediate gas mixing tank (T602), as depicted in Figure 7.22. This tank serves to concentrate CO_2 outflow from the MELiSSA compartments and feed to the HPC. Gas out-streams from the MPP are pumped to the common interface tank (T602) through a vacuum pump (P603) and a second pump (P604) is used for controlled injections (FTC A3003B) from the mixing tank to the HPC. Additionally, the O_2 enriched atmosphere of the HPC may feed directly to the MPP by metered injection.

7.5.2.3 SOLID INTERFACE

The solid interface between the HPC and the MELiSSA loop is in the form of harvested inedible biomass leading to compartment I (CI) and edible biomass leading to the crew compartment (CV). The same procedure as described for the autonomous HPC operation will be used for transferring seeds into the chamber and harvesting mature plants.

7.6 CONCLUSIONS

The HPC prototype to be integrated into the MPP at UAB has been designed and currently is under construction. The main characteristics of the detailed design presented in this chapter are the following:

- Using plant productivity data (Chapter 5) for the HPC sizing, it was concluded that 3 HPC prototypes with 5 m^2 of growing area each one will be constructed to provide 20% of the daily crew diet with beet, lettuce and wheat.
- The selected configuration is an elongated chamber with a growing area of 5 m long and 1 m wide with two air-locks at each end of the chamber. In such a configuration, seeds can be transferred periodically at one chamber end, while mature plants can be harvested simultaneously at the opposite chamber end, providing a semi-continuous production of plant biomass. The gas environment isolation during sowing and harvest is insured with the air-locks.
- Materials proposed for HPC prototype will not emit VOCs toxic to plants.
- Artificial light to the growing area will be provided with a combination of a 600 W HPS and a 400 W MH lamps. Illumination levels can be modified by switch on or off 3 separate lamp strings, resulting in 33% increment from off to maximum intensity.
- Crop irrigation will be achieved using the hydroponic nutrient film technique. The pH of the nutrient solution is controlled by additions of acid/base stock solutions. Similarly, EC of nutrient solution will be adjusted with nutrient stock additions. Condensate water will be collected in a buffer tank. Levels of the solutions tanks will be also controlled. An ultraviolet lamp and an ozone system will be used for contaminant control of the nutrient solution.
- One fan will provide forced internal air circulation inside the growing area. Temperature, humidity and CO_2 control loops will maintain such environmental conditions at desired levels. A passive control of pressure will be achieved with two expansion bags.
- Access doors will facilitate plant sowing and harvesting, chamber cleaning and other logistical tasks, while ensuring a sealed environment when closed.

Chapter 8

INTEGRATION OF THE PHOTOSYNTHETIC COMPARTMENTS WITHIN THE MPP: MASS BALANCE ANALYSIS

8.1 INTRODUCTION

The MELiSSA Pilot Plant (MPP) is envisioned as a ground based research tool for the demonstration and characterization of a closed loop life support system. The compartments of the loop include a liquefying (CI), photoheterotrophic (CII), nitrifying (CIII), and photosynthetic compartments colonized by *Arthrospira* (CIVa) and higher plants (CIVb or HPC) and a crew compartment as described in the general introduction (Figure 1.2).

Currently, plans are underway to integrate all MELiSSA compartments in the recently constructed MPP laboratory (Albiol *et al*, 2000, Gòdia *et al.*, 2004). Therefore, once the HPC prototype designed in Chapter 7 is incorporated into the MPP, the following step will involve the interconnected operation of the compartments to achieve the closure of the nitrogen, carbon dioxide and oxygen mass balances in the loop.

The purpose of this chapter is to evaluate the impact of the integration of the photosynthetic compartments (CIVa and HPC) using the empirical data gathered from the *Arthrospira* continuous cultures carried out in the pilot plant photobioreactor and from the beet

and lettuce batch and staged trials performed in the sealed environment chambers. Results obtained from the simulations of different scenarios will be used to plan the future interconnected experiments in the MPP loop, to assess the degree of closure that can be achieved and to foresee the range of conditions for which closure of the mass balances can be expected.

Although previous efforts in modelling the MELiSSA loop and in estimating the loop closure were carried out, the calculations where done using data available at that time and mainly focused at full scale rather than MPP scale compartments (Poughon *et al.*, 2000; Gòdia *et al.*, 2001; Creus, 2003).

Therefore, it was decided to develop a static mass balance model for assessing N, CO_2 and O_2 daily mass balances in the MPP for a given set of input variables. Moreover, the model was parameterized using empirical data collected from *Arthrospira* cultures and beet and lettuce production trials presented in the previous chapters (Chapter 3, 5 and 6) and from trials conducted with pilot plant or bench scale MELiSSA compartments. In the following sections, the parameters and stoichiometric relations used for the mass balance model for each compartment and the liquid, biomass and gas fluxes between them are detailed.

8.1.1 CREW COMPARTMENT

In order to sustain the crew compartment (CV), the other MELiSSA compartments operate interconnected to degrade wastes generated by the crew (mainly faeces, urine and CO_2), while providing air regeneration and food production.

As mentioned in the general introduction (Chapter 1), during the initial interconnection of the loop in the MPP, the crew compartment will be occupied by animals to mimic human O_2 consumption and CO_2 production. This compartment is still under a preliminary development phase, and the selection of the species to be used as the model animal is not yet defined. In fact, since the simulations carried out in this work will assess the CO_2 and O_2 balances inside the loop under different scenarios, the results of the amount of gas exchange required to balance the CO_2 and O_2 can be used for selecting the most appropriate type and number of animals to colonize the crew compartment.

Due to the fact that the animals will represent CV only for gas exchange, their wastes will not be introduced into the loop. Instead human faeces and urea will be collected and introduced into CI. Thus, although the animals could eat the edible biomass (EB) generated inside the loop, since their faeces will not be introduced into the loop, the complete closure of the loops is not envisaged at this point. In the mass balance calculations EB is modeled to be sent to the crew but in fact it is taken out from the MPP loop. In order to compensate this output loss, part of human faeces and urine are introduced. Although the described procedure in a way can be regarded as opening the solid component of the loop, it has the advantage of using realistic human waste streams (urine and faeces) instead of animal wastes. Therefore, this scenario has

been preferred as it will be provide very realistic data on the operation of the MELiSSA loop with humans.

As it is assumed that the N added to the loop will come from human urine, the associated CO_2 production during urea and uric acid decomposition is considered to be in the same proportions as in the standard human urine composition detailed next. The average value of the human daily production (HDP) of urine, which contains 16.67 $g \cdot L^{-1}$ urea (CH_4ON_2) and 0.56 $g \cdot L^{-1}$ uric acid ($C_5H_4O_3N_4$), is 1.5 L. Taking into account that stoichiometrically from each mol of urea 2 moles of ammonium and one of CO_2 can be obtained and that each mol of uric acid can generate 4 mols of ammonium and 5 mols of CO_2, the addition of urine into the loop results in an increase in both the N and CO_2 levels (Tortora and Grabowsky, 1992). In the MPP mass balance calculations, urine is first decomposed into ammonium and CO_2 and the corresponding amounts are introduced into the loop and accounted for in the general N and CO_2 balance, instead of considering its addition in the inlet of a particular compartment.

The HDP of faeces is 94 g fresh weight per crew member with a water content of 75% and a total N content of 4.09 % dw. Consequently, the equivalent of one day-unit of human faeces production is introduced into the loop and the corresponding dry weight load to CI would be 23.5 g $dw \cdot d^{-1}$ and 0.96 g $N \cdot d^{-1}$ (Ganong, 1977).

The amounts of faeces and urine introduced into the loop are input variables of the mass balance model and are defined for each of the scenarios studied.

The CO_2 and O_2 balances in the loop are expressed as a percentage of metabolic rates of O_2 human daily consumption (HDC), which is 27.5 mol O_2 d^{-1}, and of CO_2 human daily production (HDP), which is 25.14 mol CO_2 d^{-1} (Hanford, 2006).

Table 8.1 summarizes the daily human metabolic rates for faeces, urine and CO_2 production and O_2 consumption.

Table 8.1 Daily human metabolic rates. HDP=human daily production; HDC=Human daily consumption

Parameter	Value
Faeces HDP (g $fw \cdot d^{-1}$)	94
Faeces HDP (g $dw \cdot d^{-1}$)	23.5
Total N content in faeces (%dw)	4.09
Human daily production of N from faeces (g $N \cdot d^{-1}$)	0.96
Human daily production of N from faeces (mol $N \cdot d^{-1}$)	0.07
Urine human daily production ($L \cdot d^{-1}$)	1.5
Total CO_2 production from urine decomposition ($mol \cdot L^{-1}$)	0.29
Total N production from urine decomposition ($g \cdot L^{-1}$)	7.95
HDP of CO_2 from urine (mol $CO_2 \cdot d^{-1}$)	0.44
HDP of N from urine (g $N \cdot d^{-1}$)	11.93
HDP of N from urine (mol $N \cdot d^{-1}$)	0.85
HDP of N from urine and faeces (g $N \cdot d^{-1}$)	12.89
HDP of N from urine and faeces (mol $N \cdot d^{-1}$)	0.93
HDP of CO_2 from respiration (mol $CO_2 \cdot d^{-1}$)	25.14
HDC of O_2 from respiration (mol $O_2 \cdot d^{-1}$)	27.50

8.1.2 CI: LIQUEFYING COMPARTMENT

The liquefying compartment in the MELiSSA loop is responsible for the anaerobic biodegradation of human faeces, inedible parts of plants and *Arthrospira* and *R. rubrum* biomass not used for human consumption. The amount of each compound sent to CI is an input variable to the mass balance model and is defined for each scenario.

The products of the anaerobic fermentation process, which are mainly volatile fatty acids (VFAs) and N compounds, are fed to the CII colonized by *R. rubrum*. The CO_2 produced in CI is supplied to the photosynthetic compartments CIVa and HPC. Poorly degradable biomass emanating from CI, such as lignin, was assumed to be treated externally to the MPP in a proposed fiber degradation unit.

As the degradation efficiencies achieved in CI have different values depending on the type of organic matter considered, the degree of degradation used in the mass balance model is considered separately for bacterial biomass, higher plants and faeces. Overall, the liquefying compartment (CI) determines the fraction of organic wastes that can be recycled in the loop.

Faeces and plant biomass degradation is calculated assuming the same degradation efficiencies as obtained empirically in CI for organic matter, as summarized in Table 8.2 (Lasseur and Paillé, 2001). Although around 78% of the organic mater (faeces and inedible plant parts) can not be degraded, its content in N is lower (3%) compared to the N content in the input dry matter (5%), due to the degradation of proteins. Thus, globally CI is able to recycle around 50% of the nitrogen found in its input flow. However, this percentage of nitrogen recycling in CI increases when a different input flow composition is considered, as shown in section 8.2 where the results of the different simulation scenarios are presented.

Table 8.2 Composition of the input and output liquid flow of the first compartment (CI).

Compound	Input flow Composition ($g \cdot L^{-1}$)	Output flow composition ($g \cdot L^{-1}$)
Organic dry matter	23	18
Ash	3.7	3
Total nitrogen	1.24	1.25
$N\text{-}NH_3$	0.1	0.7
Total volatile fatty acids	0.85	2.4
Acetic acid	0.354	0.4
Propionic acid	0.218	0.85
Isobutyric acid	0.029	0.24
Butyric acid	0.167	0.26
Isovaleric acid	0.046	0.51
Valeric acid	0.033	0.03
Caproic acid	0.02	0.015
CO_2	0	0.595

The degradation efficiency of bacterial biomass (*R. rubrum* and *Arthrospira*) is assumed to be the same as the empirical degradation efficiency achieved for proteins, which is 65%, in CI (Lasseur and Vieira da Silva, 2005). The nitrogen obtained from the bacterial biomass is calculated stoichiometrically from its elemental composition.

The amount VFAs present in the outflow of CI is calculated based on the amount of carbon present in the biomass load to CI and considering the percentage of carbon used for the formation of each one of the VFAs, which is obtained from empirical data listed in Table 8.2.

8.1.3 CII: PHOTOHETEROTROPHIC COMPARTMENT (*R. RUBRUM*)

The purpose of the second compartment (CII), which is colonized by *R. rubrum*, is to consume the organic acids incoming from the liquefying compartment (CI) while generating bacterial biomass.

In work done previously, stoichiometric equations of *R. rubrum* were obtained by solving the metabolic network built using biochemistry of the *Rhodospirillaceae* (anabolism, catabolism, reserve metabolism and energetic metabolism) and elemental composition of *R. rubrum* ($CH_{1,6}O_{0,36}N_{0,22}S_{0,0036}P_{0,016}$) measured empirically (Lasseur and Fedele, 2000). These stoichiometric conversions listed in Table 8.3 are used to calculate the biomass and CO_2 production in the current mass balance model. Nitrogen uptake is determined based on the nitrogen composition of the *R. rubrum* biomass (0.22 mol N · mol^{-1} *R. rubrum*).

An iterative calculation of the production rate of *R. rubrum* biomass was used to provide starting values for the contribution of biomass made by CII to CI. The amount of *R. rubrum* biomass returned to CI is an input parameter of the mass balance model and is specified for each of the cases simulated.

Table 8.3 Stoichiometric coefficient for *R. rubrum* grown using different carbon substrates.

Volatile fatty acids (VFA)	Stoichiometric coefficients for *R. rubrum*	
	(mol *R. rubrum* ·mol^{-1} VFA)	(mol CO_2 · mol^{-1} VFA)
Acetic acid ($C_2H_4O_2$)	1.855	0.145
Propionic acid ($C_3H_6O_2$)	3.2462	-0.2462
Isobutyric acid ($C_4H_8O_2$)	4.6374	-0.6374
Butyric acid ($C_4H_8O_2$)	4.6374	-0.6374
Isovaleric acid ($C_5H_{10}O_2$)	6.0286	-1.0286
Valeric acid ($C_5H_{10}O_2$)	6.0286	-1.0286
Caproic acid ($C_6H_{12}O_2$)	7.4198	-1.4198

8.1.4 CIII: NITRIFYING COMPARTMENT

The main function of the nitrifying compartment (CIII) is to convert ammonium to nitrate to be used as a N source in the photosynthetic compartments CIVa and HPC. The bacteria selected for this conversion are a co-culture of *Nitrosomonas europaea* and *Nitrobacter winogradskyi* cells, grown in a fixed bed. Due to the slow growth of the immobilized biomass, its contribution to the daily biomass generation in the MPP is considered negligible and was therefore not included in these mass balance calculations.

Empirical values for conversion of NH_4^+ input into NO_3^- obtained in the CIII bioreactor average 98% (Pérez, 2001).

The stoichiometric equations defined for *Nitrosomonas* and *Nitrobacter* determined that for each mol of nitrogen the oxygen consumption for maintenance is 2 mol O_2·mol $^{-1}$ N and the CO_2 uptake for biosynthesis is of 0.32 mol CO_2·mol^{-1} N (Lasseur and Fedele, 2000).

8.1.5 CIVa: *ARTHROSPIRA* PHOTOSYNTHETIC COMPARTMENT

The main task of the photosynthetic compartment CIVa is to generate O_2 and edible biomass (*Arthrospira*) using the CO_2 produced in the other compartments, light as an energy source and nitrate present in the outflow of the nitrifying compartments (CIII).

An important part of the current work (Chapter 3) was devoted to the determination of maximum productivities attained with the pilot plant bioreactor. With this aim, several continuous cultures were carried out using CO_2 gas as carbon source at different dilution rates and illumination levels, which were planned using a Box-Wilson Central Composite Design (CCD).

The highest productivity values obtained in the continuous cultures of *Arthrospira* was 27 mg·L^{-1}·h^{-1} at a dilution rate of 0.044 h^{-1} and a light intensity of 194 W·m^{-2}. Considering that the pilot plant bioreactor has a volume of 77 L, the daily production of *Arthrospira* achieved up to now in the CIVa photobioreactor is 49.8 g·d^{-1}. Table 8.4 summarizes the values of the main parameters obtained in this culture.

For the mass balance model, it is assumed that the *Arthrospira* compartment is operating under conditions defined in Table 8.4 and that the same steady state values for daily biomass production, CO_2 consumption, O_2 production, N consumption are maintained.

Table 8.4 Summary of main parameters values obtained in the continuous culture of *Arthrospira* carried out using the pilot plant photobioreactor where the highest productivity was achieved. More detailed information can be obtained in Chapter 3 where the results of this culture (corresponding to Run 4) are presented and discussed.

Parameter	Values
Dilution rate (h^{-1})	0.044
Light intensity (W·m^{-2})	194
Culture volume (L)	77
DW Biomass concentration (g·L^{-1})	0.62
Biomass productivity (mg·L^{-1}·h^{-1})	27
Daily *Arthrospira* production (g·d^{-1})	49.8
CO_2 volumetric consumption, r_{CO2} (mmol·L^{-1}·h^{-1})	0.50
Daily CO_2 consumption (mol·d^{-1})	0.91
O_2 volumetric production, r_{O2} (mmol·L^{-1}·h^{-1})	1.32
Daily O_2 production (mol·d^{-1})	2.44
N volumetric uptake, r_N (mmol·L^{-1}·h^{-1})	0.28
Daily N consumption (mol·d^{-1})	0.52
Elemental composition	$CH_{1.74}N_{0.196}S_{0.005}$
Nucleic acid content (%)	5

The fraction of *Arthrospira* biomass fed to CI for degradation was calculated from the total amount produced after subtraction of the fraction reserved for human consumption, which is limited to 40 g·d^{-1} due to its nucleic content (5%).

8.1.6 CIVB: HIGHER PLANT COMPARTMENT (HPC)

Similarly to CIVa, the main task of the photosynthetic HPC is to generate O_2 and edible biomass (higher plants) using the CO_2 produced in the rest of compartments, light as an energy source and nitrate present in the outflow of the nitrifying compartment.

The collection of empirical growth, tissue composition and gas exchange data of beet and lettuce is another of the main tasks developed in this work (Chapter 5 and 6). With this objective, three batch cultures and two staged cultures were carried out for each crop in sealed environment chambers (SEC) under controlled conditions. Beet and lettuce data gathered from these empirical trials together with bibliographic values for wheat (McKeehen, 1994; Hanford, 2006) have been used for sizing the HPC to be included in the MPP (Chapter 7). Such data are used in this chapter for the mass balance simulations of the MPP loop to evaluate the impact of integrating up to the 3 HPC prototypes currently under design or construction.

Table 8.5 shows the values of the parameters used for the N, CO_2 and O_2 mass balances for each of the selected crops. Beet and lettuce values are the average of the results obtained in batch and staggered cultures.

Table 8.5 Higher Plant Chamber Data used for the mass balance model.
(1) Lettuce and beet empirical data correspond to the averaged values of the results obtained in the batch and staged cultures presented in Chapter 5.
(2) Wheat data are derived from tests performed in NASA's BPC (McKeehen, 1994; Hanford, 2006)

Parameter	Lettuce (1)	Beet (1)	Wheat(2)
Total plant productivity (g dw $m^{-2}\cdot d^{-1}$)	13.85	15.31	50
Harvest index (g·edible·g^{-1} total)	0.72	0.89	0.40
Total edible productivity (g dw edible $m^{-2}\cdot d^{-1}$)	9.97	13.62	20
Total inedible productivity (g dw edible $m^{-2}\cdot d^{-1}$)	3.88	1.68	30
Edible tissue N content (%)	4.74	4.01	3.57
Inedible tissue N content (%)	4.19	4.20	3.72
Total tissue N content (%)	4.58	4.03	3.66
Nitrogen uptake rate (mol·$m^{-2}\cdot d^{-1}$)	0.048	0.047	0.128
Tissue carbon content (%)	36.72	37.45	42
CO_2 consumption (mol·$m^{-2}\cdot d^{-1}$)	0.42	0.48	1.75
O_2 production (mol·$m^{-2}\cdot d^{-1}$)	0.42	0.48	1.75

Total edible and inedible productivity are calculated based on the total plant productivity and harvest index (HI). For beet and lettuce nitrogen content in edible and inedible tissue is the averaged value of the results obtained in batch and staged cultures presented in Chapter 5 (Table 5.7 for beet and Table 5.11 for lettuce). For wheat the values obtained by McKeehen (1994), as presented in Table 1.11, are assumed. The total tissue N content of each crop has been calculated using the edible and inedible N content and the HI. Nitrogen uptake rate for beet and lettuce was determined from the accumulated N uptake profiles as presented in Table 5.14 and 5.15. Nitrogen consumption of wheat was calculated using the wheat productivity reported by Hanford (2006) and total N tissue content (McKeehen, 1994).

In Chapter 6, it was concluded that the NCER technique was a good alternative for estimating plant growth and DW production and in fact, in Chapter 5, nutrient mass balances demonstrated that carbon tissue content matches with the CO_2 uptake for photosynthesis. For this reason, the CO_2 consumption of each crop was calculated using the total plant productivity value together with the tissue carbon content. The oxygen production is estimated using an approximate photosynthetic quotient (mol $O_2 \cdot mol^{-1}$ CO_2) of 1, as reported by some authors (Waters, 2002; Hanford, 2006).

Edible biomass (EB) from the HPC was assumed to be fed to the crew compartment. In all simulations, 100% of the inedible biomass (IEB) produced by the HPC was assumed to be transferred to CI, while in most of the scenarios EB from the HPC was sent out of the MPP loop, as mentioned in the crew compartment section (8.1.1).

8.2 RESULTS AND DISCUSSION

As determined in the HPC design chapter (Chapter 7), 3 HPC prototypes of 5 m^2 will be constructed in the MPP in order to provide a edible biomass equivalent to 20% of the daily diet of one crew member (222.3 g dw edible $\cdot d^{-1}$), each devoted to the specific culture of three crops (beet, lettuce and wheat).

However, the construction of the 3 HPC prototypes will not be installed in the MPP at the same time. This fact has motivated the evaluation of the degree of closure that can be obtained and to foresee the range of conditions for which closure of the N, CO_2 and O_2 mass balances can be expected considering that initially only one HPC prototype will be incorporated into the MPP (scenarios 1-3). Then, the incorporation of the second HPC prototype is evaluated (scenario 4). Finally the last scenario will consider the installation of all 3 HPC prototypes of 5 m^2 each (scenario 5).

Only one crop per chamber is considered in the beet and lettuce trials presented in this work (Chapter 5 and 6) and in the cultures planned in the final design of the HPC for the MPP (Chapter 7). Under the assumption that only 1 or 2 HPC prototypes are installed in the MPP, it has decided that the HPC growing area of 5 m^2 or 10 m^2 respectively would be occupied by different distributions of beet and lettuce. This will introduce some flexibility in the possible experiments to be carried out when only 1 or 2 HPC prototypes are installed in the MPP. Moreover, previous studies have demonstrated the feasibility of beet and lettuce co-cultures in the same chamber (Masot, 2004; Stasiak *et al.*, 2003). Wheat is not considered in combination with the two other crops, because its photoperiod of 24 hours (or slightly less) limits its co-culture with beet and lettuce, which both have a photoperiod requirement of 16 hours.

Once the 3 HPC prototypes are available, each chamber will be devoted to the culture of a single crop, as designed in Chapter 7. An alternative would be that 10 m^2 are used for beet and lettuce co-cultures in different proportions and that 5 m^2 are devoted for wheat production.

In these simulation studies the area was varied within the range of 0 to 15 m^2 in 5 m^2 increments. The proportion of the total area occupied by beet is user defined while the occupation by lettuce is determined by difference. Only when it is assumed that the 3 HPCs are available (scenario 5), wheat will occupy 5 m^2. The calculated rates of biomass production, CO_2 consumption, O_2 production and N uptake were derived from the areas in production for each crop and the values in Table 8.5. Thus, area production and beet and lettuce distributions are an input variable of the mass balance model and are defined for each evaluated scenario. This section includes the results obtained with the mass balance model for each of the considered scenarios.

8.2.1 SCENARIO 1: ONE HPC PROTOTYPE

In the first scenario, it is assumed that only one of the 3 HPC prototypes has been incorporated to the MPP and that the collector system for human wastes is still not available. Therefore, no human faeces or urine can be sent to the first compartment (CI). Instead, it is simulated to introduce into CI all the inedible and edible biomass (IEB and EB respectively) produced in the loop, which includes *R. rubrum* from CII, *Arthrospira* from CIVa and higher plants from HPC. The HPC growing area of 5 m^2 is occupied by different distributions of beet and lettuce, which are expressed as percentage of beet occupation (%BO of HPC area). As the animals that will colonize the crew compartment have not yet been selected, the CO_2 and O_2 balances are expressed as the percentage of the O_2 HDC and the CO_2 HDP that the loop can sustain. Such information can be then used for selecting the most appropriate species and number of animals to colonize the crew compartment also considering a possible stepwise approach in parallel to the availability of HPC in the MPP. Table 8.6 summarizes the main assumptions of the present scenario.

Table 8.6 Summary of the main conditions assumed for the first scenario (S1).
(1) Total edible and inedible production depends on crop distribution inside the HPC.

Compartment parameters	Value
CII: *R. rubrum*	
Fraction of *R. rubrum* production into CI (%)	100
CIVa: *Arthrospira*	
Arthrospira production ($g \cdot d^{-1}$)	49.80
Fraction of *Arthrospira* production into CI (%)	100
CIVb: HPC	
Number of HPC prototypes in MPP	1
Area for beet and lettuce production (m^2)	5
- Beet occupation (% of the total area)	Variable
- Lettuce occupation (% of the total area)	Variable
Area for wheat production (m^2)	0
Total edible production ($g \cdot d^{-1}$)	50-68 (1)
Fraction of edible production into CI (%)	100
Total inedible production ($g \cdot d^{-1}$)	8-19 (1)
Fraction of inedible production into CI (%)	100
CV: Crew compartment (Human wastes and animals for gas exchange)	
Fraction of HDP of faeces into CI (%)	0
Fraction of HDP of urine into the loop (%)	0

The conditions assumed in this scenario together with the production rates and the stoichiometric relations of each compartment, which are detailed in the description of the mass balance model, are used to determine the net balance of the daily N, CO_2 and O_2 exchange for each compartment.

Table 8.7 shows an example of the net exchange rates calculated at the compartment level considering the assumed conditions of this scenario (Table 8.6) and when only lettuce is inside the chamber (0% BO).

Table 8.7 Mass balance for he MPP compartments considering that (i) all the IEB and EB is sent to CI, (ii) neither human faeces nor urine are introduced into the loop and (iii) lettuce occupies the 5 m^2 growing area of the HPC prototype.

Compartment	Balances ($mol \cdot d^{-1}$)		
	N	CO_2	O_2
CI	0.87	0.65	-
CII	-0.77	-0.83	-
CIII	0.00	-0.03	-0.20
CIVa	-0.52	-0.91	2.44
HPC	-0.24	-2.12	2.12
Total balance	-0.66	-3.25	4.36

Negative and positive values indicate that the compartment is either a consumer or a evolver of the elements considered (N, CO_2 and O_2). The last row of Table 8.7 is the net balance calculated to evaluate the degree of loop closure for each of N, CO_2 and O_2 in this scenario.

The N, CO_2 and O_2 balances of the loop are depicted in Figure 8.1 for different crop distributions inside one HPC prototype.

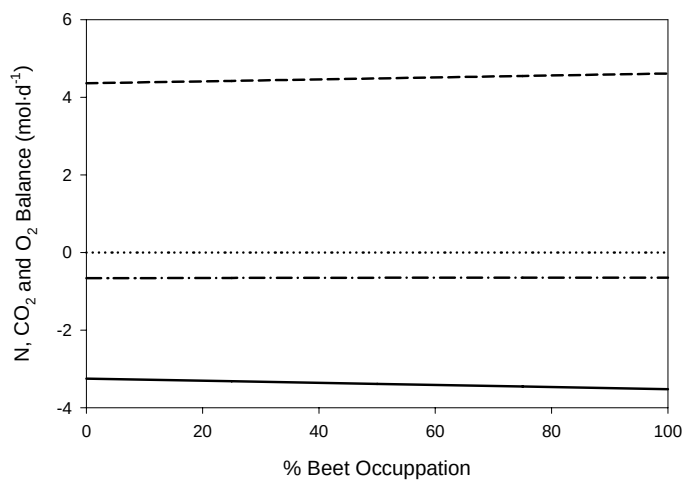

Figure 8.1 N (dashed-dotted line), CO_2 (solid line) and O_2 (dashed line) balances ($mol \cdot d^{-1}$) in the MPP as function of crop distribution (%BO of 5 m^2) for scenario 1. Negative values indicate deficiency, dotted line corresponds to the compensation point (zero) and positive values indicate element surplus in the loop. In this scenario, all the EB and IEB are sent to the CI, neither human faeces nor urine are introduced into the loop (Table 8.6).

The negative values calculated in the N balance indicate that 43% of the N recycled within the loop should be added to fulfill the nitrogen balance. Taking into account that in this scenario, all EB and IEB has been fed to CI, the N deficiency can be attributed to the degradation efficiency of CI. Although in these conditions, CI is able to recycle 57% of the N present in all the biomass (*R. rubrum*, *Arthrospira* and higher plants) introduced, currently, other techniques to increase the degradation efficiency of CI are under consideration (Lasseur *et al.*, 2005). Crop distribution inside the chamber has no significant effect on nitrogen balance, because the N uptake rate of beet (0.047 mol $N \cdot m^{-2} \cdot d^{-1}$) and lettuce (0.048 mol $N \cdot m^{-2} \cdot d^{-1}$) have been found to have similar values.

The surplus of O_2 in the loop inside the chamber indicates that in this scenario, photosynthetic compartments are able to sustain roughly 17% of the O_2 HDC. Moreover, since beet productivity (15.31 $g \cdot m^{-2} \cdot d^{-1}$) and tissue carbon content (37.4%) is higher than lettuce productivity (13.85 $g \cdot m^{-2} \cdot d^{-1}$) and carbon content (36.7%), an increase in beet occupation inside the chamber increases the percentage of daily human gas exchange rates that can be achieved.

8.2.2 SCENARIO 2: ONE HPC PROTOTYPE

As in the first scenario, it is assumed that initially only one HPC prototype with 5 m^2 of growing area is located at the MPP. However, in this case it is assumed that the collector system for human faeces and urea is already installed and a certain amount of human wastes are introduced into CI and part of the EB is sent out of the loop.

The plant EB produced is used to determine the percentage of human wastes introduced into the loop. Considering all the possible crop distributions inside the HPC prototype, edible plant production ranges from 50-68 $g \cdot d^{-1}$, which roughly represents 5% of one human daily diet. Since plant EB is taken out of the MPP loop, the corresponding 5% of the HDP of faeces (23.5 $g \cdot d^{-1}$) and urine (1.5 $L \cdot d^{-1}$) is introduced into the MPP loop.

However, it is noteworthy to mention that the use of nominal human values for urine and faeces production and composition leads to an unbalance in the crew compartment (CV). The ideal situation would be that the EB produced in the loop and sent to CV were the only source of food eaten by the human candidate from whom faeces and urine would be collected. Then, assuming that this human were living under “steady-state”, it would be possible to balance nitrogen, carbon and oxygen within the crew compartment, since the amount ingested would be found in generated wastes.

For this reason, it is evaluated to which extent the amount of N introduced into the CI via faeces and urine corresponds to the amount of N sent to the crew. If results indicate that it is not representative, the N addition would be not only expressed in percentages of HDP of urine but also as a percentage of the N taken out of the MPP loop via EB.

As the values used for faeces and urine production and composition are standard values found in bibliography and not values obtained experimentally with humans fed only with the amount of EB sent to the crew, it is emphasized that when the amount of EB sent to the crew represent 5% of the human daily diet, it does not necessarily involve that:

- such an amount represent 5% of the human nitrogen requirements
- 5% of the HDP of wastes (faeces and urine) will be introduced with the same N content as that taken out.

Faeces are directly incorporated into CI and urine is first decomposed in ammonium and CO_2 and then introduced into the loop in the general nitrogen and CO_2 balance.

Arthrospira contains 5% nucleic acids (Table 8.4). However, since humans only can eat a maximum of 2 $g \cdot d^{-1}$ nucleic acids, a maximum of 40 $g \cdot d^{-1}$ can be directed to humans. Thus, considering that the *Arthrospira* productivity of the pilot plant bioreactor is 49.8 $g \cdot d^{-1}$ (Table 8.4), the amount of *Arthrospira* to introduce into CI is 9.8 $g \cdot d^{-1}$.

In this scenario, the percentage of *R. rubrum* introduced into CI (0-100%) and the percentage of beet occupation of the HPC area were varied to evaluate its influence in N, CO_2 and O_2 balances.

The load to CI is composed by all inedible plant production (8-19 $g \cdot d^{-1}$), by 5% of faeces (1.17 $g \cdot d^{-1}$) produced daily by one human, by 20% of *Arthrospira* production (9.96 $g \cdot d^{-1}$) and by different amounts of *R. rubrum* biomass, ranging from 0 to 100%. A summary of the main conditions is included in Table 8.8.

Table 8.8 Summary of the main conditions assumed for the second scenario (S2).
(1) Total edible and inedible production depends on crop distribution inside the HPC.

Compartment parameters	Value
CII: *R. rubrum*	
Fraction of *R. rubrum* production into CI (%)	Variable
CIVa: *Arthrospira*	
Arthrospira production ($g \cdot d^{-1}$)	49.80
Fraction of *Arthrospira* production into CI (%)	20
CIVb: HPC	
Number of HPC prototypes in MPP	1
Area for beet and lettuce production (m^2)	5
- Beet occupation (% of the total area)	Variable
- Lettuce occupation (% of the total area)	Variable
Area for wheat production (m^2)	0
Total edible production ($g \cdot d^{-1}$)	50-68 (1)
Fraction of edible production into CI (%)	0
Percentage of daily human diet supplied by edible plant production (%)	5
Total inedible production ($g \cdot d^{-1}$)	8-19 (1)
Fraction of inedible production into CI (%)	100
CV: Crew compartment (Human wastes and animals for gas exchange)	
Fraction of HDP of faeces into CI (%)	5
Fraction of HDP of urine into the loop (%)	5

- **Nitrogen balance**

The N balance of the loop is presented in Figure 8.2 for various percentages of *R. rubrum* introduced into CI (0-100%) and for different crop distributions inside the HPC (% BO of the 5m^2).

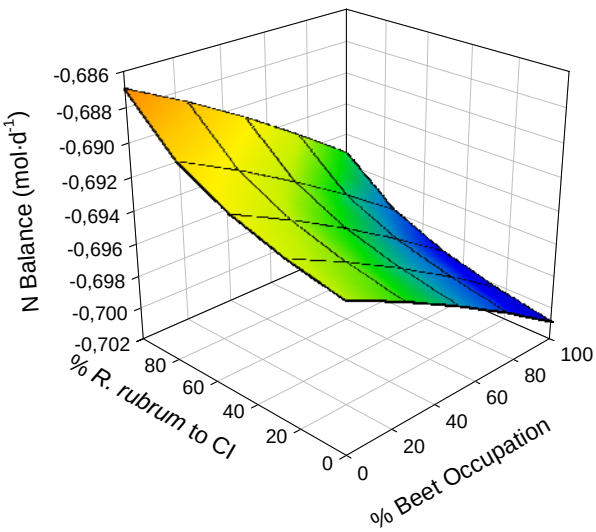

Figure 8.2 Nitrogen balance (mol·d^{-1}) for scenario 2 as function of different crop distributions (% BO of the 5 m^2) and of percentage *R. rubrum* sent to the first compartment (CI). The main assumptions for scenario 2 are listed in Table 8.8. Negative values of the balance indicate nitrogen deficiency in the loop.

The nitrogen deficiency calculated to exist across the entire range of the studied variables indicate that (i) either the nitrogen reintroduced via human wastes is much lower than the N content of EB sent to humans, which would not be a real N loss of the MELiSSA loop, or that (ii) CI is able to degrade only part of the biomass or (iii) both.

Thus, in order to evaluate to which extent the amount of nitrogen introduced into the CI as faeces and urine correspond to the N content of EB sent to the crew, the percentage of N reintroduced in to the loop is calculated for the boundary conditions (Table 8.9).

Table 8.9 Nitrogen balance for scenario 2 as function of different crop distributions inside the HPC prototype (% BO of the 5 m^2) and of percentage *R. rubrum* sent to CI. The main assumptions for scenario 2 are listed in Table 8.8.

(1) % Ratio between N introduced into the loop as human wastes and N sent out of the MPP to the crew.

(2) % Ratio between N deficiency and N recycled within the loop.

% Beet Occupation	% *R. rubrum* to CI	%N reintroduced (1)	% N deficiency (2)
0	0	8.74	84
	100	9.97	74
100	0	8.84	87
	100	9.43	77

Results indicate that only around 9-10% of the N content of the EB sent to the crew, which represent 5 % of the daily human diet, is reintroduced to the loop with the addition of 5% of HDP of urine and faeces. In fact, as the N content of the EB sent to the crew represents 57% of the N content of the HDP of wastes, obviously the introduction of 5% of the HDP of urine is not enough to compensate the N amount sent out of the loop. This fact can lead one to misidentify a N deficiency within the MPP loop, since it is mainly caused by the low N amount introduced to the loop. For the following scenarios to avoid such a misinterpretation N addition is expressed either as (i) amount of N ($g \cdot d^{-1}$) introduced into the loop as urine or (ii) as percentage of the N taken out of the MPP loop (% N reintroduced, %NR).

The effect of the introduction of different amounts of *R. rubrum* biomass into CI on the N balance is small. The highest percentage of NR (lowest apparent nitrogen deficiency) is detected when all the *R. rubrum* biomass is sent to CI and when lettuce occupies the entire chamber. A higher amount of *R. rubrum* sent to CI implies that more N is recycled in the loop and therefore N deficiency within the loop is decreased. Moreover, as less EB is sent to the crew, the %N reintroduced is higher since the amount of human wastes sent to CI are fixed.

Regarding the effect of crop distribution inside the HPC on N balance, a higher proportion of lettuce diminishes N deficiency. Taking into account that the HI of lettuce (72%) is lower than those of beets (89%), when lettuce is the only crop in the HPC the amount of IEB (19 $g \cdot d^{-1}$) introduced into CI is higher than when beet occupies all the growing area (8 $g \cdot d^{-1}$). Hence, higher N recycling in the loop is achieved with higher proportions of lettuce.

- **Gas balances (CO_2 and O_2)**

The CO_2 and O_2 balances in the MPP as function of crop distribution and of percentages of *R. rubrum* sent to CI are presented in Figure 8.3.

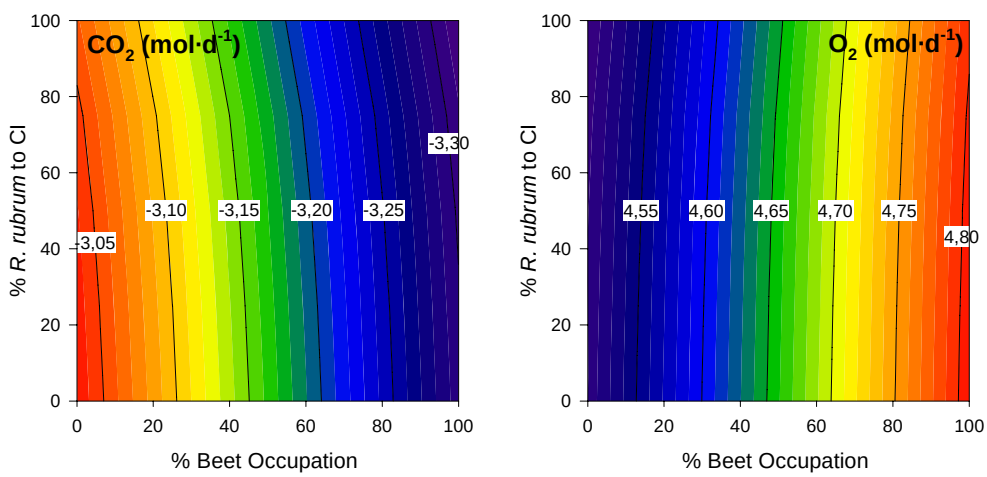

Figure 8.3 Gas balances (LEFT: CO_2 balance ($mol \cdot d^{-1}$); RIGHT: O_2 balance ($mol \cdot d^{-1}$)) for scenario 2 as function of different crop distributions inside the HPC prototype (% BO of the 5 m^2) and of percentage *R. rubrum* sent to CI. Table 8.8 summarizes the main conditions for scenario 2. Positive values of the balance indicate a surplus of CO_2 or O_2 in the loop in these conditions.

For a fixed percentage of beet occupation, for example 0% BO, CO_2 consumption increases from -3.03 to -3.06 mol·d^{-1} for 0 to 100% of the *R. rubrum* production introduced to CI respectively (Figure 8.3, left). Although the degradation in CI of higher amounts of biomass involves a higher CO_2 production, which would diminish the CO_2 consumption in the loop, more fatty acids (FAs) are also generated. Considering that the stoichiometry of CII is maintained, the consumption in CII of all the FAs produced in CI requires a higher CO_2 uptake than the CO_2 generated in CI. Hence, in the global CO_2 balance, the more *R. rubrum* reintroduced into the loop, the higher the consumption of CO_2. Alternatively, for a fixed amount of *R. rubrum* entering CI, CO_2 uptake is increased when beet occupies more growing area than lettuce, due to the higher productivity of beet.

The accumulation of O_2 in the loop is slightly higher when all *R. rubrum* is introduced into CI for a fixed crop distribution (Figure 8.3, right). In the nitrifying compartment (CIII), for each mol of N consumed, 2 mol of O_2 are also uptaken. When a higher amount of N is recovered into the loop (100% of *R. rubrum* into CI), more O_2 is required in CIII and consequently the global O_2 surplus in the loop decreases. Evaluating the effect of crop distribution on O_2 balance, the higher the lettuce proportions the lower the O_2 production in the loop because of lettuce's lower productivity.

The values found indicate that under this scenario the loop is able to supply the equivalent to 16-17% of the O_2 HDC and is capable of consuming the equivalent of 12-13% of the CO_2 HDP.

8.2.3 SCENARIO 3: ONE HPC PROTOTYPE

In the previous scenario it was calculated that only around 9-10% of the nitrogen content of the EB sent to the crew, which represent 5 % of the daily human dietary requirement, was reintroduced to the loop with the addition of 5% of the HDP of urine and faeces production. This fact lead one to misidentify a nitrogen deficiency within the MPP loop, since it was mainly caused by the low N amount reintroduced to the loop.

The next logical step is to evaluate the impact of the amount of human urine added in the loop on mass balances (N, CO_2 and O_2), which would serve as a possible compensation for the N deficiency faced in the previous cases. Moreover, it would be used to determine the conditions where the compensation point for mass balances occurs.

Thus, in this scenario the variation of the N addition from the human urine is considered together with the variation of beet occupation inside the chamber. Moreover, since the complete recirculation of the amount of *R. rubrum* produced in the loop into CI was favourable for N balance (Figure 8.2), it is assumed that all *R. rubrum* is recycled in the loop. Like in the previous scenario, only one 5 m^2 HPC prototype is used for the production of lettuce and beet. Moreover, CI receives a mix composed of 5% of the HDP of faeces, all plant IEB, all *R. rubrum* biomass produced in the loop and 20 % of the *Arthrospira* production, while plant EB and 80% *Arthrospira* production is sent to the crew compartment.

Table 8.10 summarizes conditions assumed for the simulations of scenario 3.

Table 8.10 Summary of the main conditions assumed for the third scenario (S3).
(1) Total edible and inedible production depend on crop distribution inside the HPC.

Compartment parameters	Value
CII: *R. rubrum*	
Fraction of *R. rubrum* production into CI (%)	100
CIVa: *Arthrospira*	
Arthrospira production ($g \cdot d^{-1}$)	49.80
Fraction of *Arthrospira* production into CI (%)	20
CIVb: HPC	
Number of HPC prototypes in MPP	1
Area for beet and lettuce production (m^2)	5
- Beet occupation (% of the total area)	Variable
- Lettuce occupation (% of the total area)	Variable
Area for wheat production (m^2)	0
Total edible production ($g \cdot d^{-1}$)	50-68 (1)
Fraction of edible production into CI (%)	0
Percentage of daily human diet supplied by edible plant production (%)	5
Total inedible production ($g \cdot d^{-1}$)	8-19 (1)
Fraction of inedible production into CI (%)	100
CV: Crew compartment (Human wastes and animals for gas exchange)	
Fraction of daily human production of faeces into CI (%)	5
N introduced into the loop as human urine ($g \cdot d^{-1}$)	Variable

- **Nitrogen balance**

Figure 8.4 depicts the N balance in the loop for different crop distributions (% BO of the $5m^2$) and for various amounts of N added into the loop.

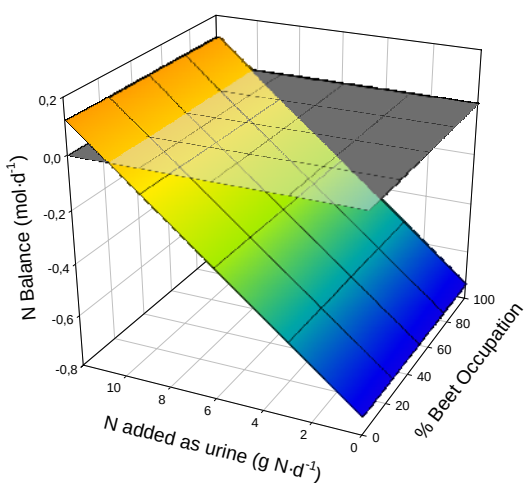

Figure 8.4 Nitrogen balance ($mol \cdot d^{-1}$) for scenario 3 as function of different crop distributions (% BO of the $5m^2$) and of N added into the loop ($g\ N \cdot d^{-1}$). The main assumptions for scenario 3 are shown in Table 8.10. The grey horizontal plane is the compensation balance plane (zero) and the colour gradient plane correspond to N balance, which is described by the following equation: N balance ($mol \cdot d^{-1}$) = -0.7293 - 0.0001·[% Beet] + 0.0714·[$g\ N \cdot d^{-1}$]; r^2=0.999.

Figure 8.4 shows that the influence of crop distribution on N balance is small. As already mentioned in the previous scenario, when there is a N deficit in the loop, it is more favourable to have a growing area stocked with lettuce, since its inedible proportion is higher than beet and consequently more N is recycled in the loop.

The addition of urine into the loop obviously decreases N deficiency until its compensation is achieved. The values for which N compensation occurs can be seen along the line formed by the intersection of the horizontal compensation balances plane and the nitrogen balance plane, which correspond to the addition of 10.3-10.4 g $N \cdot d^{-1}$ into the loop for 0% and 100% beet occupation respectively. When adding 10.3-10.4 g $N \cdot d^{-1}$, the percentage of N reintroduced in respect to the amount taken out as edible biomass ranges from 137% to 130% correspondingly. This value indicates that, in fact, the loop is able to recycle more than 60% of the N and the low N loss is due to the poorly degradable biomass sent to CI.

- **Gas balances (CO_2 and O_2)**

The effect of the urine addition on CO_2 and O_2 balances for various crop distributions can be seen in Figure 8.5.

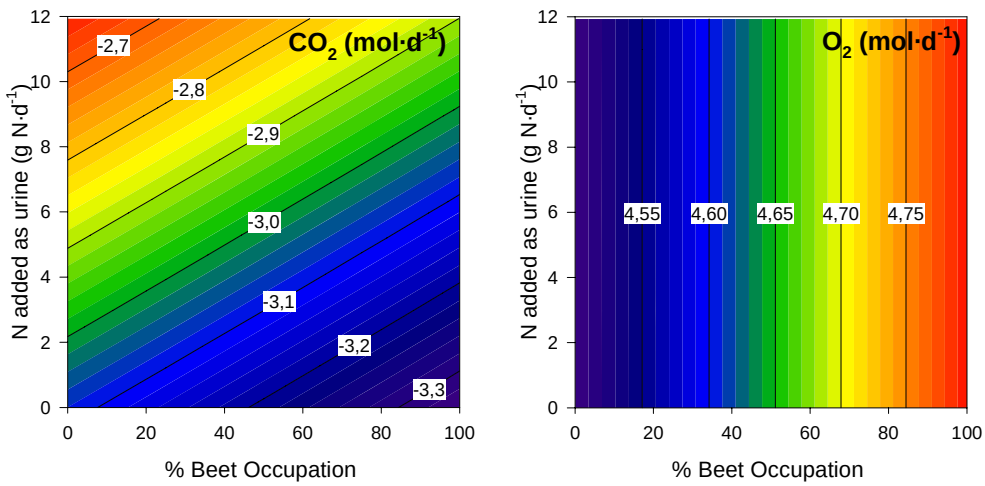

Figure 8.5 Gas balances for scenario 3 as function of different crop distributions (% BO of the $5m^2$) and of N added into the loop (g $N \cdot d^{-1}$). LEFT: CO_2 balance (mol·d^{-1}). RIGHT: O_2 balance (mol·d^{-1}). Table 8.10 includes the assumptions made in scenario 3.

For a fixed N addition rate, the CO_2 uptake and O_2 production in the loop is higher when the HPC is fully stocked (100%) with beet due to its higher productivity than lettuce (Figure 8.5). Urine addition into the loop has different impact on CO_2 and O_2 balances due to the fact that decomposition of urine produces CO_2 but no O_2. Hence, when more urine is introduced into the loop, either more CO_2 can accumulate if a surplus of CO_2 existed, or CO_2 balance can reach the compensation point if there was a CO_2 deficit. Figure 8.5 (right) shows that oxygen balance is independent from urine additions and in fact, values obtained are the same as those shown in Figure 8.3 (right) when all the *R. rubrum* was introduced into CI.

Results of O_2 balance assessments indicate that under the conditions described in Table 8.10, the photosynthetic compartments are able to produce O_2 equivalent to 16-17% of the HDC. In Table 8.11 the values of % N reintroduced into the loop and the human equivalents of CO_2 production and O_2 uptake are determined for the boundary conditions of crop proportions and amount of urine added (% HDP of urine).

Table 8.11 Results of N, CO_2 and O_2 balances for scenario 3 as function of different crop distributions inside the HPC prototype (expressed as %BO of the 5 m^2) and of percentage the HDP of urine production sent to CI. The main assumptions for scenario 3 are listed in Table 8.10.
(1) % Ratio between N introduced into the loop via human wastes (faeces and urine) and N sent out of the MPP to the crew via edible biomass (%NR).

% Beet Occupation	N added as urine (g $N \cdot d^{-1}$)	%NR (1)	% Human daily CO_2 production	% Human daily O_2 uptake
0	0	0.74	12.3	16.4
	12	185	10.5	16.4
100	0	0.70	13.3	17.4
	12	175	11.5	17.4

- **Closure of balances**

In order to determine under which conditions the N and CO_2 balances can be fulfilled simultaneously, the percentage of % CO_2 HDP, that animals should produce to compensate the CO_2 balance was calculated, (given a compensatory N addition rate of 10.3 - 10.4 g $N \cdot d^{-1}$). Results indicate that if animals can consume between 11% and 12% of the CO_2 HDP and between 130 and 137% of the N taken out from the loop is reintroduced with urine, the CO_2 and N balances are closed simultaneously for different crop distributions.

In a similar way, the conditions under which the closure of N and O_2 balances can be attained are determined. Considering that between 130 and 137% of the N taken out from the loop as EB is reintroduced with human wastes, the N and O_2 closure can be fulfilled at the same time when animals consume around 16-17% of the HDC of oxygen.

In conclusion, it is possible the achieve closure of the balances in pairs (either N and CO_2 or N and O_2) when between 130 and 137% of the N taken out from the loop as EB is reintroduced with urine under the assumptions that 5 m^2 are used for the production of beet and lettuce and that CI receives a mix of human faeces, plant IEB, *R. rubrum* and *Arthrospira* biomass (Table 8.10). In these conditions the loop supplies around 5% of the daily human diet and is able to generate around 16-17% of the HDC of O_2.

8.2.4 SCENARIO 4: TWO HPC PROTOTYPES

The aim of the scenario 4 is to evaluate under which conditions it is possible to compensate the balances when the second HPC prototype is incorporated into the MPP, which implies that growing area for beet and lettuce production increases from 5 to 10 m^2.

As in scenario 3, all the EB produced in the two HPC prototypes is sent out of the loop together with 80% of *Arthrospira* production, which is the maximum amount of *Arthrospira* that humans can ingest due to its nucleic acid content. All plant IEB and *R. rubrum* produced in the loop, together with 20% of the *Arthrospira* production and a fraction of the HDP of faeces are introduced into CI.

The amount of human faeces introduced into the loop is calculated based on the plant EB produced in 10 m^2 of the HPC prototypes, which ranges between 100 and 136 $g \cdot d^{-1}$ depending on crop proportions. Since this amount of EB, which is sent out of the loop simulating the flow that would be sent to humans, represents about 9-12% the weight of one human daily diet, the amount of faeces introduced into the loop is also 12% of the HDP.

The N, CO_2 and O_2 balances are calculated for different crop distributions and with different urea additions assuming the conditions defined in Table 8.12.

Table 8.12 Summary of the main conditions assumed for scenario 4 (S4).
(1) Total edible and inedible production depends on crop distribution inside the HPC.

Compartment parameters	Value
CII: *R. rubrum*	
Fraction of *R. rubrum* production into CI (%)	100
CIVa: *Arthrospira*	
Arthrospira production ($g \cdot d^{-1}$)	49.80
Fraction of *Arthrospira* production into CI (%)	20
CIVb: HPC	
Number of HPC prototypes in MPP	2
Area for beet and lettuce production (m^2)	10
- Beet occupation (% of the total area)	Variable
- Lettuce occupation (% of the total area)	Variable
Area for wheat production (m^2)	0
Total edible production ($g \cdot d^{-1}$)	100-136 (1)
Fraction of edible production into CI (%)	0
Percentage of daily human diet supplied by edible plant production (%)	9-12
Total inedible production ($g \cdot d^{-1}$)	17-39 (1)
Fraction of inedible production into CI (%)	100
CV: Crew compartment (Human wastes and animals for gas exchange)	
Fraction of HDP of faeces into CI (%)	12
N introduced into the loop as human urine ($g \cdot d^{-1}$)	Variable

- **Nitrogen balance**

Results obtained for N balance calculations with varying percentages of beet occupation and of urine added are presented in Figure 8.6. Increasing beet occupation inside the HPC with 10 m^2 of growing area has little impact on N balance. Nonetheless, as already discussed in the previous simulations, when a nitrogen deficiency exists it is better to use higher proportions of lettuce because of its lower harvest index, which results in a higher loading to CI and therefore a higher recovery of the nitrogen present in the inedible biomass.

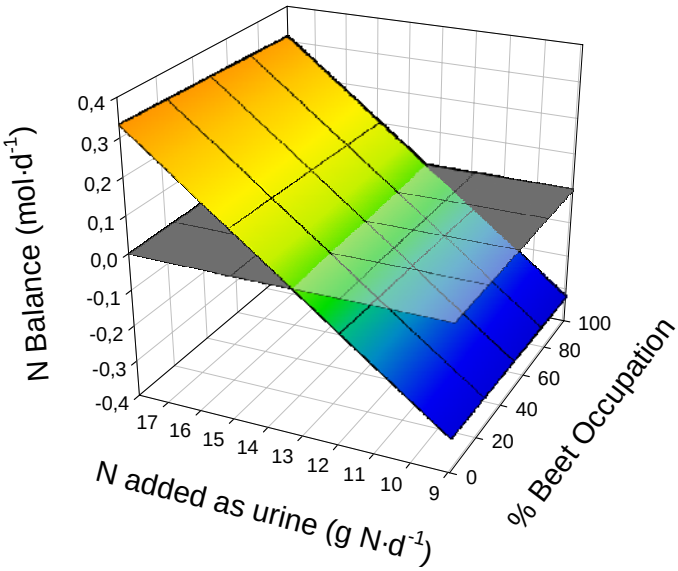

Figure 8.6 Nitrogen balance (mol·d^{-1}) for scenario 4 as function of N added into the loop (g N·d^{-1}) and of different drop distributions (% BO of the 10 m^2). The main assumptions for scenario 4 are shown in Table 8.12.

As shown in Figure 8.6, the addition of 13.2-13.5 g N·d^{-1} into the loop allows N balance when 2 HPC prototypes are installed in the MPP and assuming the conditions listed in Table 8.12. Under these conditions CI is able to recycle around 60-70% of the N content present in the biomass sent to CI for degradation.

- **Gas balances (CO_2 and O_2)**

The balances of CO_2 and O_2 calculated under conditions summarized in Table 8.12 are depicted in Figure 8.7 for various proportions of beet and lettuce inside the 10 m^2 of the HPC and for different amounts of urine added into the loop.

The influence of crop distribution and the amount of urine added into the loop on CO_2 and O_2 balances is similar to that obtained in scenario 3 (Figure 8.5). Particularly, the capability of the loop to consume higher CO_2 amounts is higher when there is more beet than lettuce inside the HPC, because of its higher photosynthetic activity, and when no urine is added into the loop, since during its decomposition CO_2 is formed. As plotted in Figure 8.7 (right), O_2 balance is independent of urine addition into the loop and the surplus detected under this condition (Table 8.12) is diminished with increasing proportions of lettuce inside the HPC due to its lower productivity compared to beet.

Results of gas balance studies indicate that under the current conditions (Table 8.12) the photosynthetic compartments can uptake the equivalent to 19-20% of the HDP of CO_2 and can supply the O_2 required for sustaining 24-26% of the HDC, when N additions range between 9 and 18 g N·d^{-1}.

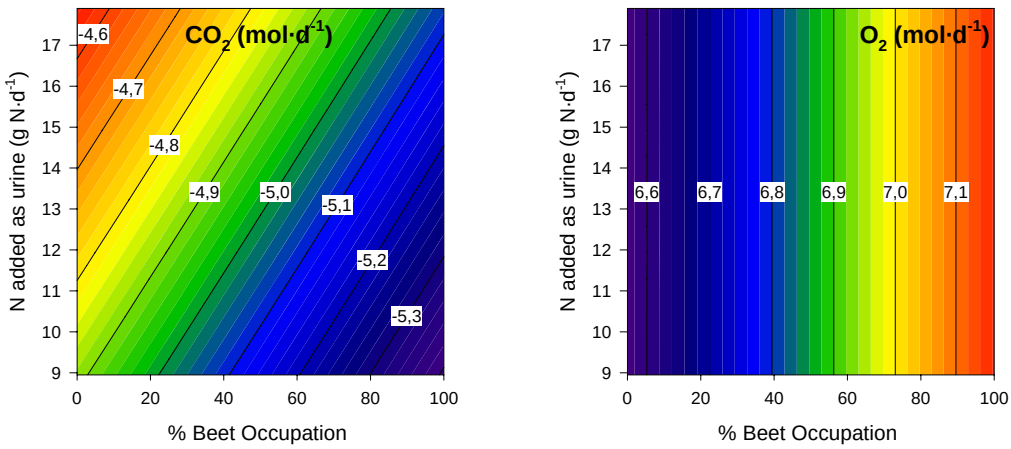

Figure 8.7 Gas balances for scenario 4 as function of N added into the loop (g $N \cdot d^{-1}$) and of different crop distributions (% BO of the 10 m^2).LEFT: CO_2 balance ($mol \cdot d^{-1}$). RIGHT: O_2 balance ($mol \cdot d^{-1}$). Table 8.12 includes the assumptions made in scenario 4.

- **Closure of balances**

Similarly as was done in scenario 3, the conditions under which the N and CO_2 balances, on one side, and the N and O_2, on the other side, can be fulfilled simultaneously, are determined. With this aim, the CO_2 and O_2 balances are simulated assuming that N added into the loop is compensatory at 13.2-13.5 g $N \cdot d^{-1}$. Results for CO_2 and O_2 balances as a function of crop distribution and of percentage of daily human gas exchange rates are plotted respectively in Figure 8.8 and in Figure 8.9.

In Figure 8.8 it can be seen that CO_2 compensation can be achieved for all crop distributions inside the 10 m^2 of the HPC and when the consumer compartments are able to consume the CO_2 equivalent to 18.7-20.8% of the HDP. As mentioned in the previous sections, under CO_2 deficits inside the loop higher occupancies of lettuce are more favourable because, for a given area, lettuce fixes less CO_2 than beet.

Figure 8.9 shows that the values for which O_2 compensation may occur are described by the line formed by the intersection the horizontal compensation balance plane (zero plane) and the oxygen balance plane. Particularly, O_2 balance is compensated when the consumers are capable of taking up the O_2 equivalent to 24-26% of the HPC for all the crop distributions inside the 2 HPC prototypes. Contrary to CO_2, under O_2 deficit increasing beet occupation inside the HPC diminishes the O_2 excess, while under O_2 deficit higher proportions of lettuce contribute to approaching the compensation point.

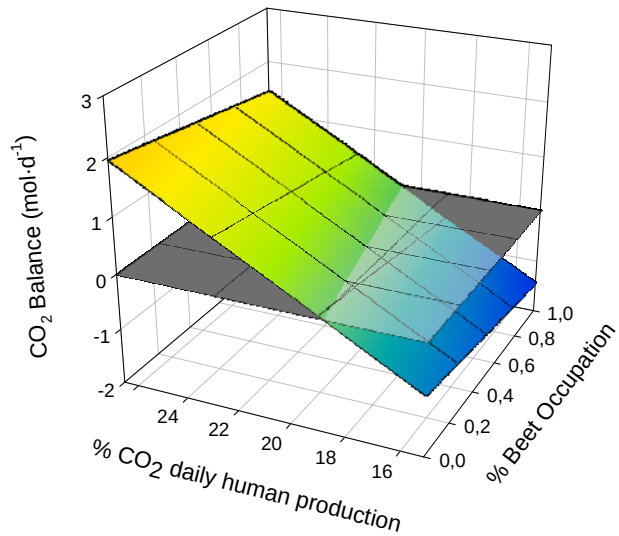

Figure 8.8 CO_2 balance ($mol \cdot d^{-1}$) for scenario 4 as function of percentage of CO_2 HDP and of different crop distributions (% BO of the 10 m^2). Conditions assumed for this simulation are as listed in Table 8.12, except for amount of N added into the loop, which is 13.36 g $N \cdot d^{-1}$. The grey horizontal plane is the compensation balance plane (zero) and the colour gradient plane correspond to CO_2 balance, which is described by the following equation: CO_2 balance ($mol \cdot d^{-1}$) = - 4.77 – 0.005·[% Beet] + 0.25·[%CO_2 HDC]; r^2=0.999.

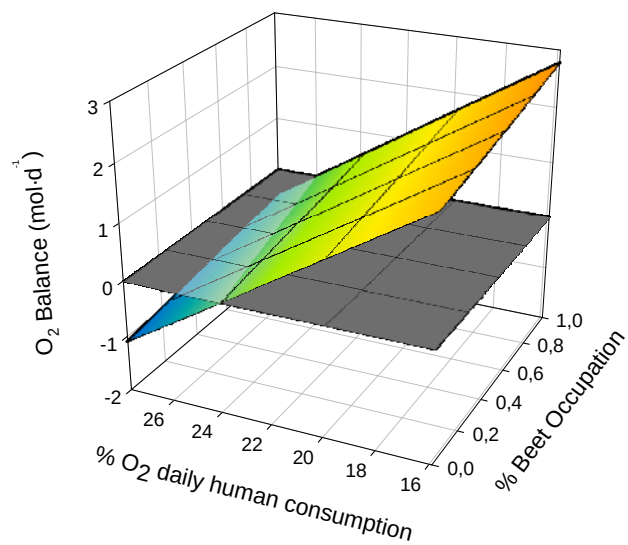

Figure 8.9 Oxygen balance ($mol \cdot d^{-1}$) for scenario 4 as function percentage of O_2 HDC and of different crop distributions (% BO of the 10 m^2). Conditions assumed for this simulation are as listed in Table 8.12, except for amount of N added into the loop, which is 13.36 g $N \cdot d^{-1}$. The grey horizontal plane is the compensation balance plane (zero) and the colour gradient plane correspond to O_2 balance, which is described by the following equation: O_2 balance ($mol \cdot d^{-1}$) = 6.57 + 0.006·[% Beet] – 0.27··[%O_2 HDC]; r^2=0.999.

In summary, the closure of the balances in pairs (either N and CO_2 or N and O_2) can be attained under the conditions of scenario 4 (Table 8.12) when the N added into the loop is 13.2-13.5 g $N \cdot d^{-1}$, which is necessary to compensate the N loss mainly caused by the fact that EB is sent out of the MPP loop. In these conditions the 2 HPC prototypes are able to supply around 9-12% of the daily human diet and the photosynthetic compartments, *Arthrospira* and HPC, are able to consume 19-21% of the HDP of CO_2 and to produce 24-26% of HDC of oxygen.

8.2.5 SCENARIO 5: THREE HPC PROTOTYPES (FINAL DESIGN)

The last scenario considered deals with the evaluation of mass balances in the MPP when the third HPC prototype is incorporated, which is the final design for which the HPC prototypes has been sized in Chapter 7.

As mentioned in the introduction, due to photoperiod restrictions, wheat is devoted to one HPC prototype of 5 m^2 and beet and lettuce occupation of the other 10 m^2 are varied as was done in the previous scenarios (%BO). In this case the production of plant EB ranges between 200 and 236 $g \cdot d^{-1}$, which correspond to 18-21% of daily human diet. Particularly, when the beet occupancy is 50%, which implies that each crop is devoted to one HPC prototype of 5 m^2, the amount of plant EB produced is equivalent to the 20% of daily human diet, as already calculated in the HPC design chapter (Chapter 7).

Considering that all the EB is sent to the crew compartments, the amount of faeces introduced into the loop is fixed to 20% of the HDP. Moreover, like in the previous scenario, 80% of *Arthrospira* production, which is the maximum amount of *Arthrospira* that humans can ingest due to its nucleic acid content, is sent also to humans. All the plant IEB, 100% of the *R. rubrum* and 20% of the *Arthrospira* production and 20% of the HDP of faeces are introduced into CI. A summary of the conditions considered for scenario 5 is found in Table 8.13.

The closure of the nitrogen balance under the present conditions is achieved when the addition of N into the loop is 19.6-19.9 g $N \cdot d^{-1}$ for different crop distributions inside 2 of the 3 HPC prototypes (Figure 8.10).

In this situation CI is able to recycle between 66 and 70% of the N content of the mix introduced in its input, which is composed of human faeces, inedible plant biomass, *R. rubrum* and part of the *Arhtrospira* biomass produced in the loop.

In order to determine under which conditions the balances can be fulfilled simultaneously (either N and CO_2 or N and O_2), the CO_2 and O_2 balances are assessed assuming that the nitrogen added into the loop is 19.8 g $N \cdot d^{-1}$, which is the amount required to attain the closure of N balance. Figure 8.11 depicts the CO_2 (left) and O_2 (right) balances for different crop distributions of beet and lettuce and as function of percentage of daily human gas exchange rates.

Table 8.13 Summary of the main conditions assumed for scenario 5 (S5).
(1) Total edible and inedible production depends on crop distribution inside the HPC.

Compartment parameters	Value
CII: *R. rubrum*	
Fraction of *R. rubrum* production into CI (%)	100
CIVa: *Arthrospira*	
Arthrospira production ($g \cdot d^{-1}$)	49.80
Fraction of *Arthrospira* production into CI (%)	20
CIVb: HPC	
Number of HPC prototypes in MPP	3
Area for beet and lettuce production (m^2)	10
- Beet occupation (% of the total area)	Variable
- Lettuce occupation (% of the total area)	Variable
Area for wheat production (m^2)	5
Total edible production ($g \cdot d^{-1}$)	200-236 (1)
Fraction of edible production into CI (%)	0
Percentage of daily human diet supplied by edible plant production (%)	18-21
Total inedible production ($g \cdot d^{-1}$)	167-189 (1)
Fraction of inedible production into CI (%)	100
CV: Crew compartment (Human wastes and animals for gas exchange)	
Fraction of HDP of faeces into CI (%)	20
N introduced into the loop as human urine ($g \cdot d^{-1}$)	Variable

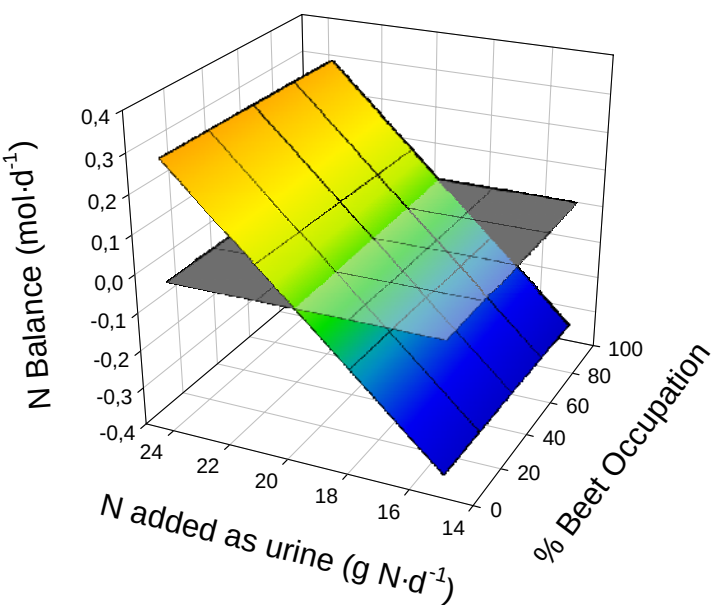

Figure 8.10 N balance ($mol \cdot d^{-1}$) for scenario 5 as function of N added into the loop ($g\ N \cdot d^{-1}$) and of different beet and lettuce distributions inside 2 of 3 HPC prototypes (% BO of the 10 m^2). The third HPC camber of 5 m^2 is devoted to wheat culture. The main assumptions for scenario 5 are shown in Table 8.13. The grey horizontal plane is the compensation balance plane (zero) and the colour gradient plane correspond to N balance, which is described by the following equation: N balance ($mol \cdot d^{-1}$) = -1.40 - 0.00002·[% Beet] + 0.0714·[$g\ N \cdot d^{-1}$]; r^2=0.999.

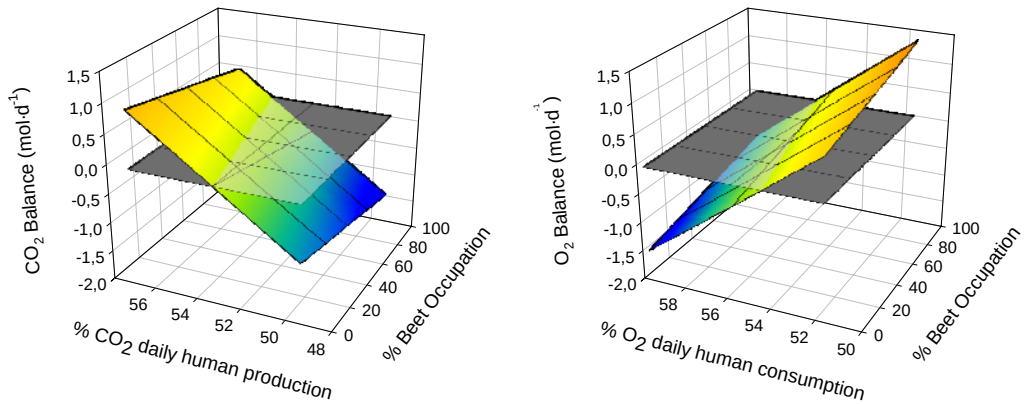

Figure 8.11 Gas balances (mol·d^{-1}) for scenario 5 as function of number of percentage of daily human gas exchange rates and of different beet and lettuce distributions inside 2 of 3 HPC prototypes (% BO of the 10 m^2). The third HPC camber of 5 m^2 is devoted to wheat culture. Conditions assumed for this simulation are as listed in Table 8.13. The grey horizontal planes are the compensation balance plane (zero) and the colour gradient plane corresponds to CO_2 (LEFT) and O_2 (RIGHT) balance. The corresponding equations are: CO_2 balance (mol·d^{-1}) = - 13.36 – 0.005·[% Beet] + 0.25·[%CO_2 HDP]; O_2 balance (mol·d^{-1}) = 14.97 + 0.006·[% Beet] – 0.27··[%O_2 HDC]

Results shown in Figure 8.11, that for all beet and lettuce distributions inside the 10 m^2 of 2 HPC prototypes, the photosynthetic compartments are able to consume 53% of the HDP of CO_2 and to produce 54-56% of the HDC of oxygen.

Finally, if we consider the scenario where each crop (beet, lettuce and wheat) is devoted to one HPC prototype of 5 m^2 and the conditions assumed in Table 8.13 the following conclusions can be drawn:

- Edible plant biomass sent to the crew compartment represents the 20% of the daily human diet.

- Regarding the N balances, it is necessary to reintroduce 19.8 g N·d^{-1} as urine into the loop to compensate the N content present in the EB sent to the crew compartment and the N loss in CI due to the presence of poorly degradable biomass. In this scenario, CI is capable to recycle 69% of the N introduced in its input, as human faeces, plant IEB, *R. rubrum* and *Arthrospira* biomass.

- The photosynthetic compartments are capable of consume 54% of the HDP of CO_2 and to produce 55% of the HDC of oxygen.

8.3 CONCLUSIONS

The static mass balance developed in this chapter was used for assessing the N, CO_2 and O_2 balances in the MPP under different scenarios considered of interest. Results contribute to the determination of the range of conditions for which closure of the mass balances can be expected. Some of the major conclusions are:

- The edible biomass sent to the crew, which correspond to a percentage 'X' of the daily human diet, has not the same N content as the N found in faeces and urine, when their amount correspond to the same percentage 'X' of the HDP of wastes. In fact, results indicate that only around 9-10% of the N content of the EB sent to the crew compartment, which represent 5 % of the daily human diet, is reintroduced to the loop with the addition of 5% of the HDP of urine and faeces. Obviously, this fact can lead one to misidentify a nitrogen deficiency within the MPP loop, since it is mainly caused by the low N amount introduced to the loop.

- Although the effect of the introduction of different amounts of *R. rubrum* biomass into CI and of crop distribution on N balance is small, the lowest Ndeficiency is detected when all the *R. rubrum* biomass is sent to CI and when lettuce occupies the entire chamber.

- The influence of crop distribution on N balance is small. However, when there is a N deficit in the loop, it is more favourable a growing area stocked with lettuce, since its inedible proportion is higher than beet and consequently more N is recycled in the loop.

- The capability of the loop to consume CO_2 and to produce O_2 amounts is higher when there is more beet than lettuce inside the HPC, because of its higher productivity.

- One HPC prototype with $5m^2$ of growing area for beet and lettuce production produces 50-68 $g \cdot d^{-1}$, which roughly represents 5% of one human daily diet. Assuming that all plant EB and 80% of the *Arthrospira* production is sent to the crew compartment and the remaining biomass produced is introduced into CI together with 5% of the HDP of faeces, the closure of N, CO_2 and O_2 balances is attained when:
  - The nitrogen reintroduced in respect to the amount taken out as edible biomass ranges from 137% to 130%.
  - The animals are able to produce the amount of CO_2 equivalent to 11% and 12% of the human daily CO_2 production and to consume the amount of O_2 equivalent to 16-17% and 12% of the human daily O_2 uptake.

- In the final scenario where each crop (beet, lettuce and wheat) is devoted to one HPC prototype of 5 m^2, all the plant EB and 80% of the *Arthrospira* production is sent to the crew compartment and the remaining biomass produced is introduced into CI together with 20% of the HDP of faeces, it can be stated that:
  - Plant EB sent to the crew compartment represents the 20% of the daily human diet.
  - It is necessary to reintroduce 19.8 g $N \cdot d^{-1}$ as urine into the loop to compensate the N content present in the EB sent to the crew compartment and the N loss in CI due to poorly degradable biomass. However, CI is capable of recycling 69% of the N introduced in its input.
  - The photosynthetic compartments are capable to consume 54% of the human daily CO_2 production and to produce 55% of the daily human oxygen requirement.

Conclusions

Chapter **9**

Conclusions

Chapter 9

CONCLUSIONS

This work has contributed to the engineering of the photosynthetic compartments of the MELiSSA life support system, while increasing the knowledge about the behaviour of *Arthrospira* and higher plant cultures in photobioreactors (Unit I) and in sealed environmental chambers (Unit II), respectively. The empirical data and the experience obtained in photosynthetic compartments has been used to design a higher plant chamber to be integrated into the MELiSSA Pilot Plant (MPP) located at UAB and to evaluate the impact of their integration into the MPP using a static mass balance model for assessing the nitrogen, CO_2 and O_2 balances (Unit III). The main conclusions drawn from this work are summarized next below.

Unit I - *Arthrospira* Compartment (CIVa):

Regarding the operational limits of *Arthrospira* culture in pilot plant photobioreactor it can be concluded that:

- The highest biomass concentration inside the bioreactor is obtained at the highest light intensity value and at low dilution rates.
- The highest *Arthrospira* productivity attained in the pilot plant photobioreactor is 27 $mg \cdot L^{-1} \cdot h^{-1}$ at a dilution rate of 0.044 h^{-1} and a light intensity of 194 $W \cdot m^{-2}$. Under these

conditions the CO_2 volumetric consumption is 0.5 $mmol \cdot L^{-1} \cdot h^{-1}$, the O_2 volumetric production is 1.32 $mmol \cdot L^{-1} \cdot h^{-1}$ and the nitrogen volumetric uptake is 0.28 $mmol \cdot L^{-1} \cdot h^{-1}$.

- Regarding the effect of light intensity on biomass composition, only the protein and the chlorophyll content are affected. In both cases, an increase in light intensity produces lower amounts of proteins and chlorophyll in *Arthrospira*.
- Disturbances of normal operating conditions affecting pH, liquid and gas flow rate affect *Arthrospira* growth, but all tested deviations allow the recovery of the initial biomass values. A batch phase is necessary before achieving normal operational conditions.

In regard to the effect of ammonium and light intensity on the growth of *Arthrospira* is concluded:

- In order to avoid inhibition of the *Arthrospira* growth, the steady-state ammonium concentration has to be lower than 5.6 mM.
- *Arthrospira* is able to recover from inhibitory conditions resulting from high ammonium concentration and high irradiance levels. Full recovery is attained after keeping the culture in batch and under low light levels.
- Biomass aggregates formed under inhibitory conditions (high ammonium or light intensities) have a lower content of carbon, hydrogen, nitrogen, protein, fatty acids and chlorophyll, but a higher amount of carbohydrates than not inhibited biomass when.
- An increase of light intensity produces a decrease in nitrogen, protein and chlorophyll content and consequently an increase in total fatty acid content. Higher protein contents were observed when using nitrate instead of ammonium as the nitrogen source.

Unit II - Higher Plant Compartment (CIVb/HPC):

The conclusions to highlight from the three batch and two staggered cultures of beet and lettuce carried out in sealed environment chambers are:

- For beet, the mean total plant productivity among batch and staggered cultures is 15.31 g $dw \cdot m^{-2} \cdot DIC^{-1}$ with a harvest index of 89%. For lettuce, total plant productivity averaged is 13.85 g $dw \cdot m^{-2} \cdot DIC^{-1}$ and the percentage of edible biomass is 72%.
- Beet and lettuce grown in these hydroponic cultures have unusually higher mineral content, protein and ash levels than beet and lettuce grown in field. This is probably caused by an excess uptake of some nutrients. In contrast, carbohydrates have lower values in both crops when compared to crops cultivated in field.
- Nutrient uptake dynamics showed that nitrogen is the nutrient with the highest consumption rate, followed by potassium. All the other nutrients analyzed (PO_4^{3-}, SO_4^{2-}, Na^+, Mg^{2+} and Ca^{2+}) present similar uptake rate values. In addition to this, the ionic uptake of the nutrient solution has been proven to be a good predictor of total

canopy mineral content using the estimated biomass, since good nutrient mass balances are obtained when comparing nutrient uptake rate from the hydroponic solution with the nutrient content present in the harvested biomass.

Some specific conclusions obtained from carbon dynamics of the above mentioned beet and lettuce cultures and from the estimation of light energy related parameters for the canopy model are:

- The net CO_2 exchange rate (NCER) technique is a good alternative to classical growth analysis for estimating plant growth and dry weight production inside the chamber without using destructive analyses. It is stressed that having a good calibration of instruments and determination of leakage rate is very important to achieve such accurate estimations of biomass from CO_2 data.
- Staggered cultures damp oscillation in gas exchange rates obtained in batch cultures. Therefore, staged cultures are rather preferred for long-term operation, such as in the continuous operation of the MELiSSA loop. This choice in the type of culture will have direct consequences on the design of HPC for the MPP.
- The rectangular hyperbola model is suitable in defining the leaf photosynthetic response to light at different CO_2 levels and crop ages. No significant differences are detected for the quantum yield (α) and dark respiration rate (R_d) among CO_2 levels, but in contrast maximum photosynthetic rate (P_{max}) has been found to depend on CO_2 concentration. Moreover, it is observed that that α, P_{max} and R_d values remain constant through crop development.
- The full canopy NCER model adequately predicts biomass accumulation for the batch cultures of beet and lettuce. More detailed work will be required to assess the performance of the full canopy model in staged cultures. It is concluded that the Thornley model coupled with direct estimation of the quantum yield, dark respiration and maximum photosynthetic rate from leaf light curve studies is an appropriate first step in the development of an HPC control law for managing gas exchange.

Unit III – Photosynthetic Compartments Integration

The main conclusions regarding the HPC designed for the MPP are:

- Using plant productivity data obtained in the previous trials, it is concluded that 3 HPC prototypes with 5 m^2 of growing area each, will be constructed to provide 20% of the daily crew diet with beet, lettuce and wheat.
- The selected configuration of the HPC prototype have the following characteristics:
  - It is an elongated chamber with a growing area 5 m long and 1 m wide with two air-locks at each end. In such a configuration a semi-continuous production of plant biomass can be provided. The gas environment isolation during sowing and harvest is insured with the air-locks. Access doors will facilitate plant sowing and

harvesting, chamber cleaning and other logistical tasks, while ensuring a sealed environment when closed.

- Artificial light to the growing area will be provided with a combination of six 600 W HPS and three 400 W MH lamps. Light intensity can be modified by switching 3 separate on/off lamp strings, resulting in 33% increment from off to maximum intensity.
- Crop irrigation will be achieved using the hydroponics based nutrient film technique. The pH of the nutrient solution is controlled by additions of acid/base stock solutions. Similarly, EC of nutrient solution will be adjusted with nutrient stock additions. Condensate water will be collected in a buffer tank. Levels of the solutions tanks will be also controlled. An ultraviolet lamp and an ozone system have been proposed for contaminant control of the nutrient solution.
- Forced internal air circulation will be provided inside the growing area. Temperature, humidity and CO_2 control loops will maintain such environmental conditions at desired levels. A passive control of pressure will be achieved with two expansion bags.

Regarding the mass balance analysis performed to evaluate the integration of the photosynthetic compartment in the MPP is concluded:

- The influence of crop distribution inside the HPC on nitrogen balance is small. Moreover, the capability of the loop to consume higher CO_2 and to produce higher O_2 amounts is higher when there is more beet than lettuce inside the HPC, because of its higher productivity.
- In the final scenario where each crop (beet, lettuce and wheat) is devoted to one HPC prototype of 5 m^2, all the edible plant biomass and 80% of the Arthrospira production is sent to the crew compartment and the remaining biomass produced is introduced into CI together with 20% of the daily human faeces production, it can be stated that:
  - Edible plant biomass sent to the crew compartment represents the 20% of the daily human diet.
  - It is necessary to reintroduce 19.8 g $N \cdot d^{-1}$ as urine into the loop to compensate the N content present in the edible biomass sent to the crew compartment and the N loss in CI due to the poorly degradable biomass. In these conditions, CI is capable of recycle 69% of the N introduced in its input.
  - The photosynthetic compartments are capable to consume 54% of the human daily CO_2 production and to produce 55% of the daily human oxygen requirement.

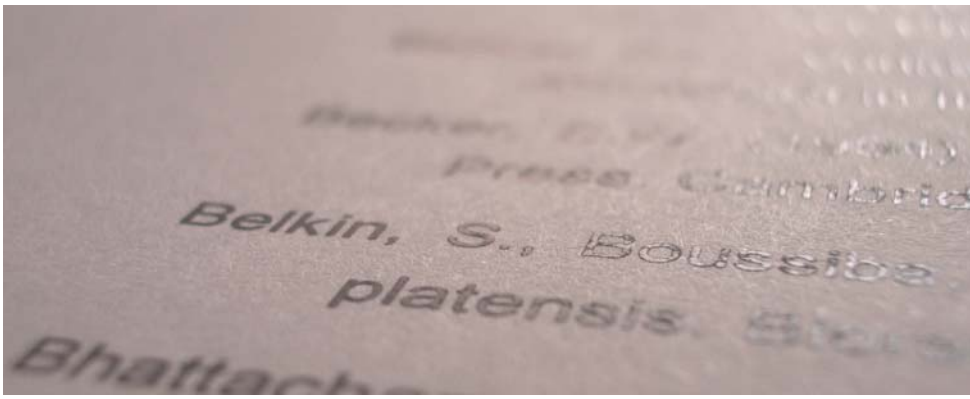

References

References

REFERENCES

A

Abadia, J., Madhusudana Rao, I., Terry, N. (1987). Changes in leaf phosphate status have only small effects on the photochemical apparatus of sugar beet leaves. *Plant Science*, 50(1): 49-55.

Abdulqader, G., Barsanti, L., Tredici, M.R. (2000). Harvest of *Arthrospira platensis* from Lake Kossorom (Chad) and its household usage among the Kanembu. J*ournal of Applied Phycology*, 12(3-5): 493-498.

Abeliovich, A., Azov, Y. (1976). Toxicity of ammonia to algae in sewage oxidation ponds. *Applied and Environmental Microbiology*, 31: 801-806.

Ahlgren, G., Gustafsson, I.B., Boberg, M. (1992). Fatty acid content and chemical composition of fresh-water microalgae. *Journal of Phycology*, 28(1): 37-50.

Akhkha, A., Reid, I., Clarke, D.D., Dominy, P. (2001). Photosynthetic light response curves determined with the leaf oxygen electrode: minimisation of errors and significance of the convexity term. *Planta*, 214(1): 135-141.

Albiol, J. (1994). Study of the MELiSSA photoheterotrophic compartment. Kinetics and effects of C limitation. ESA/YCL/2148.JAS ESTEC Working Paper. ESA-EWP-1808.

Albiol, J., Gòdia, F., Montesinos, J.L., Pérez, J., Vernerey, A., Cabello, F., Creus, N., Morist, A., Mengual, X., Lasseur, Ch. (2000). Biological Life Support System Demostration Facility: The MELiSSA Pilot Plant. Proceedings of the 30th International Conference on Environmental Systems (ICES), SAE paper No. 2000-01-2379.

Albright, L.D., Both, A.J., Chiu, A.J. (2000). Controlling greenhouse light to a consistent daily integral. *Transactions of the ASAE*, 43(2): 421-431.

Aldrich, S.R. (1980). Nitrogen in relation to food, environment, and energy, pp.97-110. Special Publication 61, Agricultural Experiment Station. College of Agriculture, University of Illinois, USA.

Allen, J., Nelson, M. (1999). Biospherics and Biosphere 2, mission one (1991-1993). *Ecological Engineering*, 13(1-4): 15-29.

Allen, J.P., Nelson, M., Alling, A. (2003). The legacy of Biosphere 2 for the study of biospherics and closed ecological systems. *Advances in Space Research*, 31(11): 1629-1639.

Ambrosio, N., Arena, C., Virzo de Santo, A. (2006). Temperature response of photosynthesis, excitation energy dissipation and alternative electron sinks to carbon assimilation in *Beta vulgaris* L.. *Environmental and Experimental Botany*, (55): 248–257.

Andrade, M.R., Costa, J.A.V. (2007). Mixotrophic cultivation of microalga *Spirulina platensis* using molasses as organic substrate. *Aquaculture*, 264: 130-134.

Andre, M., Cotte, F., Gerbaud, A., Massimino, D., Massimino, J. Richaud, C. (1989). Effect of CO_2 and O_2 on development and fructification of wheat in closed systems. A*dvances in Space Research*, 9: 17-28.

Annapurna, V.V., Deosthale, Y.G., Mahtab S. (1991). *Spirulina* as a source of vitamin A. *Plant Foods for Human Nutrition* (Formerly Qualitas Plantarum), 41(2): 125-134.

Anupama, Ravindra, P. (2000). Value-added food: Single cell protein. Biotechnology Advances, 18(6): 459-479.

AOAC - Association of Official Analytical Chemists (1990). Official Methods of Analysis. 15th ed. Washington DC, USA.

Ayala, F., Vargas, T. (1987). Experiments on *Arthrospira* culture on waste-effluent media and at the pilot-plant. *Hydrobiologia*, 151: 91-93.

Azov, Y., Goldman, J.C. (1982). Free ammonia inhibition of algal photosynthesis in intensive cultures. *Applied and Environmental Microbiology*, 43(4): 735-739.

B

Babadzhanov, A.S., Abdusamatova, N., Yusupova, F.M., Faizullaeva, N., Mezhlumyan, L.G., Malikova, M.K. (2004). Chemical composition of *Arthrospira platensis* cultivated in Uzbekistan. *Chemistry of Natural Compounds*, 40(3): 276-279.

Barta, D.J., Tibbitts, T.W., Bula, R.J., Morrow, R.C. (1992). Evaluation of light emitting diode characteristics for a space-based plant irradiation source. *Advances in Space Research*, 12(5): 141-149.

Barta, D.J., Henninger, D.L. (1996). Johnson Space Center's Regenerative Life Support Systems Test Bed. *Advances in Space Research*, 18: 211-221

Batten, J.H., Stutte, G.W., Wheeler, R.M. (1995). Effect of crop development on biogenic emissions from plant-populations grown in closed plant-growth chambers. *Phytochemistry*, 39(6): 1351-1357.

Becker, E.W., Venkataraman, L.V. (1984). Production and utilization of the blue-green alga *Spirulina* in India. *Biomass*, 4(2):105-125.

Becker, E.W. (1994). Microalgae: biotechnology and microbiology. Ed. Cambridge University Press. Cambridge.

Belay, A., Ota, Y., Miyakawa, K., Shimamatsu, H. (1993). Current Knowledge on Potential Health Benefits of *Spirulina*. *Journal of Applied Phycology*, 5(2): 235-241.

Belkin, S., Boussiba, S. (1991). High internal pH conveys ammonia resistance in *Spirulina platensis*. *Bioresource Technology*, 38(2-3): 167-169.

Bennett, A., Bogorad, L. (1973). Complementary Chromatic Adaptation in A Filamentous Blue-Green-Alga. *Journal of Cell Biology*, 58(2):, 419-435.

Berkovich, Y.A., Chetirkin, P.V., Wheeler, R.M., Sager, J.C. (2004). Evaluating and optimizing horticultural regimes in space plant growth facilities. *Advances in Space Research*, 34(7): 1612-1618.

Bhattacharya, S., Shivaprakash, M. (2005). Evaluation of three *Spirulina* species grown under similar conditions for their growth and biochemicals. *Journal of the Science of Food and Agriculture*, 85(2):333-336.

Bie, Z., Ito, T., Shinohara, Y. (2004). Effects of sodium sulfate and sodium bicarbonate on the growth, gas exchange and mineral composition of lettuce. *Scientia Horticulturae*, 99(3-4): 215-224.

Binaghi, L., del Borghi, A., Lodi, A., Converti, A., del Borghi, M. (2003). Batch and fed-batch uptake of carbon dioxide by *Spirulina platensis*. *Process Biochemistr*y, 38(9): 1341-1346.

Boussiba, S., Gibson, J. (1991). Ammonia Translocation in Cyanobacteria. *FEMS Microbiology Reviews*, 88(1): 1-14.

Bourges, S., Sotomayor, A., Mendoza, E., Chavoz, A. (1971). Utilization of the alga *Spirulina* as a protein source. *Annales de la Nutrition et de Alimentation*, 29:143-147.

Box, G.E.P., Hunter, W.G., Hunter, J.S. (1978). Statistics for experimenters. Ed. John Wiley & Sons, New York.

Bugbee, B.G., Salisbury, F.B. (1989). Current and potential productivity of wheat for a controlled environment life support system. *Advances in Space Research*, 9: 5-15.

Burton, K. (1956). A study of the conditions and mechanism of the diphenylamine reaction for the colorimetric estimation of deoxyribonucleic acid. *Biochemical Journal*, 62: 315–323.

C

Cabello, F. (2007). Cultivo en birreactores de *Rhodospirillum rubrum* en condiciones fotoheterotróficas. Tesis Doctoral. Universitat Autònoma de Barcelona.

Cannell, M.G.R., Thornley, J.H.M. (2000). Modelling the components of plant respiration: some guiding principles. *Annals of Botany*, 85(1): 45-54.

Cañizares-Villanueva, R.O., Domínguez, A.R., Cruz, M.S., Rios-Leal, E. (1995). Chemical composition of cyanobacteria grown in diluted, aerated swine wastewater. *Bioresource Technology*, 51(2-3):111-116.

Carvalho, J.C.M., Francisco, F.R., Almeida, K.A., Sato, S., Converti, A. (2004). Cultivation of *Arthrospira* (*Spirulina*) *platensis* (Cyanophyceae) by fed-batch addition of ammonium chloride at exponentially increasing feeding rates. *Journal of Phycology*, 40(3): 589-597.

Cern, M.C., Sánchez, A., Fernández, J M., Molina, E., García, F. (2005). Mixotrophic growth of the microalga *Phaeodactylum tricornutum*: Influence of different nitrogen and organic carbon sources on productivity and biomass composition. *Process Biochemistry*, 40(1): 297-305.

Chen, F., Zhang, Y. (1997). High cell density mixotrophic culture of *Spirulina platensis* on glucose for phycocyanin production using a fed-batch system. *Enzyme and Microbial Technology*, 20(3): 221-224.

Chen, T., Zheng, W., Wong, Y. S., Yang, F., Bai, Y. (2006). Accumulation of selenium in mixotrophic culture of *Spirulina platensis* on glucose. *Bioresource Technology*, 97(18): 2260-2265.

Chojnacka, K., Noworyta, A. (2004). Evaluation of *Spirulina sp*. growth in photoautotrophic, heterotrophic and mixotrophic cultures. *Enzyme and Microbial Technology*, 34(5): 461-465.

Chung, C. (2004). Analysis. In: Simulation Modeling Handbook: A practical approach. Series: Industrial and manufactruing engineering. Ed. Parsaei, H. CRC Press LLC, Boca Raton, Florida.

Ciferri, O. (1983). *Spirulina*, the edible microorganism. *Microbiological Reviews*, 47: 551-578.

Ciferri, O., Tiboni, O. (1985). The biochemistry and industrial potential of *Spirulina*. Annual *Review of Microbiology*, 39: 503-526.

Collatz, G.J., Berry, J.A., Farquhar, G.D., Pierce, J. (1990). The relationship between the Rubisco reaction mechanism and models of photosynthesis. *Plant, Cell & Environment*, 13(3): 219-225.

Cogne, G., Gros, J.B., Dussap, C.G. (2003). Identification of a metabolic network structure representative of *Arthrospira (Spirulina) platensis* metabolism. *Biotechnology and Bioengineering*, 84(6): 667-676.

Converti, A., Scapazzoni, S., Lodi, A., Carvalho, C.M. (2006). Ammonium and urea removal by *Spirulina platensis*.*Journal of Industrial Microbiology and Biotechnology*, 33(1): 8-16.

Cornet, J.F., Dussap, C.G., Dubertret, G. (1992a). A Structured Model for Simulation of Cultures of the Cyanobacterium *Spirulina platensis* in Photobioreactors 1: Coupling Between Light Transfer and Growth-Kinetics. *Biotechnology and Bioengineering*, 40(7): 817-825.

Cornet, J.F., Dussap, C.G., Cluzel, P., Dubertret, G. (1992b). A Structured Model for Simulation of Cultures of the Cyanobacterium *Spirulina platensis* in Photobioreactors 2: Identification of Kinetic-Parameters Under Light and Mineral Limitations. *Biotechnology and Bioengineering*, 40(7): 826-834.

Cornet, J.F., Dussap, C.G. Gross, J.B. (1998) Kinetics and energetics of photosynthetic microorganisms in photobioreactors: Application to *Spirulina* growth. *Advances in biochemical Engineering*, 59: 153-224.

Costa, J.A.V., Cozza, K.L., Oliveira, L., Magagnin, G. (2001). Different nitrogen sources and growth responses of *Spirulina platensis* in microenvironments. *World Journal of Microbiology and Biotechnology*, 17(5): 439-442.

Costa, J.A.V., Colla, L.M., Duarte, P., Kabke, K., Weber, A. (2002). Modelling of *Spirulina platensis* growth in fresh water using response surface methodology. *World Journal of Microbiology & Biotechnology*, 18(7): 603-607.

Costa, J.A.V., Colla, L.M., Duarte, P.F. (2004). Improving *Spirulina platensis* biomass yield using a fed-batch process. *Bioresource Technology*, 92(3): 237-241.

Creus, N. (2003). Estudi d'un Bucle de Bioreactors pel Desenvolupament d'un Sistema de Suport de Vida Biològic. Memòria de Tesi Doctoral. Universitat Autònoma Barcelona.

D

Danesi, E.D.G., Rangel-Yagui, C.O., Carvalho, J.C.M., Sato, S. (2002). An investigation of effect of replacing nitrate by urea in the growth and production of chlorophyll by *Spirulina platensis*. *Biomass and Bioenergy*, 23(4): 261-269.

Danesi, E.D.G., Rangel-Yagui, C.O., Carvalho, J.C.M., Sato, S. (2004). Effect of reducing the light intensity on the growth and production of chlorophyll by *Spirulina platensis*. *Biomass and Bioenergy*, 26(4): 329-335.

Dangeard, P. (1940). Sur une algue bleue alimentaire pour l'homme. Actes de la Société Linnéenne de Bordeaux, 91: 39–41.

Davis, T.L., Nielsen, S.S., Mitchell, C. (1988). Interactive effects of CO_2 enrichment, radiation enhancement, and nitrogen form and level on growth and nutritional values of leaf lettuce. *Hortscience*, 23(3):765.

Demmers-Derks, H., Mitchell, R.A.C., Mitchell, V.J., Lawlor, D.W. (1998). Response of sugar beet (*Beta vulgaris* L.) yield and biochemical composition to elevated CO_2 and temperature at two nitrogen applications. *Plant, Cell & Environmen*t, 21(8): 829-836.

Dent, K.C., Stephen, J.R., Finch-Savage, W.E. (2004). Molecular profiling of microbial communities associated with seeds of *Beta vulgaris* (sugar beet). *Journal of Microbiological Methods*, 56(1): 17-26.

Dixon, M.A., Grodzinski, B., Côté,R., Stasiak, M. 1999. Sealed environment chamber for canopy light interception and trace hydrocarbon analyses. *Advances in Space Research*, 24: 271-280.

Drake, B.G., Gonzalez, M.A., Long, S.P. (1997). More efficient plants: A consequence of rising atmospheric CO_2? *Annual Review of Plant Physiology and Plant Molecular Biology*, 48: 609-639.

Dubois, M., Gilles, K.A., Hamilton, J.K., Reberts, P.A. (1956). Colorometric method for determination of sugars and related substances. *Analytical Chemistry*, 28: 350-356.

Dutton, R.G., Jiao, J., Tsujita, M.J., Grodzinski, B. (1988). Whole plant CO_2 exchange measurements for nondestructive estimation of growth. *Plant Physiology*, 86(2): 355-358.

E

Emeis, J.J, Lasseur, Ch. (2006). Cholesterol-lowering preparation, food supplement and foodstuff, and methods for preparing same. United States Patent Publication US2006/0127362-A1.

Estrada, J.E.P., Bescos, P.B., del Fresno, A.M.V. (2001). Antioxidant activity of different fractions of *Spirulina platensis* protean extract. *Farmaco*, 56(5-7):497-500.

Ewert, F. (2004). Modelling plant responses to elevated CO_2: How important is leaf area index?. *Annals of Botany*, 93(6): 619-627.

F

Farrar, W.V. (1966). Tecuitlatl: A glimpse of Aztec food technology. *Nature*, 211: 341–342.

Farquhar, G.D., von Caemmerer, S., Berry, J.A. (1980). A biochemical model of photosynthetic CO_2 assimilation in leaves of C_3 plants. *Planta*, 149: 78-90.

Farquhar, G.D., von Caemmerer, S., Berry, J.A. (2001). Models of photosynthesis. *Plant Physiology*, 125(1): 42-45.

Ferentinos, K.P., Albright, L.D., Ramani, D.V. (2000). Structures and environment: optimal light integral and carbon dioxide concentration combinations for lettuce in ventilated greenhouses. *Journal of Agricultural Engineering Research*, 77(3): 309-315.

Filali-Mouhim, R., Lasseur, Ch., Dubertret, G. (1997). MELiSA: nitrogen sources for growth of the cyanobacterium *Spirulina*. Proceedings of the 6th European Symposium on Space Environmental Control Systems. ESA Special Publications, 400 (1-2):909-912.

Flores, E., Herrero, A. (1994). Assimilatory nitrogen metabolism and its regulation. In The Molecular Biology of Cyanobacteria. Ed. A. Bryant, pp. 487–517. Kluwer Academic Publishers, Dordrecht.

G

Ganong, W.F. (1977). Review of medical physiology. Ed. Lange Medical Publications, New York, USA.

Gao, Q., Zhang, X., Huang, Y., Xu, H. (2004). A comparative analysis of four models of photosynthesis for 11 plant species in the Loess Plateau. *Agricultural and Forest Meteorology*, 126: 203–222.

Gauer, L.E., Grant, C.A., Gehl, D.T., Bailey, L.D. (1992). Effects of nitrogen fertilization on grain protein content, nitrogen uptake and nitrogen use efficiency of six spring wheat (*Triticum aestivum* L.) cultivars, in relation to estimated moisture supply. *Canadian Journal of Plant Science*, 72: 235-241.

Ghoulam, C., Foursy, A., Fares, K. (2002). Effects of salt stress on growth, inorganic ions and proline accumulation in relation to osmotic adjustment in five sugar beet cultivars. *Environmental and Experimental Botany*, 47(1): 39-50.

Gòdia, F., Albiol, J., Montesinos, J. L., Pérez, J., Creus, N., Cabello, F., Mengual, X., Montràs, A., Lasseur, C. (2002). MELiSSA: a loop of interconnected bioreactors to develop life support in space. *Journal of Biotechnology*, 99(3): 319-330.

Gòdia, F., Albiol, J., Pérez, J., Creus, N., Cabello, F., Montràs, A., Masot, A., Lasseur, Ch. (2004). The MELiSSA Pilot Plant Facility As An Integration Test-Bed For Advanced Life Support Systems. *Advances in Space Research*, 34(7): 1483-1493.

Goins, G., Ruffe, L., Cranston, N., Yorio, N., Wheeler, R., Sager, J. (2001). Salad crop production under different wavelengths of red light emitting diodes (LEDs). Proceedings of the 31st International Conference on Environmental Systems (ICES), SAE paper No. 2001-01-2422.

Goins, G. (2002). Growth, stomatal conductance, and leaf surface temperature of swiss chard grown under different artificial lighting technologies. Proceedings of the 32nd International Conference on Environmental Systems (ICES), SAE paper No. 2002-01-2338.

Gomes, F.P., Oliva, M.A., Mielke, M.S., de Almeida, A.A.F., Leite, H.G. (2006). Photosynthetic irradiance-response in leaves of dwarf coconut palm (*Cocos nucifera* L. '*nana*', *Arecaceae*): Comparison of three models. *Scientia Horticulturae*, 109(1): 101-105.

Gompertz, B. (1825). On the nature of the function expressive of the law of human mortality. Philosophical Transactions of the Royal Society of London 36: 513-585.

Gordillo, F.J.L., Jiménez, C., Figueroa, F.L., Niell, F.X. (1998). Effects of increased atmospheric CO_2 and N supply on photosynthesis, growth and cell composition of the cyanobacterium *Spirulina platensis* (*Arthrospira*). J*ournal of Applied Phycology*, 10(5): 461-469.

Guerrero, M.G., Lara, C. (1987). Assimilation of inorganic nitrogen. In: The cyanobacteria. Ed. Elsevier Science Publisher, Amsterdam.

H

Hanaki, K., Wantawin, C., Ohgaki, S. (1990). Nitrification at low levels of disolved oxigen with and without organic loading in suspended-growth reactor. *Water Research*, 24: 297-302.

Hanford, A., Ewert, M. (2006). Exploration life support baseline values and assumptions document. NASA Contract Report 2006-213693.

Hansen, T. A, Germerden, H. (1972). Suplhide utilization by purple nonsulfur bacteria. *Archives of Microbiology*, 86: 49-56.

Herbert, T.D., Philiphs, P.J., Strange, R.E. (1971). Chemical analysis of microbial cells. *Methods in microbiology*, 5(b): 209-344.

Herrero, A., Muro-Pastor, A.M., Flores, E. (2001). Nitrogen control in cyanobacteria. *Journal of Bacteriology*, 183: 411–425.

Hirata, S., Hata, J.I., Taya, M., Tone, S. (1997). Evaluation of *Spirulina platensis* growth considering light intensity distribution in photoautotrophic batch culture. *Journal of Chemical Engineering of Japan*, 30(2): 355-359.

Hirata, S., Taya, M., Tone, S. (1998). Continuous cultures of *Spirulina platensis* under photoautotrophic conditions with change in light intensity. *Journal of Chemical Engineering of Japan*, 31(4): 636-639.

Hoagland, D.R., Arnon, D.I. (1950). The water culture method for growing plants without soil. California Agricultural Experiment Station Circular 347.

Hoff, J.E., Howe, J.M., Mitchell, C.A. (1982). Nutritional and cultural aspects of plant species selection for a regenerative life support system. NASA Contract Report 2982-166324.

Hunik, J.H., Bos, C.G., Den Hoogen, M.P., De Gooijer, C.D., Tramper, J. (1994). Co-inmmobilized *Nitrosomonas europaea* and *Nitrobacter agilis* cells: validation of a dynamic model for simultaneous substrate conversion and growth in K-carrageenan gel beads. *Biotechnology and Bioengineering*, 43: 1153-1163.

Hunt, R. (1982). Plant Growth curves: the functional approach to plant growth analysis. University Park Press, Baltimore.

I

Ingestad, T., Agren G.I. (1988). Nutrient uptake and allocation at steady state nutrition. *Physiologica Plantae*, 72: 450-459.

J

Jassby, A. (1988). *Spirulina*: A Model for Microalgae as Human Food. In: Algae and human affairs. Ed. by Lembi and Waaland, Cambridge University Press. Cambridge, UK.

Jensen, S., Knutsen, G. (1993). Influence of light and temperature on photoinibition of photosynthesis in *Spirulina platensis*. J*ournal of Applied Phycology*, 5: 495–504.

Jiménez, C., Cossio, B.R., Labella, D., Xavier Niell, F. (2003). The Feasibility of industrial production of *Spirulina* (*Arthrospira*) in Southern Spain. *Aquaculture*, 217(1-4): 179-190.

Jones, H., Cavazzoni, J., Keas, P. (2002). Crop Models for varying environmental conditions. Proceedings of the 32nd International Conference on Environmental Systems (ICES), SAE paper No. 2002-01-2520.

K

Källqvist, T., Svenson, A. (2003). Assessment of ammonia toxicity in tests with the microalga, *Nephroselmis pyriformis*, Chlorophyta. *Water Research*, 37(3): 477-484.

Kebede, E. (1997). Response of *Spirulina platensis* (= *Arthrospira fusiformis*) from Lake Chitu, Ethiopia, to salinity stress from sodium salts. *Journal of Applied Phycology*, 9(6), 551-558.

Kibe, S., Suzuki, K., Ashida, A., Otsubo, K., Nitta, K. (1997). Controlled Ecological Life Support System. Related Activites in Japan. *Life Support & Biosphere Science*, 4: 117-125.

Kim, H.H., Goins, G.D., Wheeler, R.M., Sager, J.C. (2004). Stomatal conductance of lettuce grown under or exposed to different light qualities. *Annals of Botany*, 94(5): 691-697.

Kitaya, Y., Shibuya, T., Yoshida, M., Kiyota, M. (2004). Effects of air velocity on photosynthesis of plant canopies under elevated CO_2 levels in a plant culture system. *Advances in Space Research*, 34(7):1466-9.

Knecth, G.N., O'Leary, J.W. (1983). The influence of carbon dioxide on growth, piment, protein, carbohydrate and mineral statues of lettuce. *Journal of Plant Nutrition*, 6: 301-312.

Knight, S.L., Mitchell, C.A. (1988). Effects of CO_2 and photosynthetic photon flux on yield, gas exchange and growth rate of *Lactuca sativa* l. 'Waldmann's Green'. J*ournal of Experimental Botany*, 39:317-328.

Kompatseva, E. I. (1981). Utilization of sulfide by nonsulfur purple bacteria *Rhodopseudomonas capsulata*. *Microbiologia*, 50: 429-436.

L

Lane, H.W., Shoeller, D.A. (1999). Nutrition in Spaceflight and weightlessness models. CRC Press. ISB-0849385679.

Langhans, R., Tibbits, T. (1997). Plant Growth Chamber Handbook. Project NCR-101, Controlled Environment Technology and Uses. North Central Regional Research Publication No. 340. Iowa Agriculture and Home Economics Experiment Station Special Report No. 99. Iowa State University, USA. ISSN: 0361-199X.

Larsen, R.U., Hiden, C. (1995). Predicting leaf unfolding in flower induced shoots of greenhouse grown chrysanthemum. *Scientia Horticulturae*, 63(3-4): 225-239.

Lasseur, Ch., Fedele, I. (2000). MELiSSA: Final report for 1999 activity: Memorandum of understanding ECT/FG/MMM/97.012. Prepared by the MELiSSA Partners. ESA/EWP-2092.

Lasseur, Ch., Paillé, C. (2001). MELiSSA: Final report for 2000 activity: Memorandum of understanding ECT/FG/MMM/97.012. Prepared by the MELiSSA Partners. ESA/EWP-2168.

Lasseur, Ch., Vieira da Silva, L. (2005). MELiSSA: Final report for 2004 activity: Memorandum of understanding TOS-MCT/2002/3161/In/CL. Prepared by the MELiSSA Partners. ESA/EWP-2287.

Lasseur, Ch., Paillé, C., Lamaze, B., Rebeyre, P., Rodriguez, A., Ordoñez, L., Marty, F. (2005). MELISSA: Overview of the Project and Perspectives. Proceedings of the 35th International Conference on Environmental Systems (ICES). SAE paper No. 2005-01-3066.

Lattenmayer, C. (2001). Preliminary evaluation of growth kinetics with ammonium as nitrogen source in the photoautotrophic compartment of MELiSSA. EWP-2127.ESTEC.

Le Bot, J., Adamowicz, S., Robin, P. (1998). Modelling plant nutrition of horticultural crops: a review. *Scientia Horticulturae*, 74(1-2): 47-82.

Lehninger, A., Nelson, D. L., Cox, M. M. (2004). Principles of Biochemistry. 4th edition. WH Freeman. ISBN-0-7167-4339-6.

Lehto, K. A., Lehto, H. J., Kanervo, E. A. (2006). Suitability of different photosynthetic organisms for an extraterrestrial biological life support system. *Research in Microbiology*, 157(1): 69-76.

Linker, R., Seginer, I., Buwalda, F. (2004). Description and calibration of a dynamic model for lettuce grown in a nitrate-limiting environment. *Mathematical and Computer Modelling*, 40(9-10), 1009-1024.

Linker, R., Johnson-Rutzke, C. (2005). Modeling the effect of abrupt changes in nitrogen availability on lettuce growth, root-shoot partitioning and nitrate concentration. *Agricultural Systems*, 86(2): 166-189.

Liotenberg, S., Campbell, D., Rippka, R., Houmard, J., Marsac, N.T. (1996). Effect of the nitrogen source on phycobiliprotein synthesis and cell reserves in a chromatically adapting filamentous cyanobacterium. *Microbiology*, 142: 611-622.

Lodi, A., Binaghi, L., Solisio, C., Converti, A., Borghi, M. (2003). Nitrate and phosphate removal by *Spirulina platensis*. J*ournal of Industrial Microbiology and Biotechnology*, 30(11): 656-660.

M

Mackowiak, C.L., Wheeler, R.M. (1996). Growth and stomatal behavior of hydroponically cultured potato (*Solanum tuberosum* L) at elevated and super-elevated CO_2. *Journal of Plant Physiology*, 149(1-2): 205-210.

Mahn, K., Hoffmann,C., Marlander, B. (2002). Distribution of quality components in different morphological sections of sugar beet (*Beta vulgaris* L.). *European Journal of Agronomy*, 17: 29-39.

Marcelis, L.F.M., Heuvelink, E., Goudriaan, J. (1998). Modelling biomass production and yield of horticultural crops: a review. *Scientia Horticulturae*, 74(1-2), 83-111.

Marino, B. D. V., Mahato, T. R., Druitt, J. W., Leight, L., Lin, G. H., Russell, R. M., Tubiello, F. N. (1999). The agricultural biome of Biosphere 2: Structure, composition and function. *Ecological Engineering*, 13(1-4): 199-234.

Marquez, F.J., Sasaki, K., Kakizono, T., Nishio, N., Nagai, S. (1993). Growth characteristics of *Spirulina platensis* in mixotrophic and heterotrophic conditions. *Journal of Fermentation and Bioengineering*, 5: 408-410.

Marquez, F. J., Nishio, N., Nagai, S., Sasaki, K. (1995). Enhancement of biomass and pigment production during growth of *Spirulina platensis* in mixotrophic culture. *Journal of Chemical Technology & Biotechnology*, 62: 159–164

Marschner, H. (1995). Mineral Nutrition of Higher Plants. 2nd Edition. Academic Pres Inc. London.

Marty, A. (1997). Etude et modélisation du comportement de *Spirulina platensis* en photobioréacteur en condition de limitation par la lumière et la source de carbone. Thèse de doctorat. Université Blaise Pascal, Clermont-Ferrand, France.

Maslova, I.P., Mouradyan, E.A., Lapina, S.S., Klyachko-Gurvich, G.L., Los, D.A. (2004). Lipid fatty acid composition and thermophilicity of cyanobacteria. *Russian Journal of Plant Physiology*, 51(3):353-360.

Masojidek, J., Papacek, S., Sergejevova, M., Jirka, V., Cerveny, J., Kunc, J., Korecko, J., Verbovikova, O., Kopecky, J., Stys, D., Torzillo, G. (2003). A closed solar photobioreactor for cultivation of microalgae under supra-high irradiance: basic design and performance. *Journal of Applied Phycology*, 15(2-3): 239-248.

Masot, A. (2004). Anàlisi i disseny del Compartiment de Plantes Superiors d'un Sistema de Suport de Vida Biològic. Memoria treball de Master en Biotecnologia. Universitat Autònoma de Barcelona.

Mathieu, J., Linker, R., Levine, L., Albright, L., Both, A.J., Spanswick, R., Wheeler, R., Wheeler, E., deVilliers, D., Langhans, R. (2006). Evaluation of the Nicolet model for simulation of short-term hydroponic lettuce growth and nitrate uptake. *Biosystems Engineering*, 95(3): 323-337.

McKeehen, J.D. (1994). Nutrient content of select controlled ecological life-support system candidate species grown under field and controlled environment conditions. PhD Thesis. University of Purdue, West Lafayette, IN, USA.

Medlyn, B.E., Dreyer, E., Ellsworth, D., Forstreuter, M., Harley, P.C., Kirschbaum, M.U.F., Le Roux, X., Montpied, P., Strassemeyer, J., Walcroft, A., Wang, K., Loustau, D. (2002). Temperature response of parameters of a biochemically based model of photosynthesis II: A review of experimental data. *Plant, Cell & Environment*, 25(9): 1167-1179.

Mergeay, M., Verstraete, W., Dubertret, G., Lefort-tran, M., Chipaux, C., Binot, R. (1998). MELiSSA: A microorganisms based model for CELSS development. Proceedings of the 3rd Symposium on Space Thermal Control and Life Support Systems, pp. 65–68.

Mertens, D.R. (2002). Gravimetric determination of amylase-treated neutral detergent fiber in feeds with refluxing in beakers or crucibles: collaborative study. *Journal of AOAC international*, 85 (6): 1217-1240.

Miller, S.R., Martin, M., Touchton, J., Castenholz, R.W. (2002). Effects of nitrogen availability on pigmentation and carbon assimilation in the cyanobacterium *Synechococcus sp* strain SH-94-5. *Archives of Microbiology*, 177(5): 392-400.

Mitchell, C. A. (1994). Bioregenerative life-support systems. *American Journal of Clinical Nutrition*, 60: 820-824.

Molina, E., Fernández, J. M., Sánchez, J. A., García, F. G. (1996). A study on simultaneous photolimitation and photoinhibition in dense microalgal cultures taking into account incident and averaged irradiances. *Journal of Biotechnology*, 45(1): 59-69.

Molina, E., Fernández, F.G.A., García, F., Chisti, Y. (1999). Photobioreactors: light regime, mass transfer, and scaleup. *Journal of Biotechnology*, 70(1-3): 231-247.

Monje, O., Bugbee, B. (1998). Adaptation to high CO_2 concentration in an optimal environment: radiation capture, canopy quantum yield and carbon use efficiency. *Plant, Cell & Environment*, 21(3): 315-324.

Monsi, M., Saeki, T. (1953). Über den lichtfaktor in den pflanzengesellschaften und seine bedeutung für die stoffproduktion. *Japanese Journal of Botany*, 14: 22-52.

Montgomery, D.C. (1991). Design and analysis of experiments. Third Edition. John Wiley & Son, Inc. New York. ISBN: 0-471-52994-x.

Montràs, A. (2003). Anàlisi en línia d'amoni i nitrat en un reactor de llit fix per a la nitrificació biològica. Memòria Treball de Màster. Universitat Autònoma Barcelona.

Morist, A., Montesinos, J.L., Cusidó, J.A., Gòdia, F. (2001). Recovery and treatment of *Spirulina platensis* cells cultured in a continuous photobioreactor to be used as food. *Process Biochemistry*, 37(5): 535-547.

Mühling, M., Belay, A., Whitton, B. (2005a). Screening *Arthrospira* (*Spirulina*) strains for heterotrophy. *Journal of Applied Phycology*, 17(2): 129-135.

Mühling, M., Belay, A., Whitton, B.A. (2005b). Variation in fatty acid composition of *Arthrospira* (*Spirulina*) strains. *Journal of Applied Phycology*, 17(2):137-146.

Muro-Pastor, M.I., Florencio, F.J. (2003). Regulation of ammonium assimilation in cyanobacteria. *Plant Physiology and Biochemistry*, 41(6-7): 595-603.

N

Nollet, L.M.L. (2004). Handbook of Food analysis. 2 edition, CRC Press.

O

Olabi, A., Hunter, J. B. (1999). Cost and quality of a bioregenerative diet. Proceedings of the 29th International Conference on Environmental Systems (ICES), SAE paper No 1999-01-2077.

Olguín, E.J., Galicia, S., Angulo-Guerrero, O., Hernández, E. (2001). The effect of low light flux and nitrogen deficiency on the chemical composition of *Spirulina sp*. (*Arthrospira*) grown on digested pig waste. *Bioresource Technology*, 77(1): 19-24.

de Oliveira, M.A.C.L., Monteiro, M.P.C., Robbs, P.G., Leite, S.G.F. (1999). Growth and chemical composition of *Spirulina maxima* and *Spirulina platensis* biomass at different temperatures. *Aquaculture International*, 7(4):261-275.

Ortega, J. J., Mazuelos, C., Hermosin, B., Saiz, C. (1993). Chemical composition of *Spirulina* and eukaryotic algae food products marketed in Spain. *Journal of applied Phycology*, 4: 425–35.

P

Pachepsky, L.B., Haskett, J.D., Acock, B. (1996a). An adequate model of photosynthesis 1: Parameterization, validation and comparison of models. *Agricultural Systems*, 50(2): 209-225.

Pachepsky, L.B., Acock, B. (1996b). An adequate model of photosynthesis 2: Dependence of parameters on environmental factors. *Agricultural Systems*, 50(2): 227-238.

Palmegiano, G.B., Agradi, E., Forneris, G., Gai, F., Gasco, L., Rigamonti, E., Sicuro, B., Zoccarato, I. (2005). *Spirulina* as a nutrient source in diets for growing sturgeon (Acipenser baeri). *Aquaculture Research*, 36(2):188-195.

Paoletti, C., Pushparaj, B., Tomaselli, L. (1975). Ricerche sulla nutrizione minerale di *Arthrospira platensis*. In: Italian Society of Microbiology (ed) Atti del XVII congresso della Societa Italiana de Microbiologia. Padua, Italy, pp 833–839.

Patel, R.K., Dodia, M.S., Joshi, R.H., Singh, S.P. (2005). Purification and characterization of alkaline protease from a newly isolated haloalkaliphilic *Bacillus sp*. *Process Biochemistry*, 41(9): 2002-2009.

Patel, A., Mishra, S., Pawar, R., Ghosh, P.K. (2005). Purification and characterization of c-phycocyanin from cyanobacterial species of marine and freshwater habitat. *Protein Expression and Purification*, 40: 248-255.

Pelizer, L.H., Danesi, E.D., Rangel, C.D., Sassano, C.E.N., Carvalho, J.C., Sato, S., Moraes, I.O. (2003). Influence of inoculum age and concentration in *Spirulina platensis* cultivation. *Journal of Food Engineering*, 56(4): 371-375.

Pérez, J. (2001). Utilización of *Nitrosomonas* y *Nitrobacter* en forma de biopelícula para la nitrificación biológica de lecho fijo. Tesis Doctoral. Universitat Autònoma de Barcelona.

Peri, P.L., Moot, D.J., McNeil, D.L. (2005). Modelling photosynthetic efficiency for the light-response curve of cocksfoot leaves grown under temperate field conditions. *European Journal of Agronomy*, 22(3): 277-292.

Pervushkin, S.V., Voronin, A.V., Kurkin, V.A., Sokhina, A.A., Shatalaev, I.F. (2001). Proteins from *Spirulina platensis* biomass. *Chemistry of Natural Compounds*, 37(5):476-481.

Piorreck, M., Baasch, K.H., Pohl, P. (1984). Biomass production, total protein, chlorophylls, lipids and fatty acids of freshwater green and blue-green algae under different nitrogen regimes. *Phytochemistry*, 23(2):207-216.

Poughon, L., Gros, J.B., Dussap, C.G. (2000). MELiSSA Loop: First Estimate of Flow Rates and Concentrations Through the Loop. Proceedings of the 30th International Conference on Environmental Systems (ICES), SAE paper No. 2000-01-2380.

Pulz, O., Gross, W. (2004). Valuable products from biotechnology of microalgae. *Applied Microbiology and Biotechnology*, 65(6): 635-648.

R

Rangel-Yagui, C.O., Danesi, E.D.G., Carvalho, J.C.M., Sato, S. (2004). Chlorophyll production from *Arthrospira platensis*: cultivation with urea addition by fed-batch process. *Bioresource Technology*, 92(2): 133-141.

Richmond, A., Grobbelaar, J.U. (1986). Factors affecting the output rate of *Spirulina platensis* with reference to mass cultivation. *Biomass*, 10(4): 253-264.

Richmond, A. (1986). Principles of pond maintenance. In: Handbook of Microalgal Mass Cultures. CRC Press.

Richmond, A. (1988). *Spirulina*. In: Microalgal Biotechnology, pp 83-121. Ed. Borowitzka M.A., Borowitzka, L.J., Cambridge University Press, Cambridge, UK.

Rodriguez, D., Ewert, F., Goudriaan, J., Manderscheid, R., Burkart, S., Weigel, H.J. (2001). Modelling the response of wheat canopy assimilation to atmospheric CO_2 concentrations. *New Phytologist*, 150(2): 337-346.

S

Salisbury, F.B., Bugbee, B., Bubenheim, D. (1987). Wheat production in controlled environments. *Advances in Space Research*, 7: 123-132.

Salisbury, F.B., Gitelson, J.I., Lisovsky, G.M. (1997). Bios-3: Siberian Experiment in Bioregenerative Life Support. *BioScience*, 47(9).

Samuelson, G., Lönneborg, A., Rosenqvist, E., Gustafsson, P., Öquist, G. (1985). Photoinhibition and reactivation of photosynthesis in the cyanobacteria *Anacystis nidulans*. *Plant Physiology*, 79: 992-995.

Sánchez, A., Cerón, M. C., García, F., Molina, E., and Chisti, Y. (2002). Growth and biochemical characterization of microalgal biomass produced in bubble column and airlift photobioreactors: studies in fed-batch culture. *Enzyme and Microbial Technology*, 31(7): 1015-1023.

Sassano, C.E.N., Carvalho, J.C.M., Gioielli, L.A., Sato, S., Torre, P., Converti, A. (2004). Kinetics and bioenergetics of *Spirulina platensis* cultivation by fed-batch addition of urea as nitrogen source. *Applied Biochemistry and Biotechnology*, 112:143–150.

Schlösser, U.G. (1982). Sammlung von Algenkulturen. Berichte der Deutschen Botanischen Gesellschaft, 95:181–276.

Seginer, I. (2003). A dynamic model for nitrogen-stressed lettuce. *Annals of Botany*, 91(6): 623-635.

Seginer, I., Albright, L.D., Ioslovich, I. (2006). Improved strategy for a constant daily light integral in greenhouses. *Biosystems Engineering*, 93(1): 69-80.

Sesták, Z. (1971). Determination of chlorophylls a and b. In: Plant Photosynthetic Production: Manual of Methods, pp. 672–701. Ed. Sesták, Z., Catsky, J., Jarvis, P. G. Publ Dr. Junk, The Hague, The Netherlands.

Siegelman, H.W., Kycia, J.H. (1982). Molecular morphology of cyanobacterial phycobilisomes. *Plant Physiology*, 70(3):887-897.

Shekharam, K., Ventakaraman, L., Salimath, P. (1987). Carbohydrate composition and characterization of two unusual sugars from the blue-green algae *Spirulina platensis*. *Phytochemistry*, 26: 2267-2269.

Shimamatsu, H. (2004). Mass production of *Spirulina*, an edible microalga. *Hydrobiologia*, 512(1-3): 39-44.

Shizhong, L., Xueming, L., Feng, C., Zijian, C. (2004). Current microalgal health food R & D activities in China. *Hydrobiologia*, 512(1): 45-48.

Siegelman, H. W., Kycia, J. H. (1982). Molecular Morphology of Cyanobacterial Phycobilisomes. *Plant Physiology*, 70(3): 887-897.

Silverstone, S.E., Nelson, M. (1996). Food production and nutrition in Biosphere 2: Results from the first mission September 1991 to September 1993. *Advances in Space Research*, 18(4-5): 49-61.

Silverstone, S. E., Harwood, R. R., Franco-Vizcaino, E., Allen, J., Nelson, M. (1999). Soil in the agricultural area of Biosphere 2 (1991-1993). *Ecological Engineering*, 13(1-4): 179-188.

Smart, D. R., Ritchie, K., Bloom, A. J., Bugbee, B.B. (1998). Nitrogen balance for wheat canopies (*Triticum aestivum* cv. Veery 10) grown under elevated and ambient CO_2 concentrations. *Plant Cell and Environment*, 21: 753-763.

Smolders, G.J.F., van der Meij, J., van Loosdrecht, M.C.M., Heijnen, J.J. (1994), Stoichiometric model for the aerobic metabolism of the biological phosphorus removal process. *Biotechnology and Bioengineering*, 44(7): 837-848.

Soletto, D., Binaghi, L., Lodi, A., Carvalho, J.C.M., Converti, A. (2005). Batch and fed-batch cultivations of *Spirulina platensis* using ammonium sulphate and urea as nitrogen sources. *Aquaculture*, 243(1-4): 217-224.

Sosulki, F.W., Imafidon, G.I. (1990). Amino acid composition and nitrogen to protein conversion factors for animal and plant food. *Journal of Agriculture and Food Chemistry*, 38: 1351-1356.

Stanca, D., Popovici, E. (1996). Urea as nitrogen source in modified Zarrouk medium. Revue Roumaine de Biologie Série de Biologie Végétale, 41: 25–31.

Stasiak, M., Waters, G., Zheng, Y., Grodzinski, B., Dixon, M. (2003). Integrated multicropping of beet and lettuce and its effect on atmospheric stability. Proceedings of the 33rd International Conference on Environmental Systems (ICES), SAE paper No. 2003-01-2357.

Stutte, G.W., Wheeler, R.M. (1997). Accumulation and effect of volatile organic compounds in closed life support systems. *Advances Space Research*, 20(10): 1913-1922.

Stutte, G.W., Mackowiak, C.L., Yorio, N.C., Wheeler, R.M. (1997). Theoretical and practical considerations for staggered production of crops in a BLSS. *Advances in Space Research*, 20(10): 1851-1854.

Subbarao, G.V., Wheeler, R.M., Stutte, G.W., Levine, L.H. (1999). How far can sodium substitute for potassium in red beet?. *Journal of Plant Nutrition*, 22(11): 1745-1761.

Subbarao, G.V., Wheeler, R.M., Stutte, G.W., Levine, L.H. (2000). Low potassium enhances sodium uptake in red-beet under moderate saline conditions. *Journal of Plant Nutrition*, 23(10): 1449-1470.

Subbarao, G.V., Wheeler, R.M., Levine, L.H., Stutte, G.W. (2001). Glycine betaine accumulation, ionic and water relations of red-beet at contrasting levels of sodium supply. *Journal of Plant Physiology*, 158(6): 767-776.

Subbarao, G.V., Ito, O., Berry, W.L., Wheeler, R.M. (2003). Sodium - A functional plant nutrient. *Critical Reviews in Plant Sciences*, 22(5): 391-416.

T

Tadros, M.G., Smith, W., Joseph, B., Phillips, J. (1993). Yield and quality of cyanobacteria – *Spirulina maxima* in continuous culture in response to light intensity. Applied *Biochemistry and Biotechnology*, 39:337-347.

Taiz, L., Zeiger, E. (1998). Plant physiology. Second edition. Publ. Sinauer associates Inc., Sunderland, Massachussets, USA. ISBN: 0-87893-831-1.

Tam, N.F.Y., Wong, Y.S. (1996). Effect of ammonia concentrations on growth of *Chlorella vulgaris* and nitrogen removal from media. *Bioresource Technology*, 57(1): 45-50.

Tamponnet, C., Savage, C. (1994). Closed ecological systems. *Journal of Biological Education*, 28: 167-173.

Tei, F., Scaife, A., Aikman, D.P. (1996a). Growth of lettuce, onion, and red beet 1: Growth analysis, light interception, and radiation use efficiency. *Annals of Botany*, 78(5): 633-643.

Tei, F., Aikman, D.P., Scaife, A. (1996b). Growth of lettuce, onion and red beet 2: Growth modelling. *Annals of Botany*, 78(5): 645-652.

Thornley, J.H.M. (1998). Dynamic model of leaf photosynthesis with acclimation to light and nitrogen. *Annals of Botany*, 81(3): 421-430.

Thornley, J.H.M., Cannell, M.G.R. (2000). Modelling the components of plant respiration: representation and realism. *Annals of Botany*, 85(1): 55-67.

Thornley, J.H.M., Johnson, I.R. (2000). Plant and crop modeling: A mathematical approach to plant and crop physiology. Caldwell, Blackburn Press.

Thornley, J.H.M. (2002). Instantaneous canopy photosynthesis: analytical expressions for sun and shade leaves based on exponential light decay down the canopy and an acclimated non-rectangular hyperbola for leaf photosynthesis. *Annals of Botany*, 89(4): 451-458.

Tomaselli, L., Boldrini, G., Margheri, M.C. (1997). Physiological behaviour of *Arthrospira* (*Spirulina*) *maxima* during acclimation to changes in irradiance. *Journal of Applied Phycology*, 9(1):37-43.

Tortora, G.J., Grabowsky, S.R. (1992). Principles of Anatomy and physiology. 7ed. Publ. Harper Collins College Publishers, New York, USA.

Torzillo, G., Pushparaj, B., Bocci, F., Balloni, W., Materassi, R., Florenzano, G. (1986). Production of *Spirulina* biomass in closed photobioreactors. *Biomass*, 11(1): 61-74.

Travieso, L., Hall, D. O., Rao, K. K., Benítez, F., Sanchez, E., Borja, R. (2001). A helical tubular photobioreactor producing *Spirulina* in a semicontinuous mode. *International Biodeterioration & Biodegradation*, 47(3): 151-155.

Tubiello, F.N., Ewert, F. (2002). Simulating the effects of elevated CO_2 on crops: approaches and applications for climate change. *European Journal of Agronomy*, 18(1-2): 57-74.

U

USDA - United States Department of Agriculture (2005). National Nutrient Database for Standard Reference, Rel 18. Available online (www.nal.usda.gov/fnic/foodcomp/search/).

V

Van Henten, E.J. (1994). Validation of a dynamic lettuce growth model for greenhouse climate control. *Agricultural Systems*, 45(1): 55-72.

Van Oijen, M. (2002). On the use of specific publication criteria for papers on process-based modelling in plant science. *Field Crops Research*, 74(2-3): 197-205.

Venables, W.N., Ripley, B.D. (2002). Modern applied statistics with S-PLUS®. 4th Edition. Springer-Verlag New York Inc., New York, USA. ISBN 0-387-95457-0.

Vernerey, A. (2000). Conception, Controle et Fonctionnement d'un Photobioreacteur pour la culture en mode continu de la cyanobacterie *Spirulina platensis*. Memòria de Tesi Doctoral. Universitat Autònoma Barcelona i Université de Technologie Compiègne.

Vernerey, A., Albiol, J., Lasseur, C., Gòdia, F. (2001). Scale-Up and Design of a Pilot-Plant Photobioreactor for the Continuous Culture of *Spirulina platensis*. *Biotechnology Progress*, 17(3): 431-438.

Vonshak, A., Abeliovich, A., Boussiba, S., Arad, S., Richmond, A. (1982). Production of *Spirulina* biomass: Effects of environmental factors and population density. *Biomass*, 2(3): 175-185.

Vonshak, A., Richmond, A. (1988). Mass production of the blue-green alga *Spirulina*: An overview. *Biomass*, 15(4): 233-247.

Vonshak, A., Torzillo, G., Tomaseli, L. (1994). Use of chlorophyll fluorescence to estimate the effect of photoinhibition in outdoor cultures of *Spirulina platensis*. *Journal of Applied Phycology*, 6: 31– 34.

Vonshak, A. (1997). *Spirulina platensis (Arthrospira)*: Physiology, Cell Biology and Biotechnology. Taylor & Francis, London. ISBN 0-7484-0674-3.

Vonshak, A., Cheung, S. M., Chen, F. (2000). Mixotrophic growth modifies the response of *Spirulina (Arthrospira) platensis* (Cyanobacteria) cells to light. *Journal of Phycology*, 36(4): 675-679.

Volk, T., Bugbee, B., Wheeler, R. (1995). An approach to crop modelling with the Energy Cascade. *Life Support and Biosphere Science*. 1:119–127.

W

Walach, M.R., Bazin, M.J., Pirt, S.J., Balyuzi, H.H.M. (1987). Computer control of carbon-nitrogen-ratio in *S. platensis*. *Biotechnology and Bioengineering*, 29: 520–8.

Wang, Z. P., Zhao, Y. (2005). Morphological reversion of *Spirulina* (*Arthrospira*) *platensis* (Cyanophyta): from linear to helical. *Journal of Phycology*, 41(4): 911.

Watanabe, Y., Hall, D.O. (1996). Photosynthetic production of the filamentous cyanobacterium *Spirulina platensis* in a cone-shaped helical tubular photobioreactor. *Applied Microbiology and Biotechnology*, 44(6): 693-698.

Waters, G.R., Olabi, A., Dixon, M.A., Hunter, J.B., Lasseur, C. (2002). Bioregenerative food system cost based on optimized menus for advanced life support. *Life Support and Biosphere Science*, 8 (3-4): 199-210.

Waters, G.C.R. (2002). Dynamic modeling of the higher plant chamber as a component of bioregenerative life support systems. PhD Thesis. University of Guelph, Canada.

Waters, G., Gidzinski, D., Zheng, Y., Dixon, M. (2005). Empirical relationships between light intensity and crop NCER at leaf and full canopy scale: Towards integration of Higher Plant Chamber in MELiSSA. Proceedings of the 35th International Conference on Environmental Systems (ICES), SAE paper No. 2005-01-3071.

Watt, B.K., Merrill, A.L. (1975). Composition of foods. United States Department of Agriculture, Handbook no.8. Washington D.C, USA.

Wheeler, R.M., Mackowiak, C.L., Sager, J.C., Yorio, N.C., Knott, W.M., Berry, W.L. (1994). Growth and gas-exchange by lettuce stands in a closed, controlled environment. *Journal of the American Society for Horticultural Science*, 119(3): 610-615.

Wheeler, R.M., Mackowiak, C.L., Sager, J.C., Knott, W.M., Berry, W.L. (1996a). Proximate composition of CELSS crops grown in NASA's Biomass Production Chamber. *Advance in Space Research*, 18(4-5): 43-47.

Wheeler, R.M., Mackowiak, C.L., Stutte, G.W., Sager, J.C., Yorio, N.C., Ruffe, L. M., Fortson, R.E., Dreschel, T.W., Knott, W.M., Corey, K.A. (1996b). NASA's biomass production chamber: A testbed for bioregenerative life support studies. *Advance in Space Research*, 18(4-5): 215-224.

Wheeler, R.M. (1996c). Gas balance in a plant-based CELSS. In: Plants in Space Biology, pp. 207-216. Ed. Hiroshi Suge. Institute of Genetic Ecology, Tohoku University, Japan.

Wheeler, R.M., Mackowiak, C.L., Yorio, N.C., Sager, J.C. (1999). Effects of CO_2 on stomatal conductance: Do stomata open at very high CO_2 concentrations?. *Annals of Botany*, 83(3): 243-251.

Wheeler, R. M., Stutte, G. W., Subbarao, G. V., Yorio, N. C. (2001). Plant Growth and Human Life Support for Space Travel. In: Hanbook of Plant and Crop Physiology. Ed. Mohammad Pessarakli. Publ. Marcel Dekker Inc. New York, USA.

Wheeler, R.M., Sager, J.C., Prince, R.P., Knott, W.M., Mackowiak, C.L., Stutte, G.W., Yorio, N.C., Ruffe, L.M., Peterson, B.V., Goins, G.D., Hinkle, C.R., Berry, W.L. (2003). Crop production for advanced life support systems – Observations from the Kennedy Space Center Breadboard Project. NASA-TM-2003-211184, National Aeronautics and Space Administration, John F. Kennedy Space Center, Florida.

X

Xue, C., Hu, Y., Saito, H., Zhang, Z., Li, Z., Cai, Y., Ou, C., Lin, H., Imbs, A.B. (2002). Molecular species composition of glycolipids from *Spirulina platensis*. *Food Chemistry*, 77(1): 9-13.

Y

Yorio, N.C., Goins, G.D., Kagie, H.R., Wheeler, R.M., Sager, J.C. (2001). Improving spinach, radish, and lettuce growth under red light-emitting diodes (LEDs) with blue light supplementation. *HortScience,* 36:380–383.

Z

Zarrouk, C. (1966). Contribution à l'étude d'une cyanophycée. Influence de divers facteurs physiques et chimiques sur la croissance et la photosynthèse de *Spirulina maxima* Geitler. Thèse de Doctorat. University of Paris, Paris.

Zhang, X.W., Zhang, Y.M., Chen, F. (1999). Application of mathematical models to the determination optimal glucose concentration and light intensity for mixotrophic culture of *Spirulina platensis*. *Process Biochemistry*, 34(5): 477-481.

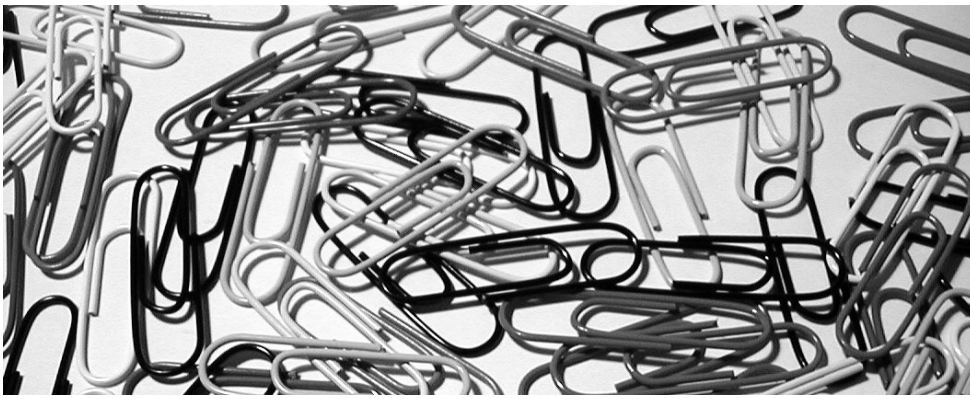

Annexes

Acronyms

Nomenclature

List of Publications

ACRONYMS

ADF	Acid Detergent Fiber
ALS	Advance Life Support
ANOVA	ANalysis Of VAriance
APC	AlloPhycocyanin
ATP	Adenosine TriPhosphate
BB	Beet Batch (culture)
BO	Beet Ocupation
BPC	Biomass Production Chamber
BS	Beet Stage (culture)
CCD	Central Composite Design
CEEF	Closed Ecology Experiment Facility
CELSS	Controlled Ecological Life-Support System
CESRF	Controlled Environment Systems Research Facility
CH	CarboHydrate
Chl	Chlorophyll
CI	Compartment I of the MELiSSA loop (thermophilic anoxygenic bacteria)
CII	Compartment II of the MELiSSA loop (photoheterotrophic bacteria *R. rubrum*)
CIII	Compartment III of the MELiSSA loop (nitrifying bacteria)
CIVa	Compartment IVa of the MELiSSA loop (photoautotrophic bacteria, *Arthrospira sp*.)
CIVb	Compartment IVb of the MELiSSA loop (Higher Plant Compartment, also called HPC)
CSA	Canadian Space Agency
CV	Compartment V of the MELiSSA loop (Crew)
D	Dilution rate
DAP	Days After Planting
Dc	Coded value for dilution rate (used for the CCD in Chapter 3)
DCG	Daily Carbon Gain
df	degrees of freedom
DIC	Days In Chamber
DRZ	Deep Root Zone
DW	Dry Weight (dw)
EB	Edible Biomass
EC	Electro-Conductivity
ESA	European Space Agency
FA	Fatty Acids

FAO	Food Agriculture Organization
FID	Flame Ionization Detector
FW	Fresh Weight (fw)
GLA	γ-Linoleic Acid
GOGAT	Glutamate synthase
GS	Glutamine synthetase
HDC	Human Daily Consumption
HDP	Human Daily Production
HI	Harvest Index
HID	High Intensity Discharge (lamp)
HPC	Higher Plant Compartment
HPLC	High Performance Liquid Chromatography
HPS	High Pressure Sodium (lamp)
I	Light Intensity
Ic	Coded value for light intensity (used for the CCD in Chapter 3)
IDCG	Integrated Daily Carbon Gain
IEB	Inedible Biomass
IRGA	Infrared Gas Analyzer
ISA	Instrument Society of America
ISS	International Space Station
KSC	Kennedy Space Center
LA	Leaf Area
LAI	Leaf Area Index
LB	Lettuce Batch (culture)
LED	Light Emitting Diode
LS	Lettuce Stage (culture)
MELiSSA	Micro-Ecological Life Support System Alternative
MH	Metal Halide (lamp)
MPP	MELiSSA Pilot Plant
MUFA	Mono-Unsaturated Fatty Acids
NA	Not Available
$NADP^+$	Nicotinamide Adenine Dinucleotide Phosphate (oxidised form)
NADPH	Nicotinamide Adenine Dinucleotide Phosphate (reduced form)
NASA	National Aeronautics and Space Administration (of USA)
NASDA	National Space Development Agency (of Japan)
NCER	Net Carbon Exchange Rate
NDF	Neutral Detergent Fiber
NDIR	Non-Dispersive Infrared
NFT	Nutrient Film Technique
NPU	Net Protein Utilization
NR	Nitrogen Reintroduction
NRH	Non-Rectangular Hyperbola
NSCORT	NASA Specialized Center of Research and Training
OD	Optical Density
PAR	Photosynthetically Active Radiation
PC	PhycoCyanin
PCC	Pasteur Culture Collection
PE	PhycoErythrin
PER	Protein Efficiency Ratio
PLC	Programmable Logic Controller
Pn	Net photosynthesis
PP	Pentose Phosphate
PPF	Photosynthetic photon flux
PQ	Photosynthetic quotient
PSII	Photosystem (PSI and PSII)
PUFA	PolyUnsaturated Fatty Acids
RE	Relative Error
RGR	Relative growth rate
RH	Rectangular Hyperbola
RMT	Root Misting Technique
Rr	Dark net respiration rate
RSE	Residuals Standard Error
RSM	Response Surface Model
Rubisco	Ribulose-1,5-bisphosphate carboxylase
RUE	Radiation Use Efficiency
RUR	Relative (nutrient) Uptake Rate
SAT	Static Aerated Technique
SCP	Single Cell Protein
SD	Standard Deviation
SE	Standard Error
SEC	Sealed Environment Chambers
SFA	Saturated Fatty Acids
SLA	Specific Leaf Area
SPSS	SigmaPlot® Statistical Software
TC	Total Carbon
TCA	TriCarboxylic Acid
TIC	Total Inorganic Carbon
TOC	Total Organic Carbon
UAB	Universitat Autònoma de Barcelona
UoG	University of Guelph
USDA	United States Department of Agriculture
VFA	Volatile Fatty Acids
VOC	Volatile Organic Compound
VPGC	Variable Plant Growth Chamber
WHO	World Health Organization

NOMENCLATURE OF INSTRUMENTATION AND CONTROL LOOP FOR HPC DESIGN

EQUIPMENT

All equipment for the HPC prototype design (Chapter 7) is labeled as EK00, where:

E: Equipment type, see table A.1.

K: Number corresponding to the HPC area where the equipment is located, see table A.2.

00: Sequential digit that indicates similar equipment inside the same HPC area.

Table A.1 Acronyms used for equipment identification in Chapter 7.

E	Explanation
A	HPC area
B	Condenser, Resistance
C	Chanel, Conveyor
F	Filter
H	Hydroponic Troughs
L	Lamp
O	Open, acces door
P	Pump, Fan, Compressor
T	Tank

Table A.2 Acronyms list used for the different HPC sub-systems area.

K	Area of HPC
1	Lighting Area (A100)
2	Liquid Area (A200)
3	Air Handling Area (A300)
4	Acess Areas (A400)
5	Growing Area (A500)
6	MPP Interface Area (A600)

Example 1: T202.- Tank (T) located in liquid sub-system area (2), the second (02) that appears.

CONTROL LOOPS

Control loops of the HPC prototype (Chapter 7) are specified as X LC EK00N, where:

X: Controlled variable, see table A.3.

LC: Control Loop.

EK00: Equipment or area at which the control loop is associated.

N: Control loop number related to an equipment or area.

Table A.3 Acronyms list used for control variables and instrumentation, proposed by ISA (Instrument Society of America).
(1) Subindex refers to the analized parameter (H: Humidity; IL: Light intensity; pH; CO_2; O_2; etc.)
(2) If corresponds to open/close equipment, High means open or almost open, and Low means Closed or almost close.
(3) Transmitter refers to the equipment constitued by transductor or sensor and transmitter itself.

LETTER	Control Variable (X)	Type (Y)
A_Z (1)	Analized Variable	Alarm
C	Conductivity	Controller
F	Flow	-
H	-	High (2)
I	-	Indicator
L	Level	Low (2)
P	Pressure	-
R	-	Regulation
T	Temperature	Transmitter (3)
V	Viscosity	Valve
X	Motor Order (On/Off)	-
Y	-	Contact/Relay

Example 2: A_{IL} LC L1011: First (1) control loop (LC) for light intensity (A_{IL}) of the lamps (L101).

INSTRUMENTATION

Instrumentation located within the HPC and associated with a control loop is described as XY EK00NA, where:

X: Controlled Variable, see table A.3.

Y: Instrumentation type, see A.3.

EK00: Equipment or area at which is associated.

N: Control loop number related to an equipment or area.

A: Optional. Sequential letter, which identifies the doubled instrumentation in the same control loop.

Example 3: A_{IL}T L1011A: First (A) transmitter (T) for light intensity (A_{IL}) in the first (1) control loop for lamps (L101).

Examples 4: A_{IL}IC L1011: Indicator (I) and Controller (C) for light intensity (A_{IL}) in the first (1) control loop for lamps (L101).

Example 5: A_{IL}ALH L1011: Alarm (A) Low/High (LW) for light intensity (A_{IL}) in the first (1) control loop for lamps (L101).

LIST OF PUBLICATIONS

Internal and confidential Technical Notes

Masot, A., Albiol, J., Gòdia, F. (2006). Review of CIVb biomass composition under different operational conditions. MELiSSA Technical Note 78.8. European Space Agency ESA/ESTEC/CONTRACT 13292/98/NL/MV.

Masot, A., Waters, G., Albiol, J., Dixon, M., Gòdia, F. (2006). Detailed design of the higher plant chamber. MELiSSA Technical Note 75.3. European Space Agency ESA/ESTEC/CONTRACT 13292/98/NL/MV.

Waters, G., Masot, A., Gòdia, F., Dixon, M. (2006). Higher Plant Chamber Prototype for the MELiSSA Pilot Plant: Detailed Design and Verification. MELiSSA Technical Note 85.5. European Space Agency ESA/ESTEC/CONTRACT 19772/06/NL/GM.

Masot, A., Albiol, J., Gòdia, F. (2005). *Spirulina platensis* ammonium uptake tests. MELiSSA Technical Note 52.5. European Space Agency ESA/ESTEC/CONTRACT 13292/98/NL/MV.

Masot, A., Waters, G., Stasiak, M., Albiol, J., Dixon, M., Gòdia, F. (2004). Higher Plant Chamber Preliminary Requirements Document. MELiSSA Technical Note 65.5. European Space Agency ESA/ESTEC/CONTRACT 13292/98/NL/MV.

Albiol, J., Creus, N., Pérez, J., Montràs, A., Masot, A., Gòdia, F. (2002). Pilot Plant Liquid Loop Review. MELiSSA Technical Note 62.3. European Space Agency ESA/ESTEC/CONTRACT 13292/98/NL/MV.

Pérez, J., Albiol, J., Creus, N., Montràs, A., Masot, A., Gòdia, F. (2002). Pilot Plant Gas Loop Review. MELiSSA Technical Note 62.4. European Space Agency ESA/ESTEC/CONTRACT 13292/98/NL/MV.

Creus, N., Montràs, A., Masot, A., Pérez, J., Albiol, J., Gòdia, F. (2002). Pilot design of the MELiSSA solid loop. MELiSSA Technical Note 62.5. European Space Agency ESA/ESTEC/CONTRACT 13292/98/NL/MV.

International Publications

Waters, G. [(1)], Gidzinski, D.[(1)], Dixon M. [(1)], Masot, A.[(2)], Gòdia, F.[(2)], Paillé, C.[(3)], Lamaze, B.[(3)], Lasseur, Ch.[(3)] (2007). Integration of a Higher Plant Chamber into the European Space Agency's MELiSSA Pilot Plant: The Canadian Role in Advanced Life Support Test-Bed Development. 2nd International Workshop-Exploring Mars and its Earth Analogues. June 19-23 2007, Trento (Italy).

Waters, G.[(1)], Gidzinski, D.[(1)], Dixon, M.[(1)], Masot, A.[(2)], Albiol, J.[(2)], Gòdia, F.[(2)], Paillé, C.[(3)], Lamaze, B.[(3)], Lasseur, Ch.[(3)] (2006). Understanding the Behaviour of Higher Plant Chambers for Bioregenerative Life Support: A Plan for Successful Integration into the European Space Agency's MELiSSA Loop. CSEW Conference, University of Toronto (Canada).

Masot, A., Albiol, J., Gòdia, F., Waters, G., Dixon, M. (2006). MELiSSA Pilot Plant Integration of a Higher Plant Compartment. Oral presentation in First Seminar Series: "What will we eat on Mars?". University of Guelph,Canada.

Waters, G.[(1)], Dixon, M.[(1)], Masot, A.[(2)], Albiol, J.[(2)], Gòdia, F.[(2)], Paillé, C.[(3)], Lamaze, B.[(3)], Lasseur, Ch.[(3)] (2006). Integration of a Higher Plant Chamber into the European Space Agency's MELiSSA Pilot Plant: Canadian Involvement in International Bioregenerative Life Support Research. Proceedings of ASTRO Conference. 13th Canadian Astronautics Conference and 53rd Annual General Meeting. April 25-27 2006. Montréal (Canada). Paper 52.

Waters, G.[(1)], Gidzinski, D.[(1)], Dixon, M.[(1)], Masot, A.[(2)], Albiol, J.[(2)], Gòdia, F.[(2)], Ordoñez, L.[(3)], Favreau, M.[(3)], Lasseur, Ch.[(3)] (2005). Integration of a Higher Plant Chamber with the MELiSSA loop (Pilot Plant Facility). Final Report to the Canadian Space Agency. CSA/CONTRACT 9F007-010129/00/ST.

Gòdia, F., Albiol, J., Pérez, J., Creus, N., Cabello, F., Montràs, A., Masot, A., Lasseur, C. (2004). The MELiSSA Pilot Plant Facility As An Integration Test-Bed For Advanced Life Support Systems. Advances in Space Research, 34(7): 1483-1493.

Waters, G., Masot, A., Albiol, J., Gòdia, F., Dixon, M. (2004). Static Mass Balance Studies of the MELiSSA Pilot Plant: Integration of a Higher Plant Chamber. Proceedings of the 34th International Conference on Environmental Systems (ICES). July 19-22 2004. Colorado Springs (USA). SAE paper No. 2004-01-2579.

Waters, G., Masot, A., Albiol, J., Gòdia, F., Dixon, M. (2004). Modeling Carbon, Oxygen and Nitrogen Balance in an Artificial Nitrogen Mineralization Loop. The Case of the European Space Agency's MELiSSA Pilot Plant Facility. Poster presented in The Centre for Research in Earth and Space Technology Innovation Network 2004 (CRESTech 2004), Toronto, Canada.

Waters, G., Gidzinski, D., Zheng,Y., Dixon, M.; Masot, A., Albiol, J., Gòdia, F.; Poughon, L., Dussap, G.; Ordoñez, L.; Paillé, C., Lasseur, Ch. (2004). Successful Integration of a Higher Plant Chamber into ESA's MELiSSA Pilot Plant. Poster presented in The Centre for Research in Earth and Space Technology Innovation Network 2004 (CRESTech 2004), Toronto, Canada.

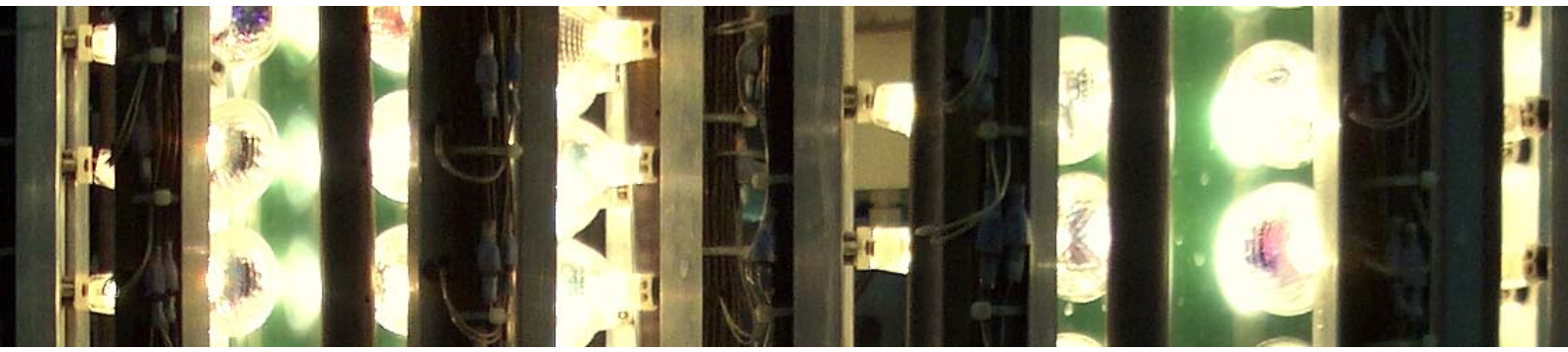

Departament d’Enginyeria Química
Escola Tècnica Superior d’Enginyeria
Universitat Autònoma de Barcelona